Chromium and Nickel Complexes with Tetradentate Diamide Ligands

by

Colin L. Weeks

A thesis submitted in fulfilment of the
requirement for the degree of
Doctor of Philosophy

School of Chemistry
University of Sydney
March 2001

Dedicated to my father

for his love, support, and encouragement over the years,

but above all for teaching me that:

"The fear of the Lord is the beginning of wisdom." Proverbs 9:10

Abstract

The higher oxidation states of Cr and Ni have been implicated in the mechanisms of Cr- and Ni-induced carcinogenesis. In the light of this the ability of deprotonated amide N-donor ligands to stabilise the higher oxidation states of Cr and Ni were explored as models for metal-peptide interactions *in vivo*. A series of acyclic tetradentate diamide ligands with pyridyl and chiral pyrrolidine terminal groups were synthesised and used to prepare the metal complexes.

Four new Ni(II) complexes with the pyrrolidine based ligands were synthesised and characterised. The two amine groups in the ligand *N,N'*-bis(*S*-prolyl)-1,2-ethanediamine (*S,S*-bprolenH_2) were oxidatively dehydrogenated during the preparation of the Ni(II) complex in air, the reaction involved O_2 and in the complex formed the ligand had 1-pyrroline terminal groups. The Ni(II) complex with *S,S*-bprolen was synthesised under anaerobic conditions, and two other Ni(II) complexes with analogous ligands were prepared in air. The $Ni^{III/II}$ reduction potentials of the complexes with pyridyl and pyrrolidine based ligands were measured by cyclic voltammetry to assess the stability of the Ni(III) oxidation state, but did not show any correlation with the ease of ligand oxidation. The production of an oxidising species from the reaction of O_2 with a Ni-amide complex indicated that some Ni-peptide complexes may well be able to cause oxidative DNA damage *in vivo*.

The ability of various oxidants to oxidise the Cr(III) complexes to Cr(V) was examined. Chromium(V) generated during the reduction of Cr(VI) by methanol was also stabilised by the tetradentate diamide ligands. EPR spectroscopy was used to monitor the formation of the Cr(V) species and their stability over time. The generation of genotoxic Cr(V) from both the reduction of carcinogenic Cr(VI) and the oxidation of Cr(III) may have important biological implications.

X-ray absorption spectroscopy was used to determine the oxidation state and coordination geometry of Cr(III) and Cr(V) complexes with alanine, 1,10-phenanthroline (phen), and *N,N'*-bis(2-pyridinecarboxamido)-1,2-benzene (bpb) ligands. Multiple-scattering XAFS calculations were used to determine the

three-dimensional structure of a dinuclear Cr(V)-alanine complex (which is the first example of an amino acid complex of Cr(V)), two Cr(III)-bpb complexes, and *cis*-$[Cr^{III}(phen)_2(OH_2)_2](NO_3)_3.2{\cdot}5H_2O$.

The complex, $[Cr^{V}O(S,S\text{-bprolben})]^{+}$, (*S,S*-bprolbenH$_2$ = *N,N′*-bis(*S*-prolyl)-1,2-benzenediamine) produced by the methanol reduction of Cr(VI) in the presence of the ligand, was a potent DNA damaging agent in plasmid DNA cleavage assays. Combined with the observed stabilisation of Cr(V) by deprotonated amide N-donor ligands, this indicated that Cr(V)-peptide complexes might play a role in the mechanism of Cr-induced carcinogenesis.

Acknowledgments

Foremost, thanks to my supervisors Dr Ron Fenton and Professor Peter Lay. Their helpfulness has been unfailing and they have provided sound advice throughout the course of this project.

I would also like to express my gratitude to the following people:

- Dr Peter Turner from the Small Molecule Crystallography Facility, University of Sydney for collecting the data and solving the structure of four of my Ni(II) complexes.
- Dr Garry Foran and Dr James Hester from the Australian National Beamline Facility at the Photon Factory in Tsukuba, Japan for their assistance in recording the X-ray absorption spectroscopy of the Cr complexes.
- Dr Aviva Levina for assistance in collecting the X-ray absorption spectroscopy data.
- Dr Ming Xie and Dr Ian Luck from the NMR facility in the School of Chemistry, University of Sydney for recording the NMR spectra on the Bruker AMX400 spectrometer. Double thanks to Dr Ming Xie who also instructed me in the use of the EPR facility at the School of Chemistry, University of Sydney.
- Dr Xiaomin Song and Dr Keith Fisher from the Mass Spectrometry Unit in the School of Chemistry, University of Sydney for measuring the ES/MS of the Cr complexes.
- Dr Carolyn Dillon for supplying the samples of $[Cr^{III}(phen)_2(OH_2)_2](NO_3)_3.2{\cdot}5H_2O$ and $[Cr^{III}(salen)(OH_2)_2]CF_3SO_3$.
- Dr Henrietta Headlam for supplying the sample of $Na_2[Cr^{V}_2O_4(S\text{-ala})_2(OCH_3)_2].0{\cdot}5CH_3OH.0{\cdot}5(S\text{-alaH})$.
- Fernando Barasoain and Jeff Armstrong, technical support staff in the School of Chemistry, University of Sydney.

I have much appreciated the friendship of the numerous members of the Fenton and Lay research groups over the past four years, especially that of my fellow residents in the "Fishbowl".

An Australian Postgraduate Award scholarship from the Australian government has helped me to keep body and soul together while doing this work. This research has been supported by funding from the Australian Research Council and the Australian Synchrotron Research Program.

Colin L. Weeks, March 2001

Table of Contents

List of Figures

List of Tables

List of Schemes

List of Abbreviations

A	absorbance
Å	angstrom
AAS	atomic absorption spectroscopy
A_{Cr}	chromium hyperfine coupling constant
ADP	adenosine diphosphate
aib	α-aminoisobutyric acid
A_{iso}	hyperfine coupling constant
ala	alanine
A_N	nitrogen superhyperfine coupling constant
ANBF	Australian National Beamline Facility
AP	apurinic/apyrimidinic
AR	analytical reagent
$bpbH_2$	*N,N′*-bis(2-pyridinecarboxamide)-1,2-benzene
$bpenH_2$	*N,N′*-bis(2-pyridinecarboxamide)-1,2-ethane
S,S-$bprolbenH_2$	*N,N′*-bis(*S*-prolyl)-1,2-benzenediamine
R,R-(*S,S*)-$bprolchxnH_2$	*N,N′*-bis(*S*-prolyl)-*R,R*-1,2-cyclohexanediamine
S,S-$bprolenH_2$	*N,N′*-bis(*S*-prolyl)-1,2-ethanediamine
br	broad
BVS	bond valence sum
CBZ	carbobenzoxy
CHE	Chinese hamster embryo (cell line)
CHO	Chinese hamster ovary (cell line)
cm	centimetre
COSY	correlation spectroscopy
$CpMe_5$	pentamethylcyclopentadienyl
cyclam	1,4,8,11-tetraazacyclotetradecane
1D	1-dimensional
2D	2-dimensional
d	day
	doublet (in NMR spectroscopy)
D_c	calculated density
dd	doublet of doublets

ddd	doublet of doublets of doublets
DMF	*N,N*-dimethylformamide
DMSO	dimethylsulfoxide
DNA	deoxyribonucleic acid
DRIFTS	diffuse reflectance infrared Fourier transform spectroscopy
dt	doublet of triplets
E	energy (in XAFS)
E^0	standard potential (in electrochemistry)
E_0	binding energy (in XAFS)
$E_{½}$	reduction potential
edta	1,2-ethanediamine-*N,N,N′,N′*-tetraacetate
ehba	2-ethyl-2-hydroxybutanoate(2−)
ΔE_p	peak-to-peak separation
EPR	electron paramagnetic resonance
ES/MS	electrospray mass spectrometry
eV	electron volt
Fc	ferrocene
g	gram
G	gauss
GeV	gigaelectron volt
GHz	gigaherz
g_{iso}	isotropic peak position
glyglyhis	glycylglycylhistidine
GoF	goodness-of-fit
GSH	glutathione
h	hour
h	Planck's constant
HPLC	high performance liquid chromatography
hmba	2-hydroxy-2-methylbutanoate(2−)
Hz	herz
I	intensity
i	current

i_{pa}	anodic peak current
i_{pc}	cathodic peak current
IR	infrared
Im	imaginary
J	coupling constant
K	Kelvin
k	photoelectron wave vector
keV	kiloelectron volt
kHz	kiloherz
L	litre
μL	microlitre
Lit.	literature
LR	laboratory reagent
m	medium (in IR spectroscopy), multiplet (in NMR spectroscopy)
M	molar
μM	micromolar
μm	micrometre
mA	milliampere
mac	3,6,9,12,14-pentaoxo-2,2,5,5,7,7,10,10-octamethyl-13,13-diethyl-1,4,8,11-tetraazacyclotridecane
mampa	5,6-(4,5-dichlorobenzo)-3,8,11,13-tetraoxo-2,2,9,9-tetramethyl-12,12-diethyl-1,4,7,10-tetraazacyclotridecane
m_e	mass of electron
mg	milligram
mL	millilitre
min	minute
mM	millimolar
mm	millimetre
m.p.	melting point
MS	multiple-scattering
msec	millisecond

mV	millivolt
mW	milliwatt
m/z	mass-to-charge ratio
N	total number of observations
N_{ind}	number of independent observations
N_{obs}	number of statistically significant observations
N_{var}	number of variables
NADH	nicotinamide adenine dinucleotide (reduced form)
NADPH	nicotinamide adenine dinucleotide phosphate (reduced form)
NHE	normal hydrogen electrode
nm	nanometre
NMR	nuclear magnetic resonance
No.	number
ORTEP	Oak Ridge thermal ellipsoid plotting program
p_e	momentum of electron
PFP	perfluoropinacolate(2−)
phen	1,10-phenanthroline
4-POBN	α-(4-pyridyl-1-oxide)-*N*-*tert*-butylnitrone
ppm	parts per million
py	pyridine
q	quartet
qa	quinic acid
R	Fourier transform distance (in XAFS)
	residual (in X-ray crystallography)
R	resistance (in electrochemistry)
	goodness-of-fit parameter including restraints (in XAFS)
R_0	bond length of unit valence
R_{as}	distance between absorbing and scattering atoms in XAFS
$r_{average}$	average radius
Re	real
R_{ij}	bond length between two atoms i and j

R_{max}	maximum effective path length for photoelectron
R_{XAFS}	goodness-of-fit parameter for XAFS curves
ROS	reactive oxygen species
rpm	revolutions per minute
s	singlet (in NMR spectroscopy)
	strong (in IR spectroscopy)
	second
s.d.	standard deviation
ss	strong and sharp
SS	single-scattering
salen	*N,N'*-ethylenebis(salicylideneiminato)
sh	shoulder
t	triplet
TBAP	tetra(*n*-butyl)ammonium perchlorate
td	triplet of doublets
TFA	trifluoroacetic acid
TMS	tetramethylsilane
tpp	tetraphenylporphyrin
UV-Vis	ultraviolet-visible
V	volt
V	volume of unit cell
+ve	positive
vs	versus
v/v	volume per unit volume
w	weak
W	watt
XAFS	X-ray absorption fine structure
XANES	X-ray absorption near-edge structure
Z	number of formula units in the unit cell

Chapter 1

Introduction

1.1 Amide Ligands

The characteristic properties and structures of proteins derive largely from their polyamide (peptide) structures.[1] The chemistry of the amide group extends far beyond its role as a structural component in proteins and in this work the focus will be upon its ability to coordinate to metal ions. The metal-amide bond need not be studied in splendid isolation; for example, examining the coordination of metal ions to the amide group can provide insights into metal-protein interactions.

A primary or secondary amide group can exist in either the neutral, protonated or deprotonated form. The main resonance structures for the neutral and deprotonated species are shown in Figure 1.1 (a) and (b), respectively. The two possible protonation sites are shown in Figure 1.1 (c). The amide group is a weak acid and a weak base, so it exists in the neutral form over most of the pH range. When the amide group is protonated, the carbonyl oxygen predominates as the site of protonation, the ratio of O-protonated to N-protonated molecules has been estimated as 10^7.[2] The partial double-bond character of the nitrogen-carbon amide bond in the neutral amide (40% double bond character[3]) due to the resonance contributor on the right means that the nitrogen lone pair is extremely unlikely to bind a proton.

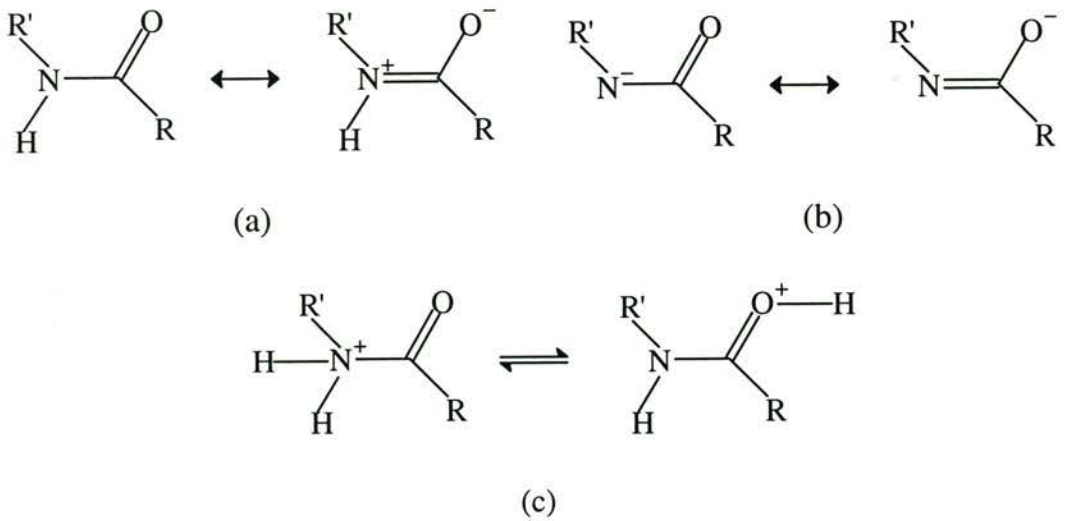

Figure 1.1 Resonance forms of the (a) neutral and (b) deprotonated amide groups; (c) equilibrium of protonated amide group

The use of molecules containing amide functional groups as ligands can lead to two different modes of metal-amide binding. The metal can bind *via* either the O or the N atoms of the amide group.[2,4] The resonance contributors for the two modes of binding are shown in Figure 1.2. The usual site of metal coordination by neutral amides is the same as the site of protonation, the oxygen atom, Figure 1.2 (c).[2,4] Coordination of a metal ion to the oxygen increases the contribution of the resonance structure on the right in Figure 1.2 (c), and an increase in the nitrogen-carbon double-bond character is observed.[2] To coordinate a metal ion to the amide nitrogen requires deprotonation of the amide group, Figure 1.2 (a), or tautomerisation, Figure 1.2 (b); deprotonation of the amide group is the more common mechanism. Tertiary amide groups, which do not have a dissociable proton, do not coordinate to metal ions *via* the amide nitrogen.[5-7]

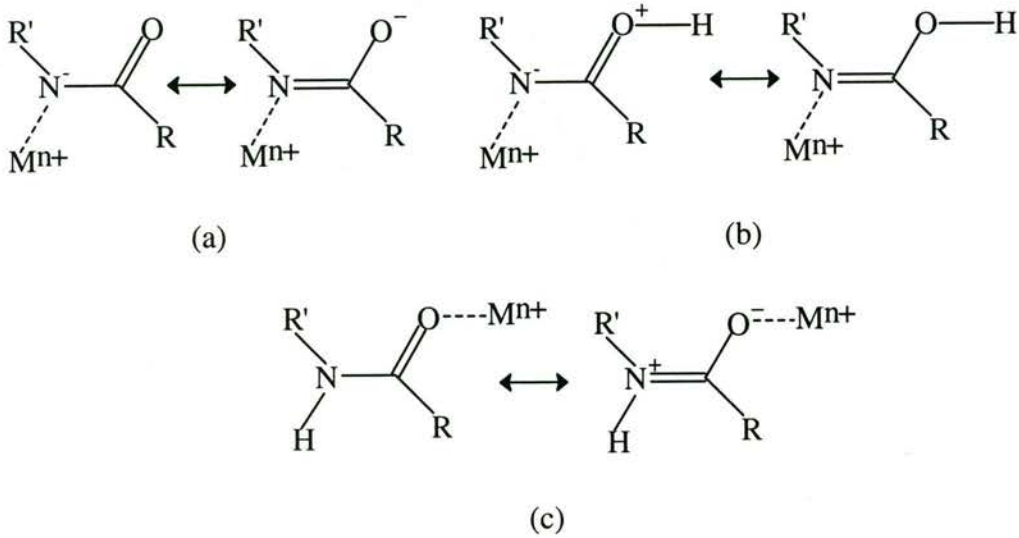

Figure 1.2 Resonance forms of the amide group coordinated to a metal ion *via* the nitrogen (a) and (b), or oxygen (c) atoms.

The weak acidity of the amide group means that high pH or the chelate effect are necessary to enable coordination of metal ions to the amide nitrogen.[2,4] Just as the nitrogen-proton bond of the amide group is strong, the bonding of metal ions to deprotonated amides results in the strongest metal-amide bonds.[2] The strength of this bond is due to the negative charge on the deprotonated amide nitrogen, making it a strong donor ligand.

The strong bonds formed by deprotonated amide nitrogens and their ability to donate electron density to coordinated metal ions make them quite effective ligands for the stabilisation of metal ions in high oxidation states. Examples of high oxidation states stabilised by deprotonated amide ligands are: Cu(III),[8-15] Ni(III),[8,9,13,16-24] Ni(IV),[25] Cr(V),[26,27] Fe(IV),[28] Mn(V),[29-31] V(IV)[32-34] and V(V).[32,34,35]

The capacity of deprotonated amide groups to stabilise high oxidation states of metal ions was the reason for choosing ligands containing secondary amide groups to synthesise complexes with Cr and Ni. Complexes of Cr and Ni in the higher oxidation states are of interest because they may play a role in Cr- and Ni-induced carcinogenesis, respectively.[36-44]

1.2 Chromium-Induced Carcinogenesis

Newman reported a tumour (nasal adeno-carcinoma) in a chrome worker in 1890.[45] Chromium(VI) has since been thoroughly documented as a carcinogen and workers exposed to it have an increased risk of developing tumours.[46-54]

Animals exposed to Cr(VI) compounds also have a significantly increased risk of developing tumours.[46,52,55-58] Finally, Cr(VI) compounds are mutagenic in yeast,[46,52,59] bacterial,[46,52,60,61] and mammalian[46,52,59,62] cells.

1.2.1 Chromium Use in Industry

The main source of Cr is the ore chromite, Cr_2O_3FeO, which is used in the production of stainless steel and refractory materials and is also refined to produce Cr metal, Cr(III) compounds, and Cr(VI) compounds. Pure Cr metal is used in the preparation of high purity alloys. Chromium(III) compounds are used as pigments, catalysts, mordants, and in leather tanning. Chromium(VI) compounds are used as pigments, mordants, in leather tanning, Cr plating, corrosion inhibition, and wood preservation.[46] There is also exposure to Cr(VI) in the smelting and welding of stainless steel and in cement production.[46] A Finnish study found that Cr(VI) compounds were the most widely used carcinogens in industry, accounting for 25% of reported exposures.[63]

1.2.2 Fundamental Chemistry of Cr

Chromium compounds exist in all the oxidation states from –II to VI, though the III and VI oxidation states are the most stable.[64,65] The oxidation states from II to VI are of most interest in biological systems since they are the forms likely to occur *in vivo* after exposure to Cr(III) and Cr(VI) used in industry. Chromium(0) in the pure metal and alloys is inert and has extremely low bioavailability; it is only when it is converted to another oxidation state, for example in the welding of stainless steel, that it becomes bioavailable.

Chromium(II) complexes are only stable under anaerobic conditions and are rapidly oxidised to Cr(III) by O_2.[64,65] Chromium(III) is the most stable oxidation state and has the greatest number of known compounds.[64] The d^3 electronic configuration of Cr(III) makes its complexes kinetically inert; they are almost always six-coordinate.[64] The most important Cr(VI) compounds are the oxides, chromic trioxide, CrO_3; chromate, CrO_4^{2-}; and dichromate, $Cr_2O_7^{2-}$. In aqueous solution chromic trioxide forms chromate and dichromate, according to the equilibria in Equations 1.1 to 1.6.[64]

$$CrO_3 + H_2O \leftrightharpoons H_2CrO_4 \quad (1.1)$$

$$H_2CrO_4 \leftrightharpoons HCrO_4^- + H^+ \quad (1.2)$$

$$HCrO_4^- \leftrightharpoons CrO_4^{2-} + H^+ \quad (1.3)$$

$$Cr_2O_7^{2-} + H_2O \leftrightharpoons 2HCrO_4^- \quad (1.4)$$

$$Cr_2O_7^{2-} + OH^- \leftrightharpoons HCrO_4^- + CrO_4^{2-} \quad (1.5)$$

$$HCrO_4^- + OH^- \leftrightharpoons CrO_4^{2-} + H_2O \quad (1.6)$$

Above pH 8 the main species is CrO_4^{2-}, while in the pH range 2-6, the $HCrO_4^-$ and $Cr_2O_7^{2-}$ ions are in equilibrium.[64,65] The existence of significant levels of $HCrO_4^-$ has been the subject of conflicting reports. Brasch *et al.* reported the formation of significant amounts of $HCrO_4^-$ and determined its $pK_a = 5.80$ using UV-Vis spectroscopy and ^{17}O NMR spectroscopy.[66] However, Poulopoulou *et al.* did not detect any $HCrO_4^-$ in the pH range 3-11 by UV-Vis spectroscopy, claiming that only CrO_4^{2-} and $Cr_2O_7^{2-}$ were present in significant amounts.[67] $HCrO_4^-$ is less absorbing

than CrO_4^{2-},[66] which is probably why it was not detected in the other study. All of the Cr(VI) oxides are strong oxidants under acidic conditions.

Chromium(V) and Cr(IV) complexes are formed when Cr(VI) is reduced by one- and two-electron reductants. Chromium(V) complexes are mostly unstable in aqueous solution, though tetraperoxochromate(V) and complexes with 2-hydroxy acid ligands and some multidentate ligands are relatively stable and have been isolated.[26,68-72] Chromium(V) complexes are readily reduced to Cr(III), and can also disproportionate to Cr(III) and Cr(VI)[73] (Equation 1.7).

$$3Cr(V) \rightarrow 2Cr(VI) + Cr(III) \qquad (1.7)$$

Few Cr(IV) complexes are stable in aqueous solution, since disproportionation to Cr(V) and Cr(III)[74,75] (Equation 1.8) occurs. Chromium(IV) is a powerful oxidant that reacts rapidly with many organic substrates, and in some complexes undergoes reduction by intramolecular ligand oxidation.[74,75]

$$2Cr(IV) \rightarrow Cr(III) + Cr(V) \qquad (1.8)$$

1.2.3 Uptake-Reduction Model of Cr-Induced Carcinogenesis

Though Cr(VI) compounds are carcinogenic, *in vitro* studies have shown that Cr(VI) itself does not interact with DNA or damage it.[60,76-80] The observation of DNA damage when Cr(VI) is reduced by cellular components has led to the uptake-reduction model of Cr(VI)-induced carcinogenesis,[77,81-84] which has been recently modified by Codd *et al.*[85] (Figure 1.3).

The uptake-reduction model may be summarised as follows: Cr(VI), which is known to be carcinogenic, is readily taken up by cells. There is also uptake of other species formed during the extracellular reduction of Cr(VI). The cell membrane is impermeable to most Cr(III) compounds. Once inside the cell, the Cr(VI) is reduced by cellular components, producing the reactive intermediates: Cr(VI)-esters, Cr(V), Cr(IV) and free radicals, with the Cr ultimately reduced to the Cr(III) oxidation state.

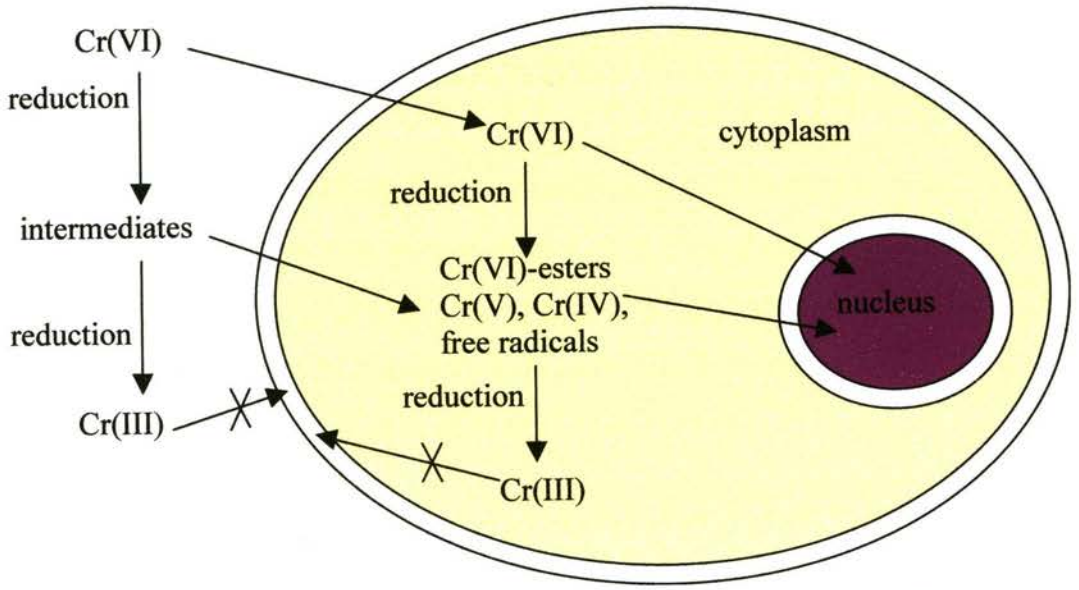

Figure 1.3 Uptake-reduction model of Cr(VI)-induced carcinogenesis[77,81-85]

The reduction of Cr(VI) to Cr(III) may take place in the cytoplasm, nucleus, membrane, mitochondria or endoplasmic reticulum. The reactive intermediates and/or the Cr(III) generated inside the cell cause damage to DNA and induce cancer.

1.2.3.1 Cellular Uptake of Cr

Chromium has been found in cells exposed to Cr(VI),[36,86-89] Cr(V),[36,37] and Cr(III)[90,91] but the uptake of cationic Cr(III) is negligible.[36,88,92] Soluble Cr(VI) enters cells as the chromate ion via the general anion channel.[93] Insoluble chromates enter cells by phagocytosis.[94-97] X-ray absorption spectroscopy (XAS) has shown that the Cr in V79 Chinese hamster lung cells exposed to Cr(VI) and Cr(V) complexes was all reduced to the Cr(III) oxidation state.[98] Although the Cr(VI) is ultimately reduced to Cr(III), some of the Cr(V) intermediates generated *in vivo* are stable enough to reach levels at which they are detectable by electron paramagnetic resonance (EPR) spectroscopy.[99,100,101]

The chemistry of the intermediates formed in the reduction of Cr(VI), and the final Cr(III) complexes, will determine their interactions with DNA and other cellular components. Understanding how the intermediates and Cr(III) complexes interact with DNA and other cellular components leads to insights into the possible mechanisms by which Cr compounds induce cancer. Interactions with DNA are

particularly important because cell growth and cell death, which are not properly regulated in cancer cells, are controlled by DNA.

1.2.3.2 Chromium(VI) Reduction in Biological Systems

The most important biological reductants of Cr(VI) are ascorbate (vitamin C),[78,82-84,102] glutathione (γ-glutamylcysteinylglycine, GSH),[82-84] and cysteine.[82,83] Some enzyme systems are also capable of reducing Cr(VI),[76,83,103] as is the membrane-bound antioxidant, vitamin E (α-tocopherol).[104]

Chromium(VI) Reduction by Ascorbate

When Cr(VI) is reduced by ascorbate, the reactive intermediates Cr(V),[105-110] Cr(IV),[108-110] and free radicals[105-111] are produced. The oxidation state of the final products depends upon the stoichiometry of the reaction, when an excess of ascorbate is used, all the Cr is reduced to Cr(III). When Cr(VI) is in excess, more of the reactive intermediate Cr(V) is detected.[105] When Cr(VI) in excess is reacted with ascorbate solutions prepared in the presence aerial O_2, additional Cr(V) complexes are detected, including Cr(V)-ascorbate-peroxo complexes. These are formed from the reaction of H_2O_2 with the Cr(V) complexes, with the H_2O_2 being produced by aerial oxidation of ascorbate prior to mixing the solutions.[105,112]

Reduction of Cr(VI) by ascorbate in the presence of DNA leads to DNA strand breaks,[78,109,113-115] Cr-DNA binding,[109] DNA-interstrand crosslinks,[114] and apurinic/apyrimidinic (AP) sites[113,115] *in vitro*.

Chromium(VI) Reduction by Glutathione

The reduction of Cr(VI) by glutathione (GSH) produced Cr(V),[116-120] and free radical intermediates.[111,120] An excess of GSH reduces Cr(VI) to Cr(III).[118,121]

The reduction of Cr(VI) by GSH in the presence of DNA causes DNA strand breaks,[115,116,121,122] DNA-protein crosslinks,[123] AP sites,[80,115,122] and Cr-DNA adducts.[116,120,124,125]

Chromium(VI) Reduction by Cysteine

The reduction of Cr(VI) by cysteine is faster than its reduction by GSH,[119,126] and produces Cr(V)[82,119] and free radicals.[82] Mechanistic studies have indicated that a Cr(IV) complex is also involved as a transient intermediate.[126,127] An excess of cysteine completely reduces Cr(VI) to Cr(III)[128] and the Cr(V) and Cr(IV) intermediates are not stable.[127]

Chromium-DNA adducts are formed when Cr(VI) is reduced by cysteine in the presence of DNA.[82,125,128,129]

Enzymatic Reduction of Cr(VI)

Chromium(VI) is reduced to Cr(III) by human[130,131] and rat[76,103,132-135] liver microsomes, where it is reduced by enzymes and requires NADPH or NADH as a cofactor. NADPH and NADH by themselves are also capable of slowly reducing Cr(VI).[132,136] The reduction of Cr(VI) by rat liver microsomes was strongly inhibited by O_2.[133,135] For human liver microsomes, O_2 is a partial inhibitor of Cr(VI) reduction.[130,131] The reduction of Cr(VI) by rat liver microsomes has been attributed primarily to the cytochrome P450 enzyme system[133-135] and the reduction by human liver microsomes has been attributed primarily to flavoproteins.[130,131] Chromium(V) is present when Cr(VI) is reduced by rat liver microsomes and NADPH.[137]

Significant amounts of Cr-DNA binding are observed when Cr(VI) is reduced by microsomes and NADPH. The amount of Cr-DNA binding from the Cr(VI) reduction by microsomes and NADPH in the presence of DNA is much higher than the amount of Cr-DNA binding in the reaction of Cr(III) with DNA.[76]

Chromium(VI) Reduction by α-Tocopherol

Reaction of α-tocopherol with Cr(VI) *in vitro* resulted in the formation of Cr(V) that was stabilised by the addition of *D*-glucose. The water-soluble vitamin E analogue, Trolox, also reduces Cr(VI), forming stable Cr(V) complexes. When Trolox is in excess the Cr(VI) is reduced to Cr(III).[104]

A role for α-tocopherol in Cr-induced carcinogenesis is based largely on the protective effect of α-tocopherol against Cr(VI) cytotoxicity, clastogenicity and mutagenicity observed in cell culture[95,138-142] and *in vivo*[143] studies. α-Tocopherol pretreatment of cultured cells reduced the amount of Cr(V) formed intracellularly after exposure to Cr(VI)[138,140,141] and reduced the level of Cr(VI)-induced DNA strand breaks in cells.[140,141,144] The protective effect of α-tocopherol against Cr-induced DNA damage in cells is postulated to be due to its reduction of Cr(V) intermediates and/or scavenging of free radicals.[138-140,144]

1.2.3.3 *In vivo* Cr(VI) Metabolism

To determine likely mechanisms of Cr-induced cancers, it is necessary to observe the effect of Cr compounds *in vivo*. As expected from the results of the *in vitro* studies, Cr(VI) is reduced *in vivo*, generating reactive intermediates and Cr(III) complexes.

Chromium(V) was detected by EPR spectroscopy in mice injected with Cr(VI).[99,100] The Cr(V) complexes detected by EPR spectroscopy had g_{iso} values consistent with coordination by diol groups, possibly from NADH. The treatment of mice with ascorbate or GSH prior to exposure to Cr(VI) decreased the levels of Cr(V) detected by EPR spectroscopy.[99,100] Chromium(V) signals have also been detected by EPR spectroscopy in the blood of rats. The rats were injected intravenously with dichromate, and a continuous circuit was set up where blood flowed from the sedated rat, through an EPR cavity, and back into the rat. The g_{iso} values of the Cr(V) species were postulated to be due to $CrO(S_2O_2)$ and $CrO(O_4)$ coordination modes.[101]

Chromium(V) and Cr(III) were found in the livers of mice injected with Cr(VI).[145] The level of Cr(V) was highest in the first sample, measured 15 minutes after the injection of the Cr(VI), but decreased significantly over the course of twelve hours. The level of Cr(III) did not change significantly over the twelve hours.

Species that are attributed to free radical adducts of the spin trap α-(4-pyridyl 1-oxide)-*N*-*tert*-butylnitrone (4-POBN) were detected by EPR spectroscopy in the bile of rats injected with Cr(VI) and 4-POBN.[146,147] Such experiments need to be viewed

with caution, however, since similar adducts are produced in non-radical processes.[85]

Occupational or environmental exposure of humans to Cr(VI) causes DNA-protein crosslinks.[148] Injection of dichromate into rats caused DNA fragmentation, DNA-protein crosslinks and nucleotide modifications.[149] DNA mutations were induced in the lung cells of mice after a Cr(VI) solution was injected into the lungs.[59] When chick embryos were exposed to Cr(VI), DNA strand breaks, DNA interstrand crosslinks and DNA-protein crosslinks, occurred in liver cells[150,151] and DNA strand breaks occurred in blood cells.[151] The frequency of micronuclei formation in bone marrow cells of rats and guinea pigs increased after they were injected with dichromate.[143]

1.2.3.4 Mechanisms of Cr-Induced DNA Damage

The biological activity of Cr(VI) is complicated because several different types of reactive intermediates form *in vivo* and *in vitro* with biological reductants. Various forms of DNA damage have also been produced *in vivo* and *in vitro* by Cr compounds. The observed metabolism of Cr(VI) *in vivo*, combined with the implications of the Cr chemistry studied *in vitro*, have led to the proposal of several mechanisms for Cr-induced carcinogenesis.

DNA Strand Breaks

Chromium(V) is produced in the reaction of Cr(VI) with all the major biological reductants listed above. The Cr(V) complexes can be stabilised by the reductants or oxidised forms of the reductants acting as ligands. Chromium(V) generated by the reaction of reductants with Cr(VI) can also be stabilised by other biological molecules. *In vitro* studies showed that *D*-glucose stabilises Cr(V) produced from the reduction of Cr(VI) by GSH[117] and α-tocopherol.[104] Oligopeptide ligands stabilised Cr(V) generated by the methanol reduction of Cr(VI).[38,152] The 2-hydroxy acid ligands are very effective at stabilising Cr(V)[68,69,153] and 2-hydroxy acids, (for example citrate and lactate) occur in biological systems.

Chromium(V) complexes with GSH,[121] 2-ethyl-2-hydroxybutanoate

(ehba),[39,40,60,154-158] quinic acid,[156] the macrocyclic tetraamide 5,6-(4,5-dichlorobenzo)-3,8,11,13-tetraoxo-2,2,9,9-tetramethyl-12,12-diethyl-1,4,7,10-tetraazacyclotridecane (mampa),[41] alanine,[38] glycine,[38] trialanine,[38] and triglycine[38] as ligands cause DNA strand breaks. The $[Cr^{V}O(mampa)]^{-}$ complex does not undergo disproportionation to Cr(VI) and Cr(III), and is not reduced by GSH.[41] The $[Cr^{V}O(mampa)]^{-}$, $[Cr^{V}O(ehba)_2]^{-}$, $[Cr^{V}(O)_2(phen)_2]^{+}$, $[Cr^{V}O(salen)]^{+}$, $[Cr^{V}_2(O)_2(\mu\text{-}O)_2(ala)_2(OCH_3)_2]^{2-}$, $[Cr^{V}O(OCH_3)(ala_3)]^{-}$, and Cr(V)-triglycine complexes are also genotoxic in cellular systems.[36-38,41] The $[Cr^{V}O(mampa)]^{-}$ and $[Cr^{V}O(ehba)_2]^{-}$ complexes are more toxic than dichromate when the level of cellular uptake is taken into account.[36] These results are consistent with the Cr(V) complexes being directly involved in DNA damage.

There is evidence that Cr(V) complexes can bind to the phosphate groups of DNA and then oxidatively cleave the DNA.[39,40,156-158] The reactions of Cr(V) complexes with smaller phosphate-containing molecules lend support to this mechanism. The $[Cr^{V}O(ehba)_2]^{-}$ complex oxidises thymidine nucleotides but not the nucleosides.[159] Chromium(V) complexes have also been observed to bind phosphate and pyrophosphate ligands.[160] EPR and ^{31}P NMR studies of the interaction of Cr(V) with nucleotides indicated that the Cr(V) bound to hydroxyl groups of the sugars and the phosphate groups.[161]

The cleavage of DNA by some Cr(V) species occurs under anaerobic conditions,[39,40,113,154-156] which shows that reactive oxygen species derived from O_2 are not necessary for DNA strand breaks to occur. This is further evidence that Cr(V) complexes can cause DNA damage directly. That is only one part of the story, however, since it has also been shown that the presence of O_2 increases the level of DNA strand breaks caused by Cr(V).[78,113,116,122,154,156,162,163] *In vitro* studies of DNA damage by Cr(VI) in the presence of biological reductants have also shown that DNA strand breaks occur both in the absence of O_2[78,113] and by O_2-dependent mechanisms.[78,113,116,122]

One explanation for the observed O_2 dependence of DNA damage is that Cr(V)-peroxo and/or Cr(IV)-peroxo complexes are involved in DNA

damage.[78,105,107,112,164] The presence of O_2 in the Cr(VI)/ascorbate system increased the levels of DNA damage.[78,113] The amount of DNA damage (at a given concentration of Cr(VI)) depends on the Cr(VI):ascorbate ratio. The damage to DNA increases with increasing ascorbate concentration to a maximum when the ratio is 1:1, then decreases as the ascorbate concentration is increased further.[78,109] The Cr(VI):ascorbate ratio at which maximum DNA damage occurs, 1:1, was the ratio at which the maximum amount of a Cr(V)-ascorbate-peroxo complex was generated when O_2 was present.[105,112]

Another explanation for the observed O_2 dependence is that it is converted into reactive oxygen species, such as singlet oxygen, superoxide and hydrogen peroxide.[162,165,166] A large number of reports have suggested that hydroxyl radicals are the ultimate DNA damaging species in chromium-induced cancer,[110,136,165,167-175] but this indirect evidence has been criticised.[85,111,115,116,122,154,155,166,176]

Addition of H_2O_2 to Cr(V)-DNA systems increases the level of DNA strand breaks.[136,154,157,163] Chromium(V) complexes are postulated by some groups to react *via* a Fenton-like reaction with H_2O_2 (Equation 1.9) to generate hydroxyl radicals.[136,154,165,169,172]

$$Cr(V) + H_2O_2 \rightarrow Cr(VI) + OH^{\bullet} + OH^{-} \qquad (1.9)$$

These methods of detection of hydroxyl radical are indirect and have been shown to be in error in the case of $[Cr^{V}O(ehba)_2]^{-}$. This complex oxidises spin traps commonly used to detect hydroxyl radicals directly, without generation of hydroxyl radicals.[177] It also reacts directly with the oxidant sensitive dyes, 2′,7′-dichlorofluorescin and dihydrorhodamine, and causes them to fluoresce without first forming a diffusible radical species. The fluorescence of these dyes observed in chromate-treated A549 cells was due to intracellular Cr(V), not reactive oxygen species.[178] $[Cr^{V}O(ehba)_2]^{-}$ also undergoes intramolecular reduction to Cr(III) when it reacts with H_2O_2 without production of such radicals.[179]

Chromium(III) complexes have also been postulated to generate hydroxyl radicals when reacted with H_2O_2[168,171,172,174,180,181] and cause DNA strand breaks in the presence of added H_2O_2.[168,180-183] The DNA cleavage has been attributed to hydroxyl radicals generated by the Haber-Weiss cycle[171] (Equations 1.10 and 1.11) and a Fenton-like reaction[168,174] (Equation 1.12). Not all Cr(III) complexes produce significant levels of DNA cleavage when H_2O_2 is added.[82]

$$Cr(III) + O_2^{\bullet-} \rightarrow Cr(II) + O_2 \quad (1.10)$$

$$Cr(II) + H_2O_2 \rightarrow Cr(III)\ {}^{\bullet}OH + OH^- \quad (1.11)$$

$$Cr(III) + H_2O_2 \rightarrow Cr(IV)\ {}^{\bullet}OH + OH^- \quad (1.12)$$

The presence of hydroxyl radicals in Cr redox chemistry, and hence their relevance to Cr-induced DNA damage, has been hotly debated. The postulated mechanisms for hydroxyl radical generation involve the reaction of H_2O_2 with Cr complexes. The indirect experimental evidence for the involvement of hydroxyl radicals has come primarily from experiments where H_2O_2 was added in concentrations from 10^{-4} – 6×10^{-3} M.[136,154,168,174,180-183] The level of H_2O_2 in cells is of the order 10^{-7} – 10^{-9} M.[166] The low natural level of H_2O_2 in cells means that even if hydroxyl radicals were produced in the reaction of H_2O_2 with Cr (which is unlikely) they are probably not a significant contributor for DNA damage *in vivo*. The possibility that large amounts of H_2O_2 could be produced by the reaction of O_2 with Cr complexes should also be taken into consideration. However, when Cr(VI), Cr(V) or Cr(IV) complexes were reacted with cysteine, GSH or ascorbate in the presence of O_2, the amount of H_2O_2 produced was very low.[111] Somewhat more peroxide is produced in the reaction of Cr(VI) with biologically important catechols, but here again the major DNA damaging species *in vitro* are Cr(V)-peroxo species.[163]

Studies by Casadevall and Kortenkamp *et al.*,[115,116,122] have demonstrated that DNA damage caused by the Cr(VI)/GSH system is not consistent with attack by hydroxyl radicals. Similarly, there is evidence that DNA damage observed in the Cr(VI)/ascorbate system,[78,115] with $[Cr^{V}O(ehba)_2]^-$,[155] and with Cr(V)-catechol complexes,[163] is not due to hydroxyl radicals.

Another explanation for the O_2 dependence of the *in vitro* DNA damage is that the O_2 is involved in reactions with thiyl radicals or carbon-based radicals and cations that are products from the oxidation of organic molecules by high-valent Cr compounds.[111,156] The main cause of the O_2 dependence is the reaction of O_2 with DNA radicals,[111,158] which facilitates oxidative damage and has nothing to do with hydroxyl radicals, though organic peracids may contribute.[111] Carbocations and carbon-based radicals are formed by hydride or hydrogen atom abstraction from the deoxyribose moiety of DNA by oxidising agents. These oxidised products of deoxyribose have several decomposition pathways, some of which involve reaction with O_2.[184-186]

There is strong evidence that Cr(III) complexes are not capable of directly cleaving DNA. The final Cr(III) products from Cr(VI) reduction with biological reductants do not cleave DNA[60,80,121,181] and isolated Cr(III) complexes with various ligands do not cleave DNA.[168,187,188]

Most of the work performed on the cleavage of DNA by Cr(IV) species has relied on indirect evidence, usually an inhibitory affect of Mn(II), to detect the involvement of Cr(IV).[159,189] This work has been shown to be in error by Levina, Lay and Dixon[158] and Zhang and Lay.[112] The concentration of Mn(II) necessary to suppress DNA strand breaks caused by $[Cr^{V}O(ehba)_2]^-$ was ten times greater than the concentration of Mn(II) necessary to suppress the formation of Cr(IV) intermediates.[158] Also, Mn(II) reacts with the Cr(V) intermediates formed in the reduction of Cr(VI) by ascorbate, and the most efficient reaction is with the mixed ligand Cr(V)-ascorbate-peroxo complexes that are the most damaging to DNA.[112] However, a characterised Cr(IV)-quinic acid complex has been shown to cause DNA strand breaks,[156] and Cr(IV) generated by the V(IV) reduction of Cr(V) increased the number of DNA strand breaks.[190] Direct evidence for the involvement of Cr(IV) in DNA cleavage is quite limited because Cr(IV) complexes are so reactive and short lived.[158]

Chromium-DNA Adducts

Several types of DNA adducts are formed when Cr(VI) is reduced in the presence of DNA. Chromium can form DNA interstrand crosslinks[129,150,151,191,192] and DNA-protein crosslinks,[123,149-151,193,194] as well as monofunctional adducts where the Cr is

also coordinated to small ligands such as GSH or amino acids.[125,128,129,148,187,195] Chromium-DNA adducts have been observed *in vitro* with isolated DNA,[38,128,187] in DNA isolated from cells exposed to Cr(VI),[123,150,193-196] and in DNA isolated from the tissues of animals exposed to Cr(VI).[148,149,151]

The chelating agent 1,2-ethanediamine-*N,N,N′,N′*-tetraacetate (edta) removes DNA adducts caused by Cr(VI).[125,194,196] This shows that some of the DNA interstrand crosslinks and crosslinks to proteins and smaller biomolecules are mediated by Cr(III). Chromium(III) chelation is not the only crosslinking mechanism; oxidative DNA-protein crosslinks that could not be removed by treatment with edta or thiols have also been observed.[194]

The incubation of Cr(III) chloride,[191,192,197,198] Cr(III)-amino acid complexes,[128,187,197] Cr(III)-GSH complexes,[187,197] and Cr(III)-ascorbate complexes[199] with DNA produced Cr-DNA adducts. This led Zhitkovich *et al.* to argue that it is the final Cr(III) products that bind to DNA when Cr(VI) is reduced inside cells.[128] The ability of Cr(III) to bind to DNA depends on the ligands coordinated to it. Chromium(III) complexes with amino acid, peptide, and ascorbate ligands showed much lower levels of DNA binding than $[Cr(H_2O)_4Cl_2]^+$ and $[Cr(H_2O)_6]^{3+}$.[197,199] Some Cr(III)-amino acid complexes did not bind to isolated DNA at all.[197] Chromium(V) peptide complexes react with isolated DNA, causing the precipitation of Cr-DNA complexes.[38] Chromium-DNA adducts may also form through the binding of reactive Cr intermediates to DNA, which are then reduced to Cr(III).[82,84,125]

Chromium(III)-amino acid or Cr(III)-GSH complexes bind to DNA *via* the phosphate group.[187] Binding of Cr complexes to nucleotides is also *via* the phosphate group,[79,128] which is further evidence for phosphate as the binding site on DNA. The identification of the phosphate group as the site where Cr is bound to DNA in Cr-DNA adducts does not distinguish between the two proposed mechanisms for the formation of the adducts; as Cr(V) complexes also bind to phosphate groups.[39,40]

The two mechanisms outlined above for the formation of Cr-DNA adducts, which are mediated by Cr(III), probably both occur in biological systems. Chromium(V)

and Cr(IV) complexes are very labile and capable of binding to DNA. Chromium(III) complexes are generally inert, but their reactivity depends on the nature of the ligands coordinated, and biological systems contain a wide variety of molecules that can bind to Cr(III). As has been shown by the reactions with amino acids and GSH ligated Cr(III), some of these complexes with biological ligands are reactive enough to bind to DNA. The Cr-DNA adducts are mutagenic in human cells, and may play a role in Cr-induced carcinogenesis.[148,187,191]

Interference with DNA Transcription

Chromium-DNA adducts cause the arrest of mammalian DNA polymerases during DNA replication.[192] Exposure to Cr(VI) *in vivo*[200,201] and *in vitro*[202-204] affected the level of gene expression. These changes to DNA transcription were correlated with the levels of DNA crosslinks and Cr-DNA adducts.[200-202] The expression of the oncogene cyclin D1 was significantly elevated in lung tumours of ex-chromate workers compared to lung tumours in non-exposed individuals.[205]

The formation of DNA lesions is not the only explanation that has been postulated for the effect of Cr on DNA trancription. Shumilla *et al.* reported that the inhibition of the transcriptional activity of nuclear factor-κB by Cr(VI) was due to Cr interactions with coactivators of transcription rather than DNA binding[203] Chromate, $[Cr^{V}O(ehba)_2]^-$ and $[Cr^{IV}O(qa)(qaH)\ ]^-$ caused oxidative damage to a model complex for the Zn binding site in Zn-finger protein;[206] similar reactions occur with Zn-finger transcription factors which changes their binding to DNA.[207]

1.3 Nickel-induced Carcinogenesis

The bulk of the epidemiological evidence for the carcinogenicity of Ni and its compounds in humans come from studies on the mortality rates of workers in Ni refineries. These studies demonstrated an increased risk of lung cancer by a factor of 5-10, and an increased risk of nasal cancer by a factor of more than 100.[46,208-210]

A study of Swedish battery workers exposed to Cd and Ni showed an increased risk of lung cancer and a highly significant increased risk of cancer of the nose and nasal sinuses.[211] Stainless-steel welders have a higher risk of lung cancer than mild steel

welders using the same techniques. This risk is thought to be due to exposure to Cr(VI) and Ni in stainless steel welding, but current epidemiological data do not indicate which of these is the more important risk factor.[212]

Crystalline Ni sulfides, Ni hydroxides, Ni oxides and metallic Ni induce tumours in animals exposed to them by various routes, including inhalation and intramuscular injections.[46,213-217] Nickel(II) compounds are not usually mutagenic in bacterial assays, though they are mutagenic in some mammalian cell assays.[218-221]

1.3.1 Nickel Use in Industry

Nickel is a common carcinogen used in industry, second only to Cr in terms of the number of workers exposed, and accounts for 20% of industrial exposures to carcinogens reported in a Finnish study.[63]

Nickel is produced from sulfidic and silicate-oxide ores, nickel sulfides and nickel oxides are produced from the ores and refined to Ni metal and salts. Crude Ni is purified by the Mond process, with $[Ni(CO)_4]$ as the intermediate, which itself is highly toxic and possibly carcinogenic. This method has been mostly superseded by electrolytic methods of purification because of the hazard. The main use of Ni is in the production of stainless and other alloy steels, other alloys, and electroplating; small amounts are used in catalysts, batteries, ceramics, magnets and salts.[46]

1.3.2 Fundamental Chemistry of Ni

Nickel compounds exist in Ni oxidation states ranging from –I to IV. Nickel(II) is by far the most common oxidation state and a huge array of compounds containing this oxidation state are known. The complexes of the lower oxidation states usually involve ligands that are strong π-acids. Of the lower oxidation states Ni(0) has the largest number of compounds, while the Ni(–I) and Ni(I) oxidation states are less common.[65] The Ni(III) and Ni(IV) oxidation states are relatively rare; complexes of these are generally very reactive and capable of oxidising some organic and inorganic substrates.[222]

Many Ni(II) salts are insoluble in water, common exceptions being: Ni(II) chloride, Ni(II) acetate, Ni(II) nitrate and Ni(II) sulfate. Nickel forms several different compounds with sulfur: Ni disulfide (NiS_2); three forms of Ni sulfide (NiS), two crystalline forms and an amorphous form; and Ni subsulfide (Ni_2S_3). The Ni oxides also vary in their composition depending on the temperature of formation, such that the content of Ni(III) varies from <0.03-0.81%, and range in colour from black to light green.[46]

1.3.3 Cellular Uptake of Ni

The main mechanism by which Ni enters mammalian cells is through the phagocytosis of crystalline particles of insoluble Ni compounds. Crystalline insoluble particles are actively phagocytised, but insoluble particles of amorphous nickel sulfide are not.[214,219,223-225] The phagocytosis of particles depends on their zeta potential, particles with a negative surface charge are phagocytised, neutral particles are not. Crystalline Ni compounds have a negative surface charge, while amorphous Ni sulfide is uncharged.[214,219]

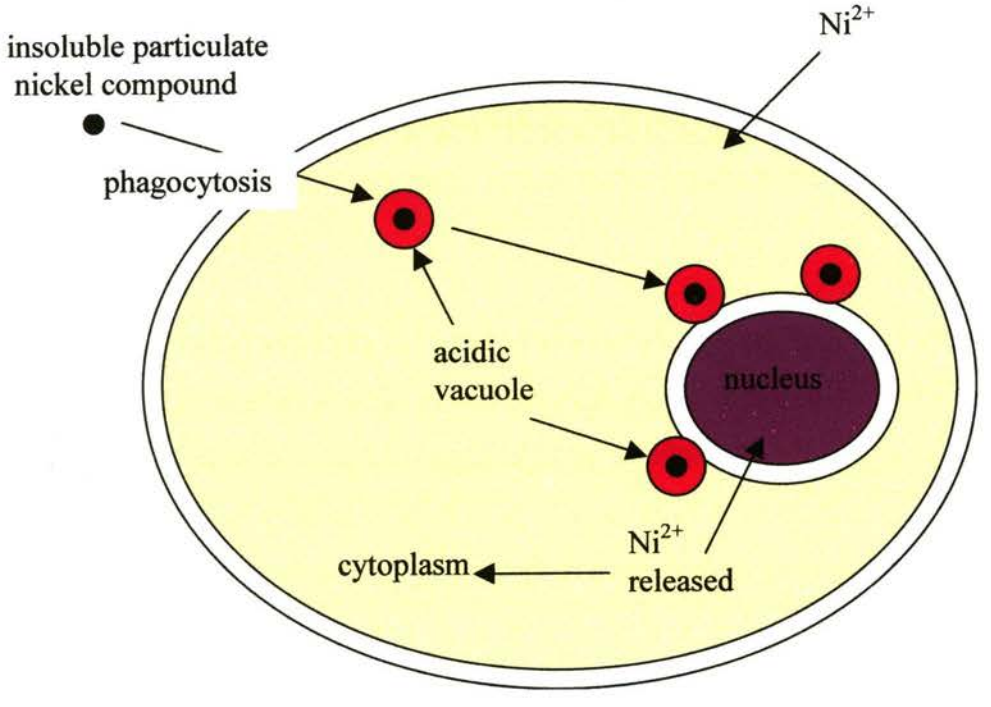

Figure 1.4 Mechanisms of the cellular uptake of nickel compounds

Treatment of amorphous Ni subsulfide with $LiAlH_4$ gave the particles a negative surface charge by attaching hydride ions to the surface and they were then phagocytised.[219] Once the insoluble particles are taken inside the cell they are surrounded by acidic vacuoles. These acidic vacuoles tend to cluster around the nucleus and can release Ni(II) ions as they dissolve the particles.[214,219,226]

Aqueous Ni(II) ions can enter mammalian cells, but they are not taken up as readily as the crystalline insoluble Ni compounds and the intracellular levels of Ni that result are lower.[220] The presence of soluble Ni(II) complexes can reduce phagocytosis.[219] The uptake of Ni from soluble Ni compounds by mammalian cells has been shown to occur by several studies,[227-232] however, the mechanism of uptake is not well understood. A study by Refsvik and Andreassen indicated that the Ni(II) ions entered human kidney epithelial cells via the Ca^{2+} channels in the cell membrane,[231] but there has also been a report that Ni(II) ions block the Ca^{2+} channels in rat melanotroph cells and do not penetrate into the cells.[233] It is likely the opposite effects observed are due to physiological differences between human kidney and rat melanotroph cells, but the reasons are not known.

1.3.4 *In vivo* Effects of Ni

Rats that received subcutaneous injections of Ni(II) chloride had elevated levels of DNA strand breaks in the lung cells,[234] DNA strand breaks and chromosome aberrations in liver cells.[235]

After interperitoneal injection of Ni(II) carbonate into rats, Ni was bound to whole chromatin, DNA + histone octamer and purified deproteinised DNA from the kidney and liver. Higher levels of Ni were present in the kidney than the liver.[236] DNA strand breaks, DNA-protein crosslinks and DNA-interstrand crosslinks were observed in kidney nuclei, and DNA strand breaks in lung nuclei.[237]

Increased amounts of oxidised DNA bases were detected in the chromatin extracted from the livers and kidneys of pregnant rats and their foetuses 24-48 hr after injections of Ni(II) acetate.[238] Chromatin from the liver and kidney of rats was monitored for oxidised DNA bases for up to 14 days after the injection of Ni(II)

acetate. In the liver, elevated amounts of five oxidised base products were detected on day 1, all except one returned to normal after 14 days. In kidneys, three oxidised bases increased significantly and one increased to just below the level of significance; the increased levels persisted for the 14 days. The faster DNA repair in rat livers may explain why rat kidneys, but not livers, are susceptible to Ni-induced carcinogenesis.[239]

1.3.5 Effects of Ni in Cultured Cells

Since Ni compounds are generally not mutagenic in bacterial cell assays, but are mutagenic in some mammalian cell assays, extensive studies have been carried out on the effect of Ni compounds on cultured mammalian cells.

Nickel subsulfide was mutagenic in a transgenic rodent fibroblast cell line.[240] Mutagenicity has also been observed in human cell lines: Ni(II) chloride was mutagenic in a human fibroblast cell line,[218] and exposure of an osteoblast-like immortal non-tumourigenic human cell line to Ni(II) sulfate transformed the cells into tumourigenic cell lines.[241] Nickel(II) sulfate also caused microsatellite mutations in three human lung tumour cell lines.[242]

Heterochromatic regions of chromosomes have been found to be particularly sensitive to Ni-induced damage. Exposure of Chinese hamster cells to Ni compounds caused a partial or complete deletion of the heterochromatic long arm of the X chromosome and immortalised the cells.[243-245] When a normal Chinese hamster X chromosome was transferred to the transformed cells, they senesced.[244] Deletion of the heterochromatic long arm of the X chromosome was the only karyotypic aberration in 80% of Ni-transformed CHE cells.[246] Chinese hamster ovary (CHO) cells treated with crystalline Ni sulfide and Ni(II) chloride had chromosome aberrations including gaps, breaks and exchanges. Nickel(II) chloride caused preferential damage to the heterochromatic centromere regions of chromosomes; crystalline nickel sulfide caused the selective fragmentation of the heterochromatic long arm of the X chromosome.[229] Chinese hamster cell lines exposed to Ni subsulfide and Ni(II) chloride initially showed decreased levels of

DNA methylation, but after three weeks the levels were significantly higher than the controls.[247]

A transgenic Chinese hamster cell line displayed Ni-induced inactivation of a gene without mutagenesis or deletion of the *gpt* transgene. Condensation of chromatin and heterochromatinisation occurred about the transgene site. Increased DNA methylation was also observed.[248]

Nickel(II) chloride and crystalline Ni sulfide caused DNA strand breaks in CHO cells while amorphous Ni sulfide did not.[227] Nickel subsulfide also induced DNA fragmentation in isolated mouse lung and nasal mucosa cells.[240] DNA strand breaks and increased levels of the DNA repair enzyme, poly(ADP-ribose) polymerase, were induced in human lung fibroblast cells by Ni subsulfide.[249] Nickel(II)-induced DNA strand breaks in human HeLa cells and partially inhibited the repair of DNA damage caused by visible light.[250] Nickel(II) sulfate and Ni subsulfide increased DNA-protein crosslinks when they were incubated with rat renal cortical cells, but Ni subsulfide was much more potent.[228] After exposure of CHO cells to nickel(II) chloride, the crosslinking of amino acids to DNA was observed; though the crosslinking was not directly mediated by Ni.[243] Nickel subsulfide increased micronuclei in BALB/3T3 cells and increased DNA-protein crosslinks in CHO cells.[251]

Some studies have also shown an increase in the levels of reactive oxygen species (ROS) in cells exposed to Ni compounds. Nickel subsulfide and Ni disulfide increased the production of hydrogen peroxide in human polymorphonuclear leukocytes; superoxide was also present in cells treated with Ni sulfide but not Ni subsulfide.[252] CHO cells treated with Ni sulfide, Ni oxide, Ni subsulfide and Ni(II) chloride had higher levels of ROS.[253]

1.3.6 Mechanisms of Ni-Induced Carcinogenesis

Nickel(II) has a higher affinity for amino acids and proteins than it does for DNA[214] so it will preferentially react with the heterochromatic regions of DNA.[246,248] The

sensitivity of the heterochromatic regions of chromosomes to Ni-induced damage is likely to play a role in nickel-induced carcinogenesis.[246,248]

The Ni-induced deletion of the heterochromatic long arm of the X chromosome in cultured Chinese hamster cells is an example of the extensive damage that can occur. The loss of the long arm of the X chromosome in these cells immortalised them. This immortalisation has been attributed to the loss of an X chromosome linked senescence gene.[244,245] Damage to, or loss of, senescence and anti-tumour genes that reside in or near heterochromatic regions of DNA is likely to be involved in Ni-induced carcinogenesis.

Nickel(II) does not just caused deletions of heterochromatic regions of DNA; there is also a proposed mechanism by which genes can be inactivated while still present. Nickel(II) binds to the histone proteins in heterochromatic regions of DNA causing increased DNA condensation in the nearby regions. The increased DNA condensation is stabilised by methylation of the DNA. Any senescence or tumour suppressor gene that becomes part of the newly condensed region of DNA would be inactivated, and this inactivation would be passed on to daughter cells, because methylation patterns are generally heritable.[226,248]

There are other types of DNA damage that have been observed in cell culture and *in vivo* studies: including DNA strand breaks, oxidised DNA bases, DNA-interstrand crosslinks and DNA-protein crosslinks. *In vitro* studies indicate that Ni-protein complexes may be involved in these forms of DNA damage.

Nickel(II) has been shown to bind at the amine terminal metal-binding site of serum albumin *via* the amine.[254,255] A large number of Ni(II)-peptide complexes containing tripeptide moieties modelled on the amine-terminal metal-binding site of serum albumin have been prepared, and their ability to cause DNA strand breaks studied. When these complexes are reacted with DNA in the presence of an oxidant (such as monoperoxyphthalic acid, monoperoxysulfate or sulfite plus oxygen) DNA strand breaks[42-44,256-262] and DNA-protein crosslinks[263] occur. Oxidative damage to guanine bases has also been detected.[264] High-valent Ni(III) or Ni(IV) complexes have been proposed as the intermediates that cause the DNA damage[42-44,259,263,264] and there is

evidence that reactive oxygen species such as hydrogen peroxide, superoxide and hydroxyl radicals are not directly involved in the DNA cleavage.[42,263]

The DNA cleavage is sequence-selective[43,44,256,258,260,261] and the selectivity changes as the amino acids in the Ni-binding tripeptide are varied.[44] The products of DNA cleavage by these metallopeptides are indicative of C4' H-atom abstraction.[44] Site-specific DNA cleavage has also been observed when the tripeptide Ni-binding moiety glyglyhis has also been added to the amine-terminal ends of DNA binding proteins and oxidants added.[260,261] Long *et al.* have proposed the following mechanism of DNA cleavage: the Ni(II)-tripeptide complex binds to the minor groove of DNA, it is activated by the oxidising agent to a Ni(III) or Ni(IV) species that reacts with DNA by a C4′ H-atom abstraction.[42,44]

The Ni(II) tripeptide complexes also undergo autoxidation of the ligand when exposed to oxidants. They ultimately lose the free carboxylate group after proceeding through several reactive intermediates. These peptide complexes also exhibit covalent binding to form DNA adducts, with guanine bases the preferred site binding site.[265]

Other Ni complexes also interact with DNA. Nickel(II) chloride, some macrocyclic Ni(II) complexes and Ni(III)-cyclam cause the conversion of B-DNA to Z-DNA. The change in DNA conformation is due to direct interaction of the Ni complexes with DNA, not just an electrostatic influence.[266] Nickel(II) salen complexes undergo ligand-centred oxidations when exposed to oxidants. DNA traps the ligand-centred radical, giving covalent DNA-complex adducts. The adducts on DNA formed almost exclusively at the guanine bases.[265] The bleomycin complex of Ni(II) can be oxidised by oxone or Ir(IV) to the Ni(III) bleomycin complex. This Ni(III) complex binds to DNA and selectively cleaves it at guanine bases. There is EPR evidence of the Ni(III) binding to guanine N-7.[267]

A Ni(II) macrocycle complex was found to cause DNA cleavage when the oxidants monoperoxysulfate or sulfite plus O_2 were present.[264,268] The postulated mechanism of DNA cleavage involved Ni(III) and sulfate radicals.[264,268]

The oxidation of Ni(II) complexes has been shown to cause DNA damage, especially DNA strand breaks. Even O_2 is capable of reacting with some Ni(II) complexes and generating reactive species.[262]

Nickel(II) complexes with tripeptide and tetrapeptide ligands that had free carboxylate termini reacted with O_2 in the air, oxidising the ligand, ultimately causing the loss of the free carboxylate group.[262,269] Peptides with carboxamide C-termini were stable on exposure to air.[262] Of relevance to the genotoxicity, Ni(III), carbon-centred ligand radicals and peroxy ligands have been postulated as intermediates in the proposed mechanism of decarboxylation. The complexes that reacted with O_2 caused DNA strand breaks, whereas complexes with carboxamide C-termini did not damage DNA in the presence of O_2 alone.[262]

There have been several other reports of Ni(II) complexes with oligopeptide ligands reacting with O_2 and undergoing ligand oxidation.[270-272] Proposed intermediates in the reaction are a complex with O_2 bound to Ni(II)[270] and Ni(III) complexes.[271,272] Nickel(II) complexes with tetrahydrosalen and an analogue of dihydrosalen as ligands react with O_2 and undergo an oxidative dehydrogenation of the amine groups.[273-275]

Nickel(II) complexes of diamidetriamine macrocycles bind oxygen.[22,276-278] With some of the ligands, the binding of O_2 was partially reversible.[22,277] The binding of O_2 leads to a Ni(III)-superoxo species.[276-278] A stable Ni(III) complex with one macrocyclic ligand was produced by electrochemical or aerial oxidation of the Ni(II) complex. The Ni(III) complex was crystallised and the crystal structure solved. The sixth coordination site was occupied by a water molecule.[23]

1.4 Chromium and Nickel Complexes with Peptide Ligands

1.4.1 Chromium(III) Complexes

The most common coordination geometry of Cr(III) complexes is octahedral; and this geometry has been reported for a wide variety of complexes with peptide

ligands.[38,279-282] Peptides coordinate to Cr(III) *via* amine N, deprotonated amide N and carboxylate O atoms.[38,279-282] Coordination of the side chains from amino acids such as histidine[280] and the S of cysteine,[125]can also occur when these residues are present in the peptide.

Non-peptide ligands with amide groups coordinated to Cr(III) also have octahedral geometry.[283-285] Coordination to the Cr in these complexes was *via* deprotonated amide N[283-285] and amide O[283,284] atoms.

1.4.2 Chromium(V) Complexes

Chromium(V) is a powerful oxidant, reacting with many organic substrates, so it is not surprising that there are few reports of Cr(V) complexes with peptide ligands. A Cr(V) complex was isolated from the reaction of chromate with glutathione (GSH), and described as $Na_4Cr(GSH)_4.8H_2O$. Coordination of carboxylate and thiolate groups to the Cr was postulated on the basis of spectroscopic evidence but the complex was not structurally characterised.[118] The Cr(V) complexes with the oligopeptides trialanine, tetraalanine, pentaalanine, triglycine, tetraglycine and pentaglycine were predicted to be six-coordinate in solution on the basis of EPR spectroscopy. The coodination of the peptides to the Cr was *via* amine N, deprotonated amide N and carboxylate O atoms.[38]

A small number of Cr(V) complexes with non-peptide amide ligands are also known. Two Cr(V) complexes with macrocyclic tetraamide ligands are five-coordinate with a square-pyramidal geometry, the four deprotonated amide N atoms at the base of the pyramid and an oxo group at the apex.[26] These complexes were very stable, even in water. In the Cr(V) complex of *N,N´*-bis(2-pyridinecarboxamido)-1,2-benzene (bpb) the Cr was coordinated to two deprotonated amide N atoms and two pyridyl N atoms; the geometry was square pyramidal with the four N atoms from the ligand at the base and a nitrido group at the apex.[27]

1.4.3 Nickel(II) Complexes

The Ni(II) complexes of oligopeptide ligands have been studied

extensively.[2,269,286-288] Both four-coordinate square-planar[2,269,286,288] and six-coordinate octahedral[2,286,287] complexes are known. The peptides coordinate to Ni(II) *via* amine N, deprotonated amide N and carboxylate O atoms.[2,286-288] The greater the number of deprotonated amide N donor atoms, the more likely that the complex will have square-planar geometry. This is because the deprotonated amide N is a strong field ligand and stabilises the low-spin d^8 configuration, which is square-planar.

Nickel(II) complexes with non-peptide amide ligands have also been reported. Square-planar,[289-293] five-coordinate,[23,294,295] and octahedral[25] complexes with deprotonated amide N coordination are known. There is also an unusual case of octahedral Ni(II) coordinated to amide O atoms in a trinuclear complex.[293]

1.4.4 Nickel(III) Complexes

Nickel(III) complexes are not very stable and most of the knowledge of their structure comes from spectroscopic and electrochemical studies on solutions. In solution, Ni(III) complexes with peptide ligands usually have a tetragonally distorted octahedral coordination geometry.[8,19-21] The amide groups are coordinated *via* deprotonated amide N atoms.[8,19-21]

The tripeptide complex Ni(III)-(aib_3) is extremely stable, acidic solutions last for weeks to months. The Ni(III) complex with a non-peptide macrocyclic tetraamide has been crystallographically characterised.[17] The Ni is coordinated to four deprotonated amide N atoms in a distorted square-planar geometry. A pentadentate macrocycle with two deprotonated amide N atoms coordinated formed a tetragonally distorted octahedral complex with Ni(III).[23]

1.5 Thesis Outline

The highly reactive Cr(V) and Ni(III) oxidation states have been postulated to play a role in the mechanisms of Cr- and Ni-induced carcinogenesis. Thus, interactions of Cr and Ni with biomolecules that lead to the formation of these higher oxidation states are of considerable interest. The objective of this thesis is to examine the ability of deprotonated amide N-donor ligands to stabilise Cr(V) and Ni(III), as models for the interactions of Cr and Ni with proteins and peptides *in vivo*.

Chapter 2 contains the synthesis of the acyclic tetradentate diamide ligands used in this work and their characterisation. Chapter 3 deals with the preparation and characterisation of Ni(II) complexes with tetradentate diamide ligands. The $Ni^{III/II}$ reduction potentials of the complexes are reported and compared to the values obtained with Ni-peptide complexes. In Chapter 4, the synthesis of the Cr(III) complexes and their oxidation to the Cr(V) analogues are reported. Chromium(V) complexes were also formed by the reduction of Cr(VI) in the presence of the tetradentate diamide ligands. EPR spectroscopy was used to characterise the Cr(V) species formed and monitor their stability. The characterisation by X-ray absorption spectroscopy of Cr(III) and Cr(V) complexes with alanine, phen, and tetradentate diamide ligands is in Chapter 5. Chapter 6 contains the results of DNA cleavage assays with the Cr(V)-amide complex $[Cr^{V}O(S,S\text{-bprolben})]^{+}$ and discusses the biological implications of the work.

1.6 References

1) J. D. Roberts and M. C. Caserio *Basic Principles of Organic Chemistry*; W. A. Benjamin Inc.: New York, New York, **1964**.

2) H. Sigel and R. B. Martin *Chem. Rev.* **1982**, *82*, 385-426.

3) L. Pauling *The Nature of the Chemical Bond*; 3rd ed.; Cornell University Press: Ithaca, New York, **1960**.

4) O. Clement, B. M. Rapko and B. P. Hay *Coord. Chem. Rev.* **1998**, *170*, 203-243.

5) M. Mulqi, F. S. Stephens and R. S. Vagg *Inorg. Chim. Acta* **1982**, *62*, 215-220.

6) M. Mulqi, F. S. Stephens and R. S. Vagg *Inorg. Chim. Acta* **1982**, *62*, 221-229.

7) M. Mulqi, F. S. Stephens and R. S. Vagg *Inorg. Chim. Acta* **1982**, *63*, 197-207.

8) M. P. Youngblood and D. W. Margerum *Inorg. Chem.* **1980**, *19*, 3068-3072.

9) S. T. Kirksey Jr., T. A. Neubecker and D. W. Margerum *J. Am. Chem. Soc.* **1979**, *101*, 1631-1633.

10) J. S. Rybka, J. L. Kurtz, T. A. Neubecker and D. W. Margerum *Inorg. Chem.* **1980**, *19*, 2791-2796.

11) L. L. Diaddario, W. R. Robinson and D. W. Margerum *Inorg. Chem.* **1983**, *22*, 1021-1025.

12) T. A. Neubecker, S. T. Kirksey Jr., K. L. Chellappa and D. W. Margerum *Inorg. Chem.* **1979**, *18*, 444-448.

13) M. Kodama and E. Kimura *J. Chem. Soc., Dalton Trans.* **1981**, 694-700.

14) I. O. Fritsky, H. Kozlowski, P. J. Sadler, O. P. Yefetova, J. Świątek-Kozlowska, V. A. Kalibabchuk and T. Glowiak *J. Chem. Soc., Dalton Trans.* **1998**, 3269-3274.

15) J. Hanss, A. Beckmann and H.-J. Krüger *Eur. J. Inorg. Chem.* **1999**, 163-172.

16) F. P. Bossu and D. W. Margerum *Inorg. Chem.* **1977**, *16*, 1210-1214.

17) T. J. Collins, T. R. Nichols and E. S. Uffelman *J. Am. Chem. Soc.* **1991**, *113*, 4708-4709.

18) F. P. Bossu and D. W. Margerum *J. Am. Chem. Soc.* **1976**, *98*, 4003-4004.

19) C. K. Murray and D. W. Margerum *Inorg. Chem.* **1982**, *21*, 3501-3506.

20) S. A. Jacobs and D. W. Margerum *Inorg. Chem.* **1984**, *23*, 1195-1201.

21) A. G. Lappin, C. K. Murray and D. W. Margerum *Inorg. Chem.* **1978**, *17*, 1630-1634.

22) E. Kimura, A. Sakonaka and R. Machida *J. Am. Chem. Soc.* **1982**, *104*, 4255-4257.

23) R. Machida, E. Kimura and Y. Kushi *Inorg. Chem.* **1986**, *25*, 3461-3466.

24) A. Tripathi, R. K. Syal and P. K. Bharadwaj *Polyhedron* **1999**, *18*, 2229-2232.

25) A. K. Patra and R. Mukherjee *Inorg. Chem.* **1999**, *38*, 1388-1393.

26) T. J. Collins, C. Slebodnick and E. S. Uffelman *Inorg. Chem.* **1990**, *29*, 3433-3436.

27) C.-M. Che, J.-X. Ma, W.-T. Wong, T.-F. Lai and C.-K. Poon *Inorg. Chem.* **1988**, *27*, 2547-2548.

28) T. J. Collins, K. L. Kostka, E. Münck and E. S. Uffelman *J. Am. Chem. Soc.* **1990**, *112*, 5637-5639.

29) C. G. Miller, S. W. Gordon-Wylie, C. P. Horowitz, S. A. Strazisar, D. K. Peraino, G. R. Clark, S. T. Weitraub and T. J. Collins *J. Am. Chem. Soc.* **1998**, *120*, 11540-11541.

30) T. J. Collins and S. W. Gordon-Wylie *J. Am. Chem. Soc.* **1989**, *111*, 4511-4513.

31) T. J. Collins, R. D. Powell, C. Slebodnick and E. S. Uffelman *J. Am. Chem. Soc.* **1990**, *112*, 899-901.

32) C. R. Cornman, E. P. Zovinka, Y. D. Boyajian, K. M. Geiser-Bush, P. D. Boyle and P. Singh *Inorg. Chem.* **1995**, *34*, 4213-4219.

33) A. J. Tasiopoulos, Y. G. Deligiannakis, J. D. Woollins, A. M. Z. Slawin and T. A. Kabanos *J. Chem. Soc., Chem. Commun.* **1998**, 569-570.

34) A. D. Keramidas, A. B. Papaioannou, A. Vlahos, T. A. Kabanos, G. Bonas, A. Makriyannis, C. P. Rapropoulou and A. Terzis *Inorg. Chem.* **1996**, *35*, 357-367.

35) F. W. B. Einstein, R. J. Batchelor, S. J. Angus-Dunne and A. S. Tracey *Inorg. Chem.* **1996**, *35*, 1680-1684.

36) C. T. Dillon, P. A. Lay, A. M. Bonin, M. Cholewa, G. J. F. Legge, T. J. Collins and K. L. Kostka *Chem. Res. Toxicol.* **1998**, *11*, 119-129.

37) C. T. Dillon, P. A. Lay, A. M. Bonin, M. Cholewa and G. J. F. Legge *Chem. Res. Toxicol.* **2000**, *13*, 742-748.

38) H. A. Headlam; PhD Thesis, The University of Sydney, 1998.

39) R. N. Bose, B. S. Fonkeng, S. Moghaddas and D. Stroup *Nucleic Acids Res.* **1998**, *26*, 1588-1596.

40) R. N. Bose and B. S. Fonkeng *J. Chem. Soc., Chem. Commun.* **1996**, 2211-2212.

41) C. T. Dillon, P. A. Lay, A. M. Bonin, N. E. Dixon, T. J. Collins and K. L. Kostka *Carcinogenesis* **1993**, *14*, 1875-1880.

42) Q. Liang, D. C. Ananias and E. C. Long *J. Am. Chem. Soc.* **1998**, *120*, 248-257.

43) D. P. Mack and P. B. Dervan *J. Am. Chem. Soc.* **1990**, *112*, 4604-4606.

44) E. C. Long *Acc. Chem. Res.* **1999**, *32*, 827-836.

45) D. Newman *Glas. Med. J.* **1890**, *33*, 469-470.

46) IARC *Chromium, Nickel and Welding*; World Health Organisation: Lyon, **1990**, Vol. 49.

47) W. Machle and F. Gregorius *Public Health Rep.* **1948**, *63*, 1114-1127.

48) H. P. Brinton, E. S. Frasier and A. L. Koven *Public Health Rep.* **1952**, *67*, 835-847.

49) M. R. Alderson, N. S. Rattan and L. Bidstrup *Br. J. Ind. Med.* **1981**, *38*, 117-124.

50) M. D. Cohen, B. Kargacin, C. B. Kline and M. Costa *Crit. Rev. Toxicol.* **1993**, *23*, 255-281.

51) M. Costa *Crit. Rev. Toxicol.* **1997**, *27*, 431-442.

52) A. Leonard and R. R. Lauwerys *Mutat. Res.* **1980**, *76*, 227-239.

53) T. Sorahan, D. C. L. Burges, L. Hamilton and J. M. Harrington *Occup. Environ. Med.* **1998**, *55*, 236-242.

54) S. Langård *Am. J. Ind. Med.* **1990**, *17*, 189-215.

55) D. Steinhoff, S. C. Gad, G. K. Hatfield and U. Mohr *Exp. Pathol.* **1986**, *30*, 129-141.

56) U. Glaser, D. Hochrainer, H. Klöppel and H. Oldiges *Toxicology* **1986**, *42*, 219-232.

57) C. Maltoni, L. Morisi and P. Chieco *Adv. Mod. Environ. Toxicol.* **1982**, *2*, 77-92.

58) L. S. Levy, P. A. Martin and P. L. Bidstrup *Br. J. Ind. Med.* **1986**, *43*, 243-256.

59) L. Cheng, S. Liu and K. Dixon *Environ. Health. Perspect.* **1998**, *106*, 1027-1032.

60) R. P. Farrell, R. J. Judd, P. A. Lay, N. E. Dixon, R. S. U. Baker and A. M. Bonin *Chem. Res. Toxicol.* **1989**, *2*, 227-229.

61) K. D. Sugden, R. J. Burris and S. J. Rogers *Mutat. Res.* **1990**, *244*, 239-244.

62) S. Itoh and H. Shimada *Mutat. Res.* **1998**, *412*, 63-67.

63) T. Kauppinen *The Finnish ASA Register*; Institute of Occupational Health, 1990.

64) L. F. Larkworthy, K. B. Nolan and P. O'Brien In *Comprehensive Coordination Chemistry*; G. Wilkinson, R. Gillard and J. A. McCleverty, Eds.; Pergamon Press: Oxford, **1987**, Vol. 3, pp 699-969.

65) F. A. Cotton and G. Wilkinson *Advanced Inorganic Chemistry*; Third ed.; Interscience: New York, **1972**.

66) N. E. Brasch, D. A. Buckingham, A. B. Evans and C. R. Clark *J. Am. Chem. Soc.* **1996**, *118*, 7969-7980.

67) V. G. Poulopoulou, E. Vrachnou, S. Koinis and D. Katakis *Polyhedron* **1997**, *16*, 521-524.

68) M. Krumpolc and J. Roček *J. Am. Chem. Soc.* **1979**, *101*, 3206-3209.

69) M. Krumpolc, B. G. DeBoer and J. Roček *J. Am. Chem. Soc.* **1978**, *100*, 145-153.

70) R. Codd, A. Levina, L. Zhang, T. W. Hambley and P. A. Lay *Inorg. Chem.* **2000**, *39*, 990-997.

71) K. Srinivasan and J. K. Kochi *Inorg. Chem.* **1985**, *24*, 4671-4679.

72) T. L. Siddall, N. Miyaura, J. C. Huffman and J. K. Kochi *J. Chem. Soc., Chem. Commun.* **1983**, 1185-1186.

73) M. Krumpolc and J. Roček *Inorg. Chem.* **1985**, *24*, 617-621.

74) M. C. Ghosh, E. Gelerinter and E. S. Gould *Inorg. Chem.* **1992**, *31*, 701-705.

75) E. S. Gould *Coord. Chem. Rev.* **1994**, *135/136*, 651-684.

76) M. J. Tsapakos and K. E. Wetterhahn *Chem.-Biol. Interact.* **1983**, *46*, 265-277.

77) M. Cieślak-Golonka *Polyhedron* **1995**, *15*, 3667-3689.

78) P. da Cruz Fresco and A. Kortenkamp *Carcinogenesis* **1994**, *15*, 1773-1778.

79) T. Wolf, R. Kasemann and H. Ottenwälder *Carcinogenesis* **1989**, *10*, 655-659.

80) M. Casadevall and A. Kortenkamp *Carcinogenesis* **1994**, *15*, 407-409.

81) K. W. Jennette *Environ. Health. Perspect.* **1981**, *40*, 233-252.

82) D. M. Stearns and K. E. Wetterhahn *NATO ASI Ser. 2* **1997**, *26*, 55-72.

83) P. H. Connett and K. E. Wetterhahn *Struct. Bond.* **1983**, *54*, 93-124.

84) A. Kortenkamp, M. Casadevall, P. D. C. Fresco and R. O. J. Shayer *NATO ASI Ser. 2* **1997**, *26*, 15-34.

85) R. Codd, C. T. Dillon, A. Levina and P. A. Lay *Coord. Chem. Rev.* **2001**, *in press*.

86) D. L. Lilien, J. L. Spivak and I. D. Goldman *J. Clin. Invest.* **1970**, *49*, 1551-1557.

87) C. J. Sanderson *Transplant.* **1976**, *21*, 526-529.

88) S. J. Gray and K. Sterling *J. Clin. Invest.* **1950**, *29*, 1604-1613.

89) S. Langård *Biol. Trace Element Res.* **1979**, *1*, 45-54.

90) D. M. Stearns, J. P. Wise Snr., S. R. Patierno and K. E. Wetterhahn *FASEB* **1995**, *9*, 1643-1649.

91) A. Kortenkamp, D. Beyersmann and P. O'Brien *Toxicol. Environ. Chem.* **1987**, *14*, 23-32.

92) P. C. Rajam and A.-L. Jackson *Proc. Soc. Exp. Biol. Med.* **1958**, *99*, 210-213.

93) B. Buttner and D. Beyersmann *Xenobiotica* **1985**, *15*, 735-741.

94) J. Singh, D. L. Carlisle, D. E. Pritchard and S. R. Patierno *Oncol. Rep.* **1998**, *5*, 1307-1318.

95) L. J. Blankenship, D. L. Carlisle, J. P. Wise Sr., J. M. Orenstein, L. E. Dye III and S. R. Patierno *Toxicol. Appl. Pharmacol.* **1997**, *146*, 270-280.

96) Z. Elias, O. Poirot, H. Perzat, H. Suquet, O. Schneider, M. C. Danière, F. Terzetti, F. Baruthio, M. Fournier and C. Cavelier *Carcinogenesis* **1989**, *10*, 2043-2052.

97) J. Singh, D. E. Pritchard, D. L. Carlisle, J. A. Mclean, A. Montaser, J. M. Orenstein and S. R. Patierno *Toxicol. Appl. Pharmacol.* **1999**, *161*, 240-248.

98) C. T. Dillon, P. A. Lay, M. Cholewa, G. J. F. Legge, A. M. Bonin, T. J. Collins, K. L. Kostka and G. Shea-McCarthy *Chem. Res. Toxicol.* **1997**, *10*, 533-535.

99) K. J. Liu, X. Shi, J. Jiang, F. Goda, N. Dalal and H. M. Swartz *Ann. Clin. Lab. Sci.* **1996**, *26*, 176-184.

100) K. J. Liu, X. Shi, J. J. Jiang, F. Goda, N. Dalal and H. M. Swartz *Arch. Biochem. Biophys.* **1995**, *323*, 33-39.

101) H. Sakurai, K. Takechi, H. Tsuboi and H. Yasui *J. Inorg. Biochem.* **1999**, *76*, 71-80.

102) P. O'Brien and N. Woodbridge *Polyhedron* **1997**, *16*, 2081-2086.

103) K. W. Jennette *Biol. Trace Element Res.* **1979**, *1*, 55-62.

104) A.-M. Dalla-Pozza; Honours Thesis, University of Sydney, 1996.

105) L. Zhang and P. A. Lay *J. Am. Chem. Soc.* **1996**, *118*, 12624-12637.

106) D. A. Dixon, N. P. Sadler and T. P. Dasgupta *J. Chem. Soc., Dalton Trans.* **1993**, 3489-3495.

107) Y. Lefebvre and H. Pézerat *Chem. Res. Toxicol.* **1992**, *5*, 461-463.

108) D. M. Stearns and K. E. Wetterhahn *Chem. Res. Toxicol.* **1994**, *7*, 219-230.

109) D. M. Stearns, L. J. Kennedy, K. D. Courtney, P. H. Giangrande, L. S. Phieffer and K. E. Wetterhahn *Biochemistry* **1995**, *34*, 910-919.

110) T.-C. Tsou, H.-J. Lai and J.-L. Yang *Chem. Res. Toxicol.* **1999**, *12*, 1002-1009.

111) P. A. Lay and A. Levina *J. Am. Chem. Soc.* **1998**, *120*, 6704-6714.

112) L. Zhang and P. A. Lay *Aust. J. Chem.* **2000**, *53*, 7-13.

113) P. da Cruz Fresco, F. Shacker and A. Kortenkamp *Chem. Res. Toxicol.* **1995**, *8*, 884-890.

114) A. Flores and J. M. Pérez *Toxicol. Appl. Pharmacol.* **1999**, *161*, 75-81.

115) M. Casadevall, P. da Cruz Fresco and A. Kortenkamp *Chem.-Biol. Interact.* **1999**, *123*, 117-132.

116) A. Kortenkamp, M. Casadevall, S. P. Faux, A. Jenner, R. O. J. Shayer, N. Woodbridge and P. O'Brien *Arch. Biochem. Biophys.* **1996**, *329*, 199-207.

117) G. Barr-David, M. Charara, R. Codd, R. P. Farrell, J. A. Irwin, P. A. Lay, R. Bramley, S. Brumby, J.-Y. Ji and G. R. Hanson *J. Chem. Soc., Faraday Trans.* **1995**, *91*, 1207-1216.

118) P. O'Brien, J. Pratt, F. J. Swanson, P. Thornton and G. Wang *Inorg. Chim. Acta* **1990**, *169*, 265-269.

119) S. Kitagawa, H. Seki, F. Kametani and H. Sakurai *Inorg. Chim. Acta* **1988**, *152*, 251-255.

120) J. Aiyar, K. M. Borges, R. A. Floyd and K. E. Wetterhahn *Toxicol. Environ. Chem.* **1989**, *22*, 135-148.

121) A. Kortenkamp, Z. Ozolins, D. Beyersmann and P. O'Brien *Mutat. Res.* **1989**, *216*, 19-26.

122) M. Casadevall and A. Kortenkamp *Carcinogenesis* **1995**, *16*, 805-809.

123) M. Capellmann, A. Mikalsen, M. Hindrum and J. Alexander *Carcinogenesis* **1995**, *16*, 1135-1139.

124) K. M. Borges and K. E. Wetterhahn *Chem. Res. Toxicol.* **1991**, *4*, 638-641.

125) K. M. Borges and K. E. Wetterhahn *Carcinogenesis* **1989**, *10*, 2165-2168.

126) P. O'Brien, G. Wang and P. B. Wyatt *Polyhedron* **1992**, *11*, 3211-3216.

127) P. A. Lay and A. Levina *Inorg. Chem.* **1996**, *35*, 7709-7717.

128) A. Zhitkovich, V. Voitkun and M. Costa *Biochemistry* **1996**, *35*, 7275-7282.

129) A. Zhitkovich, S. Shrager and J. Messer *Chem. Res. Toxicol.* **2000**, *13*, 1114-1124.

130) C. R. Myers and J. M. Myers *Carcinogenesis* **1998**, *19*, 1029-1038.

131) P. F. Pratt and C. R. Myers *Carcinogenesis* **1993**, *14*, 2051-2057.

132) J. E. Gruber and K. W. Jennette *Biochem. Biophys. Res. Commun.* **1978**, *82*, 700-706.

133) A. Mikalsen, J. Alexander and D. Ryberg *Chem.-Biol. Interact.* **1989**, *69*, 175-192.

134) J. D. Garcia and K. W. Jennette *J. Inorg. Biochem.* **1981**, *14*, 281-295.

135) A. Mikalsen, J. Alexander, H. Wallin, M. Ingelman-Sundberg and R. A. Andersen *Carcinogenesis* **1991**, *12*, 825-831.

136) M. J. Molyneux and M. J. Davies *Carcinogenesis* **1995**, *16*, 875-882.

137) K. W. Jennette *J. Am. Chem. Soc.* **1982**, *104*, 874-875.

138) M. Sugiyama, A. Ando and R. Ogura *Carcinogenesis* **1989**, *10*, 737-741.

139) M. Sugiyama, X. Lin and M. Costa *Mutat. Res.* **1991**, *260*, 19-23.

140) M. Sugiyama *Environ. Health. Perspect.* **1991**, *92*, 63-70.

141) M. Sugiyama *Environ. Health. Perspect.* **1994**, *102 Supplement 3*, 31-33.

142) J. P. Wise Sr., D. M. Stearns, K. E. Wetterhahn and S. R. Patierno *Carcinogenesis* **1994**, *15*, 2249-2254.

143) D. Chorvatovičová, E. Ginter, A. Košinová and Z. Zloch *Mutat. Res.* **1991**, *262*, 41-46.

144) M. Sugiyama, A. Ando, A. Furuno, N. B. Furlong, T. Hidaka and R. Ogura *Cancer Lett.* **1987**, *38*, 1-7.

145) S. Ueno, N. Susa, Y. Furukawa and M. Sugiyama *Toxicol. Appl. Pharmacol.* **1995**, *135*, 165-171.

146) M. B. Kadiiska, Q.-H. Xiang and R. P. Mason *Chem. Res. Toxicol.* **1994**, *7*, 800-805.

147) M. B. Kadiiska, J. D. Morrow, J. A. Awad, L. J. Roberts II and R. P. Mason *Chem. Res. Toxicol.* **1998**, *11*, 1516-1520.

148) A. Zhitkovich, V. Voitkun, T. Kluz and M. Costa *Environ. Health. Perspect.* **1998**, *106*, 969-974.

149) A. Izzotti, M. Bagnasco, A. Camoirano, M. Orlando and S. De Flora *Mutat. Res.* **1998**, *400*, 233-244.

150) M. J. Tsapakos, T. J. Hampton, P. R. Sinclair, J. F. Sinclair, W. J. Bement and K. E. Wetterhahn *Carcinogenesis* **1983**, *4*, 959-966.

151) J. W. Hamilton and K. E. Wetterhahn *Carcinogenesis* **1986**, *7*, 2085-2088.

152) H. A. Headlam and P. A. Lay *Inorg. Chem.* **2001**, *40*, 78-86.

153) S. Signorella, M. Santoro, C. Palopoli, C. Brondino, J. M. Salas-Peregrin, M. Quiroz and L. F. Sala *Polyhedron* **1998**, *17*, 2739-2749.

154) K. D. Sugden and K. E. Wetterhahn *Chem. Res. Toxicol.* **1997**, *10*, 1397-1406.

155) R. N. Bose, S. Moghaddas, P. A. Mazzer, L. P. Dudones, L. Joudah and D. Stroup *Nucleic Acids Res.* **1999**, *27*, 2219-2226.

156) A. Levina, G. Barr-David, R. Codd, P. A. Lay, N. E. Dixon, A. Hammershøi and P. Hendry *Chem. Res. Toxicol.* **1999**, *12*, 371-381.

157) K. D. Sugden *J. Inorg. Biochem.* **1999**, *77*, 177-183.

158) A. Levina, P. A. Lay and N. E. Dixon *Inorg. Chem.* **2000**, *39*, 385-395.

159) K. D. Sugden and K. E. Wetterhahn *J. Am. Chem. Soc.* **1996**, *118*, 10811-10818.

160) K. D. Sugden and K. E. Wetterhahn *Inorg. Chem.* **1996**, *35*, 3727-3728.

161) M. Rizzotto, V. Moreno, S. Signorella, V. Daier and L. F. Sala *Polyhedron* **2000**, *19*, 417-423.

162) J. Ye, S. Wang, S. S. Leonard, Y. Sun, L. Butterworth, J. Antonini, M. Ding, Y. Rojanasakul, V. Vallyathan, V. Castranova and X. Shi *J. Biol. Chem.* **1999**, *274*, 34974-34980.

163) D. I. Pattison, P. A. Lay and M. J. Davies *Redox Rep.* **2000**, *5*, 130-132.

164) L. Zhang and P. A. Lay *Inorg. Chem.* **1998**, *37*, 1729-1733.

165) X. Shi, A. Chiu, C. T. Chen, B. Halliwell, V. Castranova and V. Vallyathan *J. Toxicol. Environ. Health, Part B* **1999**, *2*, 87-104.

166) A. M. Standeven and K. E. Wetterhahn *Chem. Res. Toxicol.* **1991**, *4*, 616-625.

167) P. Jones, A. Kortenkamp, P. O'Brien, G. Wang and G. Yang *Arch. Biochem. Biophys.* **1991**, *286*, 652-655.

168) T.-C. Tsou and J.-L. Yang *Chem.-Biol. Interact.* **1996**, *102*, 133-153.

169) F. Chen, J. Ye, X. Zhang, Y. Rojanasakul and X. Shi *Arch. Biochem. Biophys.* **1997**, *338*, 165-172.

170) J. Ye, X. Zhang, H. A. Young, Y. Mao and X. Shi *Carcinogenesis* **1995**, *16*, 2401-2405.

171) X. Shi, S. S. Leonard, K. J. Liu, L. Zang, P. M. Gannett, Y. Rojanasakul, V. Castranova and V. Vallyathan *J. Inorg. Biochem.* **1998**, *69*, 263-268.

172) A. Chiu, N. Chiu, X. Shi, J. Beaubier and N. S. Dalal *Environ. Carcino. Ecotox. Rev.* **1998**, *C16*, 135-148.

173) X. Shi and N. S. Dalal *Arch. Biochem. Biophys.* **1990**, *277*, 342-350.

174) W. Qi, R. J. Reiter, D.-X. Tan, J. J. Garcia, L. C. Manchester, M. Karbownik and J. R. Calvo *Environ. Health. Perspect.* **2000**, *108*, 399-402.

175) S. Leonard, S. Wang, L. Zang, V. Castranova, V. Vallyathan and X. Shi *J. Environ. Pathol. Toxicol. Oncol.* **2000**, *19*, 49-60.

176) K. D. Sugden and D. M. Stearns *J. Environ. Pathol. Toxicol. Oncol.* **2000**, *19*, 215-230.

177) K. D. Sugden and K. E. Wetterhahn *Inorg. Chem.* **1996**, *35*, 651-657.

178) B. D. Martin, J. A. Schoenhard and K. D. Sugden *Chem. Res. Toxicol.* **1998**, *11*, 1402-1410.

179) S. K. Ghosh and E. S. Gould *Inorg. Chem.* **1986**, *25*, 3357-3359.

180) A. Parand, A. C. Royer, T. L. Cantrell, M. Weitzel, N. Memon, J. B. Vincent and M. W. Crowder *Inorg. Chim. Acta* **1998**, *268*, 211-219.

181) S. P. Kaiwar, A. Sreedhara, M. S. S. Raghavan, C. P. Rao, V. Jadhav and K. N. Ganesh *Polyhedron* **1996**, *15*, 765-774.

182) J. K. Speetjens, R. A. Collins, J. B. Vincent and S. A. Woski *Chem. Res. Toxicol.* **1999**, *12*, 483-487.

183) R. Vijayalakshmi, M. Kanthimathi, V. Subramanian and B. U. Nair *Biochim. Biophys. Acta* **2000**, *1475*, 157-162.

184) W. K. Pogozelski and T. D. Tullius *Chem. Rev.* **1998**, *98*, 1089-1107.

185) G. Pratviel, J. Bernadou and B. Meunier *Angew. Chem., Int. Ed. Engl.* **1995**, *34*, 746-769.

186) G. A. Neyhart, W. A. Kalsbeck, T. W. Welch, N. Grover and H. H. Thorpe *Adv. Chem.* **1995**, *246*, 405-429.

187) V. Voitkun, A. Zhitkovich and M. Costa *Nucleic Acids Res.* **1998**, *26*, 2024-2030.

188) J. K. Speetjens, A. Parand, M. W. Crowder, J. B. Vincent and S. A. Woski *Polyhedron* **1999**, *18*, 2617-2624.

189) H. Luo, Y. Lu, Y. Mao, X. Shi and N. S. Dalal *J. Inorg. Biochem.* **1996**, *64*, 25-35.

190) G. Barr-David, T. W. Hambley, J. A. Irwin, R. J. Judd, P. A. Lay, B. D. Martin, R. Bramley, N. E. Dixon, P. Hendry, J.-Y. Ji, R. S. U. Baker and A. M. Bonin *Inorg. Chem.* **1992**, *31*, 4906-4908.

191) T.-C. Tsou, R.-J. Lin and J.-L. Yang *Chem. Res. Toxicol.* **1997**, *10*, 962-970.

192) L. C. Bridgewater, F. C. R. Manning and S. R. Patierno *Mol. Carcinog.* **1998**, *23*, 201-206.

193) S. N. Mattagajasingh and H. P. Misra *J. Biol. Chem.* **1996**, *271*, 33550-33560.

194) S. N. Mattagajasingh and H. P. Misra *Mol. Cell. Biochem.* **1999**, *199*, 149-162.

195) A. Zhitkovich, V. Voitkun and M. Costa *Carcinogenesis* **1995**, *16*, 907-913.

196) C. A. Miller III and M. Costa *Mol. Carcinog.* **1988**, *1*, 125-133.

197) A. S. Hneihen, A. M. Standeven and K. E. Wetterhahn *Carcinogenesis* **1993**, *14*, 1795-1803.

198) H. Arakawa, R. Ahmad, M. Naoui and H.-A. Tajmir-Riahi *J. Biol. Chem.* **2000**, *275*, 10150-10153.

199) B. Gulanowski, M. Cieślak-Golonka, K. Szyba and J. Urban *BioMetals* **1994**, *7*, 177-184.

200) K. E. Wetterhahn and J. W. Hamilton *Sci. Total Environ.* **1989**, *86*, 113-129.

201) J. W. Hamilton and K. E. Wetterhahn *Mol. Carcinog.* **1989**, *2*, 274-286.

202) F. C. R. Manning, J. Xu and S. R. Patierno *Mol. Carcinog.* **1992**, *6*, 270-279.

203) J. A. Shumilla, R. J. Broderick, Y. Wang and A. Barchowsky *J. Biol. Chem.* **1999**, *274*, 36207-36212.

204) R. C. Kaltreider, C. A. Pesce, M. A. Ihnat, J. P. Lariviere and J. W. Hamilton *Mol. Carcinog.* **1999**, *25*, 219-229.

205) M. Katabami, H. Dosaka-Akita, T. Mishina, K. Honma, K. Kimura, Y. Uchida, K. Morikawa, H. Mikami, S. Fukuda, Y. Inuyama, Y. Ohsaki and Y. Kawakami *Hum. Pathol.* **2000**, *31*, 973-979.

206) A. Levina, A. M. Bailey, G. Champion and P. A. Lay *J. Am. Chem. Soc.* **2000**, *122*, 6208-6216.

207) A. M. O'Connell; Honours Thesis, University of Sydney, 1997.

208) R. Doll, L. G. Morgan and F. E. Speizer *Br. J. Cancer* **1970**, *24*, 623-632.

209) J. Kaldor, J. Peto, D. Easton, R. Doll, C. Hermon and L. Morgan *J. Natl. Cancer Inst.* **1986**, *77*, 841-848.

210) H. M. Shen and Q. F. Zhang *Environ. Health. Perspect.* **1994**, *102 Suppl.*, 275-282.

211) L. Jarup, T. Bellander, C. Hogstedt and G. Spang *Occup. Environ. Med.* **1998**, *55*, 755-759.

212) S. Langård *Sci. Total Environ.* **1994**, *148*, 303-309.

213) A. D. Ottolenghi, J. K. Haseman, W. W. Payne, H. L. Falk and H. N. MacFarland *J. Natl. Cancer Inst.* **1974**, *54*, 1165-1172.

214) M. Costa *Toxicol. Environ. Chem.* **1995**, *49*, 145-148.

215) K. S. Kasprzak, R. V. Quander and L. A. Poirier *Carcinogenesis* **1985**, *6*, 1161-1166.

216) T. Ohmori, K. Okada, M. Terada and R. Tabei *Cancer Lett.* **1999**, *136*, 53-58.

217) N. T. Christie, D. M. Tummolo, N. W. Biggart and E. C. Murphy *Cell Biol. Toxicol.* **1988**, *4*, 427-445.

218) J. Li, R. Ayyadevara and R. J. S. Reis *Mutat. Res.* **1997**, *385*, 173-193.

219) M. Costa *Ann. Rev. Pharmacol. Toxicol.* **1991**, *31*, 321-337.

220) C. B. Klein, K. Frenkel and M. Costa *Chem. Res. Toxicol.* **1991**, *4*, 592-604.

221) W. F. Sunderman Jr. *Environ. Health. Perspect.* **1981**, *40*, 131-141.

222) S. Bhattacharya, B. Saha, A. Dutta and P. Banerjee *Coord. Chem. Rev.* **1998**, *170*, 47-74.

223) M. Costa and H. H. Mollenhauer *Science* **1980**, *209*, 515-517.

224) A. Oskarsson, Y. Andersson and H. Tjalva *Cancer Res.* **1979**, *39*, 4175-4182.

225) M. Costa, J. Simmons-Hansen, C. W. M. Bedrossian, J. Bonura and R. M. Caprioli *Cancer Res.* **1981**, *41*, 2868-2876.

226) A. R. Oller, M. Costa and G. Oberdörster *Toxicol. Appl. Pharmacol.* **1997**, *143*, 152-166.

227) S. Robinson, O. Cantoni and M. Costa *Carcinogenesis* **1982**, *3*, 657-662.

228) S. K. Chakrabarti, C. Bai and K. S. Subramanian *Toxicol. Appl. Pharmacol.* **1999**, *154*, 245-255.

229) P. Sen and M. Costa *Cancer Res.* **1985**, *45*, 2320-2325.

230) M. Nishimura and M. Umeda *Mutat. Res.* **1979**, *68*, 337-349.

231) T. Refsvik and T. Andreassen *Carcinogenesis* **1995**, *16*, 1107-1112.

232) M. P. Abbracchio, R. M. Evans, J. D. Heck, O. Cantoni and M. Costa *Biol. Trace Element Res.* **1982**, *4*, 289-301.

233) I. Shibuya and W. W. Douglas *Endocrinology* **1992**, *131*, 1936-1941.

234) U. Şaplakoglu, M. Işcan and M. Işcan *Mutat. Res.* **1997**, *394*, 133-140.

235) T. J. Stinson, S. Jaw, E. H. Heffery and M. J. Plewa *Toxicol. Appl. Pharmacol.* **1992**, *117*, 98-103.

236) R. B. Ciccarelli and K. E. Wetterhahn *Cancer Res.* **1984**, *44*, 3892-3897.

237) R. B. Ciccarelli and K. E. Wetterhahn *Cancer Res.* **1982**, *42*, 3544-3549.

238) K. S. Kasprzak, B. A. Diwan, J. M. Rice, M. Misra, C. W. Rigss, R. Olinski and M. Dizdaroglu *Chem. Res. Toxicol.* **1992**, *5*, 809-815.

239) K. S. Kasprzak, P. Jaruga, T. H. Zastawny, S. L. North, C. W. Riggs, R. Olinski and M. Dizdaroglu *Carcinogenesis* **1997**, *18*, 271-277.

240) C. Mayer, R. G. Klein, H. Wesch and P. Schmezer *Mutat. Res.* **1998**, *420*, 85-98.

241) A. S. Rani, D.-Q. Qu, M. K. Sidhu, F. Panagakos, V. Shah, K. M. Klein, N. Brown, S. Pathak and S. Kumar *Carcinogenesis* **1993**, *14*, 947-953.

242) S. Zienolddiny, D. H. Svendsrud, D. Ryberg, A. B. Mikalsen and A. Haugen *Mutat. Res.* **2000**, *452*, 91-100.

243) M. Costa, Z. Zhuang, X. Huang, S. Cosentino, C. B. Klein and K. Salnikow *Sci. Total Environ.* **1994**, *148*, 191-199.

244) C. B. Klein, K. Conway, X. W. Wang, R. K. Bhamra, X. Lin, M. D. Cohen, L. Annab, J. C. Barrett and M. Costa *Science (Washington, D. C.)* **1991**, *251*, 796-799.

245) X. W. Wang, X. Lin, C. B. Klein, R. K. Bhamra, Y.-W. Lee and M. Costa *Carcinogenesis* **1992**, *13*, 555-561.

246) K. Conway and M. Costa *Biol. Trace Element Res.* **1989**, *21*, 437-444.

247) Y.-W. Lee, L. Broday and M. Costa *Mutat. Res.* **1998**, *415*, 213-218.

248) Y.-W. Lee, C. B. Klein, B. Kargacin, K. Salnikow, J. Kitahara, K. Dowjat, A. Zhitkovich, N. T. Christie and M. Costa *Mol. Cell. Biol.* **1995**, *15*, 2547-2557.

249) Z. X. Zhuang, H. M. Sheng, V. Ng and C. N. Ong *Hum. Exp. Toxicol.* **1996**, *15*, 891-897.

250) H. Dally and A. Hartwig *Carcinogenesis* **1997**, *18*, 1021-1026.

251) Y. C. Hong, S. R. Paik, H. J. Lee, K. H. Lee and S. M. Jang *Environ. Health. Perspect.* **1997**, *105*, 744-748.

252) Z. Zhong, W. Troll, K. L. Koenig and K. Frenkel *Cancer Res.* **1990**, *50*, 7564-7570.

253) X. Huang, Z. Zhuang, K. Frenkel, C. B. Klein and M. Costa *Environ. Health. Perspect.* **1994**, *102*, 281-284.

254) G. Gill, A. A. Richter-Rusli, M. Ghosh, C. J. Burrows and S. E. Rokita *Chem. Res. Toxicol.* **1997**, *10*, 302-309.

255) W. Bal, V. Karantza, E. N. Moudrianakis and K. S. Kasprzak *Arch. Biochem. Biophys.* **1999**, *364*, 161-166.

256) Q. Liang, P. D. Eason and E. C. Long *J. Am. Chem. Soc.* **1995**, *117*, 9625-9631.

257) D. F. Shullenberger, P. D. Eason and E. C. Long *J. Am. Chem. Soc.* **1993**, *115*, 11038-11039.

258) M. Footer, M. Egholm, S. Kron, J. M. Coull and P. Matsudaira *Biochemistry* **1996**, *35*, 10673-10679.

259) C. Harford, S. Narindrasorasak and B. Sarkar *Biochemistry* **1996**, *35*, 4271-4278.

260) D. P. Mack and P. B. Dervan *Biochemistry* **1992**, *31*, 9399-9405.

261) M. Nagaoka, M. Hagihara, J. Kuwahara and Y. Sugiura *J. Am. Chem. Soc.* **1994**, *116*, 4085-4086.

262) C. J. Burrows, R. J. Perez, J. G. Muller and S. E. Rokita *Pure Appl. Chem.* **1998**, *70*, 275-278.

263) K. C. Brown, S.-H. Yang and T. Kodadek *Biochemistry* **1995**, *34*, 4733-4739.

264) J. G. Muller, R. P. Hickerson, R. J. Perez and C. J. Burrows *J. Am. Chem. Soc.* **1997**, *119*, 1501-1506.

265) J. G. Muller, L. A. Kayser, S. J. Paikoff, V. Duarte, N. Tang, R. J. Perez, S. E. Rokita and C. J. Burrows *Coord. Chem. Rev.* **1999**, *185-186*, 761-774.

266) H.-C. Shih, N. Tang, C. J. Burrows and S. E. Rokita *J. Am. Chem. Soc.* **1998**, *120*, 3284-3288.

267) L. L. Guan, J. Kuwahara and Y. Sugiura *Biochemistry* **1993**, *32*, 6141-6145.

268) R. P. Hickerson, F. Prat, J. G. Muller, C. S. Foote and C. J. Burrows *J. Am. Chem. Soc.* **1999**, *121*, 9423-9428.

269) W. Bal, M. I. Djuran, D. W. Margerum, E. T. Gray Jr., M. A. Mazid, R. T. Tom, E. Nieboer and P. J. Sadler *J. Chem. Soc., Chem. Commun.* **1994**, 1889-1890.

270) E. B. Paniago, D. C. Weatherburn and D. W. Margerum *J. Chem. Soc., Chem. Commun.* **1971**, 1427-1428.

271) F. P. Bossu, E. B. Paniago, D. W. Margerum, S. T. Kirksey Jr. and J. L. Kurtz *Inorg. Chem.* **1978**, *17*, 1034-1042.

272) S. A. Ross and C. J. Burrows *Inorg. Chem.* **1998**, *37*, 5358-5363.

273) A. Böttcher, H. Elias, L. Müller and H. Paulus *Angew. Chem., Int. Ed. Engl.* **1992**, *31*, 623-625.

274) A. Böttcher, H. Elias, E.-G. Jäger, H. Langfelderova, M. Mazur, L. Müller, H. Paulus, P. Pelikan, M. Rudolph and M. Valko *Inorg. Chem.* **1993**, *32*, 4131-4138.

275) A. Berkessel, J. W. Bats and C. Schwarz *Angew. Chem., Int. Ed. Engl.* **1990**, *29*, 106-108.

276) D. Chen, R. J. Motekaitis and A. E. Martell *Inorg. Chem.* **1991**, *30*, 1396-1402.

277) E. Kimura, R. Machida and M. Kodama *J. Am. Chem. Soc.* **1984**, *106*, 5497-5505.

278) E. Kimura and R. Machida *J. Chem. Soc., Chem. Commun.* **1984**, 499-500.

279) J.-H. Choi and P. E. Hoggard *Polyhedron* **1992**, *11*, 2399-2407.

280) C. M. Murdoch, M. K. Cooper, T. W. Hambley, W. N. Hunter and H. C. Freeman *J. Chem. Soc., Chem. Commun.* **1986**, 1329-1331.

281) J.-H. Choi, I.-H. Suh and S.-H. Kwak *Acta Crystallogr., Sect. C* **1995**, *C51*, 1745-1748.

282) V. Subramaniam, K.-W. Lee, R. G. Garvey and P. E. Hoggard *Polyhedron* **1988**, *7*, 523-527.

283) T. J. Collins, B. D. Santarsiero and G. H. Spies *J. Chem. Soc., Chem. Commun.* **1983**, 681-682.

284) T. Weyhermüller, K. Weighardt and P. Chaudhuri *J. Chem. Soc., Dalton Trans.* **1998**, 3805-3813.

285) W.-H. Leung, J.-X. Ma, V. W.-W. Yam, C.-M. Che and C.-K. Poon *J. Chem. Soc., Dalton Trans.* **1991**, 1071-1076.

286) H. C. Freeman, J. M. Guss and R. L. Sinclair *Acta Crystallogr., Sect. B* **1978**, *B34*, 2459-2466.

287) H. C. Freeman, J. M. Guss and R. L. Sinclair *J. Chem. Soc., Chem. Commun.* **1968**, 485-487.

288) W. R. Kennedy and D. W. Margerum *Inorg. Chem.* **1985**, *24*, 2490-2495.

289) F. S. Stephens and R. S. Vagg *Inorg. Chim. Acta* **1982**, *57*, 9-13.

290) F. S. Stephens and R. S. Vagg *Inorg. Chim. Acta* **1986**, *120*, 165-171.

291) M. Mulqi, F. S. Stephens and R. S. Vagg *Inorg. Chim. Acta* **1981**, *52*, 73-77.

292) F. S. Stephens and R. S. Vagg *Inorg. Chim. Acta* **1984**, *90*, 17-24.

293) Z.-N. Chen, H.-X. Zhang, K.-B. Yu, C.-Y. Su and B.-S. Kang *Polyhedron* **1998**, *17*, 1535-1540.

294) M. Nonoyama *Inorg. Chim. Acta* **1974**, *10*, 59-63.

295) Y. Kushi, R. Machida and E. Kimura *J. Chem. Soc., Chem. Commun.* **1985**, 216-218.

Chapter 2

Synthesis of Tetradentate Diamide Ligands

2.1 Introduction

Vagg and coworkers developed a series of acyclic tetradentate ligands with two central amide groups and two terminal pyridyl groups (Figure 2.1).[1,2] These ligands were used to prepare a range of complexes with M(II) ions.[2-22]

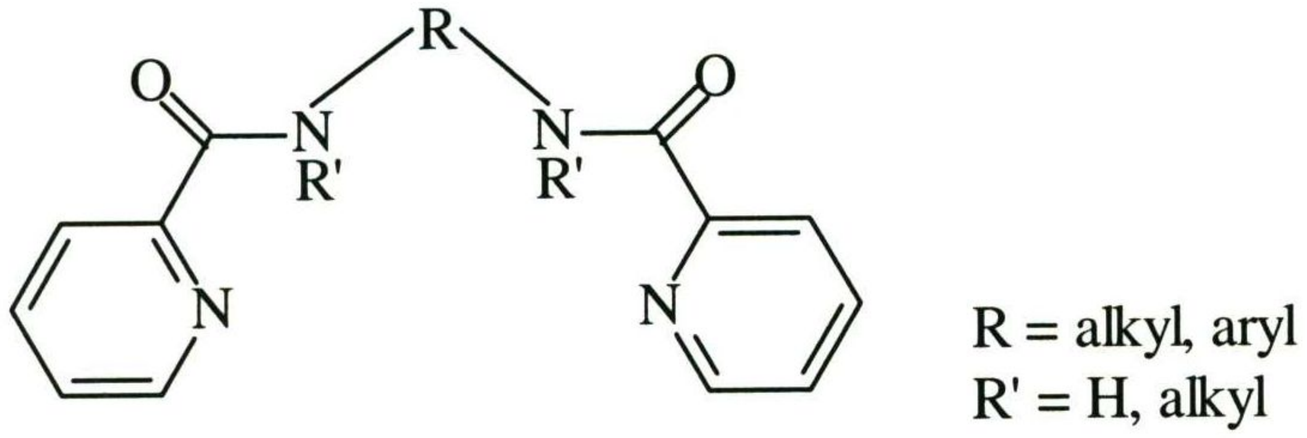

R = alkyl, aryl
R' = H, alkyl

Figure 2.1 General structure of the tetradentate diamide-dipyridyl ligands

Two of these ligands, *N,N´*-bis(2-pyridinecarboxamide)-1,2-ethane ($bpenH_2$) and *N,N´*-bis(2-pyridinecarboxamide)-1,2-benzene ($bpbH_2$) (Figure 2.2) were chosen as potential ligands for stabilising the higher oxidation states Cr(V) and Ni(III).

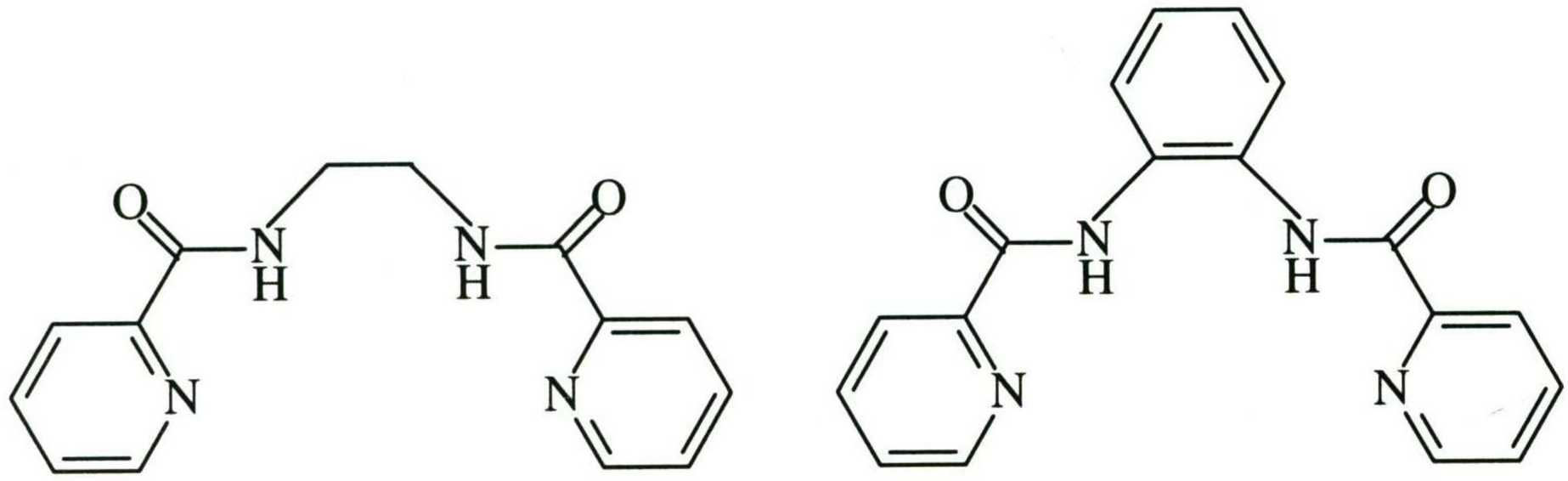

(a) (b)

Figure 2.2 Molecular structures of (a) $bpenH_2$ and (b) $bpbH_2$

A second class of acyclic tetradentate ligands with two central amide groups was also developed. These have pyrrolidine terminal groups instead of the pyridyl terminal groups used by Vagg and coworkers.

The ligands *N,N´*-bis(*S*-prolyl)-1,2-ethanediamine (*S,S*-$bprolenH_2$) and *N,N´*-bis(*S*-prolyl)-*R,R*-1,2-cyclohexanediamine (*R,R*-(*S,S*)-$bprolchxnH_2$) (Figure 2.3) were used by Jun and Liu as intermediates in the synthesis of acyclic tetraamine ligands,[23,24] but they were only obtained in crude forms as oils. The dihydrochloride salt of

S,S-bprolenH_2 was also reported as an intermediate in the synthesis of a bivalent affinity label for the crosslinking of immunoglubulin G but was not characterised.[25] The ^1H and ^{13}C NMR spectral data of the bis-TFA salt of *S,S*-bprolenH_2, a product of the photolytic degradation of prolylglycine, has also been reported.[26]

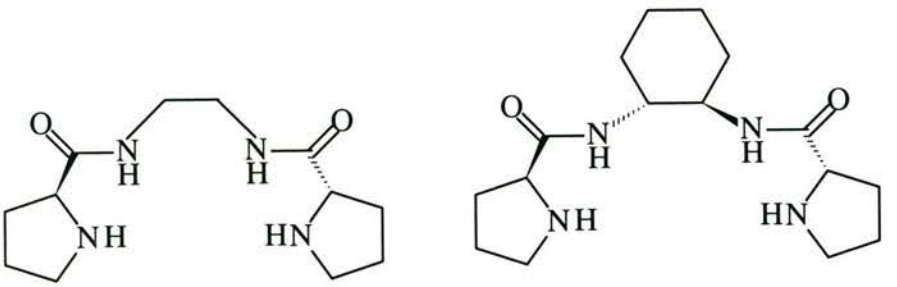

(a) (b)

Figure 2.3 Molecular structures of (a) *S,S*-bprolenH_2 and (b) *R,R*-(*S,S*)-bprolchxnH_2

There have been several articles reporting Cu(II) complexes of the *S,S*-bprolenH_2 ligand. It was used in studies on the activity of Cu(II) complexes in the catalytic dismutation of superoxide (O_2^-)[27] and the decomposition of H_2O_2.[28] The Cu(II) complexes were only characterised in solution, as they decomposed during the course of the reactions, and no details on the synthesis or characterisation of the ligands were given. The synthesis and crystal structure of a Cu(II) complex of *S,S*-bprolenH has been recently reported,[29] the complex is dinuclear and two ligands act as bis-bidentates, bridging the two Cu centres. The ligands bind to one Cu *via* a pyrrolidine N and an amide O atom (from the protonated amide group) and to the other Cu *via* a pyrrolidine N and an amide N atom (from the deprotonated amide group). The *S,S*-bprolenH_2 ligand was characterised by ^{13}C NMR spectroscopy.[29]

Reported here is the synthesis and detailed characterisation of three acyclic tetradentate ligands with two central amide groups and terminal pyrrolidine groups.

2.2 Experimental

2.2.1 Synthesis of Ligands

2.2.1.1 bpenH_2

The ligand bpenH_2 was synthesised from 1,2-ethanediamine and 2-pyridinecarboxylic acid by the method of Barnes *et al.*[1] The product was recrystallised from chloroform followed by repeated recrystallisation from ethanol, giving the pure product in 75% yield. ^{1}H NMR* ($CDCl_3$): ppm; 3.77 (t, 4H); 7.42 (ddd, 2H); 7.84 (td, 2H); 8.19 (dt, 2H); 8.4 (s, 2H); 8.55 (dt, 2H). IR† (DRIFTS in KBr) cm^{-1}: 3334 (ss); 1662 (ss); 1533 (ss); 1466 (m); 1449 (m); 1435 (m); 1328 (m); 1291 (m); 1256 (m); 1232 (m); 996 (m); 888 (m); 747 (m); 678 (s); 620 (m).

2.2.1.2 bpbH_2

The compound bpbH_2 was synthesised from 1,2-benzenediamine and 2-pyridinecarboxylic acid by the method of Barnes *et al.*[1] The product was purified by repeated recrystallisation from chloroform, giving the pure product in 55% yield. ^{1}H NMR ($CDCl_3$): ppm; 7.30 (dd, 2H); 7.46 (ddd, 2H); 7.8-8.0 (m, 4H); 8.32 (dt, 2H); 8.56 (dt, 2H); 10.26 (br, 2H). IR (DRIFTS in KBr) cm^{-1}: 3317 (m); 1677 (ss); 1668 (ss); 1594 (m); 1527 (s); 1519 (s); 1487 (m); 1465 (m); 1451 (m); 1432 (m); 1280 (w); 759 (m); 748 (m); 690 (m); 673 (br, sh).

2.2.1.3 *S,S*-bprolenH_2

Carbobenzoxy-*S*-proline

Carbobenzoxy-*S*-proline was synthesised from *S*-proline and benzyl chloroformate according to the method of Berger *et al.*,[30] the product was isolated as an oil and not a solid as they reported.

***N,N′*-Bis(carbobenzoxy-*S*-prolyl)-1,2-ethanediamine**

The method of Jun and Liu[23] was used to synthesise *N,N′*-bis(carbobenzoxy-*S*-

---

* Abbreviations for NMR: br, broad; d, doublet; m, multiplet; ppm, parts per million; q, quartet; s, singlet; t, triplet.

† Abbreviations for IR: br, broad; m, medium; s, strong; ss, strong and sharp; sh, shoulder; w, weak.

prolyl)-1,2-ethanediamine. Carbobenzoxy-*S*-proline (39.6 g) in toluene (400 mL, Merck, 99.5%), chloroform (50 mL), and triethylamine (27 mL, Merck, 99%) were chilled in an ice/salt bath to −5 °C. *Iso*-butylchloroformate (20.5 mL, Aldrich, 98%) was added and the mixture was stirred for 1 h. 1,2-Ethanediamine (4.3 mL, Merck, 99%) in chloroform (300 mL) and triethylamine (27 mL, Merck, 99%) were cooled in an ice bath and the mixture was added to the chilled toluene mixture. The resultant mixture was removed from the ice bath and stirred at room temperature for 24 h. The reaction mixture was washed with water (300 mL), sodium hydrogen carbonate solution (3%, 300 mL), and water (300 mL). The organic layer was dried over anhydrous sodium sulfate, filtered and the solvent was removed on a rotary evaporator to give the crude product. Yield: 34.63 g (>100%). ^{1}H NMR ($CDCl_3$): ppm; 1.8-2.2 (m, 8H); 3.22 (m, 2H); 3.5 (m, 6H); 4.21 (m, 4H); 5.12 (q, 4H); 7.33 (s, 10H). IR (DRIFTS in KBr) cm^{-1}: 3377 (m); 3345 (w); 1706 (ss); 1666 (m); 1645 (m); 1531 (ss); 1444 (m); 1415 (ss); 1357 (m).

_N,N′_-Bis(*S*-prolyl)-1,2-ethanediamine (*S,S*-bprolenH_2)

Palladium on activated carbon (~1 g, Aldrich, 10%) was added to crude _N,N′_-bis(carbobenzoxy-*S*-prolyl)-1,2-ethanediamine (34.6 g) in methanol (450 mL). Hydrogen was gently bubbled through the mixture until carbon dioxide production ceased (monitored by lime water, ~90 h). The mixture was filtered through a celite pad and the residue was washed with methanol (~100 mL). The combined filtrate and washings were filtered through a filter paper and the solvent was removed on a rotary evaporator. Ethanol (~100 mL) was added and evaporated to remove any residual water as an azeotrope. The product, a yellow coloured oil, was stored under nitrogen in the refrigerator for 5 d, during which time most of it solidified forming white crystals. This crude product was recrystallised from methanol/ethyl acetate as the hemihydrate. Yield: 7.40 g (42%). M.p. 105-108 °C. IR (DRIFTS in KBr; cm^{-1}): 3306 (s); 3076 (w); 2965 (m); 2943 (m); 2921 (w); 2860 (m); 2825 (w); 1652 (ss); 1541 (s); 1444 (m); 1376 (w); 1311 (m); 1255 (m); 1235 (m); 1110 (m); 1065 (w); 966 (w); 910 (m); 773 (w); 692 (m, br); 514 (w); 436 (w). Calculated for $C_{12}H_{22}N_4O_2.0{\cdot}5H_2O$: C, 54.73%; H, 8.80%; N, 21.28%. Found: C, 54.84%; H, 8.39%; N, 21.02%.

2.2.1.4 *R,R*-(*S,S*)-bprolchxnH_2

_N,N´_-Bis(carbobenzoxy-*S*-prolyl)-*R,R*-1,2-cyclohexanediamine

The method of Jun and Liu[24] was used to synthesise _N,N´_-bis(carbobenzoxy-*S*-prolyl)-*R,R*-1,2-cyclohexanediamine. Carbobenzoxy-*S*-proline (33.17 g) was dissolved in toluene (300 mL, Ajax, AR) and triethylamine (19.5 mL, Ajax, 99%) was added. The solution was chilled to –5 °C in an ice/acetone bath and *iso*-butylchloroformate (17.3 mL, ICN Biomedicals) was added, followed by toluene (50 mL, Ajax, AR). The solution was stirred for 1 h. *R,R*-1,2-Cyclohexanediamine (7.59 g) was dissolved in chloroform (200 mL) and triethylamine (19.5 mL, Ajax, 99%) was added. The *R,R*-1,2-cyclohexanediamine solution was cooled in an ice bath then added to the carbobenzoxy-*S*-proline solution. The flask was removed from the ice/acetone bath, sealed with a $CaCl_2$ drying tube, and left stirring overnight. The reaction mixture was filtered at the pump and the residue was washed with chloroform (50 mL). The combined filtrate and washings were extracted with water (200 mL), sodium hydrogen carbonate solution (200 mL, 3%), and water (200 mL). The organic layer was dried over anhydrous sodium sulfate and filtered. The solvent from the filtrate was removed on a rotary evaporator to give a white solid, which was recrystallised from acetone/diethyl ether. Yield 26.37 g (69%). ^{1}H NMR ($CDCl_3$): ppm; 0.7-1.3 (m, 4H); 1.4-2.3 (m, 12H); 3.50 (m, 6H); 4.25 (t, 2H); 5.18 (t, 4H); 6.3 (br, 1H); 6.7 (br, 1H); 7.35 (s, 10H).

_N,N´_-Bis(*S*-prolyl)-*R,R*-1,2-cyclohexanediamine (*R,R*-(*S,S*)-bprolchxnH_2)

Palladium on activated carbon (~3 g, Aldrich, 10%) was added to _N,N´_-bis(carbobenzoxy-*S*-prolyl)-*R,R*-1,2-cyclohexanediamine (26.37 g) in methanol (300 mL). Hydrogen gas was gently bubbled through the stirred reaction mixture until carbon dioxide production ceased (~156 h). The reaction mixture was filtered through a celite pad and the celite pad was washed with methanol (3 × ~10 mL). The combined filtrate and washings were removed on a rotary evaporator. Methanol (~100 mL) was added and evaporated to remove any remaining water as an azeotrope. The product, a white solid, was dried over silica gel. Yield: 14.27 g (~100%). M.p. 179-181 °C. IR (DRIFTS in KBr; cm^{-1}): 3315 (ss); 3248 (w); 2972

(w); 2935 (m); 2860 (m); 1637 (ss); 1523 (s); 1510 (s); 1456 (w); 1297 (w); 1110 (w); 880 (w); 695 (w); 655 (w); 579 (w); 416 (w). Calculated for $C_{16}H_{28}N_4O_2$: C, 62.30%; H, 9.15%; N, 18.17%. Found: C, 62.10%; H, 8.88%; N, 17.95%.

2.2.1.5 *S,S*-bprolbenH_2

_N,N´_-Bis(carbobenzoxy-_S_-prolyl)-1,2-benzenediamine

Carbobenzoxy-*S*-proline (48.48 g) was dissolved in toluene (400 mL, Ajax, AR) and triethylamine (28.5 mL, Ajax, 99%) was added. The solution was chilled to –10 °C in an ice/acetone bath and *iso*-butylchloroformate (25.5 mL, ICN Biomedicals) was added, followed by toluene (125 mL, Ajax, AR). The solution was stirred for 1 h. 1,2-Benzenediamine (10.43 g) was dissolved in chloroform (300 mL) and triethylamine (28.5 mL, Ajax, 99%) was added. The 1,2-benzenediamine solution was cooled in an ice bath before being added to the carbobenzoxy-*S*-proline solution. The flask was removed from the ice/acetone bath, sealed with a $CaCl_2$ drying tube and left stirring overnight. The reaction mixture was filtered at the pump and the residue was washed with toluene (~50 mL, Ajax, AR). The combined filtrate and washings were extracted with water (400 mL), sodium hydrogen carbonate solution (400 mL, 3%), and water (400 mL). The organic layer was dried over anhydrous sodium sulfate (~5 g) and filtered. The solvent from the filtrate was removed on a rotary evaporator, giving a very viscous brown coloured oil that solidified on cooling. The product was dissolved in boiling ethanol (500 mL) and activated carbon (14.5 g, BDH, LR) was added. The mixture was boiled for 30 min and the hot solution was filtered twice. The filtrate was evaporated to dryness to give a pale brown coloured solid. This crude product was not purified further. Yield: 46.92 g (85%). ^{1}H NMR ($CDCl_3$): ppm; 1.8-2.4 (m, 8H); 3.51 (m, 4H); 4.49 (m, 2H); 5.16 (m 4H); 7.34 (m, 14H); 7.64 (m, 1H); 8.91 (m, 1H).

_N,N´_-Bis(_S_-prolyl)-1,2-benzenediamine (_S,S_-bprolbenH_2)

A solution of HBr in acetic acid (130 mL, BDH, 45%) was added to *N,N´*-bis(carbobenzoxy-*S*-prolyl)-1,2-benzenediamine (46.53 g). The mixture was heated for $2^1/_4$ h on a steam bath then sealed and left to cool. The reaction mixture was filtered and the solvent was removed on a rotary evaporator. Ethanol (200 mL) was added to the residue, then it was evaporated on a steam bath. Diethyl ether was

added to the cooled residue, which was triturated and left to stand. The supernatant was decanted and discarded. The residue was dissolved by shaking with sodium hydroxide solution (200 mL, 1 M; 50 mL, 10 M) and chloroform (200 mL). The two layers were separated and the aqueous layer was extracted with chloroform (4 × 100 mL). The combined organic layers were dried over anhydrous sodium sulfate (~10 g), filtered and the solvent was removed on a rotary evaporator. The crude product was recrystallised from chloroform/diethyl ether. This gave a pale brown coloured powder. Yield: 7.14 g (29%). IR (DRIFTS in KBr; cm^{-1}): 3312 (m); 3254 (m, br); 2969 (m); 2946 (w); 2915 (w); 1665 (ss); 1594 (m); 1528 (ss); 1473 (m); 1301 (m); 1104 (m); 906 (w); 869 (m); 771 (m); 576 (w); 477 (w). A small amount of the product was purified by chromatography on a silica column. A methanol solution of the crude product was loaded onto the column (11 × 2 cm, silica gel 60, 35-70 mesh) and a yellow band was eluted with methanol, which was discarded. The fraction that was eluted with methanol after the yellow band and a subsequent fraction eluted with dichloromethane contained pure *S,S*-bprolbenH_2. The solvent was removed from these fractions on a rotary evaporator and the residues were combined. The purified product was a white solid and after drying over silica gel it was used to record the NMR spectra and for the elemental analyses. *S,S*-bprolbenH_2.0.5CH_3OH, calculated for $C_{16.5}H_{24}N_4O_{2.5}$: C, 62.24%; H, 7.60%; N, 17.60%. Found: C, 62.34%; H, 7.26%; N, 16.69%. M.p. 154-159 °C.

2.2.2 Analysis and Instrumentation

$CDCl_3$ solutions were used to record the NMR spectra of ligands and the synthetic intermediates. 1D ^1H NMR spectra were recorded on a Bruker AC200 NMR spectrometer or a Bruker AMX400 NMR spectrometer; 2D COSY ^1H NMR spectra were recorded on a Bruker AMX400 NMR spectrometer. The ^1H-decoupled ^{13}C NMR spectra were recorded on a Bruker AC200 NMR spectrometer. The ^1H and ^{13}C spectra were referenced against the internal standard TMS.

The IR spectra of the complexes were recorded by diffuse reflectance infrared Fourier transform spectroscopy (DRIFTS) on a Bio Rad FTS-40 spectrophotometer. KBr was used as the matrix and background for spectra recorded over the range 400-4000 cm^{-1}.

Melting points were measured on a Gallenkamp melting point apparatus and are reported uncorrected. C, H, and N microanalyses were carried out at the Research School of Chemistry at the Australian National University; and the University of Otago, New Zealand.

2.3 Results and Discussion

2.3.1 Synthesis of $bpenH_2$ and $bpbH_2$

The ligands $bpenH_2$ and $bpbH_2$ were synthesised according to the literature method, the yields obtained were lower than those reported in the literature[1] because they were based on the recrystallised products instead of the crude products.

The ^1H NMR and IR spectra were consistent with the data reported in the literature.[1,3,9] The resonances at 7.30 ppm and 7.46 ppm, and 8.32 ppm and 8.56 ppm in the spectrum of $bpbH_2$ were overlapped in the data reported in the literature; but they were resolved into separate signals by the use of a 200 MHz spectrometer.

2.3.2 Synthesis of *S,S*-$bprolenH_2$, *R,R*-(*S,S*)-$bprolchxnH_2$ and *S,S*-$bprolbenH_2$

The synthetic scheme for the three ligands with pyrrolidine terminal groups is outlined in Scheme 2.1. The syntheses of these three ligands all started from *S*-proline (the naturally occurring form). A carbobenzoxy (CBZ) protecting group was added to the amine N to prevent the condensation of two proline molecules together during the coupling of the carboxylic acid to the amine to form the amide. The CBZ-*S*-proline was reacted with the appropriate diamine to give the diamide with protected amine-N atoms. This reaction proceeded in good yield with all three diamines. The products were not purified, which is why the yield of *N,N'*-bis(carbobenzoxy-*S*-prolyl)-1,2-ethanediamine was greater than the theoretical amount. The yield of *N,N'*-bis(carbobenzoxy-*S*-prolyl)-*R,R*-1,2-cyclohexanediamine was significantly greater than the yield obtained in the literature[24] probable due to the fact that the literature preparation only used a 1.2:1 mole ratio of CBZ-S-proline:*trans*-1,2-cyclohexanediamine.

Scheme 2.1 Synthesis of tetradentate ligands with pyrrolidine terminal groups

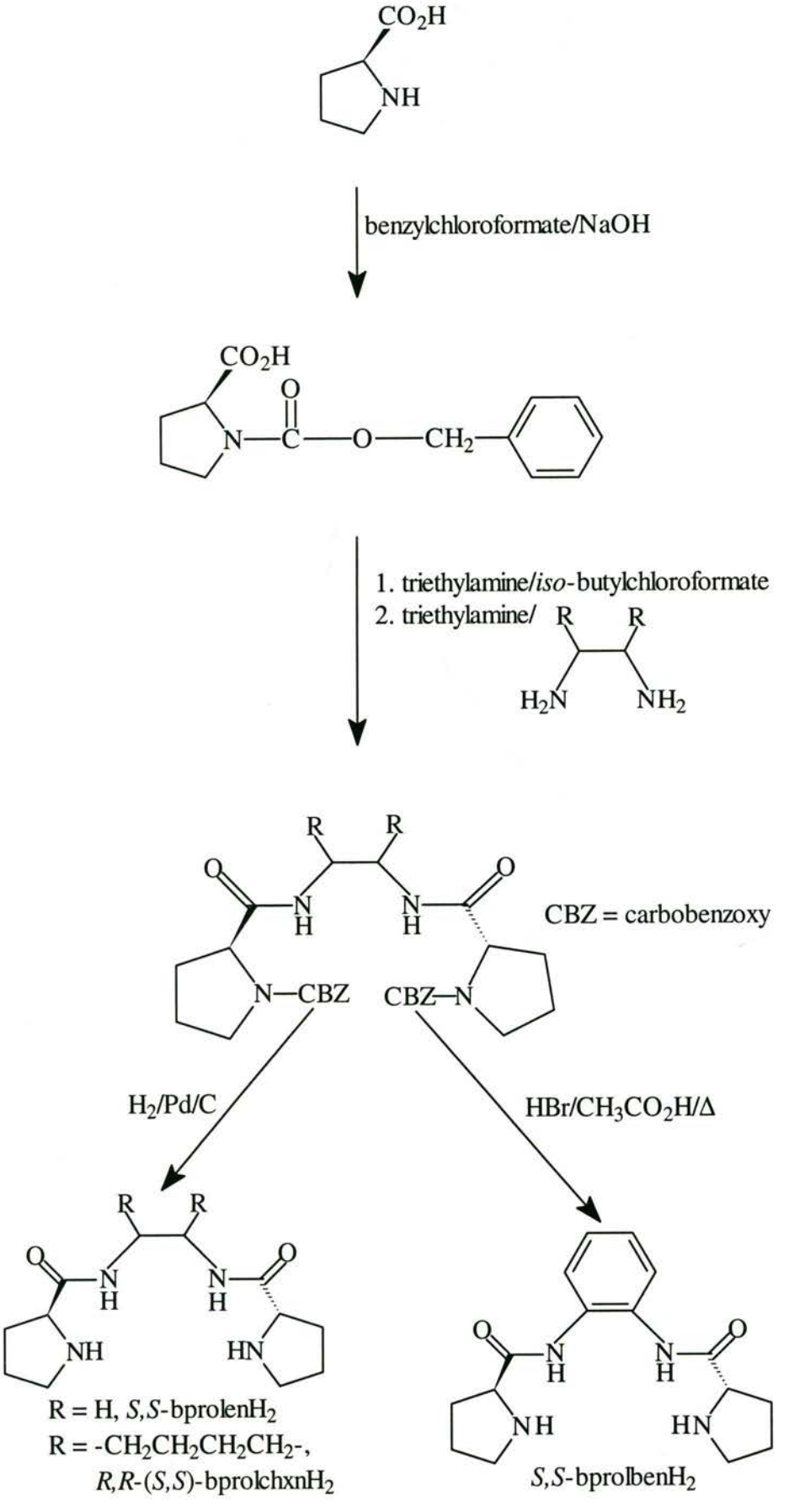

Two different methods were used to remove the CBZ protecting groups. For *N,N'*-bis(carbobenzoxy-*S*-prolyl)-1,2-ethanediamine and *N,N'*-bis(carbobenzoxy-*S*-prolyl)-*R,R*-1,2-cyclohexanediamine hydrogenation over Pd on activated carbon was used. Jun and Liu[23,24] also used hydrogenation over a Pd on C catalyst but they carried the hydrogenation out under pressure for a shorter time period and were unable to isolate a pure product. The *S,S*-bprolenH_2 was difficult to recrystallise, which is why the yield was lower than for *R,R*-(*S,S*)-bprolchxnH_2, which was obtained directly from the deprotection reaction as a solid. The yield of crude *R,R*-(*S,S*)-bprolchxnH_2 was greater than the theoretical amount (101%); however, the results of the elemental analysis were in good agreement with the calculated values; therefore, it was considered to be of sufficient purity and it was not recrystallised.

The removal of the CBZ protecting group by hydrogenation over Pd on C catalyst was a rather slow process and a quicker method was desirable. A solution of HBr in acetic acid[31] was used to remove the protecting group from *N,N'*-bis(carbobenzoxy-*S*-prolyl)-1,2-benzenediamine. This method was faster, but the yield was only 29%. This was because an approximately equal amount of a second product formed in the reaction. A white solid was removed from the HBr in acetic acid reaction mixture during the first filtration. It was dissolved in alkaline solution and extracted, giving the second product. The ^{1}H NMR spectrum of this product was similar to the spectrum of the genuine product, but there were extra signals and the aromatic region of the spectrum was not as symmetric. The white solid formed during the latter stages of heating the HBr in acetic reaction mixture and there was no evidence of the CBZ groups in the NMR spectrum, so it is likely that a side reaction is occurring with the deprotected ligand. The yield of the desired product could probably be improved by decreasing the heating period.

2.3.3 NMR Spectra of Ligands

2.3.3.1 *S,S*-bprolenH_2

The 1D ^{1}H NMR spectrum of *S,S*-bprolenH_2 is shown in Figure 2.4 and the 2D COSY ^{1}H NMR spectrum in Figure 2.5. The assignment of the ^{1}H and ^{13}C NMR spectra was made according to the atom numbering scheme in Figure 2.6. The

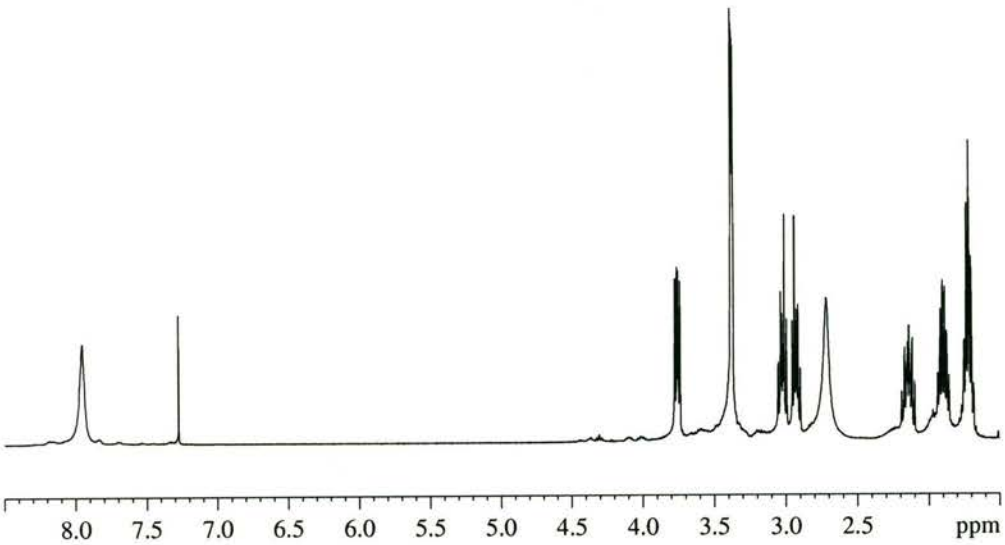

Figure 2.4 1D ^{1}H NMR spectrum of *S,S*-bprolenH_2 in $CDCl_3$. The residual solvent peak occurs at 7.27 ppm.

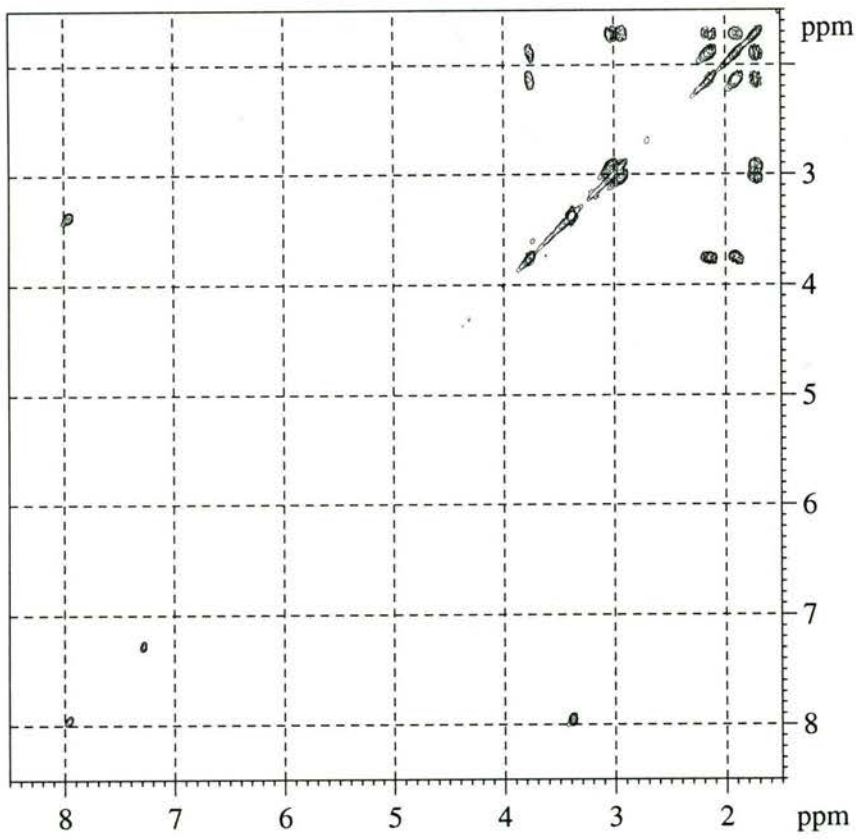

Figure 2.5 2D COSY ^{1}H NMR spectrum of *S,S*-bprolenH_2 in $CDCl_3$. The residual solvent peak occurs at 7.27 ppm.

assignment of the ^{1}H NMR spectra are in Table 2.1, and the ^{13}C NMR data and their assignments are in Table 2.2.

The total number of protons and their positions are consistent with the molecular structure of *S,S*-bprolenH_2. The broad resonances of the amide and amine protons

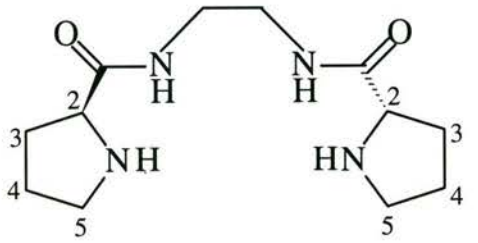

Figure 2.6 Atom numbering scheme for *S,S*-bprolenH_2 used in the assignment of the NMR spectra

Table 2.1 Assignment of the ^{1}H NMR spectra of *S,S*-bprolenH_2

Chemical Shift (ppm)	Description	Number of Protons	Assignment
1.72	multiplet	4	Position 4 of the pyrrolidine rings
1.90	multiplet	2	Either the axial or the equatorial protons on position 3 of the pyrrolidine rings
2.14	multiplet	2	Either the equatorial or the axial protons on position 3 of the pyrrolidine rings
2.72	broad singlet	2	Amine protons
2.97	multiplet	4	Position 5 of the pyrrolidine rings
3.37	triplet	4	Central ethylene bridge
3.76	doublet of doublets	2	Position 2 of the pyrrolidine rings
7.95	broad singlet	2	Amide protons

are clear proof that the removal of the CBZ protecting groups was successful. The central ethylene bridge give an unusually shaped triplet, the centre peak is weaker than the two outer peaks. A triplet of the same type is observed for the protons of the central ethene linkage in the ^{1}H NMR spectrum of the bpenH_2 ligand (where it is the only signal apart from the aromatic protons and so is easily assigned), which makes the assignment to the central ethene linkage in *S,S*-bprolenH_2 clear. The axial and equatorial protons on position 3 of the pyrrolidine rings are not equivalent and give separate resonances at 1.90 ppm and 2.14 ppm. Both sets of protons on position 3 have cross-peaks in the 2D COSY spectrum to the protons on position 2 and 4, making it difficult to determine which are the axial protons and which are the equatorial protons.

The ^{1}H NMR data of the bis-TFA salt in D_2O have been reported,[26] though not assigned. The literature data differ significantly from those reported here as there were no signals from the amine and amide protons (based on the number of protons reported) and only four signals were reported for the remaining eighteen protons.

Table 2.2 ^{13}C NMR spectral data for *S,S*-bprolenH_2 in $CDCl_3$

Chemical Shift (ppm)	Assignment
26.1	Position 4 of the pyrrolidine rings
30.7	Position 3 of the pyrrolidine rings
39.1	Central ethene bridge
47.2	Position 5 of the pyrrolidine rings
60.5	Position 2 of the pyrrolidine rings
175.8	Carbonyl of the amide groups

The ^{13}C NMR data were assigned by comparison of the chemical shifts to those of proline.[32] The ^{13}C NMR spectral data have been reported previously for D_2O solutions of *S,S*-bprolenH_2[29] and its bis-TFA salt.[26] The ^{13}C chemical shifts reported for these two substances differed by between 3 ppm and 10 ppm, the largest difference being for the carbonyl groups. The ^{13}C chemical shifts determined in this work lie between the values previously reported for *S,S*-bprolenH_2 and its bis-TFA

salt. The only assignment of the ^{13}C NMR data was by Lee *et al.*,[29] who assigned the carbonyl from the amide group and position 2 of the pyrrolidine rings.

The ^{1}H and ^{13}C NMR spectra could be assigned to the structure in Figure 2.6, which showed that the synthesis of *S,S*-bprolenH_2 was successful.

2.3.3.2 *R,R*-(*S,S*)-bprolchxnH_2

The 1D ^{1}H NMR spectrum of *R,R*-(*S,S*)-bprolchxnH_2 is shown in Figure 2.7 and the 2D COSY ^{1}H NMR spectrum in Figure 2.8. The assignments of the ^{1}H (Table 2.3) and ^{13}C NMR (Table 2.4) spectra were made according to the atom numbering scheme in Figure 2.9.

The ^{1}H NMR spectra of *R,R*-(*S,S*)-bprolchxnH_2 exhibited overlap between the resonances from the cyclohexane ring and the pyrrolidine rings. The interactions between the protons within each of the two types of ring were not simple first-order couplings, and for some resonances from the cyclohexane ring not all the couplings were resolved in the 1D spectrum, leading to broad peaks in the multiplets. The pattern and intensity of the cross peaks in the 2D COSY spectrum were used to assign the spectrum. There were no cross peaks between protons on the cyclohexane ring and protons on the pyrrolidine rings, which made it easy to determine which ring system to assign the resonances, even when signals from protons on the cyclohexane ring overlapped with those from protons on the pyrrolidine rings.

The number of protons present and their positions were consistent with the structure in Figure 2.9. The axial and equatorial protons on several ring positions were not equivalent and gave separate resonances, but it was difficult to determine unambiguously which resonance was due to the equatorial protons and which was due to the axial protons. The assignment of these resonances to either the axial or the equatorial protons was difficult because they had cross peaks in the 2D COSY spectrum to the same resonances and not all the couplings were resolved in the 1D spectrum.

The protons from the amide groups and the amine groups appeared as broad singlets in the 1D spectrum. In the 2D COSY spectrum there were cross peaks from the amide protons to the protons on positions 1 and 2, and 3 and 6 of the cyclohexane ring, but these couplings were not resolved in the 1D spectrum. There was no

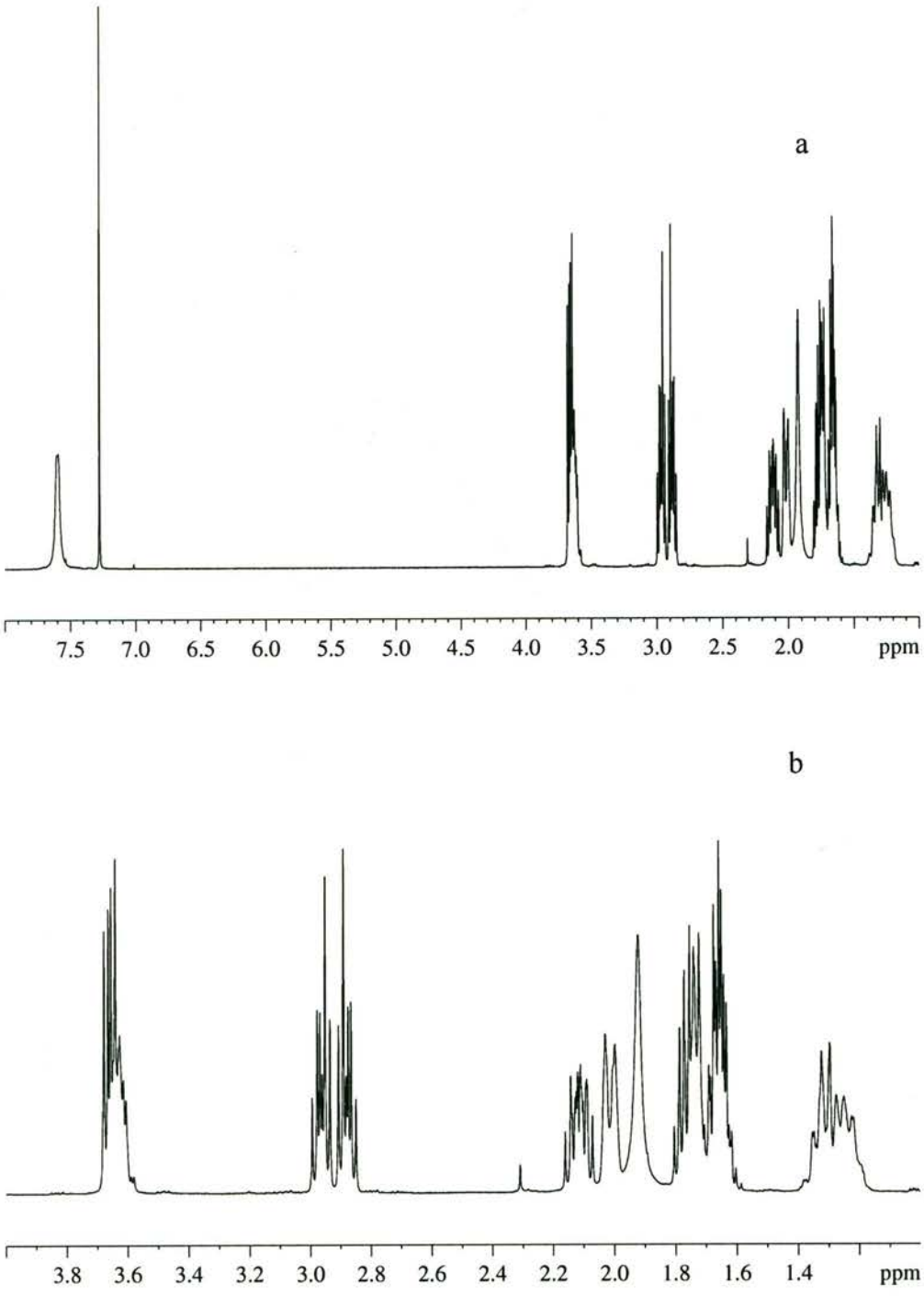

Figure 2.7 1D ^{1}H NMR spectra of *R,R*-(*S,S*)-bprolchxnH_2 in $CDCl_3$: (a) full spectrum, (b) expansion (1-4 ppm). The residual solvent peak occurs at 7.27 ppm.

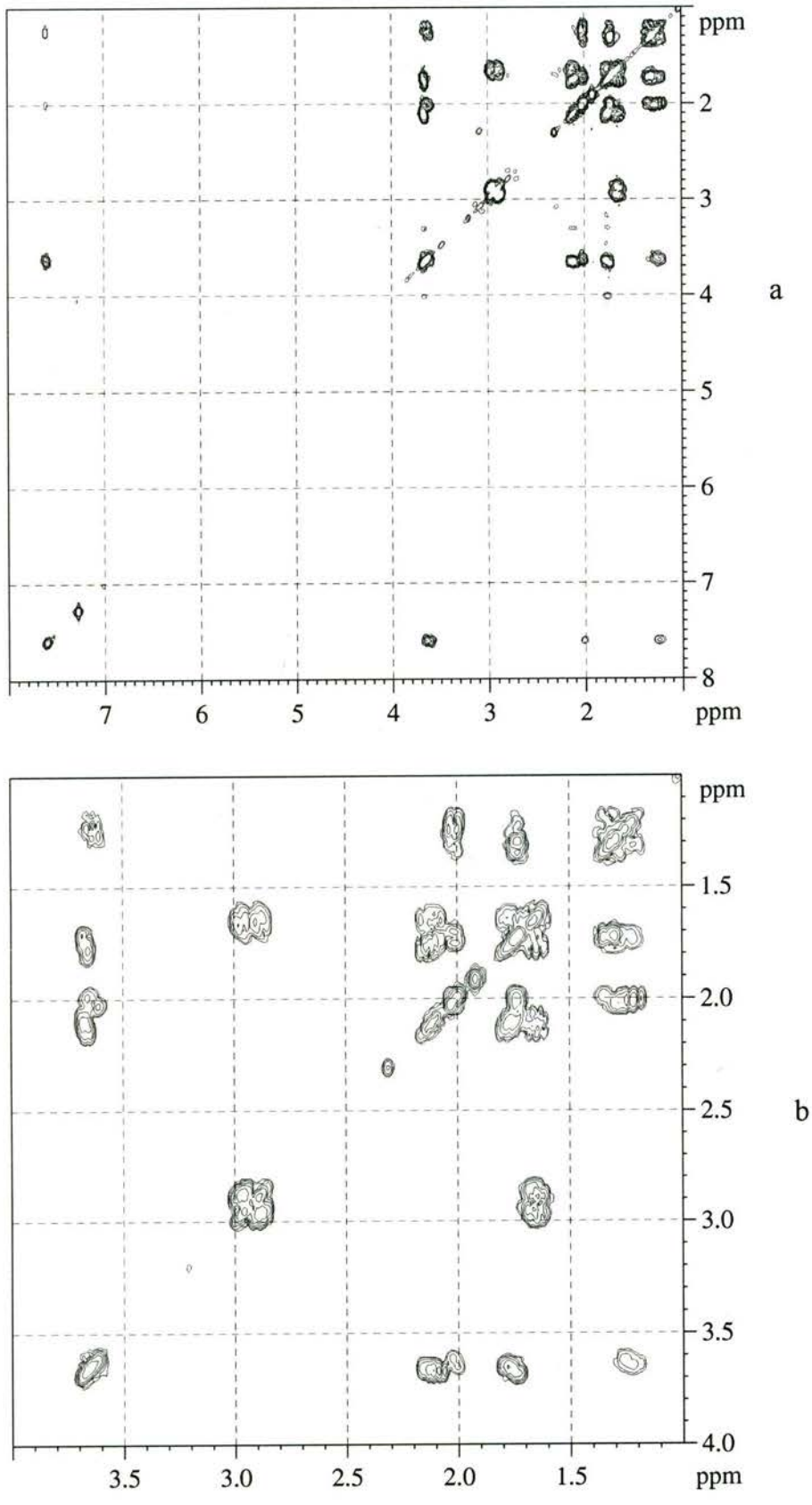

Figure 2.8 2D COSY ^{1}H NMR spectra of *R,R*-(*S,S*)-bprolchxnH_2 in $CDCl_3$: (a) full spectrum, (b) expansion (1-4 ppm). The residual solvent peak occurs at 7.27 ppm.

Table 2.3 Assignment of the ^{1}H NMR spectrum of *R,R*-(*S,S*)-bprolchxnH_2

Chemical Shift (ppm)	Description	Number of Protons	Assignment
1.25	multiplet	2	Either the axial or the equatorial protons on positions 3 and 6 of the cyclohexane ring
1.31	multiplet	2	Either the axial or the equatorial protons on positions 4 and 5 of the cyclohexane ring
1.66	multiplet	4	Position 4 of the pyrrolidine rings
1.73	multiplet	2	Either the equatorial or the axial protons on positions 4 and 5 of the cyclohexane ring
1.77	multiplet	2	Either the axial or the equatorial protons on position 3 of the pyrrolidine rings
1.92	broad singlet	2	Amine protons
2.01	mutliplet	2	Either the equatorial of the axial protons on positions 3 and 6 of the cyclohexane ring
2.11	multiplet	2	Either the equatorial or the axial protons on position 3 of the pyrrolidine rings
2.92	multiplet	4	Position 5 of the pyrrolidine rings
3.62	multiplet	2	Positions 1 and 2 of the cyclohexane ring
3.66	doublet of doublets	2	Position 2 of the pyrrolidine rings
7.59	broad singlet	2	Amide protons

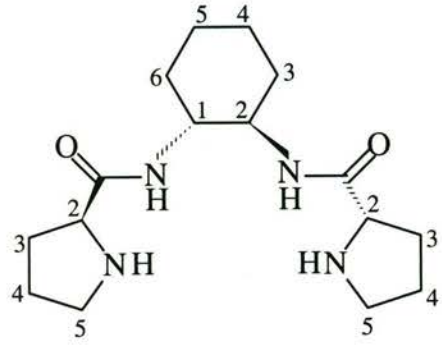

Figure 2.9 Atom numbering scheme for *R,R*-(*S,S*)-bprolchxnH_2 used in the assignment of the NMR spectra.

evidence that the amine protons were coupled to other protons in the molecule. The presence of the amine protons in the ^{1}H NMR spectrum and the absence of any aromatic protons were proof that the carbobenzoxy protecting groups had been successfully removed.

The resonances from the cyclohexane and pyrrolidine ring carbons were quite close together in the 20-35 ppm region, but it was possible to assign them by comparison to the ^{13}C NMR data for *S,S*-bprolenH_2 (Table 2.2) and *S,S*-bprolbenH_2 (Table 2.6). The ^{13}C NMR data for *S,S*-bprolenH_2 and *S,S*-bprolbenH_2 demonstrated that the chemical shifts of the pyrrolidine ring carbons were not significantly affected by the nature of the bridge linking the amide groups.

Table 2.4 ^{13}C NMR spectral data for *R,R*-(*S,S*)-bprolchxnH_2 in $CDCl_3$

Chemical Shift (ppm)	Assignment
24.8	Positions 4 and 5 of the cyclohexane ring
26.3	Position 4 of the pyrrolidine rings
30.8	Position 3 of the pyrrolidine rings
32.7	Positions 3 and 6 of the cyclohexane ring
47.2	Position 5 of the pyrrolidine rings
52.5	Positions 1 and 2 of the cyclohexane ring
60.6	Position 2 of the pyrrolidine rings
175.3	Carbonyl of the amide groups

The assignment of the ^{1}H and ^{13}C NMR spectra to the structure in Figure 2.9 showed, together with the microanalytical data, that the synthesis of *R,R*-(*S,S*)-bprolchxnH_2 was successful.

2.3.3.3 *S,S*-bprolbenH_2

The 1D ^{1}H NMR spectrum of *S,S*-bprolbenH_2 is shown in Figure 2.10 and the 2D COSY ^{1}H NMR spectrum is in Figure 2.11. The assignments of the ^{1}H and ^{13}C NMR spectra were made according to the atom numbering scheme in Figure 2.12. The assignment of the ^{1}H NMR spectra are in Table 2.5 and the ^{13}C NMR data and their assignment are in Table 2.6.

The ^{1}H NMR spectra of *S,S*-bprolbenH_2 displayed a complicated non-first-order coupling pattern for the protons of the pyrrolidine rings; the cross peaks in the 2D COSY spectra were used to assign the spectra. There were three tiny peaks in the 1.0-1.6 ppm region; these were due to low levels of impurities that were not removed by the flash chromatography.

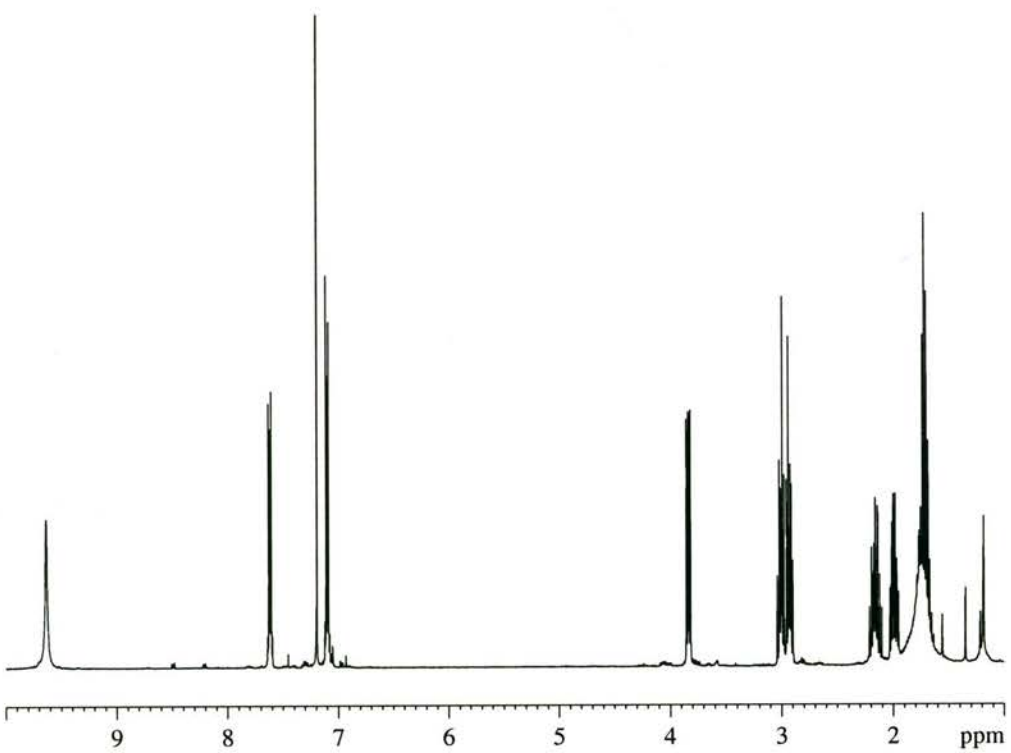

Figure 2.10 1D ^{1}H NMR spectra of *S,S*-bprolbenH_2 in $CDCl_3$. The residual solvent peak occurs at 7.19 ppm.

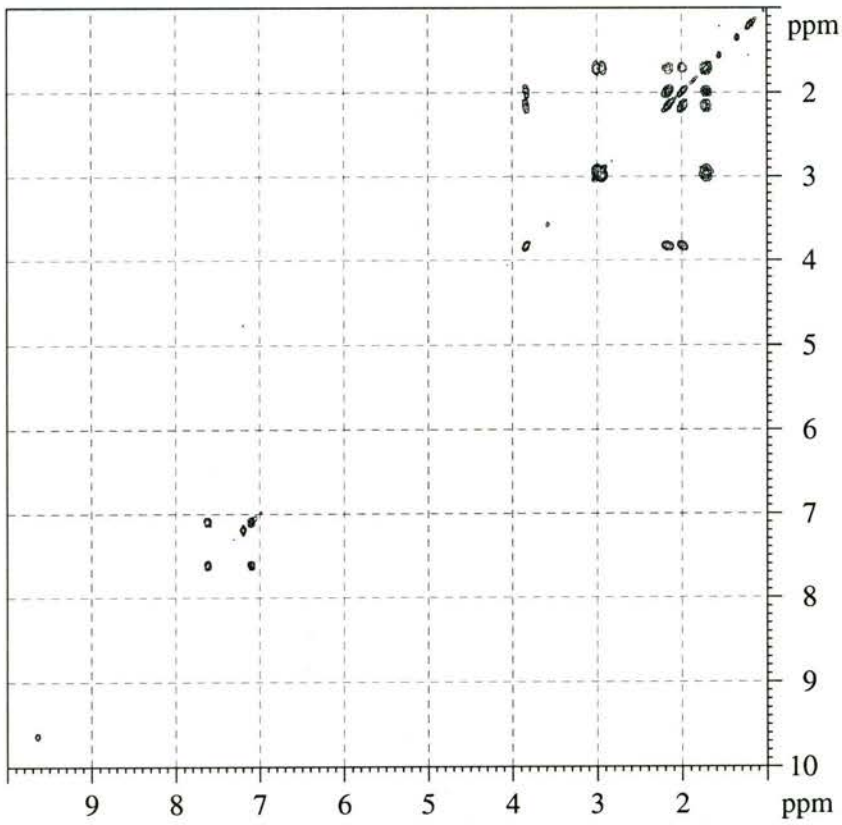

Figure 2.11 2D COSY ^{1}H NMR spectrum of *S,S*-bprolbenH_2 in $CDCl_3$. The residual solvent peak occurs at 7.19 ppm.

The resonance of the amide protons occurred further downfield than in the spectra of *S,S*-bprolenH_2 and *R,R*-(*S,S*)-bprolchxnH_2, which was due to the ring current effect of the benzene ring to which the amide N atoms are attached. The presence of the benzene ring did not have a significant effect on the chemical shifts of the resonances from the pyrrolidine rings. The axial and the equatorial protons on the pyrrolidine rings were not equivalent, but it was difficult to determine which of the resonances was due to the axial protons and which was due to the equatorial protons. The signal from the amine protons overlapped the signal from the protons on position 4 of the pyrrolidine ring and gave rise to the broad underlying feature at 1.72 ppm.

Table 2.5 Assignment of the ^{1}H NMR spectrum of *S,S*-bprolbenH_2

Chemical Shift (ppm)	Description	Number of Protons	Assignment
1.72	multiplet	6	The overlap of two signals: a multiplet from the four protons on position 4 of the pyrrolidine rings and a broad signal from the two amine protons.
2.00	multiplet	2	Either the axial or the equatorial protons on position 3 of the pyrrolidine rings
2.15	multiplet	2	Either the equatorial or the axial protons on position 3 of the pyrrolidine rings
2.96	multiplet	4	Position 5 of the pyrrolidine rings
3.84	doublet of doublets	2	Position 2 of the pyrrolidine rings
7.09	multiplet	2	Positions 4 and 5 of the benzene ring
7.62	multiplet	2	Positions 3 and 6 of the benzene ring
9.64	broad singlet	2	Amide protons

5 4

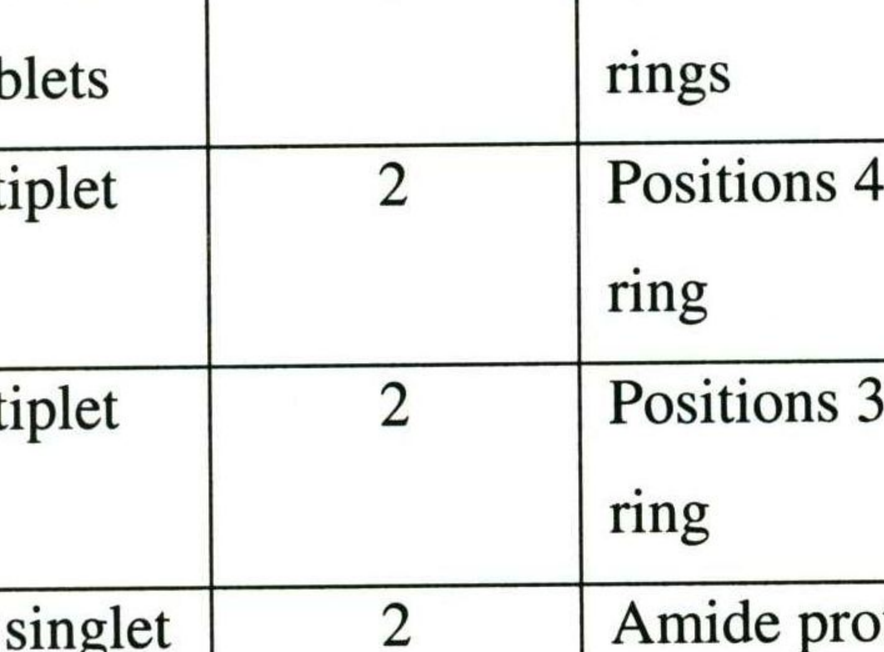

Figure 2.12 Atom numbering scheme for *S,S*-bprolbenH_2 used in the assignment of the NMR spectra

Table 2.6 ^{13}C NMR spectral data for *S,S*-bprolbenH_2 in $CDCl_3$

Chemical Shift (ppm)	Assignment
26.3	Position 4 of the pyrrolidine rings
30.9	Position 3 of the pyrrolidine rings
47.4	Position 5 of the pyrrolidine rings
61.1	Position 2 of the pyrrolidine rings
124.0	Positions 3 and 6 of the benzene ring
125.7	Positions 4 and 5 of the benzene ring
129.8	Positions 1 and 2 of the benzene ring
174.2	Carbonyl of the amide groups

The ^{1}H and ^{13}C NMR spectra were consistent with the structure in Figure 2.10 and together with the microanalytical data, it can be concluded that the synthesis of *S,S*-bprolbenH_2 was successful.

The signals from the pyrrolidine rings in the ^{1}H and ^{13}C NMR spectra of *S,S*-bprolenH_2, *R,R*-(*S,S*)-bprolchxnH_2, and *S,S*-bprolbenH_2 were very similar. The changes in the chemical shifts were slight and the coupling patterns of the protons on positions 2, 3 and 5 of the pyrrolidine rings essentially identical. This close similarity in the NMR spectra indicated that the structure of the pyrrolidine rings was not affected by the nature of the substituent on the amide N.

2.3.4 IR Spectra of Ligands

The characteristic peaks in the IR spectra of *S,S*-bprolenH_2, *R,R*-(*S,S*)-bprolchxnH_2, and *S,S*-bprolbenH_2 and their assignments are given in Table 2.7. The bands were assigned according to Bellamy[33] and by comparison to the assignments of the IR spectra of bpenH_2[9] and bpbH_2.[3]

There are only small variations in the positions of the amide N–H stretching band and the amide I, II and III bands between the three ligands. Several C–H stretching bands occur between 2800-3000 cm^{-1} and three of these bands are at approximately

Table 2.7 Characteristic IR bands of *S,S*-bprolenH_2, *R,R*-(*S,S*)-bprolchxnH_2, and *S,S*-bprolbenH_2

Wavenumber (cm^{-1})			Assignment
S,S-bprolenH_2,	*R,R*-(*S,S*)-bprolchxnH_2	*S,S*-bprolbenH_2	
3306	3315	3312	amide ν(N–H)
2965	2972	2969	ν(C–H)
2943	2935	2946	ν(C–H)
2860	2860	2915	ν(C–H)
2825		2869	ν(C–H)
1652	1637	1665	amide I band
		1594	aromatic ring skeletal vibration
1541	1523	1528	amide II band
1444	1456		C–H deformation
		1473	C–H deformation or aromatic ring skeletal vibration
1311	1297	1301	amide III band
691	695		amide V band

the same frequency in each ligand. The peaks at 3248 cm^{-1} in the spectrum of *R,R*-(*S,S*)-bprolchxnH_2 and 3254 cm^{-1} in the spectrum of *S,S*-bprolbenH_2 may be the amine N–H stretching bands. The IR spectra show that the syntheses of the three ligands with pyrrolidine rings were successful, confirming the results of the NMR spectroscopy.

2.4 Conclusion

The acyclic tetradentate ligands *S,S*-bprolenH_2, *R,R*-(*S,S*)-bprolchxnH_2, and *S,S*-bprolbenH_2 were synthesised and the identity of the products were confirmed by elemental analysis, and NMR and IR spectroscopies. This is the first time that these compounds have been isolated as pure solids and detailed characterisation

performed. Previous reports of *S,S*-bprolenH_2 only contained limited characterisation details and the spectral data reported were not completely assigned.

2.5 References

1) D. J. Barnes, R. L. Chapman, R. S. Vagg and E. C. Watton *J. Chem. Eng. Data* **1978**, *23*, 349-350.

2) R. R. Fenton, F. S. Stephens and R. S. Vagg *J. Coord. Chem.* **1991**, *23*, 291-311.

3) R. L. Chapman and R. S. Vagg *Inorg. Chim. Acta* **1979**, *33*, 227-234.

4) R. L. Chapman, F. S. Stephens and R. S. Vagg *Inorg. Chim. Acta* **1980**, *43*, 29-33.

5) R. L. Chapman, F. S. Stephens and R. S. Vagg *Acta Crystallogr., Sect. B* **1981**, *B37*, 75-79.

6) M. Mulqi, F. S. Stephens and R. S. Vagg *Inorg. Chim. Acta* **1981**, *53*, L91-L93.

7) M. Mulqi, F. S. Stephens and R. S. Vagg *Inorg. Chim. Acta* **1981**, *51*, 9-14.

8) F. S. Stephens and R. S. Vagg *Inorg. Chim. Acta* **1981**, *51*, 149-154.

9) D. J. Barnes, R. L. Chapman, F. S. Stephens and R. S. Vagg *Inorg. Chim. Acta* **1981**, *51*, 155-162.

10) M. Mulqi, F. S. Stephens and R. S. Vagg *Inorg. Chim. Acta* **1981**, *52*, 73-77.

11) R. L. Chapman, F. S. Stephens and R. S. Vagg *Inorg. Chim. Acta* **1981**, *52*, 161-168.

12) R. L. Chapman, F. S. Stephens and R. S. Vagg *Inorg. Chim. Acta* **1981**, *52*, 169-176.

13) M. Mulqi, F. S. Stephens and R. S. Vagg *Inorg. Chim. Acta* **1981**, *52*, 177-182.

14) F. S. Stephens and R. S. Vagg *Inorg. Chim. Acta* **1982**, *57*, 9-13.

15) F. S. Stephens and R. S. Vagg *Inorg. Chim. Acta* **1982**, *57*, 43-49.

16) M. Mulqi, F. S. Stephens and R. S. Vagg *Inorg. Chim. Acta* **1982**, *62*, 215-220.

17) M. Mulqi, F. S. Stephens and R. S. Vagg *Inorg. Chim. Acta* **1982**, *62*, 221-229.

18) M. Mulqi, F. S. Stephens and R. S. Vagg *Inorg. Chim. Acta* **1982**, *63*, 197-207.

19) F. S. Stephens and R. S. Vagg *Inorg. Chim. Acta* **1984**, *88*, 7-14.

20) F. S. Stephens and R. S. Vagg *Inorg. Chim. Acta* **1984**, *90*, 17-24.

21) F. S. Stephens and R. S. Vagg *Inorg. Chim. Acta* **1986**, *120*, 165-171.

22) F. S. Stephens and R. S. Vagg *Inorg. Chim. Acta* **1988**, *142*, 43-50.

23) M.-J. Jun and C. F. Liu *Inorg. Chem.* **1975**, *14*, 2310-2314.

24) M.-J. Jun and C. F. Liu *Inorg. Chim. Acta* **1975**, *15*, 111-116.

25) D. M. Segal and E. Hurwitz *Biochemistry* **1976**, *15*, 5253-5258.

26) R. R. Hill, J. D. Coyle, D. Birch, E. Cave, G. E. Jeffs, D. Randall, I. Stec and T. M. Stevenson *J. Am. Chem. Soc.* **1991**, *113*, 1805-1817.

27) R. P. Bonomo, E. Conte, R. Marchelli, A. M. Santoro and G. Tabbi *J. Inorg. Biochem.* **1994**, *53*, 127-138.

28) R. P. Bonomo, R. Marchelli and G. Tabbi *J. Inorg. Biochem.* **1995**, *60*, 205-218.

29) B.-W. Lee, J.-H. Park, D.-K. Son, B.-G. Kim, C.-E. Oh and M.-K. Doh *Bull. Korean Chem. Soc.* **1999**, *20*, 749-752.

30) A. Berger, J. Kurtz and E. Katchalski *J. Am. Chem. Soc.* **1954**, *76*, 5552-5554.

31) D. Ben-Ishai and A. Berger *J. Org. Chem.* **1952**, *17*, 1564-1570.

32) W. Bremser, L. Ernst, B. Franke, R. Gerhards and A. Hardt *Carbon-13 NMR Spectral Data*; Verlag Chemie: Weinheim, **1981**.

33) L. J. Bellamy *The Infra-red Spectra of Complex Molecules*; 2nd ed.; Methuen and Co. Ltd.: London, **1959**.

Chapter 3

Nickel Complexes with Tetradentate Diamide Ligands

3.1 Introduction

Vagg and coworkers have reported the synthesis and characterisation of Ni(II) complexes with the tetradentate diamides $bpenH_2$ and $bpbH_2$, where the ligands were in both protonated (LH_2) and deprotonated (L^{2-}) forms.[1,2] The protonation state of the ligand in the metal complexes depended upon the reaction conditions. The mixing of solutions of the ligand with solutions of Ni(II) chloride or Ni(II) nitrate produced complexes with the protonated ligands.[1,2] Conversely, to form complexes of the deprotonated ligands required more basic conditions. The use of Ni(II) acetate as the starting material gave the complex with the deprotonated ligand $[Ni^{II}(bpb)]$.[1] The addition of NaOH solution to the reaction mixture was necessary to form the complex $[Ni^{II}(bpen)]$.[2]

The UV-Vis spectral data and magnetic moments showed that the coordination geometry about the Ni in the complexes with the protonated ligands was octahedral.[1,2] A square-planar geometry (Figure 3.1) was predicted for complexes with the deprotonated ligands,[1,2] and observed in the X-ray crystal structures of $[Ni^{II}(bpen)]$[3] and $[Ni^{II}(bpb)]$.[4] Deprotonated amide Ns are strong-field ligands and stabilise low-spin square-planar Ni(II) complexes.

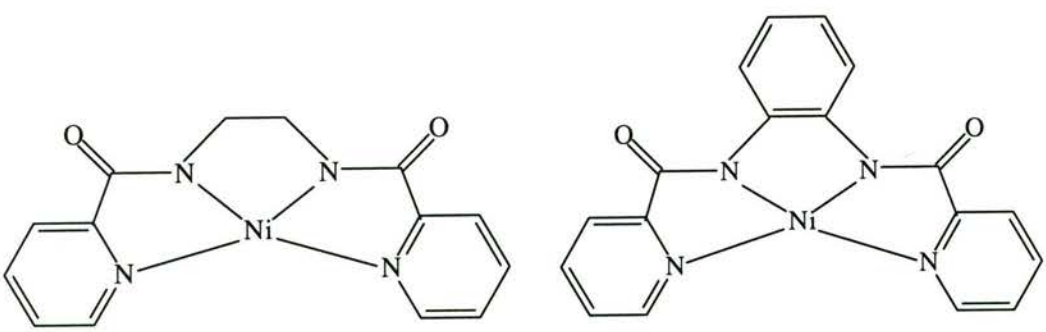

(a) (b)

Figure 3.1 Molecular structures of (a) $[Ni^{II}(bpen)]$ and (b) $[Ni^{II}(bpb)]$

Coordination of deprotonated amide N is known to stabilise the higher oxidation states of transition metals;[5] therefore, the Ni(II) complexes with bpen, bpb and the analogous pyrrolidine-based ligands were synthesised in this work. It was anticipated that they would stabilise Ni(III) and the pyrrolidine ligands could be used

in studies of the enantioselectivity of DNA damage in relation to the potential role of Ni(III)-peptides in Ni-induced cancer.

3.2 Experimental

3.2.1 Synthesis of Ni(II) complexes

3.2.1.1 [Ni^{II}(bpen)]

This complex was synthesised according to the method of Barnes, *et al.*[2] Nickel(II) acetate (0.46 g, Merck, LR) was dissolved in water (15 mL) by heating on a steam bath. The hot solution of Ni(II) acetate was added to a solution of $bpenH_2$ in boiling ethanol (25 mL). The solution was further heated and then water (20 mL) was added. Sodium hydroxide solution (~8 mL, 1 M) was added dropwise to the hot solution until the pH value was ~11. The heating of the solution was ceased and it was cooled in an ice bath. The precipitate was collected at the pump and the residue was washed with ice-cold water (2 × 5 mL), and ethanol (5 mL), and air dried. The product was dried under reduced pressure over silica gel to give a bright yellow coloured powder. Yield: 0.498 g (82%). The product was recrystallised from methanol for use in subsequent experiments. IR (DRIFTS in KBr; cm^{-1}): 1633 (ss); 1604 (ss); 1418 (m); 755 (m); 685 (m). Lit.: 1630 (s); 1420 (m). UV-Vis (CH_3OH) λ_{max} (ε): 256 nm (1.5×10^4 M^{-1} cm^{-1}), 382 nm (7.4×10^3 M^{-1} cm^{-1}).

3.2.1.2 [Ni^{II}(bpb)]

This complex was synthesised according to the method of Chapman and Vagg.[1] Nickel(II) acetate (0.40 g, Merck, LR) was dissolved in hot water (20 mL). A solution of $bpbH_2$ (0.51 g) in hot ethanol (15 mL) was added to the nickel solution and an orange-coloured precipitate formed immediately. The mixture was covered with a watch glass and heated on a steam bath for 50 min. The solution was cooled to room temperature and the precipitate was collected at the pump. The residue was washed with water (2 × 10 mL), followed by ethanol (~2 mL). Finally, it was air dried, then dried over silica gel under reduced pressure. The product was a dark, orange-coloured powder. Yield: 0.583 g (97%). The product was recrystallised from *N,N*-dimethylformamide (DMF) for use in subsequent experiments. IR (DRIFTS in KBr; cm^{-1}): 1639 (ss); 1604 (ss); 1576 (m); 1485 (m); 1398 (m); 745 (ss); 680 (m).

Lit.: 1640 (ss); 1605 (ss); 1570 (m); 1485 (m); 1390 (m); 750 (m); 680 (m). UV-Vis (DMF) λ_{max} (ε): 324 nm (1.9×10^4 M^{-1} cm^{-1}), 372 nm (sh, 8.1×10^3 M^{-1} cm^{-1}), 446 nm (sh, 3.1×10^3 M^{-1} cm^{-1}).

3.2.1.3 $[Ni^{II}(bprolenH_{-4})].H_2O$

Method 1

Nickel(II) acetate tetrahydrate (0.196 g, Merck, LR) was dissolved in water (15 mL) and *S,S*-bprolenH_2 (0.200 g) was added. The green-coloured solution was heated on a steam bath then allowed to evaporate slowly. The non-crystalline residue thus formed was dissolved in water (~5 mL), further heated, and NaOH solution (1 M) was added dropwise until the colour of the solution changed to orange. The solution was filtered and the filtrate was left to evaporate slowly. Small yellow needle-like crystals formed over several days and were collected at the pump and dried under reduced pressure over silica gel. The product was recrystallised from methanol. Yield: 0.0073 g (3%). ^{1}H NMR (CD_3OD): ppm; 2.09 (q, 4H); 2.71 (m, 4H); 3.24 (s, 4H); 3.77 (m, 4H). IR (DRIFTS in KBr; cm^{-1}): 3479 (m, br); 2940 (m); 2847 (m); 1627 (ss); 1612 (ss); 1411 (m); 1328 (m); 1032 (m); 508 (m). Calculated for $C_{12}H_{18}N_4O_3Ni$: C, 44.34%; H, 5.58%; N, 17.24%. Found: C, 44.39%; H, 5.53%; N, 17.01%.

Method 2

Nickel(II) acetate tetrahydrate (0.196 g, Merck, LR) was dissolved in water (10 mL) and a solution of *S,S*-bprolenH_2 (0.208 g) in water (10 mL) was added. The pH value was raised to ~8 by the addition of $NaHCO_3$ solution (10 mL, 1 M) and a fine precipitate started to form. Sodium carbonate (20 mL, 1 M) was added to raise the pH value to ~10, and this resulted in the precipitation of a large amount of fine solid. The mixture was heated on a steam bath for an hour to dissolve most of the solid and the colour changed from green-yellow to bright yellow. The mixture was filtered, and the pH value of the filtrate was ~10. Slow evaporation of the filtrate gave tiny needle-like yellow-coloured crystals, which were collected at the pump, washed with ice-cold water (2×2 mL), and dried under reduced pressure over silica gel. A second crop formed in the filtrate and washings; it was collected at the pump, washed with water (~2 mL), and recrystallised from methanol. Yield: 0.055 g (22%).

^{1}H NMR (CD_3OD): ppm; 2.09 (m, 4H); 2.71 (m, 4H); 3.24 (s, 4H); 3.78 (m, 4H). UV-Vis (CH_3OH) λ_{max} (ε): 242 nm (sh, 6.8×10^3 M^{-1} cm^{-1}), 382 nm (8.3×10^3 M^{-1} cm^{-1}), 424 nm (sh, 3.3×10^3 M^{-1} cm^{-1}).

3.2.1.4 [Ni^{II}(*S,S*-bprolen)].H_2O

The syntheses were carried out using Schlenk techniques under an Ar atmosphere. All solvents and prepared solutions were degassed thoroughly before use by repeated evacuation followed by purging with Ar (BOC Gases, high purity).

Method 1

Nickel(II) acetate tetrahydrate (0.196 g, Merck, LR) was dissolved in water (10 mL) and a solution of *S,S*-bprolenH_2 (0.203 g) in water (10 mL) was added. A NaOH solution (3 mL, 0.4 M) was added and the solutions were mixed thoroughly. The water was evaporated under reduced pressure, and the residue was dissolved in methanol (30 mL, Prolabo, AR) and filtered. The filtrate was evaporated under reduced pressure, and the residue was dissolved in methanol (20 mL, Prolabo, AR) and filtered. Methanol (Prolabo, AR) was added to the filtrate to increase the volume to ~40 mL and acetonitrile (15 mL, Ajax, AR) was added. Slow evaporation of the methanol/acetonitrile solution over a period of several days under Ar did not produce crystals, so diethyl ether (15 mL) was added and the mixture was allowed to stand for a further 2 d. The supernatant was decanted, leaving orange-coloured crystals that were washed with methanol/acetonitrile in a 1:5 ratio (12 mL) and dried under reduced pressure to give a yellow-coloured powder. Yield: 0.055 g (21%). ^{1}H NMR (CD_3OD): ppm; 1.6-1.9 (m, 4H); 1.9-2.2 (m, 4H); 2.81 (m, 2H); 2.98 (s, 4H); 3.2-3.4 (m, 2H); 3.61 (m, 2H); 4.37 (q, 2H). IR (DRIFTS in KBr; cm^{-1}): 3092 (m, br); 2955 (m); 2881 (m); 2867 (m); 1599 (ss); 1449 (w); 1425 (m); 1317 (w); 1222 (w); 1071 (w); 1051 (w); 1005 (w); 934 (m); 765 (w); 512 (w). Calculated for $C_{22}H_{22}N_4O_3Ni$: C, 43.67%; H, 6.71%; N, 16.98%. Found: C, 43.25%; H, 6.49%; N, 16.76%.

Method 2

Nickel(II) chloride hexahydrate (0.279 g, Merck, LR) was dissolved in water (10 mL) and a solution of *S,S*-bprolenH_2 (0.311 g) in water (10 mL) was added. NaOH solution (10 mL, 1 M) was added and the solutions were mixed thoroughly. The

water was evaporated under reduced pressure, the residue was dissolved in methanol (25 mL) and filtered. The filtrate was evaporated under reduced pressure, the residue was dissolved in methanol (20 mL) and filtered. The filtrate was evaporated under reduced pressure and the residue was removed from the Ar atmosphere. The remainder of the synthesis was carried out in air. The residue was dissolved in methanol (15 mL) and loaded onto a LH20 lipophilic Sephadex column (2.5 × 14 cm) and the complexes were eluted with methanol. A major fast moving yellow band and a minor, slower moving light orange band were eluted. The faster moving yellow band was collected and slowly evaporated to dryness. The residue was recrystallised from methanol yielding light orange crystals. Yield 0.188 g (49%). ^{1}H NMR (DMSO-d_6): ppm; 1.5-1.8 (m, 4H); 1.8-2.1 (m, 4H); 2.69 (m, 2H); 2.75 (s, 4H); 3.14 (m, 2H); 3.5 (m, 2H); 4.40 (q, 2H). UV-Vis (CH_3OH) λ_{max} (ε): 252 nm (sh, 7.9×10^3 M^{-1} cm^{-1}), 380 nm (3.9×10^2 M^{-1} cm^{-1}).

3.2.1.5 [Ni^{II}(*R,R*-(*S,S*)-bprolchxn)].2·5H$_2$O

Nickel(II) acetate tetrahydrate (0.203 g, Merck, LR) was dissolved in water (10 mL) by heating on a steam bath. The ligand (0.252 g) dissolved in water (10 mL) was added to the Ni(II) acetate solution. Sodium hydroxide solution (3 mL, 1 M) was added and the solution changed colour from green to yellow. The solution was filtered, and the filtrate was left to evaporate slowly. Orange crystals formed in the filtrate and were collected at the pump, washed with water (2 × ~5 mL), and dried under reduced pressure. A second crop of crystals was obtained from the filtrate and washings. Yield: 0.165 g (50%). The product was recrystallised from methanol. ^{1}H NMR (CD_3OD): ppm; 1.15 (m, 4H); 1.54 (m, 2H); 1.65 (m, 2H); 1.91 (m, 4H); 2.03 (m, 2H); 2.76 (m, 2H); 2.87 (m, 4H); 3.23 (m, 2H); 3.65 (t, 2H); 4.17 (q, 2H). UV-Vis (CH_3OH) λ_{max} (ε): 238 nm (1.4×10^4 M^{-1} cm^{-1}), 418 nm (2.3×10^2 M^{-1} cm^{-1}). IR (DRIFTS in KBr; cm^{-1}): 3439 (w, br); 3364 (w, br); 3106 (m, br); 2981 (w); 2971 (w); 2934 (m); 2903 (w); 2870 (m); 2855 (w); 2839 (w); 1611 (m); 1575 (ss); 1444 (m); 1417 (m); 1343 (m); 1297 (w); 1238 (w); 932 (m); 513 (w). Calculated for $C_{16}H_{31}N_4O_{4.5}Ni$: C, 46.86%; H, 7.62%; N, 13.66%. Found: C, 47.14%; H, 7.60%; N, 13.42%.

3.2.1.6 [Ni^{II}(*S,S*-bprolben)].2H_2O

Nickel(II) acetate tetrahydrate (0.167 g, Merck, LR) was dissolved in water (10 mL) by heating on a steam bath. A solution of *S,S*-bprolbenH_2 (0.204 g) in methanol (10 mL) was added to the hot Ni(II) acetate solution. The colour of the solution changed immediately from green to orange. The product crystallised as the solution cooled, and was collected at the pump after the mixture had stood for 2 d. The dark yellow, crystalline product was washed with ice-cold water (5 mL), air dried, then dried under reduced pressure over silica gel. Yield: 0.182 g (69%). ^{1}H NMR (CD_3OD): ppm; 1.75 (m, 2H); 1.96 (m, 2H); 2.15 (m, 4H); 2.89 (m, 2H); 3.45 (m, 2H); 3.72 (m, 2H); 4.51 (q, 2H); 6.71 (dd, 2H); 8.08 (dd, 2H). UV-Vis (CH_3OH) λ_{max} (ε): 216 nm (3.1×10^4 M^{-1} cm^{-1}), 244 nm (sh, 1.3×10^4 M^{-1} cm^{-1}), 274 nm (1.5×10^4 M^{-1} cm^{-1}), 294 nm (1.7×10^4 M^{-1} cm^{-1}), 416 nm (2.1×10^2 M^{-1} cm^{-1}). IR (DRIFTS in KBr; cm^{-1}): 3456 (w, br); 3248 (w); 3117 (w, br); 2972 (w); 2872 (w); 1605 (ss); 1569 (ss); 1481 (m); 1454 (m); 1403 (m); 1033 (w); 755 (m); 543 (w). Calculated for $C_{16}H_{24}N_4O_4Ni$: C, 48.63%; H, 6.12%; N, 14.18%. Found: C, 49.11%; H, 5.23%; N, 14.45%.

3.2.2 X-ray Crystallography

All data were collected and structures were solved by Dr Peter Turner at the Small Molecule Crystallography Facility, University of Sydney. The details of the data collection and structure solutions for the compounds below are given in Appendix 1.

3.2.2.1 [Ni^{II}(bprolenH_4)].H_2O

Slow evaporation of a methanol solution of the product from Method 1 produced orange crystals of suitable quality for X-ray diffraction studies.

3.2.2.2 [Ni^{II}(*S,S*-bprolen)].H_2O

The recrystallisation of the product from methanol using Method 2 afforded crystals suitable for X-ray diffraction studies.

3.2.2.3 [Ni^{II}(*R,R*-(*S,S*)-bprolchxn)].3H_2O

Slow evaporation of a methanol/acetonitrile solution of the product produced crystals suitable for X-ray crystallography.

3.2.3.4 [Ni^{II}(*S,S*-bprolben)].D_2O.CD_3OD

A CD_3OD solution of the complex prepared for NMR spectroscopy with 3 drops of D_2O added was left standing in a sealed NMR tube for 2 weeks. Yellow crystals suitable for X-ray crystallography formed during this time.

3.2.3 Analysis and Instrumentation

1D ^1H NMR spectra were recorded on a Bruker AC200 NMR spectrometer. Other 1D ^1H NMR and 2D COSY ^1H NMR spectra were recorded on a Bruker AMX400 NMR spectrometer. The samples of the complexes were dissolved in CD_3OD or DMSO-d_6, in some experiments a few drops of D_2O were added to identify labile protons. The spectra were referenced against the internal standard TMS. The ^{13}C NMR spectra were recorded on a Bruker AC 200 NMR spectrometer or a Bruker AMX400 NMR spectrometer. The samples were dissolved in CD_3OD or DMSO-d_6. The spectra were referenced against the internal standard TMS or the solvent resonance.

The IR spectra of the complexes were recorded by the DRIFTS technique on a Bio Rad FTS-40 spectrophotometer. KBr was used as the matrix and background for spectra recorded in the range from 400-4000 cm^{-1}.

Cyclic voltammetry was carried out using a BAS 100B Electrochemical Analyzer controlled by BAS 100W software. The complexes were dissolved in *N,N*-dimethylformamide (DMF) (Ajax, HPLC grade) or distilled water with 0.10 M tetra(*n*-butyl)ammonium perchlorate (TBAP) (Fluka, electrochemistry grade) or $NaClO_4$ (Aldrich, 99.99%), respectively, as the supporting electrolytes. A three-electrode system with a glassy-carbon working electrode, a Ag/AgCl reference electrode and a Pt wire auxiliary electrode was used. Full *iR* compensation was applied for all scans. The ferrocenium/ferrocene ($Fc^{+/0}$) couple was used as an internal redox potential standard for the DMF solutions.

UV-Visible spectra were recorded on a Hewlett Packard 8452A diode array spectrophotometer using a 1 cm path length quartz cell. The complexes were

dissolved in DMF (Ajax, HPLC grade) or methanol (APS Finechem, 99.8%) and the solvent was used as the blank.

3.3 Results and Discussion

3.3.1 Synthesis and Characterisation of Ni(II) Complexes

3.3.1.1 [Ni^{II}(bprolenH$_{-4}$)] and [Ni^{II}(S,S-bprolen)]

Two different complexes, [Ni^{II}(bprolenH$_{-4}$)] and [Ni^{II}(*S,S*-bprolen)], were obtained from the reaction of *S,S*-bprolenH$_2$ with Ni(II), depending on the conditions under which the reaction took place (Scheme 3.1).

Initially the reaction of Ni(II) and *S,S*-bprolenH$_2$ was carried out in the air. The synthesis of the Ni(II) complex with *S,S*-bprolenH$_2$ required the addition of base to deprotonate the amide N atoms, enabling them to coordinate to the Ni. The acetate from the starting Ni(II) salt did not raise the pH value sufficiently to deprotonate the amide N atoms, and no solid product could be isolated without the addition of base. The addition of hydroxide solution raised the pH value sufficiently for coordination

Scheme 3.1 Synthesis of Ni(II) complexes with *S,S*-bprolen

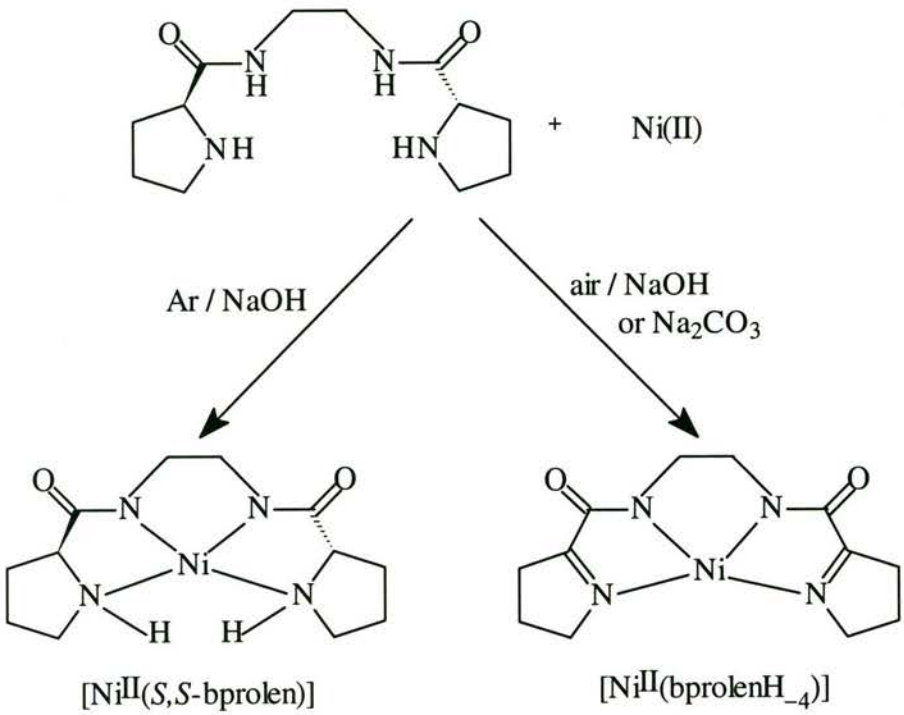

via deprotonated amide N to occur. The use of carbonate solution instead of hydroxide solution also achieved deprotonated amide N coordination and produced a higher yield. When the carbonate solution was added (Method 2) a large amount of precipitate, that was presumed to be Ni(II) carbonate, formed. The precipitate gradually dissolved as the ligand coordinated to the Ni, forming a soluble yellow complex. The ability of *S,S*-bprolenH_2 to facilitate the dissolution of Ni(II) carbonate by complexing the Ni shows the high affinity of Ni for the ligand with deprotonated amide N atoms.

During the aerobic synthesis, however, the two amine groups of the ligand were oxidised to imine groups. This occurred when either hydroxide or carbonate was used as the base to deprotonate the amide N atoms. The oxidation of the amine groups was not expected, but was evident in the crystal structure. The most significant feature of the crystal structure (Figure 3.2) are the N1–C4 and N4–C9 bond lengths (Table 3.1) of 1.281(5) Å and 1.285(5) Å, respectively, which show that these are N–C double bonds. The sp^2 hybridisation of N1 and N4 is also shown by their trigonal planar geometry. Four protons have been lost from N1, C4, N4, and C9 in going from the free ligand to the complex. The heterocyclic rings were changed from pyrrolidine to 1-pyrroline rings by the formation of the C–N double bonds. The formation of the double bonds made the terminal groups of the ligand planar 1-pyrroline rings (Planes 2 and 3 in Table 3.2), while pyrrolidine rings are usually puckered. The 1-pyrroline rings are almost coplanar with the plane defined by the four nitrogen atoms, the dihedral angles are 6.99° and 4.14°. The angle between the two 1-pyrroline rings is 11.11°.

The crystal structure of [Ni^{II}(bprolenH_{-4})] shows the nickel coordination geometry is square-planar, with two Ni–N(amide) and two Ni–N(imine) bonds. The Ni atom lies almost in the plane (0.034 Å above) defined by the four N atoms (Plane 1 in Table 3.2). The sum of the four angles around the Ni atom is 360.0° (Table 3.3), another indicator of the planarity of the coordination around the Ni.

As expected, the amide N atoms are deprotonated. This is consistent with the Ni–N(amide) bond lengths of 1.835(3) Å and 1.827(3) Å, which are within the range

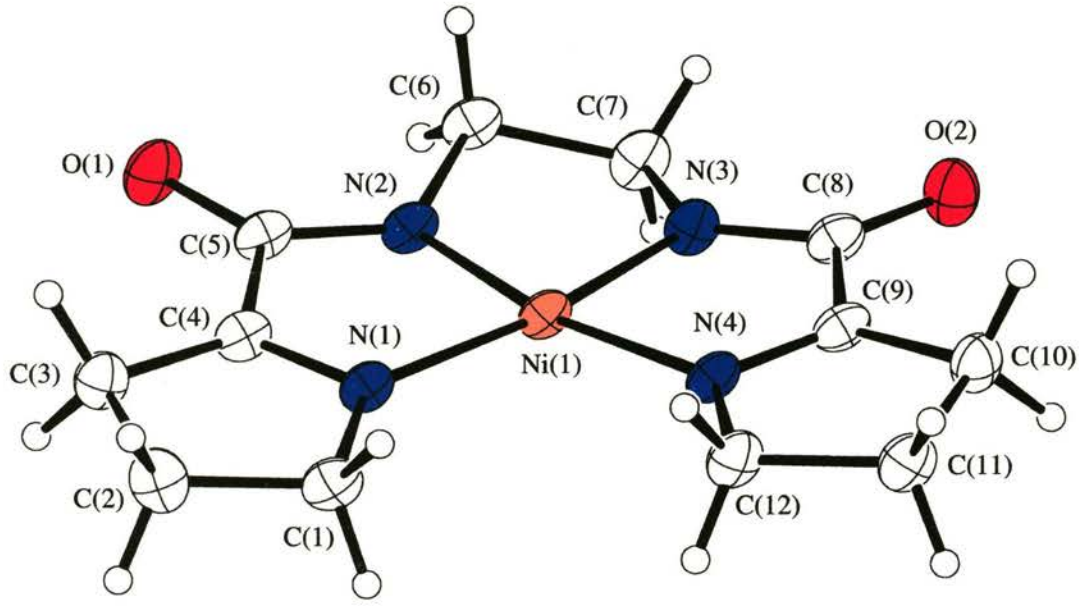

Figure 3.2 ORTEP[12] representation with 25% probability thermal ellipsoids of the complex in the crystals of $[Ni^{II}(bprolenH_{-4})].H_2O$

Table 3.1 Bond lengths from the crystal structure of $[Ni^{II}(bprolenH_{-4})]$ involving the non-hydrogen atoms[a]

atom–atom	distance (Å)	atom–atom	distance (Å)
Ni1–N1	1.893(3)	N4–C9	1.285(5)
Ni1–N2	1.835(3)	N4–C12	1.466(5)
Ni1–N3	1.827(3)	C1–C2	1.526(6)
Ni1–N4	1.898(3)	C2–C3	1.534(6)
O1–C5	1.243(5)	C3–C4	1.470(5)
O2–C8	1.230(5)	C4–C5	1.508(5)
N1–C1	1.478(4)	C6–C7	1.515(6)
N1–C4	1.281(5)	C8–C9	1.524(5)
N2–C5	1.325(5)	C9–C10	1.481(6)
N2–C6	1.461(4)	C10–C11	1.537(6)
N3–C7	1.470(5)	C11–C12	1.529(6)
N3–C8	1.316(5)		

[a] The estimated standard deviations in the least significant figure are in parentheses.

Table 3.2 Least-squares planes in $[Ni^{II}(bprolenH_{-4})]^a$

Plane 1	
atoms defining plane	distance from plane (Å)
N1	0.016(3)
N2	−0.021(3)
N3	0.027(3)
N4	−0.017(3)
additional atoms	
Ni1	0.034
Plane 2	
atoms defining plane	distance from plane (Å)
N1	−0.006(3)
C1	0.008(3)
C2	−0.005(5)
C3	−0.002(4)
C4	0.006(4)
additional atoms	
Ni1	−0.108
C5	−0.012
Plane 3	
atoms defining plane	distance from plane (Å)
N4	0.009(3)
C9	0.006(4)
C10	−0.035(5)
C11	0.040(4)
C12	−0.034(4)
additional atoms	
Ni1	−0.067
C8	0.031

[a] The estimated standard deviations in the least significant figure are in parentheses.

(1.820-2.02 Å) reported for Ni–N(amide) in other complexes.[3,4,6-11] The Ni–N(imine) bond lengths of 1.893(3) Å and 1.898(3) Å are also within the range

(1.840-2.065 Å) reported in the crystal structures of other complexes.[13-19] The Ni–N(amide) bonds are shorter and stronger than the Ni–N(imine) bonds because of the negative charge on the amide N atoms.

The average amide C–N bond length of 1.321 Å indicates a high degree of double-bond character, which is attributed to the predominance of the resonance structure shown in Figure 1.2 (a). The sums of the angles (Table 3.3) around N2 and N3 are 358.0(7)° and 359.7(8)°, respectively. This shows that they are almost planar, with

Table 3.3 Bond angles from the crystal structure of $[Ni^{II}(bprolenH_{-4})].H_2O$ involving the non-hydrogen atoms[a]

atom–atom–atom	angle (°)	atom–atom–atom	angle (°)
N1–Ni1–N2	84.5(1)	C1–C2–C3	105.6(3)
N1–Ni1–N3	169.1(1)	C2–C3–C4	102.8(3)
N1–Ni1–N4	106.5(1)	N1–C4–C3	115.7(4)
N2–Ni1–N3	84.7(1)	N1–C4–C5	115.5(4)
N2–Ni1–N4	168.5(1)	C3–C4–C5	128.8(3)
N3–Ni1–N4	84.3(1)	O1–C5–N2	129.0(4)
Ni1–N1–C1	136.3(3)	O1–C5–C4	121.4(4)
Ni1–N1–C4	113.2(3)	N2–C5–C4	109.6(3)
C1–N1–C4	110.4(3)	N2–C6–C7	106.8(3)
Ni1–N2–C5	116.7(2)	N3–C7–C6	107.7(3)
Ni1–N2–C6	117.7(3)	O2–C8–N3	129.3(4)
C5–N2–C6	123.6(3)	O2–C8–C9	122.7(4)
Ni1–N3–C7	116.7(3)	N3–C8–C9	107.9(3)
Ni1–N3–C8	118.8(3)	N4–C9–C8	116.3(3)
C7–N3–C8	124.2(3)	N4–C9–C10	115.3(3)
Ni1–N4–C9	112.6(2)	C8–C9–C10	128.4(4)
Ni1–N4–C12	136.5(3)	C9–C10–C11	102.6(3)
C9–N4–C12	110.7(3)	C10–C11–C12	105.2(3)
N1–C1–C2	105.5(3)	N4–C12–C11	105.9(3)

[a] The estimated standard deviations in the least significant figure are in parentheses.

only a slight tetrahedral distortion. This planarity can also be attributed to the double-bond character of the amide C–N bond.

The angles around the Ni atom deviate from the ideal value of 90° for a square-planar complex. The three chelate rings form angles of 84.5(1)°, 84.3(1)°, and 84.7(1)° about the nickel atom. The larger N1–Ni–N4 angle of 106.5(1)° compensates for the smaller angles enforced about the nickel by the chelate rings.

The ^{1}H NMR spectrum of [Ni^{II}(bprolenH$_{-4}$)] in Figure 3.3 is much simpler than that of the free ligand *S,S*-bprolenH$_2$ (Figure 2.4). There are only four signals, and their assignments are given in Table 3.4. The individual proton-proton couplings were determined along with the coupling constants by selective decoupling experiments (Appendix 2). The resonances at 2.71 ppm and 3.76 ppm are triplets of triplets; the stronger coupling is to the two protons on position 4 of the 1-pyrroline ring, while the weaker triplet splitting is due to coupling to each other. The resonance at

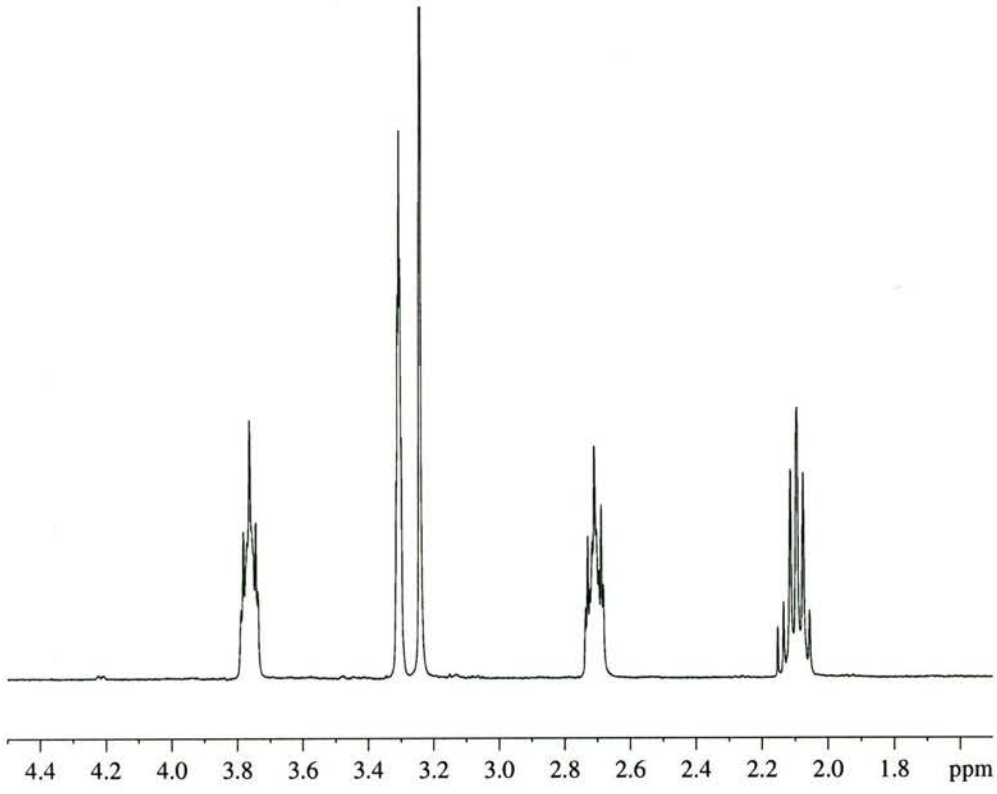

Figure 3.3 1D ^{1}H NMR spectrum of [Ni^{II}(bprolenH$_{-4}$)] in CD_3OD. The residual solvent peak occurs at 3.31 ppm.

Table 3.4 ^{1}H NMR spectral data for [Ni^{II}(bprolenH$_{-4}$)]

Chemical Shift (ppm)	Description	Number of Protons	Assignment
2.09	quintet	4	position 4 on the 1-pyrroline rings
2.71	triplet of triplets	4	position 3 on the 1-pyrroline rings
3.24	singlet	4	central ethylene bridge
3.76	triplet of triplets	4	position 5 on the 1-pyrroline rings
Coupling constant (Hz)	$J_{34} = 8.0$	$J_{35} = 2.4$	$J_{45} = 7.6$

2.09 ppm is a quintet as the coupling to the two protons on position 3 of the 1-pyrroline ring and the coupling to the two protons on position 5 of the 1-pyrroline ring are approximately equal, so there are four "equivalent" neighbours.

The assignments of the ^{13}C NMR data are contained in Table 3.5. The NMR spectra show that the complexes remain square-planar in solution and there is no evidence of paramagnetic five- or six-coordinate species.

The IR spectral data and their assignments for [Ni^{II}(bprolenH$_{-4}$)] are listed in Table 3.6. The absence of the amide N–H stretch and the amide II band confirm the deprotonation of the amide N on coordination. The band at 1612 cm^{-1} is tentatively assigned to the imine ν(C=N) stretch. The amide II and amide III bands of the free ligand (which are combinations of δ(N–H) and ν(C–N)) are replaced by the band at 1411 cm^{-1} (due to amide ν(C–N)) in the spectrum of the complex.[2] The IR spectrum is consistent with the structure of the complex as determined by X-ray crystallography and NMR spectroscopy.

The NMR and IR spectral data demonstrate that the bulk product from the reaction of *S,S*-bprolenH$_2$ with Ni(II) in the presence of air has the same structure as that in the

Table 3.5 ^{13}C NMR spectral data for [Ni^{II}(bprolenH$_{-4}$)] in DMSO-d_6

Chemical Shift (ppm)	Assignment
20.3	Position 4 on the 1-pyrroline rings
32.7	Position 3 on the 1-pyrroline rings
48.0	Position 5 on the 1-pyrroline rings
57.9	Central ethylene bridge
164.6	Imine carbons, position 2 on the 1-pyrroline rings
177.4	Carbonyl groups

Table 3.6 Characteristic IR bands of [Ni^{II}(bprolenH$_{-4}$)]

Wavenumber (cm^{-1})	Assignment
2940	ν(C–H)
2847	ν(C–H)
1627	amide I band
1612	imine ν(C=N)
1411	amide ν(C–N)

crystal used in the determination of the X-ray crystal structure. To investigate how the amine groups of the ligand were being dehydrogenated, the reaction was carried out in the absence of O_2.

When the reaction of Ni(II) acetate and *S,S*-bprolenH$_2$ was carried out under Ar using Schlenk techniques, the complex, [Ni^{II}(*S,S*-bprolen)], with the unoxidised ligand was obtained. Once the base used to deprotonate the amide groups and water had been removed, the product can be handled in the air as a solid without significant decomposition or ligand oxidation. The methanol solution of the complex is also air-stable, a CD_3OD solution was exposed to the air and its stability was monitored by ^1H NMR spectroscopy. After one month, no [Ni^{II}(bprolenH$_{-4}$)] or other decomposition products were detected. Once the stability of the complex in methanol solution had been established, the purification of crude product in Method 2 could be carried out in the air using column chromatography, greatly improving the yield. The crystal used to determine the structure by X-ray diffraction was obtained by slow evaporation under atmospheric conditions of a methanol solution.

The molecular structure of [Ni^{II}(*S,S*-bprolen)] as determined by X-ray crystallography (Figure 3.4), has a two-fold symmetry axis through the metal atom. The non-hydrogen bond lengths and non-hydrogen bond angles are given in Tables 3.7 and 3.8, respectively. The crystal structure showed that the amines in the pyrrolidine rings of the ligand were preserved during the formation of the complex. The N1–C4 bond length is 1.503(4) Å, and the geometries about N1 and C4 are tetrahedral. The amine N atoms are chiral and both have the *S* configuration. The Ni atom is coordinated to two deprotonated amide N atoms and two amine N atoms in square-planar geometry (Table 3.9). The pyrrolidine rings of the ligand are non-planar and are at a ~60° angle to the coordination plane.

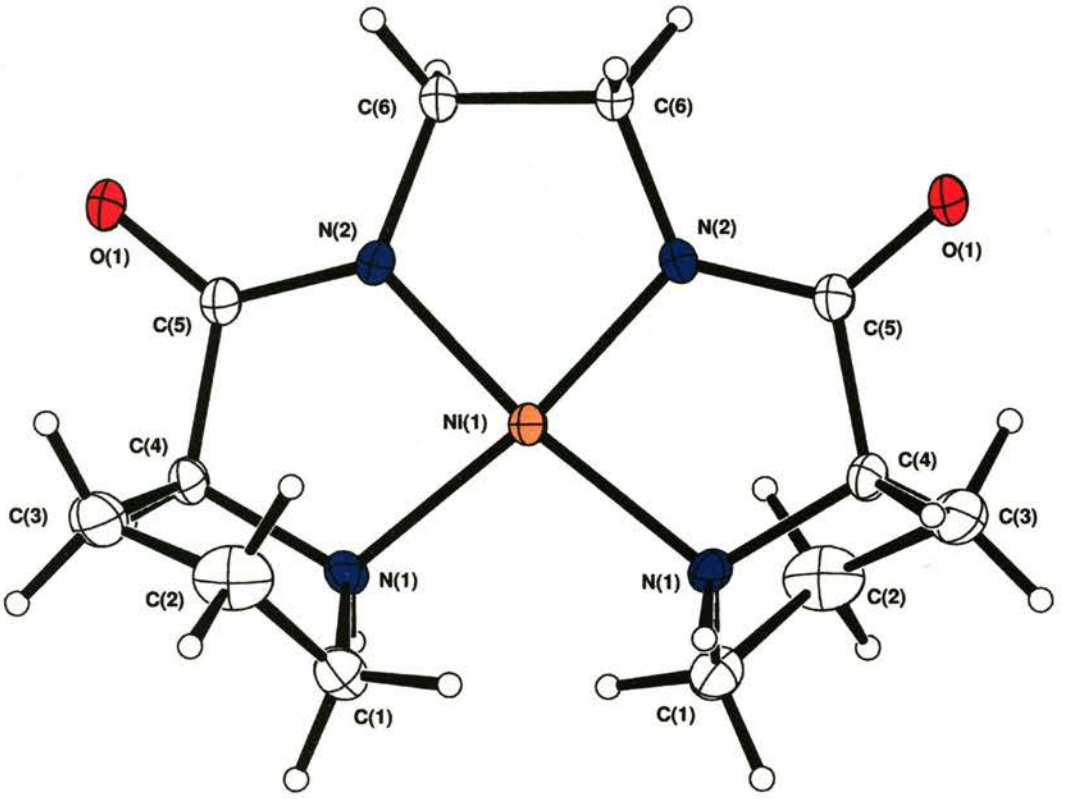

Figure 3.4 ORTEP[12] representation with 25% probability thermal ellipsoids of the complex in the crystals of [Ni^{II}(*S,S*-bprolen)].H_2O.

The Ni–N(amide) bond length of 1.822(2) Å is significantly shorter than the Ni–N(amine) bond length of 1.925(2) Å, and indicates deprotonated amide coordination. The Ni–N(amide) bond length is slightly, but not significantly, shorter than the average value in [Ni^{II}(bprolenH_{-4})], and the Ni–N(amine) bond length is

Table 3.7 Bond lengths from the crystal structure of [Ni^{II}(*S,S*-bprolen)] involving the non-hydrogen atoms[a]

atom–atom	distance (Å)	atom–atom	distance (Å)
Ni1–N1	1.925(2)	Ni1–N2	1.822(2)
O1–C5	1.249(4)	N1–C1	1.498(4)
N1–C4	1.503(4)	N2–C5	1.314(4)
N2–C6	1.462(4)	C1–C2	1.485(6)
C2–C3	1.514(7)	C3–C4	1.542(5)
C4–C5	1.510(5)	C6–C6′	1.528(6)

[a] The estimated standard deviations in the least significant figure are in parentheses.

Table 3.8 Bond angles from the crystal structure of [Ni^{II}(*S,S*-bprolen)] involving the non-hydrogen atoms[a]

atom–atom–atom	angle (°)	atom–atom–atom	angle (°)
N1–Ni1–N1′	101.5(2)	C2–C1–N1	103.6(3)
N1–Ni1–N2	86.4(1)	C1–C2–C3	103.6(4)
N1–Ni1–N2′	171.4(1)	C2–C3–C4	103.6(3)
N2–Ni1–N2′	86.0(2)	N1–C4–C5	110.5(2)
C1–N1–C4	107.3(3)	N1–C4–C3	105.1(3)
C1–N1–Ni1	113.7(2)	C5–C4–C3	112.4(3)
C4–N1–Ni1	110.0(2)	O1–C5–N2	126.3(3)
C5–N2–C6	123.4(2)	O1–C5–C4	120.6(3)
C5–N2–Ni1	119.3(2)	N2–C5–C4	113.1(3)
C6–N2–Ni1	115.8(2)	N2–C6–C6′	106.7(2)

[a] The estimated standard deviations in the least significant figure are in parentheses

significantly longer than the Ni–N(imine) bonds in [Ni^{II}(bprolenH_{-4})]. The angles about Ni1 between the atoms in the chelate rings are less than the ideal 90°, and the N1–Ni1–N1′ angle is larger (101.5(2)°) to compensate. The coordination about the Ni atom is square-planar, and the Ni lies in the plane defined by the four N atoms, though the deviation of the N atoms from the least-squares plane is slightly

Table 3.9 Least-squares plane in [Ni^{II}(*S,S*-bprolen)][a]

atoms defining plane	distance from plane (Å)
N1	–0.037(3)
N2	0.078(4)
N1′	0.037(3)
N2′	–0.078(4)
additional atoms	
Ni1	–0.000(1)

[a] The estimated standard deviations in the least significant figure are in parentheses.

larger than in [Ni^{II}(bprolenH$_{-4}$)], probably due to the non-planarity of the heterocyclic rings of the ligand.

The 1D ^{1}H NMR spectrum (Figure 3.5) of [Ni^{II}(*S,S*-bprolen)] has a larger number of signals and a much more complicated spin-coupling pattern than the spectrum of [Ni^{II}(bprolenH$_{-4}$)]. The assignment of the spectrum was made on the basis of the 2D COSY ^{1}H NMR spectrum (Figure 3.6) and is summarised in Table 3.10.

A deuterium-exchange experiment was performed to confirm the identity of the amine protons. When three drops of D_2O were added to a solution of [Ni^{II}(*S,S*-bprolen)] in CD_3OD, the signal at 4.37 ppm disappeared and the multiplet at 3.6 ppm (corresponding to the signal at 3.3 ppm in DMSO-d_6) became a triplet. The exchange of the amine protons was slow; an hour after the D_2O was added the quartet at 4.37 ppm was weaker but still present; a day later it had completely disappeared. Once the identity of the signal from the amine protons had been unambiguously established, the pattern and intensity of the cross-peaks in the COSY spectrum were used to assign the remaining signals. In the spectrum recorded in DMSO-d_6, the signal at 3.3 ppm is obscured by the water peak, but the cross-peaks, due to couplings with the amine protons and the axial and equatorial protons on position 3 of the pyrrolidine rings, are clearly observed.

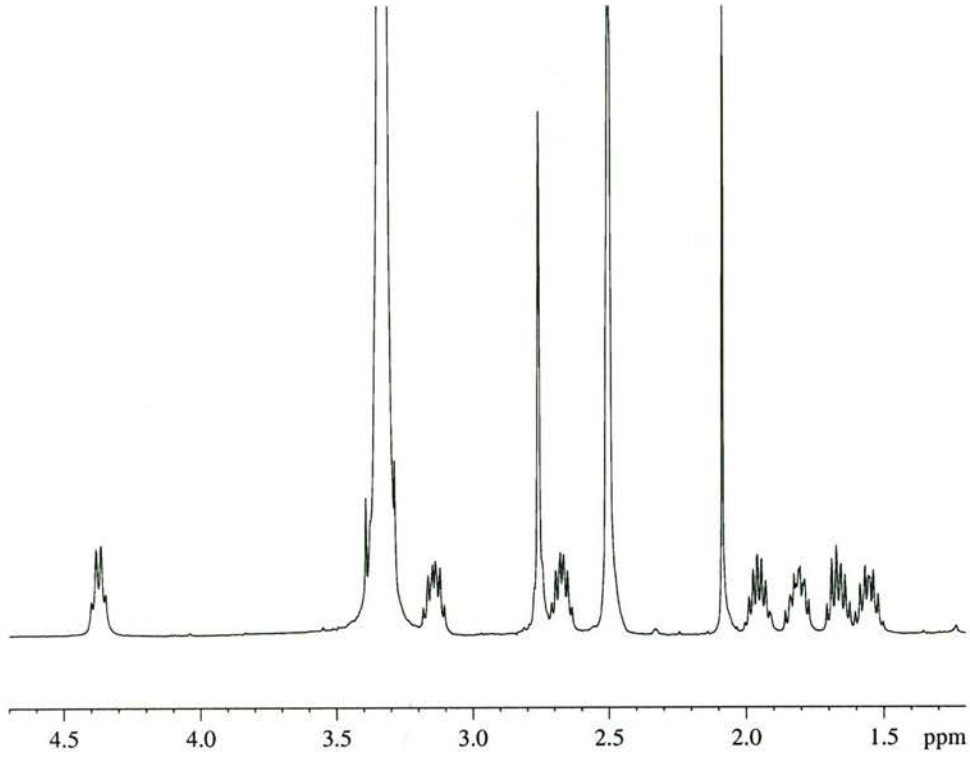

Figure 3.5 1D ^{1}H NMR spectrum of [Ni^{II}(*S,S*-bprolen)] in DMSO-d_6. The residual solvent peak is at 2.48 ppm, residual acetone at 2.07 ppm and the water peak at 3.32 ppm.

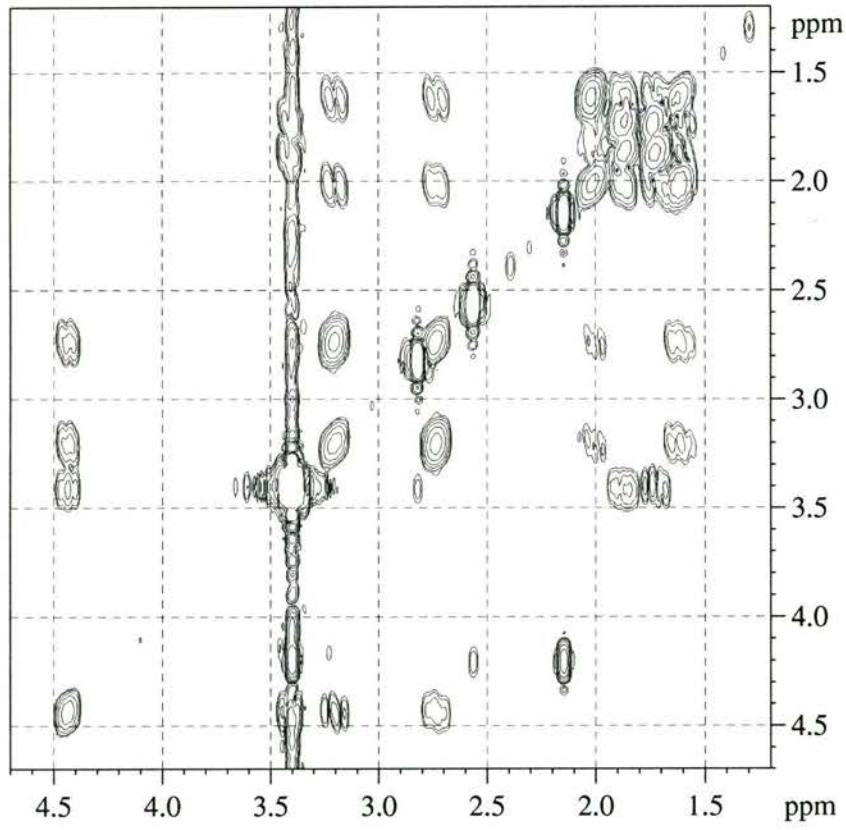

Figure 3.6 2D COSY ^{1}H NMR spectrum of [Ni^{II}(*S,S*-bprolen)] in DMSO-d_6.

Table 3.10 ^{1}H NMR spectral data for [Ni^{II}(*S,S*-bprolen)]

Chemical Shift (ppm)	Description	Number of Protons	Assignment
1.54	multiplet	2	Either the axial or the equatorial protons on position 4 of the pyrrolidine rings
1.66	multiplet	2	Either the axial or the equatorial protons on position 3 of the pyrrolidine rings
1.80	multiplet	2	Either the equatorial or the axial protons on position 3 of the pyrrolidine rings
1.95	multiplet	2	Either the equatorial or the axial protons on position 4 of the pyrrolidine rings
2.67	multiplet	2	Either the axial or the equatorial protons on position 5 of the pyrrolidine rings
2.76	singlet	4	Central ethylene bridge
3.14	multiplet	2	Either the equatorial or the axial protons on position 5 of the pyrrolidine rings
~3.3	multiplet	2	Position 2 of the pyrrolidine rings
4.37	quartet	2	Amine protons on position 1 of the pyrrolidine rings

The assignments of the ^{13}C NMR data are given in Table 3.11. There is no signal in the region where imine carbons appear and an increase in the number of signals in the aliphatic region compared to the oxidised species.

The protons on the amine groups and position 2 of the pyrrolidine rings were clearly identified in the ^{1}H NMR spectra and both the ^{1}H and ^{13}C NMR spectra were

assigned to the complex with unoxidised amine groups, in accordance with the X-ray crystallography results.

Table 3.11 ^{13}C NMR spectral data for [Ni^{II}(*S,S*-bprolen)] in DMSO-d_6

Chemical Shift (ppm)	Assignment
25.5	Position 4 of the pyrrolidine rings
29.3	Position 3 of the pyrrolidine rings
47.0	Central ethylene bridge
49.0	Position 5 of the pyrrolidine rings
66.2	Position 2 of the pyrrolidine rings
177.1	Carbonyl groups

Table 3.12 Characteristic IR bands of [Ni^{II}(*S,S*-bprolen)]

Wavenumber (cm^{-1})	Assignment
2955	ν(C–H)
2881	ν(C–H)
2867	ν(C–H)
1599	amide I band
1425	amide ν(C–N)

The absence of the amide ν(N–H), amide II and amide III bands from the IR spectrum is due to the deprotonation of the amide N atoms on coordination to Ni. The amide I band is shifted to a lower wavenumber than for the free ligand and for [Ni^{II}(bprolenH$_{-4}$)].

3.3.1.2 Oxidative Dehydrogenation of [Ni^{II}(*S,S*-bprolen)]

The characterisation of the products from the different synthetic methods demonstrated that there were two conditions necessary for oxidative dehydrogenation of the ligand to occur in [Ni^{II}(*S,S*-bprolen)]: (i) there must be O_2 present; and (ii) the complex must be dissolved in a basic solution.

The syntheses of [Ni^{II}(*S,S*-bprolen)] under Ar were carried out in highly basic solution with hydroxide as the base. The ^1H NMR spectrum of the crude product

from Method 1 did not show evidence of any Ni complexes other than [Ni^{II}(*S,S*-bprolen)], and the exclusion of O_2 during the synthesis prevented oxidation of the ligand.

The oxidative dehydrogenation only occurred in basic aqueous solution. The success of the synthesis of [Ni^{II}(bprolenH_{-4})] by Method 2 proved that it was not necessary to have a strong base present, since the reaction occurred at pH 10 with the use of the more moderate base, carbonate. It is not possible to say categorically that a high pH value is necessary for the actual dehydrogenation reaction because the high pH value is necessary to achieve coordination of the amide groups to Ni through deprotonated amide N atoms. However, the high stability of solutions of [Ni^{II}(*S,S*-bprolen)] in methanol in the presence of O_2 indicates that the base added to deprotonate the amide groups may also be involved in the dehydrogenation.

There were few prior reports of the oxidative dehydrogenation of amines coordinated to Ni. The oxidation of tetrahydrosalen derivatives coordinated to Ni(II) to the dihydrosalen derivatives by O_2 (Scheme 3.2) has been reported by Böttcher, *et. al.*[20] who identified the dihydrosalen complexes spectroscopically.

Scheme 3.2 Oxidative dehydrogenation of Ni(II)-tetrahydrosalen complexes

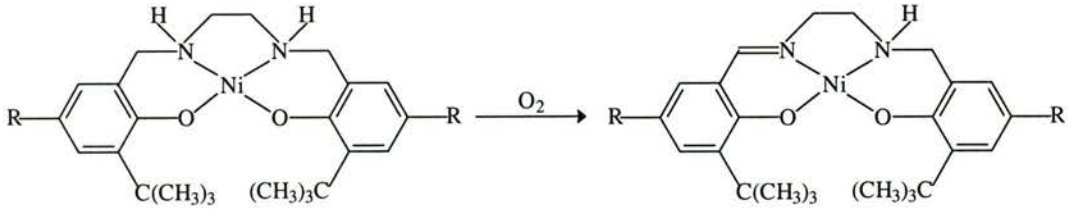

R = H, CH_3 or Cl

Berkessel, Bats and Schwartz have also reported the oxidative dehydrogenation of a dihydrosalen derivative coordinated to Ni(II) (Scheme 3.3).[21] The thioether coordinated in the axial position is also oxidised in the reaction and diphenyl sulfide is a product of the reaction.

Scheme 3.3 Oxidative dehydrogenation of a Ni(II)-dihydrosalen derivative

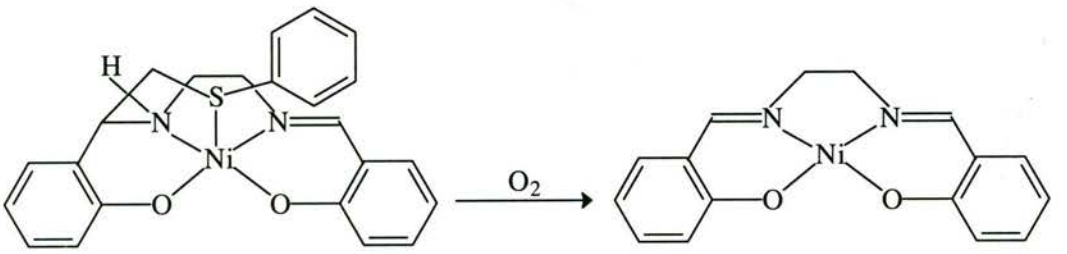

In the oxidative dehydrogenation of the tetrahydrosalen derivatives coordinated to Ni(II), there was evidence that the mechanism involved O_2 binding to the Ni.[20] There are several reports of O_2 binding to Ni(II) complexes with amide ligands,[9,22-29] which caused ligand oxidation in some instances.[9,22-25] There is also evidence that higher oxidation states of Ni are intermediates in the ligand oxidation.[22,24,25] The oxidative dehydrogenation of *S,S*-bprolen ligand observed in this work is postulated to occur by a mechanism involving O_2 binding to the Ni, leading to the formation of a higher oxidation state Ni species followed by an intramolecular oxidative dehydrogenation of an amine group with concomitant reduction of the Ni to Ni(II). The oxidation of the two amine groups to imines observed would mean that this happens twice for each molecule. This is unlike the oxidative dehydrogenation of the tetrahydrosalen and dihydrosalen derivatives[20,21] where only a single amine group was oxidised.

The mechanism of DNA damage by Ni(II)-peptide complexes in the presence of oxidants is postulated to involve oxidation of Ni(II)-peptide complexes to higher Ni oxidation states;[30-33] therefore, the aerial oxidation may have direct relevance as a biomimetic reaction leading to the biological oxidation of DNA species.

3.3.1.3 [Ni^{II}(*R,R*-(*S,S*)-bprolchxn)]

The synthesis of the complex required the addition of hydroxide solution to deprotonate the amide N atoms in order for them to coordinate to the Ni.

The ORTEP[12] diagram of the complex in the crystal structure of [Ni^{II}(*R,R*-(*S,S*)-bprolchxn)].3H_2O is given in Figure 3.7. The non-hydrogen bond lengths are in Table 3.13, and the non-hydrogen bond angles are in Table 3.15. The

Ni atom is bound to two amine N and two amide N atoms and has square-planar coordination geometry (Table 3.14), though the N atoms are slightly displaced from the least-squares plane. These deviations of the N atoms are larger than those observed in the crystal structures of [Ni^{II}(bprolenH$_{-4}$)], [Ni^{II}(*S,S*-bprolen)] and [Ni^{II}(*S,S*-bprolben]; and are due to the central *trans*-cyclohexane bridge. The amine Ns are chiral and both have a *S* configuration.

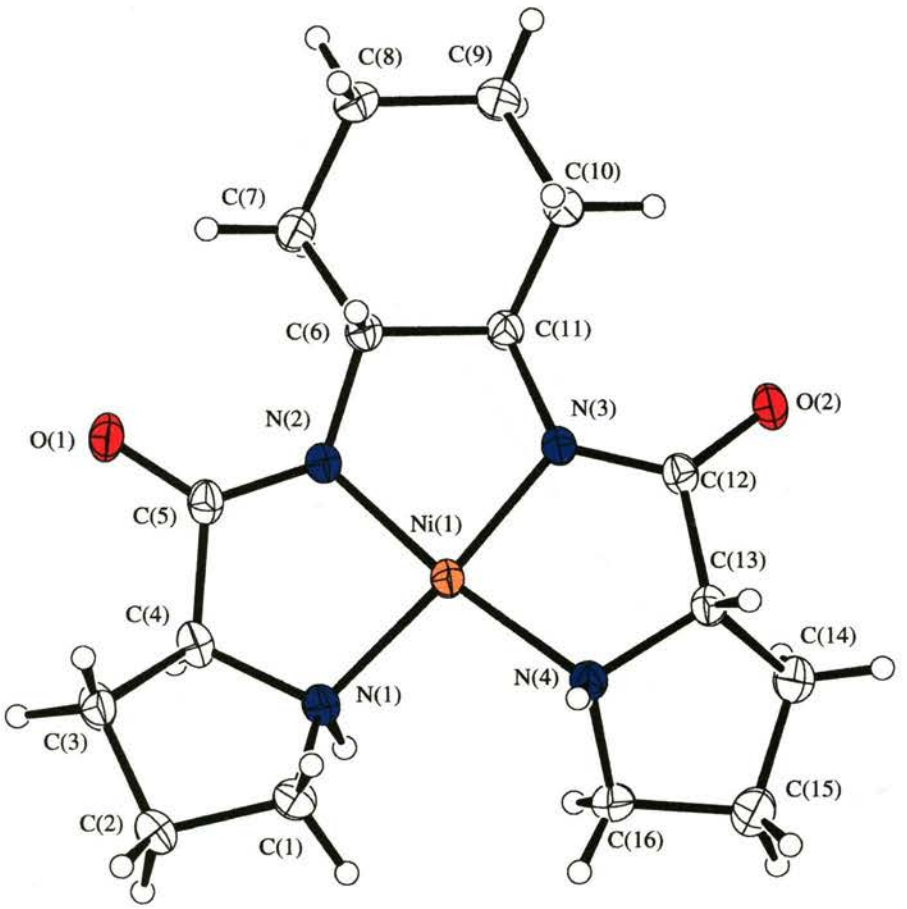

Figure 3.7 ORTEP[12] representation with 25% probability thermal ellipsoids of the complex in the crystals of [Ni^{II}(*R,R*-(*S,S*)-bprolchxn)].3H_2O.

The Ni–N(amide) bond lengths of 1.839(2) Å and 1.845(2) Å show that the amide N atoms are deprotonated, as expected. The average Ni–N(amide) bond length of 1.842 Å is 0.02 Å longer than the Ni–N(amide) bond length of [Ni^{II}(*S,S*-bprolen)], but the average Ni–N(amine) bond length of 1.927 Å is not significantly different from the Ni–N(amine) bond length of 1.925(2) Å in [Ni^{II}(*S,S*-bprolen)]. The longer Ni–N(amide) bond lengths may be due to the distortion caused by the central

Table 3.13 Bond lengths from the crystal structure of $[Ni^{II}(R,R\text{-}(S,S)\text{-bprolchxn})].3H_2O$ involving the non-hydrogen atoms[a]

atom–atom	distance (Å)	atom–atom	distance (Å)
Ni1–N3	1.839(2)	Ni1–N2	1.845(2)
Ni1–N1	1.921(2)	Ni1–N4	1.932(2)
O1–C5	1.259(3)	O2–C12	1.262(3)
N1–C1	1.486(3)	N1–C4	1.515(3)
N2–C5	1.314(3)	N2–C6	1.482(3)
N3–C12	1.320(3)	N3–C11	1.475(3)
N4–C16	1.507(3)	N4–C13	1.510(3)
C1–C2	1.520(4)	C2–C3	1.518(4)
C3–C4	1.529(3)	C4–C5	1.526(3)
C6–C7	1.525(3)	C6–C11	1.529(3)
C7–C8	1.537(3)	C8–C9	1.517(4)
C9–C10	1.531(3)	C10–C11	1.522(3)
C12–C13	1.518(3)	C13–C14	1.517(3)
C14–C15	1.497(4)	C15–C16	1.492(4)

[a] The estimated standard deviations in the least significant figure are in parentheses.

Table 3.14 Least-squares plane in $[Ni^{II}(R,R\text{-}(S,S)\text{-bprolchxn})].3H_2O$[a]

atoms defining plane	distance from plane (Å)
N1	–0.0778(9)
N2	0.091(1)
N3	–0.091(1)
N4	0.0779(9)
additional atoms	
Ni1	0.028(1)

[a] The estimated standard deviations in the least significant figure are in parentheses

trans-cyclohexane bridge. The bond angles about the Ni involving the coordinated atoms from the three chelate rings are less than the ideal value of 90°, forcing the opening up of the N1–Ni1–N4 angle to 100.24(8)°.

Table 3.15 Bond angles from the crystal structure of $[Ni^{II}(R,R\text{-}(S,S)\text{-bprolchxn})].3H_2O$ involving the non-hydrogen atoms[a]

atom–atom–atom	angle (°)	atom–atom–atom	angle (°)
N3–Ni1–N2	86.70(8)	C5–C4–C3	115.4(2)
N3–Ni1–N1	170.36(8)	O1–C5–N2	128.2(2)
N2–Ni1–N1	86.80(8)	O1–C5–C4	119.2(2)
N3–Ni1–N4	86.68(7)	N2–C5–C4	112.6(2)
N2–Ni1–N4	172.34(8)	N2–C6–C7	118.6(2)
N1–Ni1–N4	100.24(8)	N2–C6–C11	105.3(2)
C1–N1–C4	106.4(2)	C7–C6–C11	109.8(2)
C1–N1–Ni1	120.6(2)	C6–C7–C8	108.8(2)
C4–N1–Ni1	109.7(1)	C7–C8–C9	113.4(2)
C5–N2–C6	125.6(2)	C8–C9–C10	111.0(2)
C5–N2–Ni1	118.3(2)	C9–C10–C11	109.2(2)
C6–N2–Ni1	113.5(1)	N3–C11–C10	117.7(2)
C12–N3–C11	123.4(2)	N3–C11–C6	106.4(2)
C12–N3–Ni1	116.6(2)	C10–C11–C6	109.7(2)
C11–N3–Ni1	113.5(1)	O2–C12–N3	128.1(2)
C16–N4–C13	106.1(2)	O2–C12–C13	118.9(2)
C16–N4–Ni1	119.4(2)	N3–C12–C13	113.0(2)
C13–N4–Ni1	109.0(1)	N4–C13–C14	105.8(2)
N1–C1–C2	105.4(2)	N4–C13–C12	110.5(2)
C3–C2–C1	102.4(2)	C12–C13–C14	113.9(2)
C2–C3–C4	103.5(2)	C13–C14–C15	103.4(2)
N1–C4–C5	110.4(2)	C14–C15–C16	103.5(2)
N1–C4–C3	106.5(2)	C15–C16–N4	105.4(2)

[a] The estimated standard deviations in the least significant figure are in parentheses.

The 1D and 2D COSY ^{1}H NMR spectra of $[Ni^{II}(R,R\text{-}(S,S)\text{-bprolchxn})]$ in DMSO-d_6 are shown in Figures 3.8 and 3.9, respectively. The 1D ^{1}H NMR spectrum of $[Ni^{II}(R,R\text{-}(S,S)\text{-bprolchxn})]$ in CD_3OD was also recorded to determine the structure

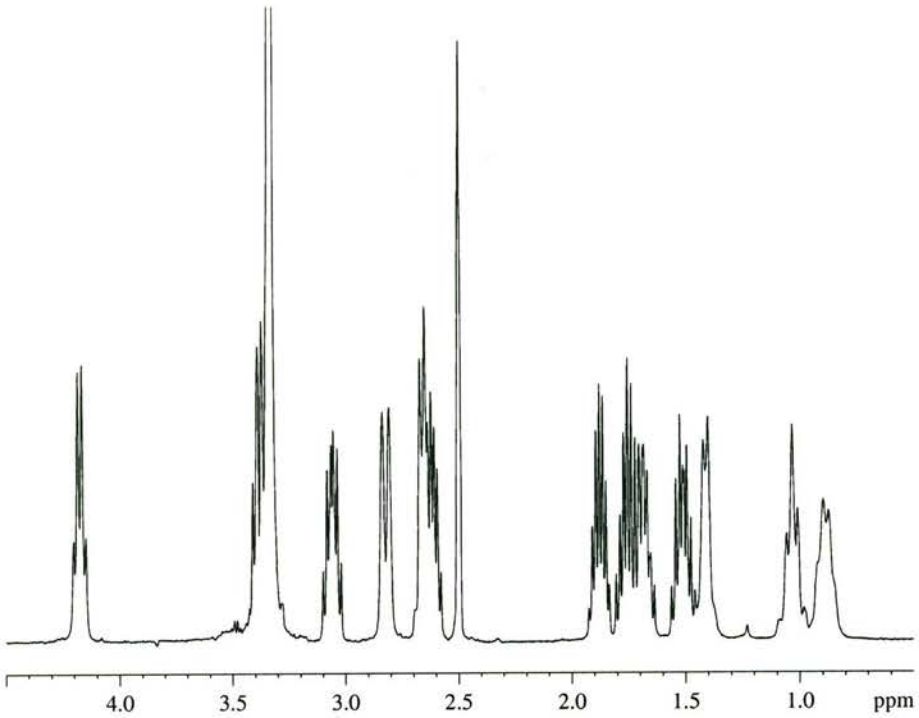

Figure 3.8 1D ^{1}H NMR spectrum of [Ni^{II}(*R*,*R*-(*S*,*S*)-bprolchxn)] in DMSO-d_6. The residual solvent peak is at 2.50 ppm and the water peak is at 3.34 ppm.

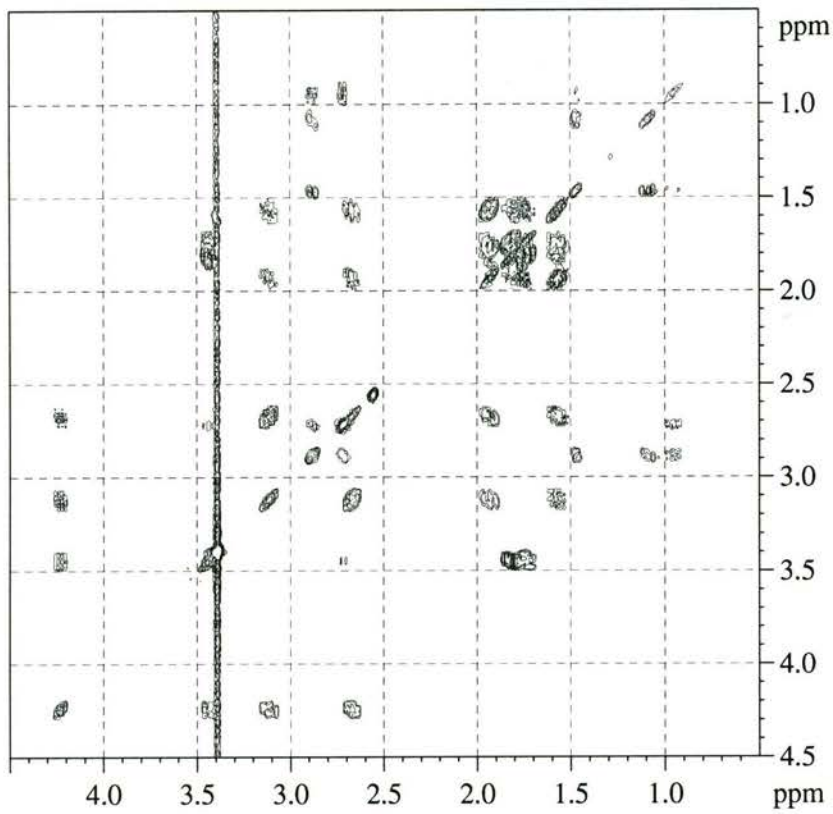

Figure 3.9 2D COSY ^{1}H NMR spectrum of [Ni^{II}(*R*,*R*-(*S*,*S*)-bprolchxn)] in DMSO-d_6.

Table 3.16 ^{1}H NMR spectral data for [Ni^{II}(*R,R*-(*S,S*)-bprolchxn)]

Chemical Shift (ppm)	Description	Number of Protons	Assignment
0.88	multiplet	2	Either the axial or the equatorial protons on positions 3 and 6 of the cyclohexane ring
1.03	multiplet	2	Either the equatorial or the axial protons on positions 4 and 5 of the cyclohexane ring
1.41	multiplet	2	Either the axial or the equatorial protons on positions 4 and 5 of the cyclohexane ring
1.51	multiplet	2	Either the axial or the equatorial protons on position 4 of the pyrrolidine rings
1.69	multiplet	2	Either the axial or the equatorial protons on position 3 of the pyrrolidine rings
1.76	multiplet	2	Either the equatorial or the axial protons on position 3 of the pyrrolidine rings
1.88	multiplet	2	Either the equatorial or the axial protons on position 4 of the pyrrolidine rings
2.62	multiplet	2	Either the axial or the equatorial protons on position 5 of the pyrrolidine rings
2.66	multiplet	2	Positions 1 and 2 of the cyclohexane ring
2.82	multiplet	2	Either the equatorial or the axial protons on positions 3 and 6 of the cyclohexane ring
3.06	multiplet	2	Either the equatorial or the axial protons on position 5 of the pyrrolidine rings
3.38	quartet	2	Position 2 of the pyrrolidine rings
4.17	quartet	2	Amine protons on position 1 of the pyrrolidine rings

Table 3.17 ^{13}C NMR spectral data for [Ni^{II}(*R,R*-(*S,S*)-bprolchxn)] in DMSO-d_6

Chemical Shift (ppm)	Assignment
25.2	Either positions 4 and 5 of the cyclohexane ring or postion 4 of the pyrrolidine rings
25.4	Either position 4 of the pyrrolidine rings or positions 4 and 5 of the cyclohexane ring
28.8	Position 3 of the pyrrolidine rings
31.6	Positions 3 and 6 of the cyclohexane ring
49.0	Position 5 of the pyrrolidine rings
65.8	Position 2 of the pyrrolidine rings
68.6	Positions 1 and 2 of the cyclohexane ring
177.9	Carbonyl groups

of the multiplet hidden under the water peak in DMSO-d_6. Partial exchange of the amine protons for deuterium occurred in CD_3OD solution; addition of D_2O led to the complete exchange of the amine protons. The signal due to the protons on position 2 of the pyrrolidine rings was initially a quartet but it changed to a triplet as the amine protons were replaced by deuterium. The assignment of the spectrum was made on the basis of the 2D COSY ^1H NMR spectrum and the deuterium exchange observed in CD_3OD solution (Table 3.16). The rigidity of the molecule results in proton-proton couplings over quite long paths. There are even weak cross peaks in the COSY ^1H NMR spectrum between the 2.66 ppm resonance, the protons on positions 1 and 2 of the cyclohexane ring, and the 3.38 ppm resonance, the protons on position 2 of the pyrrolidine rings.

The ^1H and ^{13}C NMR spectra demonstrated that the Ni retains its square-planar geometry in solution, and that the molecule is symmetric about the axis passing through the Ni atom and between the two amide Ns and the two amine Ns. The identification of the amine protons and the absence of a signal in the region due to imine carbons in the ^{13}C NMR spectrum showed that the amine groups had not been oxidised in the product.

The IR spectral data and their assignments for [Ni^{II}(*R,R*-(*S,S*)-bprolchxn)] are listed in Table 3.18. The amide N–H stretching band and the amide II band are absent, which is consistent with deprotonation of the amide groups. The strong band at 1575 cm^{-1} is assigned to the amide I vibration and the peak at 1417 cm^{-1} is tentatively assigned to the amide ν(C–N).

Table 3.18 Characteristic IR bands of [Ni^{II}(*R,R*-(*S,S*)-bprolchxn)]

Wavenumber (cm^{-1})	Assignment
2981	ν(C–H)
2971	ν(C–H)
2934	ν(C–H)
2903	ν(C–H)
2870	ν(C–H)
2855	ν(C–H)
2839	ν(C–H)
1575	amide I band
1444	C–H deformation
1417	amide ν(C–N)

No Ni complexes with oxidised ligands were isolated during the synthesis or detected in the NMR spectra of the product, yet the reaction conditions for the synthesis of [Ni^{II}(*R,R*-(*S,S*)-bprolchxn)] were the same as the conditions under which the amine groups of *S,S*-bprolen were oxidatively dehydrogenated. This does not completely rule out oxidation of the ligand as the yield was only 50%, but it shows that the amine groups in the Ni complex of *R,R*-(*S,S*)-bprolchxn are considerably less susceptible to oxidative dehydrogenation than the amine groups in the Ni complex of *S,S*-bprolen. It is possible that the relative solubilities of the complexes with the oxidatively dehydrogenated and unoxidised forms of the ligands may be different for the various ligands and also affect which complex is isolated.

3.3.1.4 [Ni^{II}(*S,S*-bprolben)]

The synthesis of this complex did not require the addition of excess base, since the acetate counterion was sufficient to deprotonate the amide groups. The amide

protons are more labile than in the analogous ligands with aliphatic central bridges because the deprotonated amide groups are stabilised by the delocalisation of the negative charge into the benzene ring. The product was only slightly soluble in water and precipitated from the reaction mixture as it cooled.

The ORTEP[12] diagram (Figure 3.10) shows that the Ni atom is square-planar and coordinated to two amine N and two amide N atoms. The Ni–N(amide) bond lengths (Table 3.19) of 1.833(3) Å and 1.842(3) Å are significantly shorter than the Ni–N(amine) bond lengths of 1.919(3) Å and 1.922(3) Å, characteristic of Ni–N(deprotonated amide) bonds. The bond angles (Table 3.20) around the Ni atom are less than 90° for the chelate rings, forcing the N1–Ni1–N4 angle to open up to 101.1(1)°. The coordinated N atoms are planar (Table 3.21), as are the carbon atoms of the benzene ring in the ligand. The benzene ring is almost coplanar with the coordination plane, since the dihedral angle between them is 1.4(2)°.

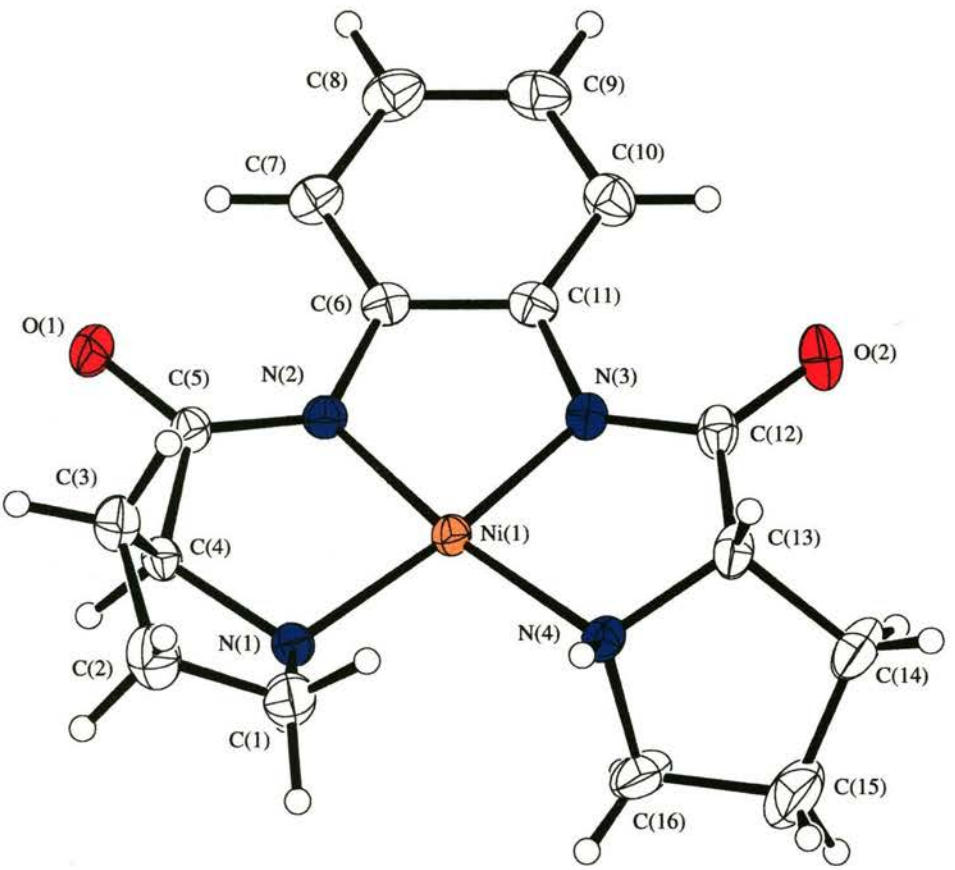

Figure 3.10 ORTEP[12] representation with 25% probability thermal ellipsoids of the complex in the crystals of $[Ni^{II}(S,S\text{-bprolben})].D_2O.CD_3OD$

Table 3.19 Bond lengths from the crystal structure of $[Ni^{II}(S,S\text{-bprolben})].D_2O.CD_3OD$ involving the non-hydrogen atoms[a]

atom–atom	distance (Å)	atom–atom	distance (Å)
Ni1–N2	1.833(3)	Ni1–N3	1.842(3)
Ni1–N1	1.919(3)	Ni1–N4	1.922(3)
O1–C5	1.243(4)	O2–C12	1.250(5)
O3–C17	1.375(7)	N1–C1	1.509(5)
N1–C4	1.512(4)	N2–C5	1.327(5)
N2–C6	1.416(4)	N3–C12	1.323(4)
N3–C11	1.415(5)	N4–C16	1.487(5)
N4–C13	1.499(5)	C1–C2	1.486(6)
C2–C3	1.534(6)	C3–C4	1.514(5)
C4–C5	1.526(5)	C6–C7	1.396(5)
C6–C11	1.406(5)	C7–C8	1.389(6)
C8–C9	1.381(6)	C9–C10	1.389(6)
C10–C11	1.389(5)	C12–C13	1.510(5)
C13–C14	1.541(5)	C14–C15	1.503(9)
C15–C16	1.494(7)		

[a] The estimated standard deviations in the least significant figure are in parentheses.

The pyrrolidine rings were not oxidised during the synthesis of the complex. They are puckered and are not coplanar with the coordination plane. The amine Ns are chiral and both have the *S* configuration. The amine N in $[Ni^{II}(S,S\text{-bprolen})]$ and $[Ni^{II}(R,R\text{-}(S,S)\text{-bprolchxn})]$ also have *S* configuration, which indicates that the chirality of the amine Ns in these three complexes is determined by the fixed *S* configuration at position 2 of the pyrrolidine ring.

The 1D and 2D COSY ^1H NMR spectra of $[Ni^{II}(S,S\text{-bprolben})]$ in CD_3OD are shown in Figures 3.11 and 3.12, respectively. The assignment of the spectrum was made on the basis of the 2D COSY spectrum (Table 3.22). When 3 drops of D_2O were added to a CD_3OD solution of $[Ni^{II}(S,S\text{-bprolben})]$, the exchange of the amine protons for deuterium was not observed. Even after 2 d the quartet due to the amine protons was

Table 3.20 Bond angles from the crystal structure of $[Ni^{II}(S,S\text{-bprolben})].D_2O.CD_3OD$ involving the non-hydrogen atoms[a]

atom–atom–atom	angle (°)	atom–atom–atom	angle (°)
N2–Ni1–N3	85.6(1)	C3–C4–C5	113.3(3)
N2–Ni1–N1	86.8(1)	O1–C5–N2	128.7(3)
N3–Ni1–N1	172.3(1)	O1–C5–C4	118.6(3)
N2–Ni1–N4	172.0(1)	N2–C5–C4	112.7(3)
N3–Ni1–N4	86.6(1)	C7–C6–C11	120.1(3)
N1–Ni1–N4	101.1(1)	C7–C6–N2	127.4(3)
C1–N1–C4	106.3(3)	C11–C6–N2	112.5(3)
C1–N1–Ni1	118.6(2)	C6–C7–C8	119.1(4)
C4–N1–Ni1	108.9(2)	C7–C8–C9	120.5(4)
C5–N2–C6	125.9(3)	C8–C9–C10	121.0(4)
C5–N2–Ni1	118.2(2)	C9–C10–C11	119.2(4)
C6–N2–Ni1	114.8(2)	C10–C11–C6	120.0(3)
C12–N3–C11	126.8(3)	C10–C11–N3	127.1(3)
C12–N3–Ni1	118.1(3)	C6–C11–N3	112.8(3)
C11–N3–Ni1	114.3(2)	O2–C12–N3	126.8(4)
C16–N4–C13	106.0(3)	O2–C12–C13	120.3(3)
C16–N4–Ni1	117.3(2)	N3–C12–C13	112.9(3)
C13–N4–Ni1	108.6(2)	N4–C13–C12	111.1(3)
C2–C1–N1	107.4(3)	N4–C13–C14	107.4(4)
C1–C2–C3	103.2(3)	C12–C13–C14	113.5(4)
C2–C3–C4	102.6(3)	C13–C14–C15	104.5(4)
N1–C4–C3	104.4(3)	C14–C15–C16	106.2(4)
N1–C4–C5	110.6(3)	N4–C16–C15	105.3(4)

[a] The estimated standard deviations in the least significant figure are in parentheses.

still visible, though the signal partially overlapped the water peak, which had shifted; therefore, an accurate integration value could not be determined. However, the resonance at 3.72 ppm due to the protons on position 2 of the pyrrolidine rings was still observed as a quartet; it had not changed to a triplet as the equivalent resonances

Table 3.21 Least-squares planes in [Ni^{II}(*S,S*-bprolben)].$D_2O.CD_3OD$[a]

Plane 1	
atoms defining plane	distance from plane (Å)
N1	−0.023(1)
N2	0.027(2)
N3	−0.027(2)
N4	0.023(1)
additional atoms	
Ni1	−0.003(2)
Plane 2	
atoms defining plane	distance from plane (Å)
C6	−0.002(3)
C7	0.001(3)
C8	0.001(3)
C9	−0.002(3)
C10	0.002(3)
C11	0.000(3)
additional atoms	
Ni1	0.008(7)
N2	0.021(6)
N3	0.024(6)

[a] The estimated standard deviations in the least significant figure are in parentheses.

in the spectra of [Ni^{II}(*S,S*-bprolen)] and [Ni^{II}(*R,R*-(*S,S*)-bprolchxn)] did when the amine protons were replaced by deuterium. This showed that none of the amine protons had been replaced by deuterium.

The ^1H and ^{13}C NMR spectra demonstrate that the complex retains its square-planar coordination geometry in solution and has an axis of symmetry that passes through the Ni atom, between the two amide Ns and the two amine Ns. No Ni complexes with oxidised forms of the ligand were detected in the NMR spectra.

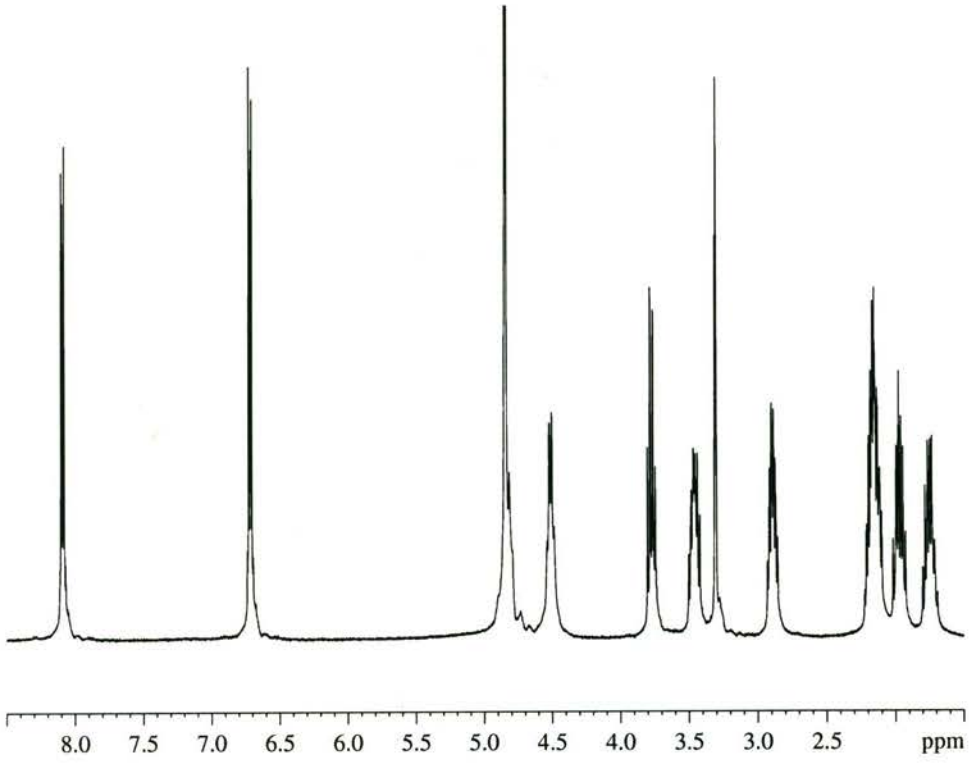

Figure 3.11 1D ^{1}H NMR spectrum of [Ni^{II}(*S,S*-bprolben)] in CD_3OD. The residual solvent peak occurs at 3.31 ppm and the water peak at 4.84 ppm.

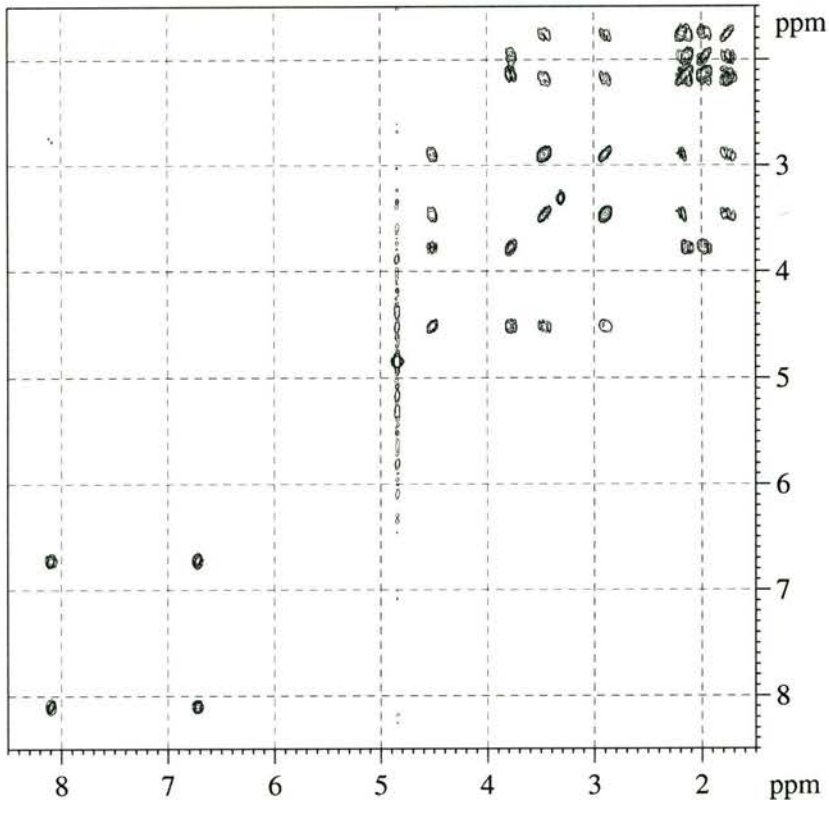

Figure 3.12 2D COSY ^{1}H NMR spectrum of [Ni^{II}(*S,S*-bprolben)] in CD_3OD.

Table 3.22 ^{1}H NMR spectral data for [Ni^{II}(*S,S*-bprolben)]

Chemical Shift (ppm)	Description	Number of Protons	Assignment
1.75	multiplet	2	Either the axial or the equatorial protons on position 4 of the pyrrolidine rings
1.96	multiplet	2	Either the equatorial or the axial protons on position 4 of the pyrrolidine rings
2.15	multiplet	4	Position 3 of the pyrrolidine rings
2.89	quintet	2	Either the axial or the equatorial protons on position 5 of the pyrrolidine rings
3.45	multiplet	2	Either the equatorial or the axial protons on position 5 of the pyrrolidine rings
3.72	quartet	2	Position 2 of the pyrrolidine rings
4.51	quartet	2	Amine protons on position 1 of the pyrrolidine rings
6.71	doublet of doublets	2	Positions 4 and 5 of the benzene ring
8.08	doublet of doublets	2	Positions 3 and 6 of the benzene ring

The IR spectral data and their assignments for [Ni^{II}(*S,S*-bprolben)] are listed in Table 3.24. The absence of the amide ν(N–H) and the amide II bands from the IR spectrum was consistent with the deprotonation of the amide groups. It was not possible to identify the amide ν(C–N) band as it fell in the same region as the skeletal vibrations from the benzene ring.

Table 3.23 ^{13}C NMR spectral data for [Ni^{II}(*S,S*-bprolben)] in DMSO-d_6

Chemical Shift (ppm)	Assignment
25.6	Position 4 of the pyrrolidine rings
29.8	Position 3 of the pyrrolidine rings
49.4	Position 5 of the pyrrolidine rings
66.8	Position 2 of the pyrrolidine rings
118.6	Positions 3 and 6 of the benzene ring
120.3	Positions 4 and 5 of the benzene ring
142.9	Positions 1 and 2 of the benzene ring
177.0	Carbonyl groups

Table 3.24 Characteristic IR bands of [Ni^{II}(*S,S*-bprolben)]

Wavenumber (cm^{-1})	Assignment
2972	ν(C–H)
2872	ν(C–H)
1605	amide I band
1569	aromatic ring skeletal vibration
1481	C–H deformation or benzene ring
1454	skeletal vibration
755	C–H deformation

3.3.2 Electrochemistry

Cyclic voltammetry was used to determine the $Ni^{III/II}$ reduction potentials (Table 3.25). The complexes were not all soluble in a single solvent, which prevented quantitative comparisons from being made between all the complexes in the same solvent. No reversible oxidation was observed for [Ni^{II}(bpb)], the other complexes showed reversible or quasi-reversible redox couples. The complexes with terminal amine ligands had the lowest $Ni^{III/II}$ reduction potentials. The presence of a central benzene bridge made the reduction potential more positive. This is probably because delocalisation of the negative charge on the deprotonated amide groups into the benzene ring means the ligand is not as effective at stabilising the Ni(III) oxidation state.

Table 3.25 $Ni^{III/II}$ reduction potentials

Couple	$E_{1/2}$ vs NHE (V)[a]	$E_{1/2}$ vs $Fc^{+/0}$ (V)[b]
$[Ni(bpen)]^{+/0}$	–	0.311
$[Ni(S,S\text{-bprolben})]^{+/0}$	–	0.220
$[Ni(R,R\text{-}(S,S)\text{-bprolchxn})]^{+/0}$	0.870	0.033
$[Ni(S,S\text{-brolen})]^{+/0}$	0.918	–
$[Ni(bprolenH_{-4})]^{+/0}$	0.950	0.316

[a] solvent: H_2O, supporting electrolyte: $NaClO_4$ (0.1 M)

[b] solvent: *N,N*-dimethylformamide, supporting electrolyte: TBAP (0.1 M)

The most easily oxidised complex was $[Ni^{II}(R,R\text{-}(S,S)\text{-bprolchxn})]$, yet it is the complex with *S,S*-bprolen that undergoes oxidative dehydrogenation of the amines during the synthesis. This indicates that factors besides the oxidation potential of the Ni, such as the strain induced in the ligand upon coordination, influence whether the amine groups undergo aerial dehydrogenation or not.

At lower scan rates (Figure 1.13(b) and Figure 3.14(b)), the $Ni^{III/II}$ couple was almost fully reversible, as the scan rate increased the anodic and cathodic peaks moved farther apart and the relative intensity of the cathodic peak decreased (Figure 3.13.(a) and Figure 3.14(a)). As the scan rate increased from 10 mV s^{-1} to 100 mV s^{-1} for $[Ni^{II}(bpen)]$ the ratio of the peak currents, i_{pc}/i_{pa}, decreased from 0.91 to 0.46 and the peak-to-peak separation, ΔE_p, increased from 70 mV to 87 mV. As the scan rate increased from 100 mV s^{-1} to 500 mV s^{-1} for $[Ni^{II}(bprolenH_{-4})]$ i_{pc}/i_{pa} decreased from 0.73 to 0.52 and ΔE_p increased from 73 mV to 82 mV.

The decrease in the ratio of i_{pc}/i_{pa} is counter-intuitive for a reversible process. However, the Ni(II) complexes are four-coordinate and have square-planar geometry about the Ni, whereas Ni(III) complexes are usually six-coordinate,[34-36] so there is a conformational change when the oxidation state of the Ni changes between II and III. At slower scan rates, the scan rate was slow compared to the rate of conformational rearrangement, so a single reversible reduction couple was seen. As the scan rate increased, the timescale of the experiment became comparable to the rate of conformational rearrangement; i.e., the redox couples for the four-coordinate species

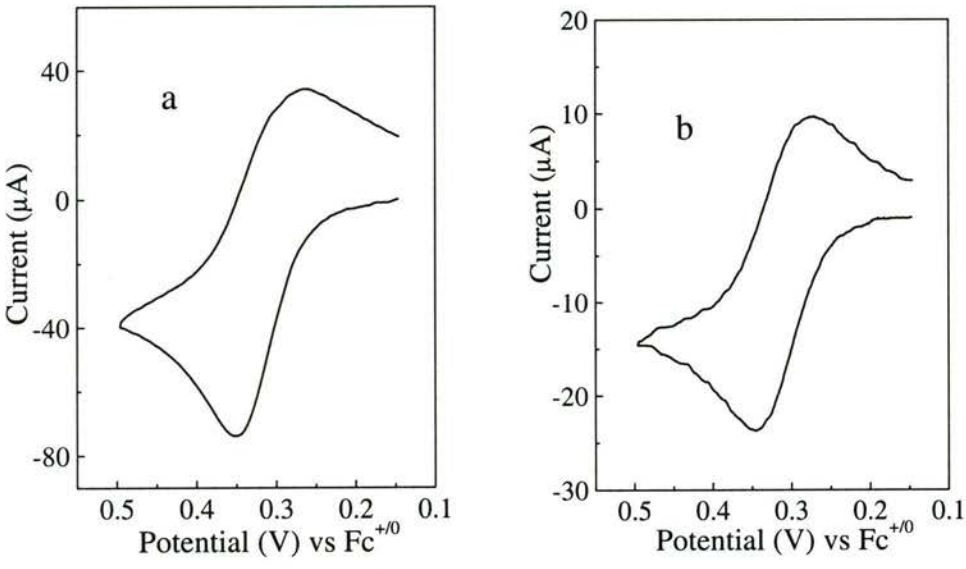

Figure 3.13 Cyclic voltammograms of [Ni^{II}(bpen)] (5 mM) in DMF, supporting electrolyte: TBAP (0.1 M), at scan rates of (a) 100 mV s^{-1} and (b) 10 mV s^{-1}

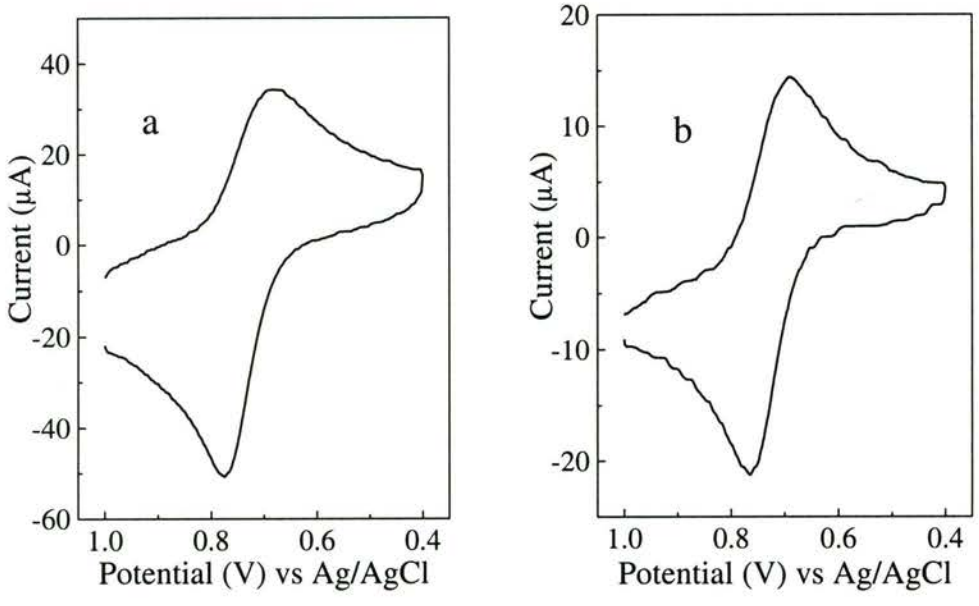

Figure 3.14 Cyclic voltammograms of [Ni^{II}(bprolenH_{-4})] (2 mM) in H_2O, supporting electrolyte: $NaClO_4$ (0.1 M), at scan rates of (a) 500 mV s^{-1} and (b) 100 mV s^{-1}

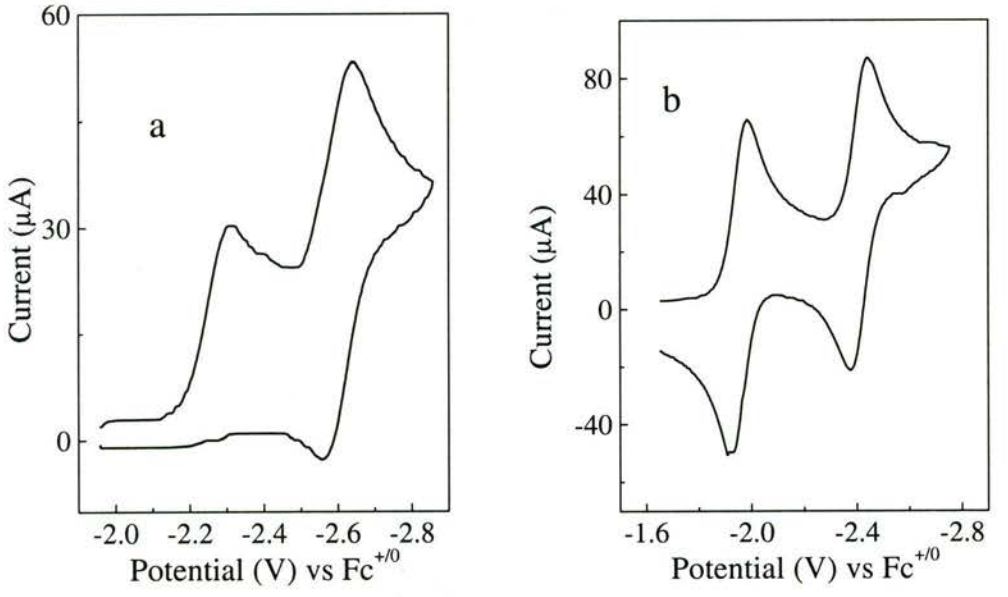

Figure 3.15 Cyclic voltammograms of (a) $bpbH_2$ (3.5 mM) and (b) [Ni^{II}(bpb)] (4 mM) in DMF, supporting electrolyte: TBAP (0.1 M), at a scan rate of 100 mV s^{-1}

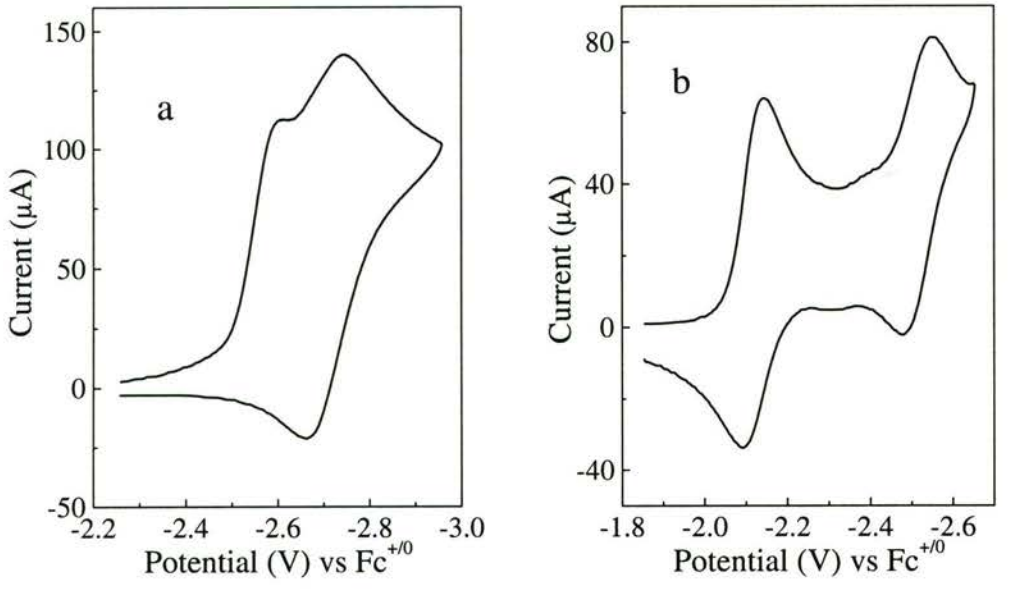

Figure 3.16 Cyclic voltammograms of (a) $bpenH_2$ (3.5 mM) and (b) [Ni^{II}(bpen)] (5 mM) in DMF, supporting electrolyte: TBAP (0.1 M), at scan rates of (a) 300 mV s^{-1} and (b) 100 mV s^{-1}

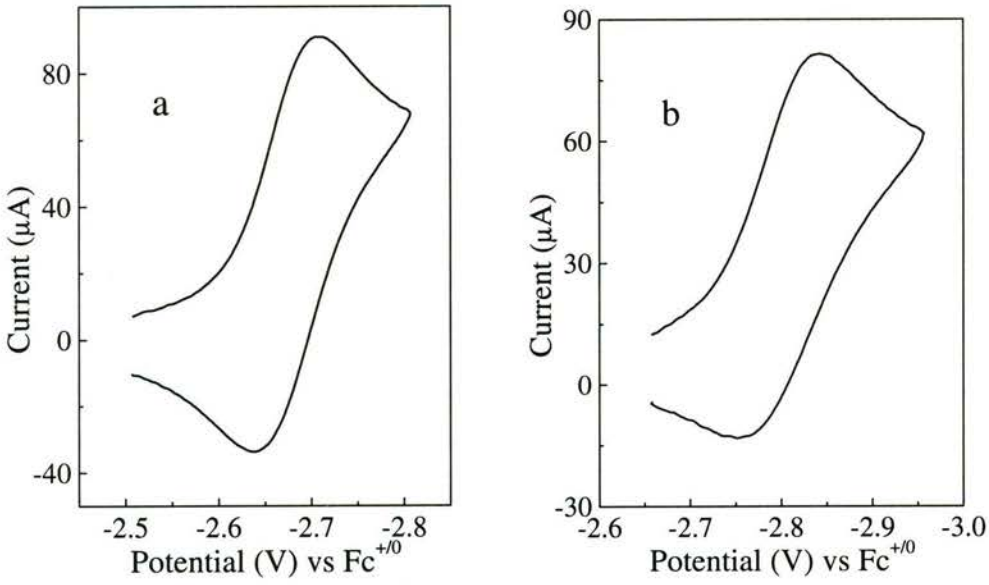

Figure 3.17 Cyclic voltammograms of (a) [Ni^{II}(*S,S*-bprolben)] (5 mM) and (b) [Ni^{II}(*R,R*-(*S,S*)-bprolchxn)] (5 mM) in DMF, supporting electrolyte: TBAP (0.1 M), at a scan rate of 100 mV s^{-1}

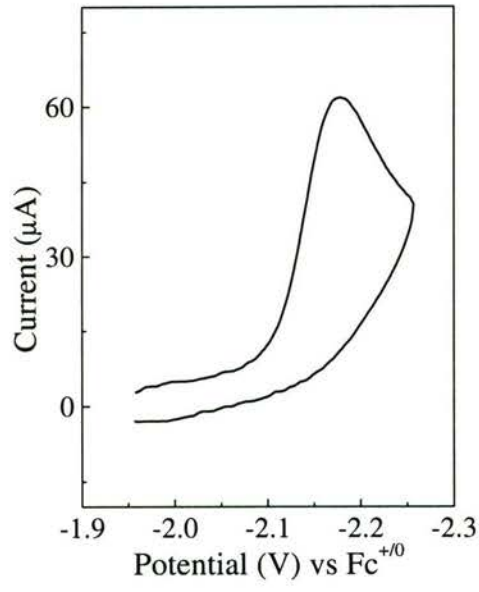

Figure 3.18 Cyclic voltammogram of [Ni^{II}(bprolenH_{-4})] (2 mM) in DMF, supporting electrolyte: TBAP (0.1 M), at a scan rate of 100 mV s^{-1}

and the six-coordinate species started to separate, and the reversibility was lost. Although scan rates of up to 2,000 mV s^{-1} were used, distinct redox couples for the four-coordinate and six-coordinate species could not be resolved in the potential window.

Bossu and Margerum reported the E^0 values for a large number of Ni(II) complexes with oligopeptide ligands in water.[34] The values for tripeptide ligands (2 deprotonated amide Ns coordinated) ranged from 0.84-0.96 V vs NHE, for tetrapeptides, peptide amides and higher order peptides (3 deprotonated amide Ns coordinated), the values ranged from 0.79-0.84 V vs NHE. These $Ni^{III/II}$ reduction potentials are not are not the lowest ones known, since $E_{1/2}$ values of 0.48-0.49 V vs NHE have been reported for some Ni(II) complexes with pentadentate macrocyclic ligands bound *via* two deprotonated amide Ns and three amine Ns.[27,28,37]

The $Ni^{III/II}$ reduction potentials observed in this work are similar to the values obtained for the Ni complexes with tripeptide ligands. The Ni(II) complexes of these tetradentate diamide ligands have fairly low $Ni^{III/II}$ reduction potentials, which indicates that the deprotonated amides are effective at stabilising the Ni(III) oxidation state. Two reversible reductions were observed in the cyclic voltammograms of [Ni^{II}(bpb)] (Figure 3.15 (b)) and [Ni^{II}(bpen)] (Figure 3.16 (b)). These reductions are ligand centred, two reductions were also observed in the cyclic voltammograms of the ligands (Figure 3.15 (a) and Figure 3.16 (a)), though only the reduction at more negative potential was reversible. The reduction potentials shifted to more positive values when the ligands were coordinated to Ni, and the shift was greater for the first reduction, so the separation between the two redox couples increased upon coordination. The first reduction became reversible in the Ni(II) complexes because the delocalisation of the charge onto the Ni stabilised the reduced form. The shift of the reduction potentials to more positive values is also evidence that the coordination of the ligands to Ni stabilises both of the reduced forms. These two reductions probably involve the pyridyl rings in the ligand as no reductions, either reversible or irreversible, were observed in the cyclic voltammograms of the pyrrolidine based ligands *S,S*-bprolenH_2, *R,R*-(*S,S*)-bprolchxnH_2 and *S,S*-bprolbenH_2.

[Ni^{II}(*S,S*-bprolben)] and [Ni^{II}(*R,R*-(*S,S*)-bprolchxn)] had a single reversible reduction at negative potentials (Figure 3.17); while [Ni^{II}(bprolenH$_{-4}$)] displayed an irreversible reduction (Figure 3.18) at approximately 0.6 V more positive potential. It is not known whether these reductions are primarily ligand based or primarily Ni based. The cyclic voltammograms of [Ni^{II}(*S,S*-brolen)] were only recorded in water (due to its limited solubility in DMF), so it was not possible to examine its redox behaviour with a C electrode at the more negative potentials where the other Ni(II) complexes were reduced.

3.4 Conclusions

Four new Ni(II) complexes with tetradentate diamide ligands were synthesised and characterised by X-ray crystallography, and NMR and IR spectroscopies. The pyrrolidine groups in the ligands made the complexes chiral, though the oxidative dehydrogenation of [Ni^{II}(bprolenH$_{-4}$)] resulted in the loss of the chiral centres in this complex. The [Ni^{II}(*R,R*-(*S,S*)-bprolchxn)] complex contained an additional two chiral centres in the 1,2-cyclohexane bridge between the amide groups. The fixed chirality at position 2 of the pyrrolidine rings controlled the stereochemistry of the amine Ns coordinate to the Ni. The procedures developed can be used to prepare the enantiomeric complexes, but time did not permit these to be synthesised.

The $Ni^{III/II}$ reduction potentials of the complexes with pyrrolidine based ligands, and the pyridyl based analogue, bpen, were quite low, indicating that deprotonated amide ligands are effective at stabilising the Ni(III) oxidation state. Nickel(III) species may be involved in site-selective DNA cleavage by Ni(II)-peptide/oxidant systems.[30,31] These chiral amide ligands that stabilise Ni(III) may prospectively be used to examine the enantioselectivity of such interactions with DNA.

3.5 References

1) R. L. Chapman and R. S. Vagg *Inorg. Chim. Acta* **1979**, *33*, 227-234.

2) D. J. Barnes, R. L. Chapman, F. S. Stephens and R. S. Vagg *Inorg. Chim. Acta* **1981**, *51*, 155-162.

3) F. S. Stephens and R. S. Vagg *Inorg. Chim. Acta* **1982**, *57*, 9-13.

4) F. S. Stephens and R. S. Vagg *Inorg. Chim. Acta* **1986**, *120*, 165-171.

5) T. J. Collins, K. L. Kostka, E. S. Uffelman and T. L. Weinberger *Inorg. Chem.* **1991**, *30*, 4204-4210.

6) T. J. Collins, T. R. Nichols and E. S. Uffelman *J. Am. Chem. Soc.* **1991**, *113*, 4708-4709.

7) M. Mulqi, F. S. Stephens and R. S. Vagg *Inorg. Chim. Acta* **1981**, *52*, 73-77.

8) F. S. Stephens and R. S. Vagg *Inorg. Chim. Acta* **1984**, *90*, 17-24.

9) W. Bal, M. I. Djuran, D. W. Margerum, E. T. Gray Jr., M. A. Mazid, R. T. Tom, E. Nieboer and P. J. Sadler *J. Chem. Soc., Chem. Commun.* **1994**, 1889-1890.

10) H. C. Freeman, J. M. Guss and R. L. Sinclair *Acta Crystallogr., Sect. B* **1978**, *B34*, 2459-2466.

11) H. C. Freeman, J. M. Guss and R. L. Sinclair *J. Chem. Soc., Chem. Commun.* **1968**, 485-487.

12) C. K. Johnson *ORTEP: ORTEPII Report ORNL-5138*; **1976**, Oak Ridge National Laboratory: Oak Ridge.

13) T. Kawamoto, H. Kuma and Y. Kushi *Bull. Chem. Soc. Jpn.* **1997**, *70*, 1599-1606.

14) G. Brewer, P. Kamaras, L. May, S. Prytkhov and M. Rapta *Inorg. Chim. Acta* **1998**, *279*, 111-115.

15) H. Keypour, S. Salehzadeh, R. G. Pritchard and R. V. Parish *Trans. Met. Chem.* **1998**, *23*, 605-607.

16) A. Garoufis, S. Kasselouri, C.-A. Mitsopoulou, J. Sletten, C. Papadimitriou and N. Hadjiliadis *Polyhedron* **1998**, *18*, 39-47.

17) A. Garoufis, S. Kasselouri, C. P. Raptopoulou and A. Terzis *Polyhedron* **1998**, *18*, 585-591.

18) E. Kwiatkowski, M. Klein and G. Romanowski *Inorg. Chim. Acta* **1999**, *293*, 115-122.

19) E. Szłyk, A. Wojtczak, E. Larsen, A. Surdykowski and J. Neumann *Inorg. Chim. Acta* **1999**, *293*, 239-244.

20) A. Böttcher, H. Elias, L. Müller and H. Paulus *Angew. Chem., Int. Ed. Engl.* **1992**, *31*, 623-625.

21) A. Berkessel, J. W. Bats and C. Schwarz *Angew. Chem., Int. Ed. Engl.* **1990**, *29*, 106-108.

22) C. J. Burrows, R. J. Perez, J. G. Muller and S. E. Rokita *Pure Appl. Chem.* **1998**, *70*, 275-278.

23) E. B. Paniago, D. C. Weatherburn and D. W. Margerum *J. Chem. Soc., Chem. Commun.* **1971**, 1427-1428.

24) F. P. Bossu, E. B. Paniago, D. W. Margerum, S. T. Kirksey Jr. and J. L. Kurtz *Inorg. Chem.* **1978**, *17*, 1034-1042.

25) S. A. Ross and C. J. Burrows *Inorg. Chem.* **1998**, *37*, 5358-5363.

26) D. Chen, R. J. Motekaitis and A. E. Martell *Inorg. Chem.* **1991**, *30*, 1396-1402.

27) E. Kimura, A. Sakonaka and R. Machida *J. Am. Chem. Soc.* **1982**, *104*, 4255-4257.

28) E. Kimura, R. Machida and M. Kodama *J. Am. Chem. Soc.* **1984**, *106*, 5497-5505.

29) E. Kimura and R. Machida *J. Chem. Soc., Chem. Commun.* **1984**, 499-500.

30) Q. Liang, D. C. Ananias and E. C. Long *J. Am. Chem. Soc.* **1998**, *120*, 248-257.

31) D. P. Mack and P. B. Dervan *J. Am. Chem. Soc.* **1990**, *112*, 4604-4606.

32) C. Harford, S. Narindrasorasak and B. Sarkar *Biochemistry* **1996**, *35*, 4271-4278.

33) E. C. Long *Acc. Chem. Res.* **1999**, *32*, 827-836.

34) F. P. Bossu and D. W. Margerum *Inorg. Chem.* **1977**, *16*, 1210-1214.

35) C. K. Murray and D. W. Margerum *Inorg. Chem.* **1982**, *21*, 3501-3506.

36) R. Machida, E. Kimura and Y. Kushi *Inorg. Chem.* **1986**, *25*, 3461-3466.

37) Y. Kushi, R. Machida and E. Kimura *J. Chem. Soc., Chem. Commun.* **1985**, 216-218.

Chapter 4

Chromium Complexes with Tetradentate Diamide Ligands

4.1 Introduction

Chromium(V) complexes are usually synthesised by the reduction of Cr(VI) in the presence of the ligand[1-4] or the oxidation of Cr(II) and Cr(III) complexes.[5-12] They can also be formed by ligand-exchange reactions with a previously formed Cr(V) complex.[13-15]

Chromium(V) complexes are highly reactive, often unstable in aqueous solution and difficult to isolate. Few Cr(V) complexes have been isolated and characterised; among them are tetraperoxochromate(V),[16] the oxo-Cr(V) complexes with 2-hydroxy acids,[1-3,17] salen and its derivatives,[6,7] and macrocyclic tetraamides.[5] Nitrido-Cr(V) complexes with salen,[9-11] 5,10,15,20-tetra-*p*-tolylporphyrin,[8] and bis(2-pyridylcarboxamido)-1,2-benzene (bpb)[12] have also been reported. Strong σ and π donors, such as oxo and nitrido groups, alkoxides and deprotonated amide groups are necessary to stabilise the Cr(V) oxidation state.

Chromium(V) complexes have been studied extensively in solution due to the fact that the high reactivity of many Cr(V) complexes prevents them from being isolated as solids[18] and because Cr(V) species are intermediates in the Cr(VI) oxidation of inorganic[19,20] and organic[13,21-29] substrates.

Chromium(V) complexes with oligopeptide ligands were produced by the reduction of Cr(VI) and the oxidation of the Cr(III) analogues,[30] and macrocyclic tetraamido complexes by the oxidation of the Cr(II) complexes.[5] The nitrido-Cr(V) complex of bpb has been synthesised by the photolysis of the Cr(III)-azido complex and characterised by X-ray crystallography, but no details were reported for the Cr(III) intermediates.[12] Complexes of Cr(III)-bpb are used as catalysts in the oxidation of alkenes by iodosobenzene, and an oxo-Cr(V) species was postulated as the reactive intermediate, but it was not characterised.[31]

In this work, both the oxidation of Cr(III) and the reduction of Cr(VI) have been used to generate Cr(V) complexes with deprotonated amide ligands.

4.2 Experimental

4.2.1 Synthesis of Cr(III) Complexes

4.2.1.1 *trans*-[Cr^{III}(bpb)Cl(OH_2)]

Method 1: *trans*-[Cr^{III}(bpb)Cl(OH_2)].DMF

Chromium(III) chloride hexahydrate (0.419 g, Merck, extra pure) was dissolved with heating in DMF (25 mL). A solution of $bpbH_2$ (0.502 g) in DMF (35 mL) was added, followed by triethylorthoformate (20 mL, Aldrich, 98%). The solution was boiled for 4½ h and in the process the volume was reduced to ~ 5 mL. The reaction mixture was cooled and DMF (5 mL) was added to redissolve some dark brown solid that had formed. Diethyl ether (25 mL) was added and a dark brown solid precipitated. The precipitate was collected at the pump and the residue was washed with diethyl ether (2 × 25 mL) and dried under vacuum over silica gel. Yield: 0.4706 g (60%). IR (DRIFTS in KBr; cm^{-1}): 3061 (w); 2941 (w); 1654 (ss); 1626 (ss); 1596 (ss); 1574 (ss); 1474 (ss); 1450 (m); 1363 (ss); 1291 (m); 1147 (w); 1091 (w); 1051 (w); 1029 (w); 964 (m); 811 (w); 755 (m); 690 (m); 655 (w); 565 (w); 510 (m); 450 (w); 424(w); 406 (w). IR (DRIFTS in polyethylene; cm^{-1}): 382 (w); 328 (w); 323 (w); 280 (w). UV-Vis (DMF) λ_{max} (ε): 342 nm (1.02×10^4 M^{-1} cm^{-1}); 438 nm (3.90×10^3 M^{-1} cm^{-1}, sh). ES/MS (CH_3OH) (+ve ion): 368, 753, 767, 887, 1167 m/z. Calculated for $C_{21}H_{21}N_5O_4ClCr$: C, 50.96%; H, 4.28%; N, 14.16%; Cr, 10.51%. Found: C, 51.86%; H, 4.35%; N, 14.47%; Cr, 10.7%.

Method 2: *trans*-[Cr^{III}(bpb)Cl(OH_2)]

The Cr(III) complex of bpb was also prepared by a modification of the method of Leung *et al.*[31] Chromium(III) chloride hexahydrate (0.84 g, Merck, 95%) and $bpbH_2$ (1.00 g) were dissolved in DMF (35 mL, Prolabo, AR) and triethylorthoformate (10 mL, Aldrich, 98%) was added. A $CaCl_2$ drying tube was attached to the top of the condenser and the mixture was refluxed for 4½ h. The condenser was removed and the mixture was boiled for 40 min to reduce the volume of the solution to ~20 mL. The solution was cooled and water was gradually added until a precipitate formed. The product was collected at the pump and the residue was washed with water (20 mL) and dried under vacuum over silica gel. Yield: 0.973 g (70%). IR (DRIFTS in KBr; cm^{-1}): 3487 (w, br); 2700-3400 (m, br); 1667 (w); 1615 (m); 1591

(ss); 1561 (s); 1473 (s); 1449 (m); 1393 (m); 1368 (m); 1290 (m); 1149 (w); 1097 (w); 1051 (w); 1037 (w); 1030 (w); 967 (m); 898 (w); 807 (w); 754 (s); 687 (m); 654 (w); 516 (m); 454 (w). IR (DRIFTS in polyethylene; cm^{-1}): 377(w); 335 (w); 317 (w); 278 (w). UV-Vis (DMF) λ_{max} (ε): 340 nm (9.52×10^3 M^{-1} cm^{-1}); 438 nm (3.97×10^3 M^{-1} cm^{-1}, sh). Calculated for $C_{18}H_{14}N_4O_3ClCr$: C, 51.25%; H, 3.35%; N, 13.29%. Found: C, 50.95%; H, 3.83%; N, 13.12%.

4.2.1.2 *trans*-$[Cr^{III}(bpb)(OH_2)_2]ClO_4.H_2O$*

The complex was synthesised according to the method of Leung *et al.*[31] *trans*-$[Cr^{III}(bpb)Cl(OH_2)]$ (0.100 g) was dissolved in NaOH solution (10 mL, 0.05 M) and heated to boiling for 20 min. The dark red solution was cooled and perchloric acid (Merck, 70%, AR) was added dropwise until a precipitate formed. The precipitate was collected at the pump and was washed with water (10 mL). The residue was dissolved in water/acetone (15 mL, 1:3 v/v) and brown crystals formed upon slow evaporation of the acetone. The product was collected at the pump, washed with water (10 mL) and air dried. Yield 81.4 mg (66%). IR (DRIFTS in KBr; cm^{-1}): 3400-2400 (m, br); 1610 (m); 1585 (m); 1544 (ss); 1469 (m); 1450 (m); 1398 (m); 1297 (w); 1149 (m); 1116(m); 1087 (m); 1029 (w); 803 (w); 754 (m); 685 (m); 655 (w); 637 (w); 513 (m) 445 (w). IR (DRIFTS in polyethylene; cm^{-1}): 384(w); 352 (w); 336 (w); 302 (w); 279 (w). UV-Vis (DMF) λ_{max} (ε): 336 nm (1.03×10^4 M^{-1} cm^{-1}); 434 nm (4.13×10^3 M^{-1} cm^{-1}, sh). Calculated for $C_{18}H_{18}N_4O_9ClCr$: C, 41.43%; H, 3.48%; N, 10.74%. Found: C, 41.59%; H, 3.38%; N, 10.76%.

4.2.1.3 $[Cr^{III}(S,S\text{-bprolben})L_2]^{n+}$

A solution of *S,S*-bprolbenH_2 (0.4947 g) and $CrCl_3.6H_2O$ (0.4413 g, Merck, 95%) in DMF (20 mL, Ajax, AR) and triethylorthoformate (12 mL, Aldrich, 98%) was refluxed for 26 h then boiled for 1½ h and the volume reduced to ~10 mL. The solution was cooled and the product was precipitated by the addition of water (15 mL). The dark brown powder was collected at the pump and dried under vacuum over silica gel. Yield: 0.1629 g. IR (DRIFTS in KBr; cm^{-1}): 3062 (w); 2968 (m);

---

* ***Caution: Perchlorate salts of metal complexes are potentially explosive and should be handled with care.***[32]

2876 (m); 1721 (s); 1660 (ss); 1566 (s); 1501 (m); 1452 (m); 1409 (m); 1366 (m); 1210 (w); 1095 (m); 1036 (m); 896 (w); 757 (m); 701 (w); 568 (m, br). UV-Vis (DMF) λ_{max}: 342 nm. Calculated for $C_{16}H_{22}N_4O_3ClCr$: C, 47.84%; H, 5.46%; N, 13.81%. Found: C, 51.25%; H, 5.73%; N, 11.86%.

4.2.1.4 $[Cr^{III}(bpen)Cl(OH_2)].2H_2O.2CH_3OH$

Chromium(III) chloride hexahydrate (0.49 g, Merck, 95%) was dissolved in DMF (30 mL) with heating and a solution of $bpenH_2$ (0.52 g) in DMF (45 mL) was added. The mixture was boiled and triethylorthoformate (15 mL, Aldrich, 98%) was added in four portions over the course of 2 h. The mixture was boiled for 1 h and the volume was reduced to ~10 mL. Diethyl ether (15 mL) was added and the precipitate was collected at the pump and washed with diethyl ether (15 mL). A second crop was obtained by adding diethyl ether (25 mL) to the filtrate and collecting the precipitate that formed as described above. The crude product was dissolved in methanol (~3 mL) and loaded onto a column of LH20 lipophilic Sephadex (25 × 2 cm) and then eluted with methanol. The large maroon band that eluted was collected and after slow evaporation of the solvent the product was collected as a dark maroon coloured powder. Yield: 0.134 g (15%). IR (DRIFTS in KBr; cm^{-1}): 3062 (w); 2925 (w); 2850 (w); 1582 (ss); 1563 (ss); 1441 (m); 1391 (m); 1378 (m); 1293 (m); 1261 (m); 1193 (w); 1097 (m); 1052 (m); 1031 (m); 815 (w); 763 (m); 692 (m); 656 (m); 545 (m); 429 (w). IR (DRIFTS in polyethylene; cm^{-1}): 358 (w). UV-Vis (DMF) λ_{max} (ε): 338 nm (2.91×10^3 M^{-1} cm^{-1}, sh); 544 nm (1.09×10^2 M^{-1} cm^{-1}). ES/MS (CH_3OH) (+ve ion): 271, 293, 316, 352, 425, 632, 699 m/z. Calculated for $C_{16}H_{26}N_4O_7ClCr$: C, 40.56%; H, 5.53%; N, 11.82%. Found: C, 40.55%; H, 4.96%; N, 11.94%.

4.2.2 Oxidation of Cr(III) Complexes to the Cr(V) Analogues*

4.2.2.1 Oxidation of *trans*-[Cr^{III}(bpb)Cl(OH_2)]

Method 1

Lead(IV) oxide (0.105 g, Merck, pure) was added to a solution of *trans*-[Cr^{III}(bpb)Cl(OH_2)] (25.3 mg) in DMF (4 mL, Ajax, AR). The mixture was stirred for 1 h, filtered to remove the unreacted PbO_2, and the EPR spectrum of the filtrate was recorded.

Method 2

trans-[Cr^{III}(bpb)Cl(OH_2)] (20.8 mg) in acetonitrile (10 mL, Ajax, 99.7%) was agitated in a sonicating water bath for 20 min and the mixture was filtered to remove any undissolved solid. Iodosobenzene (30 mg) was added to the filtrate and EPR spectra were recorded at regular intervals over 90 min to monitor the development of Cr(V) species.

Method 3

A solution of *trans*-[Cr^{III}(bpb)Cl(OH_2)] (2.2 mg) in acetonitrile (5 mL, Ajax, 99.7%) and *tert*-butylhydroperoxide (100 μL, Fluka, ~5.5 M in nonane) were mixed. EPR spectra were recorded at regular intervals over 90 min to monitor the development of Cr(V) species.

Method 4

Iodosobenzene (11.5 mg) was added to a solution of *trans*-[Cr^{III}(bpb)Cl(OH_2)] (5.9 mg) in DMF (5 mL, Ajax, AR). EPR spectra were recorded at regular intervals over 90 min to monitor the development of Cr(V) species.

4.2.2.2 Oxidation of [Cr^{III}(bpen)Cl(OH_2)].$2H_2O$.$2CH_3OH$

Iodosobenzene (9.8 mg) was added to a solution of [Cr^{III}(bpen)Cl(OH_2)].$2H_2O$.$2CH_3OH$ (9.9 mg) in DMF (5 mL, BDH, 99.9%).

Caution: Chromium(V) complexes are mutagenic and potentially carcinogenic,[33-36] contact with skin and inhalation must be avoided.

EPR spectra were recorded at regular intervals over 90 min to monitor the development of Cr(V) species.

4.2.2.3 Oxidation of $[Cr^{III}(S,S\text{-bprolben})L_2]^{n+}$

Iodosobenzene (12.7 mg) was added to a solution of $[Cr^{III}(S,S\text{-bprolben})L_2]^{n+}$ (10.8 mg) in DMF (5 mL, BDH, 99.9%). EPR spectra were recorded at regular intervals over 90 min and at 22 h to monitor the development of Cr(V) species.

4.2.3 Reduction of Cr(VI) in the Presence of Tetradentate Diamide Ligands

4.2.3.1 Reduction of Cr(VI) in Acetone/Methanol

A solution of $Na_2Cr_2O_7.2H_2O$ (0.056 g, Merck, 99.5%) in acetone (25 mL) and methanol (5 mL) was stirred under a fluorescent desk lamp (~20 cm away, Norax brand fitted with a 45 × 2.5 cm 15 W tube). The reaction mixture was monitored by EPR spectroscopy over 7 d to follow the development of Cr(V) signals.

4.2.3.2 Reduction of Cr(VI) in the Presence of $bpenH_2$

Method 1: $C_{16}Cr_4H_{24}N_4Na_3O_{22}$

Sodium dichromate dihydrate (0.731 g, Merck, 99%) was added to a mixture of $bpenH_2$ (2.04 g) in acetone (40 mL, Merck, 99.5%). When the colour of the reaction mixture had not changed after stirring for 2 d, hydrochloric acid (2 drops, BDH, 32%) was added. No change occurred over the course of the next day so methanol (5 mL, Rhone Poulenc Prolabo, 99.8%) was added and the mixture was stirred for a further 4 d. The reaction mixture was filtered at the pump and the residue was dried over silica gel. To remove unreacted $bpenH_2$, a chloroform mixture of the residue was sonicated and the insoluble residue was collected at the pump. The brown powder was dried over silica gel under reduced pressure. Yield 101 mg (9%). IR (DRIFTS in KBr; cm^{-1}): 3254 (w, br); 3074 (w); 1636 (ss); 1604 (m); 1559 (m); 1540 (m); 1473 (w); 1436 (w); 1054 (w); 1031 (w); 945 (s, br); 811 (w); 784 (s, br); 684 (w); 547 (w). UV-Vis (DMF) λ_{max}: 268 nm; 384 nm (sh). ES/MS (CH_3OH) (+ve ion): 293, 372, 413, 563, 757, 955, 1497 m/z. Calculated for $C_{16}H_{24}N_4O_{22}Cr_4Na_3$: C, 21.32%; H, 2.68%; N, 6.24%; Cr, 23.1%; Na, 7.65%. Found:

C, 21.38%; H, 2.69%; N, 6.34%; Cr, 23%; Na, 7.7%.

Method 2

Sodium dichromate dihydrate (0.0555 g, Merck, 99%) was added to a mixture of bpenH_2 (0.1079 g) in acetone (10 mL, Merck, 99.5%) and methanol (5 mL, Prolabo, AR). Hydrochloric acid (2 drops, BDH, 32%) was added and the mixture was stirred for three days. The reaction mixture was filtered at the pump and the residue was then washed with acetone (3 × ~2 mL, Merck, 99.5%) and dried over silica gel. Yield 56.7 mg. IR (DRIFTS in KBr; cm^{-1}): 3217 (m. br); 3066 (m); 1638 (ss); 1606 (m); 1554 (m); 1536 (w); 1475 (w); 1435 (w); 1055 (m); 1029 (m); 948 (m); 917 (m); 811 (m); 758 (m); 684 (w); 549 (br, m).

4.2.3.3 Reduction of Cr(VI) in the Presence of bpbH_2

To an acetone solution (50 mL) of bpbH_2 (0.2575 g) was added a solution of $Na_2Cr_2O_7.2H_2O$ (0.1145 g, Merck, 99.5%) in methanol (10 mL, Prolabo, AR). Acetone (20 mL) was added, the reaction mixture was stirred, and the reaction was monitored by EPR spectroscopy over 8 d to follow the development of Cr(V) signals.

4.2.3.4 Reduction of Cr(VI) in the Presence of *S,S*-bprolbenH_2

Method 1: Dark Reaction

A solution of *S,S*-bprolbenH_2 (0.2520 g) in acetone (40 mL) and a solution of $Na_2Cr_2O_7.2H_2O$ (0.1175 g, Merck, 99.5%) in methanol (10 mL) were mixed. Acetone (20 mL) was added and the flask was covered with aluminium foil to protect the reaction mixture from light. The stirred reaction mixture was monitored by EPR spectroscopy over 3 d to follow the development of Cr(V) signals.

Method 2: Light Reaction

A solution of *S,S*-bprolbenH_2 (0.2564 g) in acetone (40 mL) and a solution of $Na_2Cr_2O_7.2H_2O$ (0.1226 g, Merck, 99.5%) in methanol (10 mL) were mixed. Acetone (20 mL) was added and the mixture was stirred under a fluorescent desk lamp (~20 cm away, Norax brand fitted with a 45 × 2.5 cm 15 W tube). The reaction mixture was monitored by EPR spectroscopy over 6 d to follow the development of Cr(V) signals.

Isolation of $[Cr^{V}O(S,S\text{-bprolben})]^{+}$

A solution of *S,S*-bprolbenH_2 (0.255 g) in acetone (40 mL) was mixed with a solution of $Na_2Cr_2O_7.2H_2O$ (0.118 g, Merck, 99.5%) in methanol (10 mL). Acetone (20 mL) was added and the mixture was exposed to the ambient light in the laboratory and stirred for 9 d. The reaction mixture changed colour from orange to dark brown and contained a fine precipitate. The reaction mixture was centrifuged ($r_{average}$ = 11.94 cm, 5000 rpm, 10 min) in a Sorvall RC-5B superspeed centrifuge. The supernatant was decanted and reserved; the residue was washed with acetone (50 mL), the mixture centrifuged ($r_{average}$ = 11.94 cm, 5000 rpm, 15 min), the supernatant was decanted and the residue was dried under reduced pressure over silica gel. The volume of the original supernatant was reduced to ~10 mL on a rotary evaporator (water bath < 25 °C) and it was loaded onto a column of LH20 lipophilic Sephadex (11 × 2 cm) and eluted with methanol. Several fractions were eluted as a faster moving grey-brown band and a slower moving orange-brown band, which overlapped. EPR spectroscopy was used to identify the Cr(V) species in the fractions. The solvent was removed from the fraction containing the orange-brown band on a rotary evaporator. The residue was dissolved in water and the stability of the Cr(V) complex was monitored by EPR spectroscopy.

4.2.4 Analysis and Instrumentation

EPR measurements were carried out on a Bruker EMX X-band spectrometer equipped with an ER 041XG microwave bridge, an EMX 148T microwave bridge controller, an EMX 035M NMR gaussmeter, an EMX 032T field controller, and an EMX 120 modulation amplifier. Spectra were recorded at room temperature from solutions contained in a quartz flat cell. EPR spectrometer operating parameters were as follows: operating frequency, ~9.7 GHz; modulation frequency, 100 kHz; other parameters are as indicated in figure captions. Simulations of the EPR spectra were performed using the program WinSim.[37]

Solutions for the determination of Cr content were prepared by digesting samples of the complex for 40 min on a steam bath in a mixture of NaOH solution (~2 M, 20 mL) and hydrogen peroxide (3%, 20 mL) then making up to volume with distilled water. The Cr content was determined by flame AAS using a Varian SpectrAA 800.

Solutions for the determination of Na content were prepared by dissolving the complex in hydrochloric acid (32%, BDH, AR) and making up to volume with distilled water. The Na content was determined using a Sherwood 410 flame photometer. Microanalyses for C, H and N were carried out at the Research School of Chemistry, Australian National University and the University of Otago, New Zealand.

The IR spectra were recorded by DRIFTS on a Bio Rad FTS-40 spectrometer with KBr as the matrix and the background in the 400-4000 cm^{-1} range, and polyethylene as the matrix and background in the 250-400 cm^{-1} range, resolution: 4 cm^{-1}. The IR bands were assigned by comparison to the spectra of the free ligands and according to Bellamy[38] and Ferraro.[39] UV-Visible spectra were recorded from 300-800 nm on a Hewlett Packard 8452A diode array spectrophotometer using a 1 cm path length quartz cell.

Electrospray mass spectra were recorded by Dr Xiaomin Song and Dr Keith Fisher on a Finnigan LCQ ES1-APC1 Triple-Quadrupole Mass Spectrometer. Theoretical molecular isotope distributions were calculated using *Molecular Isotope Distribution Calculator Program.*[40]

4.3 Results and Discussion

4.3.1 Synthesis and Characterisation of Cr(III) Complexes

The synthesis of the Cr(III) complexes with the tetradentate diamide ligands was difficult due to the inert nature of the Cr(III) oxidation state and the need to deprotonate the amide groups. The complexes were synthesised by boiling a mixture of $CrCl_3.6H_2O$ and the ligand in DMF. Due to the kinetic inertness of Cr(III) to substitution reactions, it is difficult to remove the aqua ligands from the starting material; therefore, triethylorthoformate was added as a water scavenger.

4.3.1.1 *trans*-[Cr^{III}(bpb)Cl(OH_2)]

The reaction mixture gradually changed colour from dark green to dark brown as it boiled. The product was quite soluble in DMF requiring precipitation by the addition

of diethyl ether (Method 1) or water (Method 2). The elemental analysis showed that complexes produced by the two methods differed only by the inclusion of a DMF of crystallisation in the product of Method 1.

The νN–H band (at 3317 cm^{-1} for $bpbH_2$) was absent from the IR spectra (Table 4.1), which showed that bpb was coordinated *via* the deprotonated amide N to the Cr. There was little difference in the position of most of the characteristic IR bands of the two products. The amide I band was one that differed significantly between the two samples. This was probably because the amide group of the DMF of crystallisation, which was only in the product of Method 1, also occurs in this region.

The ligand, bpb, is a planar tetradenate and is expected to fill the four equatorial sites of the six-coordinate Cr(III), leaving the two axial positions for the coordination of monodentate ligands. The axial positions must be occupied by Cl^- and H_2O in the product from Method 2 as these were the only options. In the product resulting from Method 1 there was also the molecule of DMF that can coordinate to metal ions through the O atom.[41] The band at ~810 cm^{-1} in the IR spectra was evidence that H_2O was coordinated in both products. However, it was difficult to determine from the IR spectrum whether the second axial coordination site in the product from Method 1 was occupied by Cl^- or DMF. The νCr–Cl vibration in Cr(III) complexes has been reported in the range 303-375 cm^{-1},[39,42] and the band at ~320 cm^{-1} (which was absent from the IR spectrum of $[Cr^{III}(bpb)(OH_2)_2]ClO_4$) may be due to νCr–Cl, but as νCr–N vibrations also occur in the 300-400 cm^{-1} region,[39] the ligand in the second axial coordination site could not be unambiguously assigned from the low frequency region of the IR spectra, without isotopic substitution.

The most abundant ions in the ES/MS spectra were the mononuclear species (Table 4.2). The calculated and observed isotopic distributions for the two most abundant molecular ions are shown in Table 4.3. In all the species the Cr:ligand ratio was 1:1, dimers and trimers were observed but they all involved OH^- or OCH_3^-. The OCH_3^- came from the solvent used in the ES/MS experiment, an indication that the dimers and trimers were probably formed by aggregation of monomers as the solution

Table 4.1 Characteristic IR bands of *trans*-[Cr^{III}(bpb)Cl(OH_2)]

Wavenumber (cm^{-1})		Assignment
Method 1	Method 2	
3061		νC–H
2941		νC–H
1626	1615	amide I
1596	1591	aromatic ring
1574	1561	skeletal vibrations
1474	1473	and C–H
1450	1449	deformation
811	807	coordinated H_2O rock
755	754	C–H deformation

Table 4.2 Assignment of the +ve ion ES/MS data for *trans*-[Cr^{III}(bpb)Cl(OH_2)].DMF

m/z	Relative Intensity	Molecular Formula	Assignment
368	100	$C_{18}H_{12}N_4O_2Cr$	$[Cr(bpb)]^+$
753	8	$C_{36}H_{25}N_8O_5Cr_2$	$[Cr_2(bpb)_2(OH)]^+$
767	30	$C_{37}H_{27}N_8O_5Cr_2$	$[Cr_2(bpb)_2(OCH_3)]^+$
1167	7	$C_{56}H_{43}N_{12}O_8Cr_3$	$[Cr_3(bpb)_3(OCH_3)(CH_3OH)]^+$

became more concentrated as it evaporated. The OCH_3^- may be acting as a bridging group in the dimers and trimers.

Structural characterisation of the product from Method 1 was carried out by multiple-scattering XAFS analysis, the experimental details and results are in Chapter 5. The results indicated that Cl^- and O were coordinated in the axial positions, since the IR spectra indicated that H_2O was one of the axial ligands, thus the formulation of the complex is *trans*-[Cr^{III}(bpb)Cl(OH_2)].DMF.

Table 4.3 Observed and calculated molecular isotope distributions for +ve ion ES/MS data for *trans*-[Cr^{III}(bpb)Cl(OH_2)].DMF

Molecular Formula	m/z	Relative Intensity	
		Calculated	Observed
$C_{18}H_{12}N_4O_2Cr$	366	5.2	5
	367	1.1	2
	368	100	100
	369	32.5	32
	370	7.7	10
	371	1.1	1
$C_{37}H_{27}N_8O_5Cr_2$	765	10.1	14
	766	5.5	6
	767	100	100
	768	65.4	68
	769	26.6	29
	770	7.5	11

4.3.1.2 *trans*-[Cr^{III}(bpb)(OH_2)$_2$]ClO_4

The Cl^- ligand in *trans*-[Cr(bpb)Cl(OH_2)] was removed by boiling an alkaline solution, resulting in a complex with two aqua ligands in the axial position, which was isolated as the perchlorate salt.

The IR spectrum (Table 4.4) showed a broad O–H stretching band from 3400-2400 cm^{-1} due to the aqua ligands. The was also a νCl–O band at 1116 cm^{-1} due to the perchlorate counterion.[43,44] The other identifiable bands only varied by small amounts from the frequencies observed for *trans*-[Cr^{III}(bpb)Cl(OH_2)] (Table 4.1).

This complex with known axial ligands was synthesised as a model complex for the XAFS analysis of the Cr(III)-bpb complexes (Chapter 5). Since its axial ligands were known, the XAFS structural parameters obtained could be used as a check on the accuracy of the refinements of models with different axial ligands to fit the XAFS data for *trans*-[Cr(bpb)Cl(H_2O)].DMF.

Table 4.4 Characteristic IR bands of *trans*-$[Cr^{III}(bpb)(OH_2)_2]ClO_4$

Wavenumber (cm^{-1})	Assignment
3400-2400	νO–H
1610	amide I
1585	aromatic ring
1544	skeletal vibrations
1469	and C–H
1450	deformation
1116	νCl–O
803	coordinated H_2O rock
754	C–H deformation

4.3.1.3 $[Cr^{III}(S,S\text{-bprolben})L_2]^{n+}$

The reaction of Cr(III) with *S,S*-bprolbenH_2 was considerably slower than the analogous reaction with bpbH_2. A much longer reaction time was required and the first sign of a colour change was only observed after 12 h. After refluxing for 26 h, the green colour of the starting material had all disappeared and the reaction mixture was dark brown in colour. The microanalysis results showed that the product was impure. The values for C and N differed significantly from those calculated for $[Cr^{III}(S,S\text{-bprolben})Cl(OH_2)]$, and it was difficult to find an alternative formulation that gave reasonable agreement between the experimental and calculated values. The IR spectrum indicated that the ligand was coordinated *via* deprotonated amide N so the crude product was used without further purification in the reaction with iodosobenzene to generate Cr(V).

The νN–H band (at 3312 cm^{-1} for *S,S*-bprolbenH_2) was absent from the IR spectrum (Table 4.5), which showed that the ligand was coordinated *via* deprotonated amide Ns to the Cr. The peak at 1660 cm^{-1} is due to the amide I band.

Table 4.5 Characteristic IR bands of $[Cr^{III}(S,S\text{-bprolben})L_2]^{n+}$

Wavenumber (cm^{-1})	Assignment
2968	νC–H
2876	νC–H
1660	amide I
1566	aromatic ring skeletal
1501	vibration or C–H
1452	deformation
757	C–H deformation

4.3.1.4 $[Cr^{III}(bpen)Cl(OH_2)].2H_2O.2CH_3OH$

The product was very soluble in DMF so it was precipitated by the addition of diethyl ether. This led to a crude product that was purified by column chromatography on LH20 Sephadex.

The νN–H band (at 3334 cm^{-1} for $bpenH_2$) was absent from the IR spectrum, which was evidence that the ligand was probably coordinated to Cr via deprotonated amide N atoms. The bands at 815 cm^{-1} and 544 cm^{-1} indicated that there was also H_2O coordinated, but this does not show whether H_2O occupies just one or both of the axial sites, so the complex could also be formulated as $[Cr^{III}(bpen)(OH_2)_2]Cl.H_2O.2CH_3OH$.

The predominant species in the +ve ion ES/MS spectrum was the protonated adduct of $bpenH_2$ (Table 4.7), for which the observed and calculated molecular isotope distribution is shown in Table 4.8. There were also small amounts of a Cr(III)-bpen complex. The low level of the Cr(III)-bpen complex observed indicated that it was less stable under ES/MS conditions than the analogous Cr(III)-bpb complexes.

Table 4.6 Characteristic IR bands of $[Cr^{III}(bpen)Cl(OH_2)].2H_2O.2CH_3OH$

Wavenumber (cm^{-1})	Assignment
3062	νC–H
2925	νC–H
2850	νC–H
1582	amide I
1441	C–H deformation
1193	pyridyl ring
1097	vibration
1052	or C–H
1031	deformation
815	coordinated H_2O rock
763	C–H deformation
544	coordinated H_2O wag

Table 4.7 Assignment of the +ve ion ES/MS data for $[Cr^{III}(bpen)Cl(OH_2)].2H_2O.2CH_3OH$

m/z	Relative Intensity	Molecular Formula	Assignment
271	100	$C_{14}H_{15}N_4O_2$	$[bpenH_3]^+$
293	9	$C_{14}H_{14}N_4O_2Na$	$[Na(bpenH_2)]^+$
352	8	$C_{15}H_{16}N_4O_3Cr$	$[Cr(bpen)(CH_3OH)]^+$
425	12	–	–

Table 4.8 Observed and calculated molecular isotope distributions for +ve ion ES/MS data for $[Cr^{III}(bpen)Cl(OH_2)].2H_2O.2CH_3OH$

Molecular Formula	m/z	Relative Intensity	
		Calculated	Observed
$C_{14}H_{15}N_4O_2$	271	100	100
	272	16.8	18

4.3.2 Oxidation of Cr(III) Complexes to the Cr(V) Analogues

4.3.2.1 Oxidation of *trans*-[Cr^{III}(bpb)Cl(OH_2)]

The use of PbO_2 as an oxidant in Method 1 produced three Cr(V) EPR signals (Figure 4.1). The signal at g_{iso} = 1.9835 was the strongest, and five lines due to superhyperfine couplings were observed. The pattern of the couplings was the same as those observed for signal from the species produced in Method 2, Method 3 and Method 4, but the sixth line was hidden due to overlap with the signal at g_{iso} = 1.9783.

The compound *trans*-[Cr^{III}(bpb)Cl(OH_2)].DMF was only partially soluble in acetonitrile, so a saturated solution was prepared to maximise the concentration for the oxidation reaction using Method 2. The solution of the Cr(III) complex changed colour from orange-brown to green-brown in less than a minute when the iodosobenzene was added with concomitant growth of the Cr(V) EPR signals over

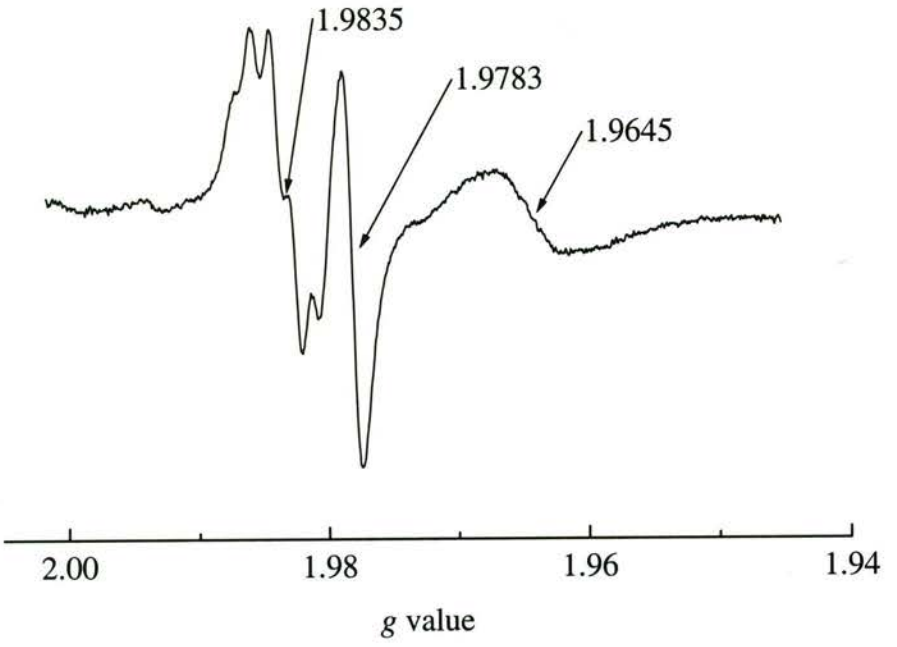

Figure 4.1 EPR spectrum of the Cr(V) species produced in the PbO_2 oxidation of *trans*-[Cr^{III}(bpb)Cl(OH_2)] in DMF. Parameters: receiver gain, 6.32×10^4; sweep width, 100 G; power, 20.12 mW; modulation amplitude, 1.00 G; time constant, 40.96 msec; conversion time, 40.96 msec; scans, 30.

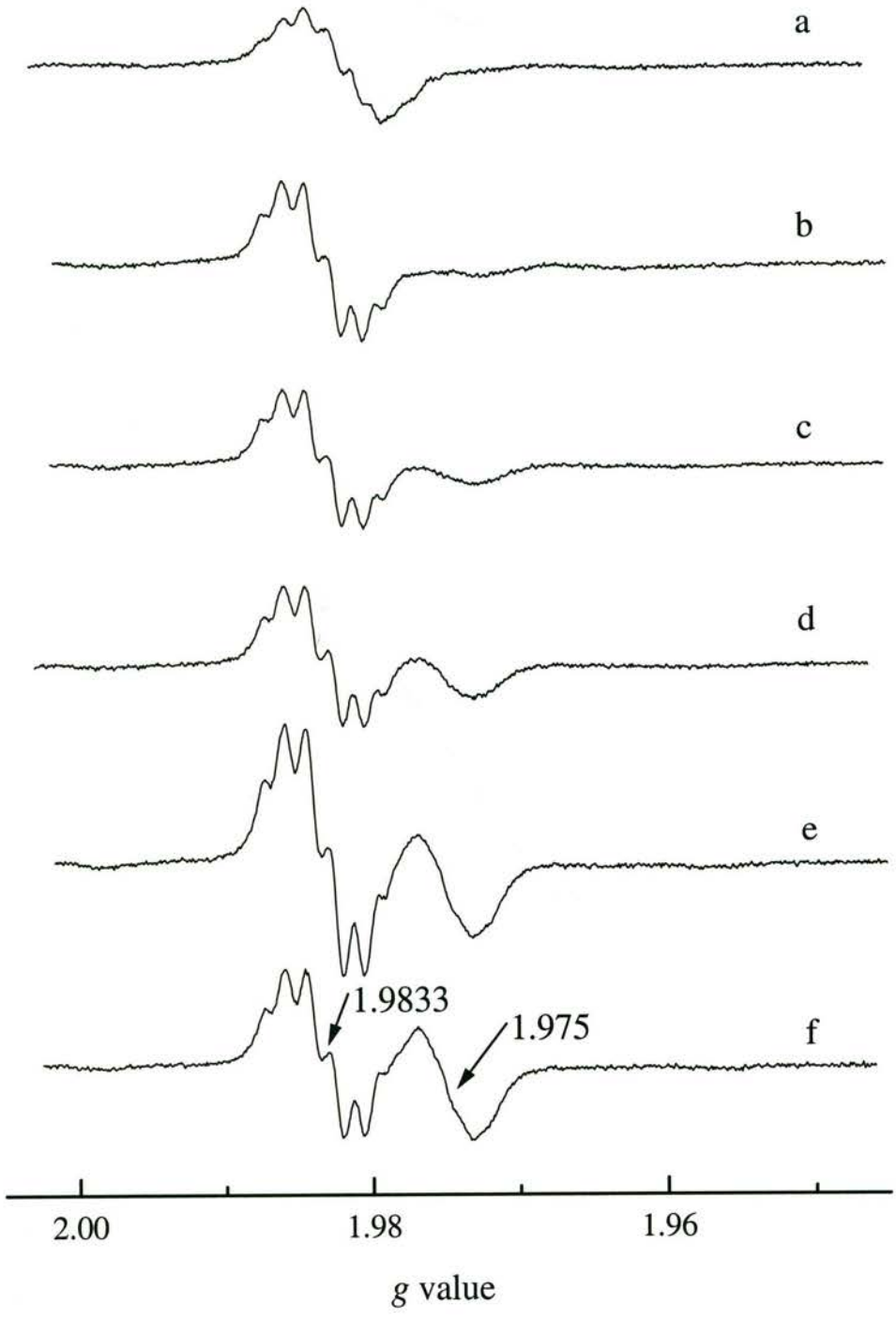

Figure 4.2 EPR spectra of the Cr(V) products of the iodosobenzene oxidation of *trans*-[Cr^{III}(bpb)Cl(OH_2)] in acetonitrile recorded at: (a) 5 min, (b) 10 min, (c) 20 min, (d) 30 min, (e) 60 min, and (f) 90 min after the addition of the oxidant. Parameters: sweep width, 100 G; receiver gain, 6.32×10^4; power, 20.12 mW; modulation amplitude, 1.00 G; time constant, 20.48 msec; conversion time, 20.48 msec; scans, 5.

time (Figure 4.2). A six-line signal centred at g_{iso} = 1.9833 was present in all of the spectra and increased in intensity with time until it reached its maximum value at 60 min. As the intensity of the signal increased, the resolution improved, but the superhyperfine couplings were still not fully resolved, showing that more than one species was present. A second EPR signal with g_{iso} = 1.975 appeared after 10 min; it was weak initially, but rapidly increased in intensity with time. Though this signal was broad, no superhyperfine coupling was resolved.

When *tert*-butylhydroperoxide was used as the oxidant using Method 3, the solution changed colour rapidly from orange-brown to dark red-brown, and three signals were observed in the EPR spectrum after 5 min (Figure 4.3). The six-line signal centred at g_{iso} = 1.9832 was the strongest; it increased slightly in intensity and the resolution of the superhyperfine couplings improved up to about 20 min, after that the intensity did not change significantly over 1 h. The broad signals with g_{iso} = 1.975 and 1.963 decreased in intensity with time; the signal at g_{iso} = 1.963 decayed more rapidly. The EPR spectrum of the solution after 1 day still showed a six-line Cr(V) signal with g_{iso} = 1.9831, but the intensity had decreased by ~70%.

There was little change in colour as a result of oxidation via Method 4, since the orange-brown solution of the Cr(III) complex only darkened slightly after the iodosobenzene was added. A single six-line signal centred at g_{iso} = 1.9832 was observed after 5 min (Figure 4.4). The intensity of this signal increased with time, reaching a maximum value after 40 min and then slowly decreased. A second very broad signal at g_{iso} = 1.962 was just visible after 10 min, and then slowly increased in intensity with time. The resolution of the superhyperfine structure of the six-line signal was better in the spectra recorded for this oxidation method than that in the spectra obtained using Methods 1-3. The presence of a shoulder on the fourth peak showed that there was more than one species present, but they were still not fully resolved.

Another sample of *trans*-[Cr^{III}(bpb)Cl(OH_2)] in DMF was oxidised with iodosobenzene and the EPR spectrum was recorded after ~1 h (Figure 4.5(a)). The use of a smaller modulation amplitude improved the resolution of the peaks from the different species, while the receiver gain and number of scans were increased to

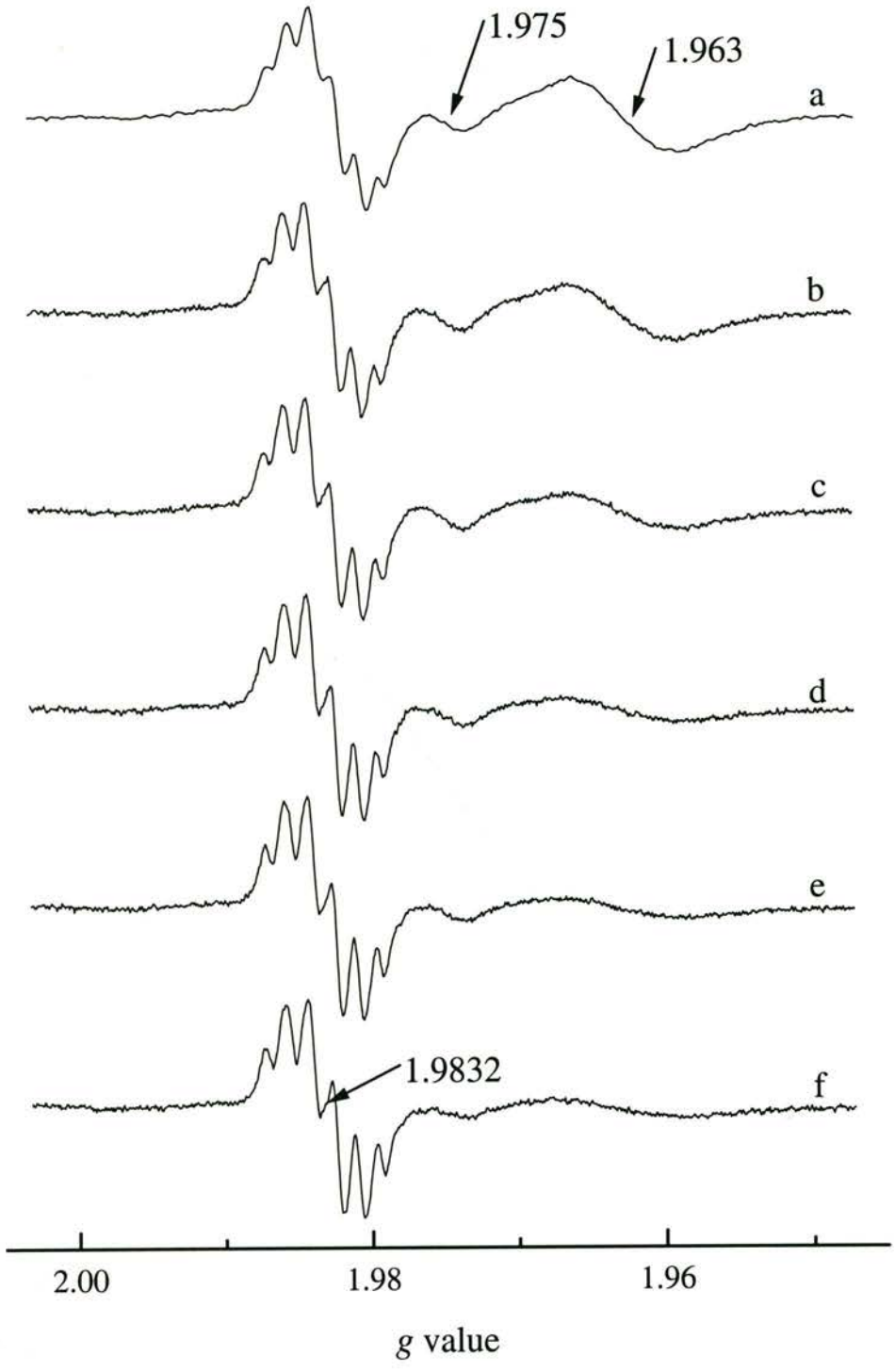

Figure 4.3 EPR spectra of the Cr(V) products obtained during the *tert*-butylhydroperoxide oxidation of *trans*-[Cr^{III}(bpb)Cl(OH_2)] in acetonitrile recorded at: (a) 5 min, (b) 10 min, (c) 20 min, (d) 40 min, (e) 60 min, and (f) 90 min after the addition of the oxidant. Parameters: receiver gain, 6.32×10^4; sweep width, 100 G; power, 20.17 mW; modulation amplitude, 1.00 G; time constant, 20.48 msec; conversion time, 20.48 msec; scans, (a) 5, (b)-(f) 2.

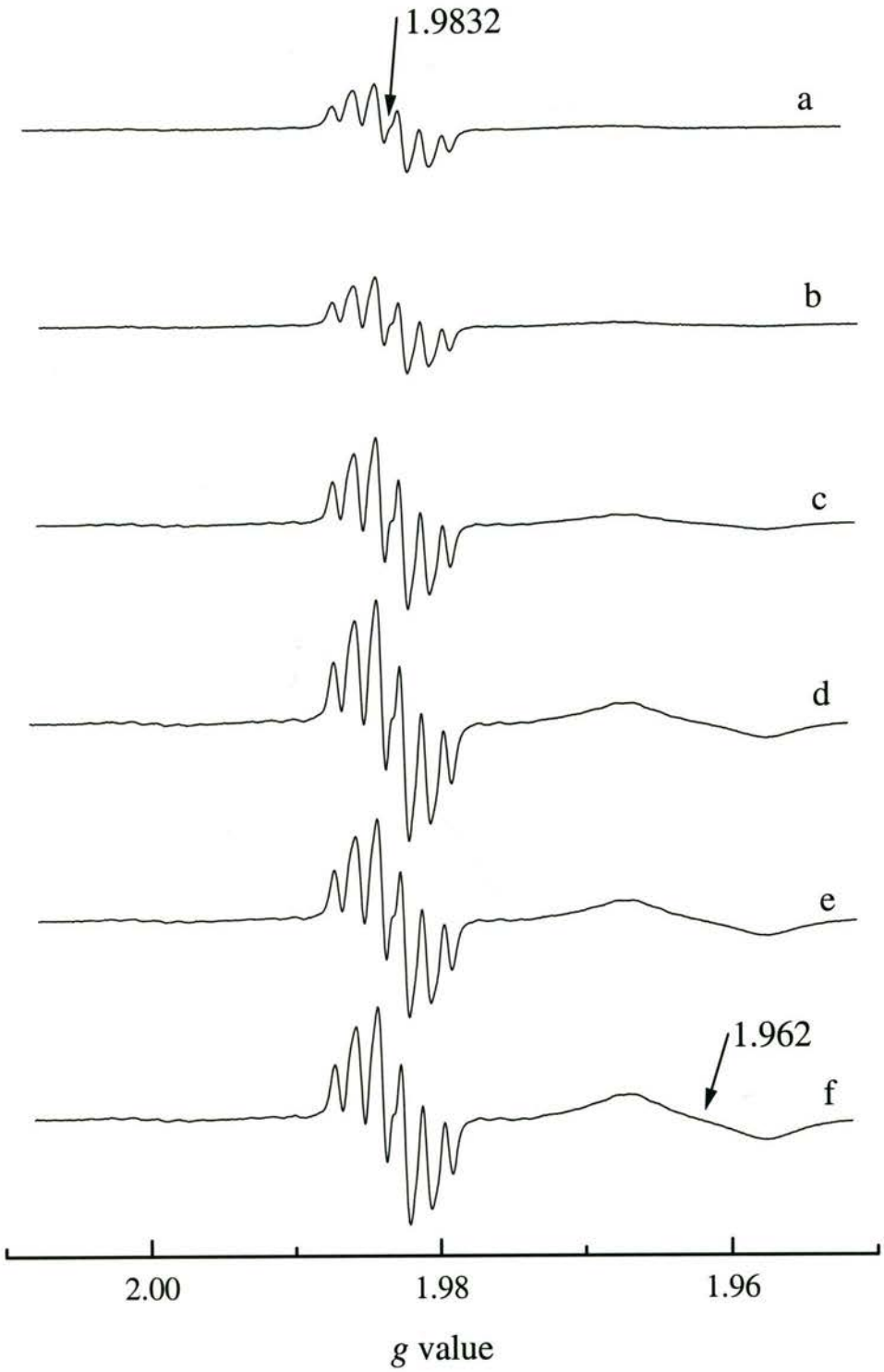

Figure 4.4 EPR spectra of the Cr(V) products obtained during the iodosobenzene oxidation of *trans*-[Cr^{III}(bpb)Cl(OH_2)] in DMF recorded at: (a) 5 min, (b) 10 min, (c) 20 min, (d) 40 min, (e) 60 min, and (f) 90 min after the addition of the oxidant. Parameters: receiver gain, 6.32×10^4; sweep width, 100 G; power, 20.17 mW; modulation amplitude, 1.00 G; time constant, 20.48 msec; conversion time, 20.48 msec; scans, 3.

improve the signal-to-noise ratio. The spectrum was simulated as two five-line species and a species with two different sets of superhyperfine couplings, which gave excellent agreement (correlation coefficient = 0.989) between the experimental and simulated spectra (Figure 4.5). Attempts to simulate the spectrum with only two five-line species were not successful. The EPR parameters used to simulate the spectrum are in Table 4.9. The size of the A_{iso} values indicated that there was superhyperfine coupling to two ^{14}N atoms in all the species.[45] The five-line species arose from coupling due to two ^{14}N atoms, and the third species exhibited coupling to two ^{14}N atoms and a weaker coupling that was assigned to two ^{1}H. The magnitude of the A_N values, 2.36-2.39 $\times 10^{-4}$ cm^{-1}, showed that the coupling was to the amide Ns.[45] In comparison, the A_N values due to coupling to the imine N in a series of $[Cr^{V}O(L)]^{+}$ complexes (where L is salen or a salen analogue) were in the range 2.05-2.18 $\times 10^{-4}$ cm^{-1}.[7] Simulation of the spectrum as two five-line species and a

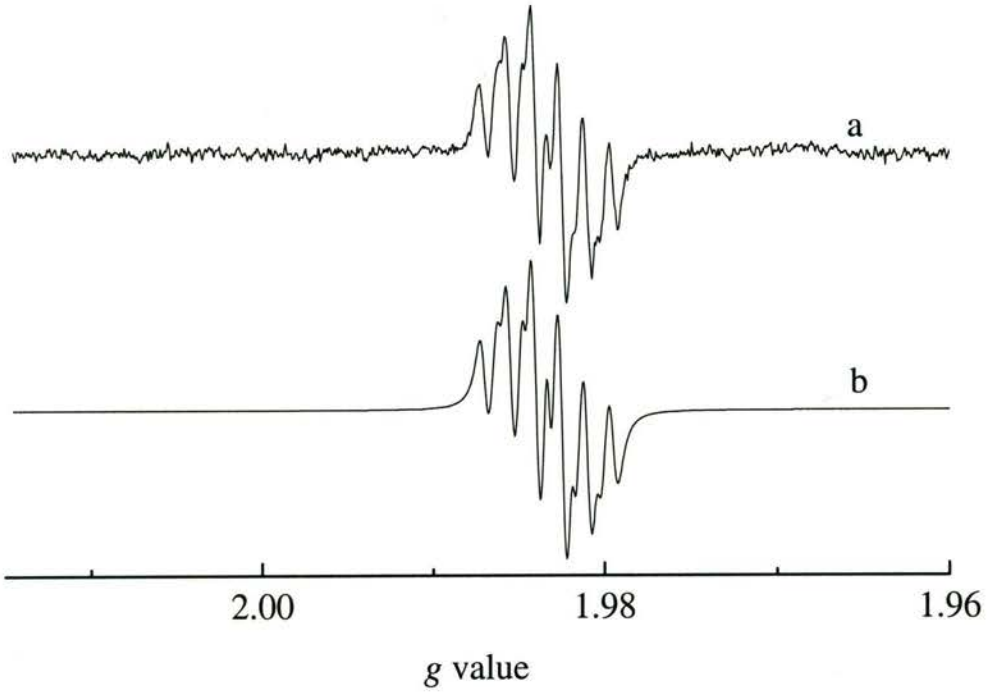

Figure 4.5 (a) Experimental and (b) simulated spectra of the Cr(V) species produced in the iodosobenzene oxidation of *trans*-$[Cr^{III}(bpb)Cl(OH_2)]$ in DMF. Experimental parameters: receiver gain, 6.32×10^{5}; sweep width, 100 G; power, 20.12 mW; modulation amplitude 0.20 G; time constant, 20.48 msec; conversion time, 20.48 msec; scans, 10. The parameters used in the simulation are in Table 4.9.

Table 4.9 Chromium(V) EPR parameters obtained from the simulated spectrum of the iodosobenzene oxidation of *trans*-[Cr^{III}(bpb)Cl(OH_2)] in DMF

Cr(V) Species	g_{iso} value	relative concentration (%)	A_{iso} ($\times 10^{-4}$ cm^{-1})	Number of atoms
1	1.9842	22.7	2.36	2 N
2	1.9833	46.8	2.39 1.21	2 N 2 H
3	1.9823	30.5	2.37	2 N

species with coupling to two sets of two N atoms gave a slightly worse fit between the experimental and simulated spectra (correlation value = 0.983). The A_N value calculated for the second set of N atoms was 1.15×10^{-4} cm^{-1}, considerably lower than the value for imine N in Cr(V)-salen complexes. However, the imine Ns are *trans* to the amides and hence might be expected to have longer Cr–N bonds. Since superhyperfine coupling is a contact splitting, the longer the bond length, the weaker the coupling. The second coupling is tentatively assigned to two ^1H as the correlation value was slightly higher, but the difference may not be significant. The observation of coupling to ring protons is not unprecedented, there were weak superhyperfine couplings to ring protons in Cr(V)-catechol complexes.[26] Attempts to record the Q-band EPR spectrum to facilitate a more definitive assignment were unsuccessful, due to the difficulty of generating sufficiently concentrated solutions of the Cr(V) complexes.

The three Cr(V) species had very similar g_{iso} values, which indicated that they had similar sets of donor ligands and the same coordination number. The appearance of the six-line signal did not alter over time (Figure 4.4), which showed that the relative amounts of different species did not change significantly. These two factors indicated that the different species may have been due to different conformations of the complex, but the evidence was not conclusive. The absence of superhyperfine coupling to the imine N does not rule out their coordination to Cr in some or all of the Cr(V) species detected, the coupling to the imine N may have been too small to be resolved.

There were broad signals at g_{iso} = ~1.975 and ~1.963 in several of the spectra, but their identity is uncertain as they did not exhibit any hyperfine or superhyperfine couplings. The apparent six-line species centred at 1.9833 was present under all oxidation conditions, but the superhyperfine couplings were not well resolved in the spectra obtained during the oxidations using Methods 1, 2, and 3. The number and identities of the species that gave rise to the six-line signal were not determined in these reactions; but it is likely that the major Cr(V) species are the same.

4.3.2.2 Oxidation of $[Cr^{III}(bpen)Cl(OH_2)].2H_2O.2CH_3OH$

Two Cr(V) species were detected in the EPR spectra recorded during the first 90 min of the oxidation of $[Cr^{III}(bpen)Cl(OH_2)].2H_2O.2CH_3OH$ in DMF by iodosobenzene (Figure 4.6). There was little change in the relative intensities of the g_{iso} = 1.9736 signal and the g_{iso} = 1.9713 signal over the initial 90 min of the reaction. The g_{iso} = 1.9736 signal was the stronger of the two and in some spectra shoulders due to other species were also apparent. The shoulders were weak and only partially resolved, so it was difficult to determine whether they were due to small amounts of other Cr(V) species or to superhyperfine coupling.

The Cr(V) species present in the EPR spectrum of the 1-day-old oxidation reaction mixture were different to those observed during the first 90 min of the oxidation reaction (Figure 4.7). The two new Cr(V) signals had g_{iso} values of 1.9826 and 1.9801, but their intensities were considerably lower than those of the Cr(V) species observed in the freshly oxidised solution. The presence of weak Cr(V) signals in the EPR spectrum of the 1-day-old solution indicated that the bpen ligand was moderately effective at stabilising the Cr(V) oxidation state.

The EPR spectra of the fresh solution and the 1-day-old solution from the oxidation of $[Cr^{III}(bpen)Cl(OH_2)].2H_2O.2CH_3OH$ both showed two Cr(V) signals, the stronger signal occurring at the higher g_{iso} value. Interestingly, the differences in the g_{iso} values of the two Cr(V) signals were 0.0023 for the fresh solution and 0.0025 for the 1-day-old solution.

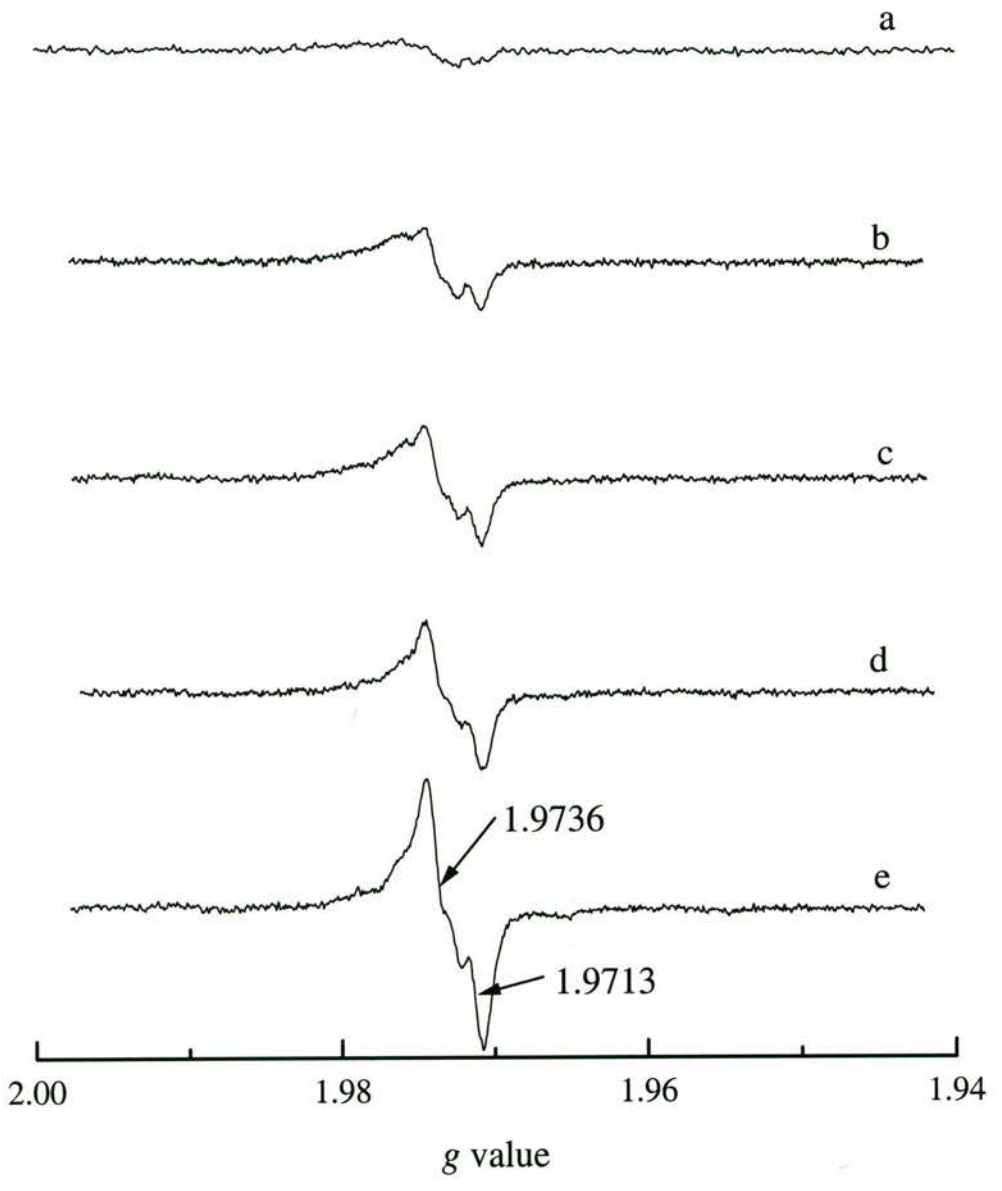

Figure 4.6 EPR spectra of the Cr(V) species generated during the iodosobenzene oxidation of $[Cr^{III}(bpen)Cl(OH_2)].2H_2O.2CH_3OH$ in DMF recorded at: (a) 10 min, (b) 20 min, (c) 30 min, (d) 60 min, and (e) 90 min after the addition of the oxidant. Parameters: receiver gain, 6.32×10^5; sweep width, 100 G; power, 20.12 mW; modulation amplitude, 1.00 G; time constant, 20.48 msec; conversion time, 20.48 msec; scans, 5.

This raises the question of whether the initially formed Cr(V) species underwent similar transformations to give the Cr(V) species observed after 24 h. The observed increase in the g_{iso} values would be consistent with a change from a six-coordinate to five-coordinate geometry as five-coordinate Cr(V) species have higher g_{iso} values

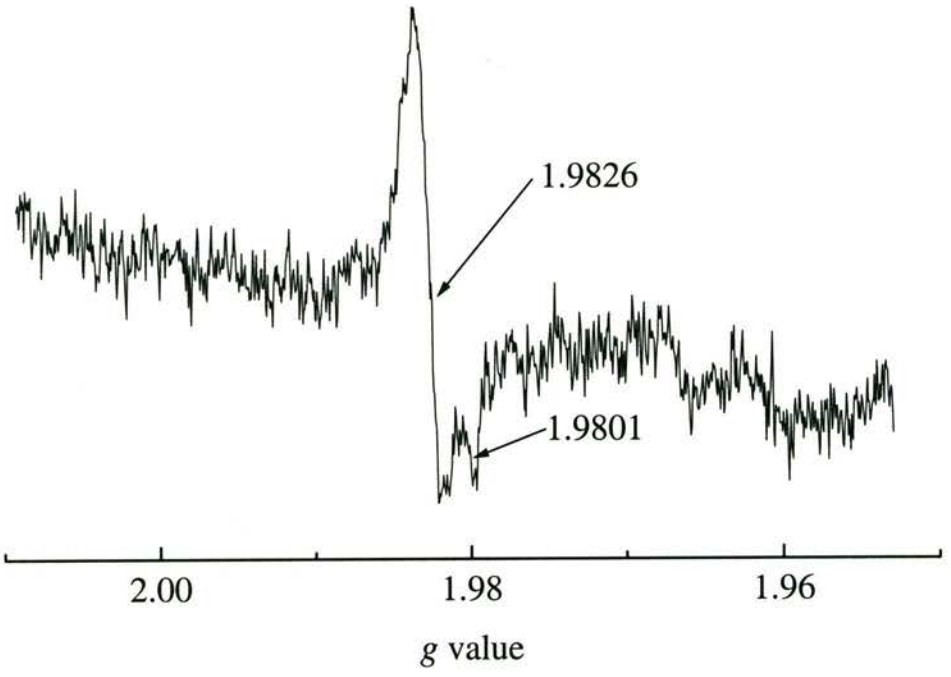

Figure 4.7 EPR spectrum of the Cr(V) species generated during the iodosobenzene oxidation of $[Cr^{III}(bpen)Cl(OH_2)].2H_2O.2CH_3OH$ in DMF recorded 24 h after the addition of the oxidant. Parameters: receiver gain, 6.32×10^5; sweep width, 100 G; power, 20.12 mW; modulation amplitude, 1.00 G; time constant, 20.48 msec; conversion time, 20.48 msec; scans, 50.

than their six-coordinate analogues.[45] However, a definitive assignment of the coordination number and donor ligands of the species that gave rise to the Cr(V) signals was not made, as all the Cr(V) species were too weak to detect the hyperfine coupling to the ^{53}Cr isotope (9.5% abundant, spin = $^3/_2$), and no superhyperfine couplings were resolved.

4.3.2.3 Oxidation of $[Cr^{III}(S,S\text{-bprolben})L_2]^{n+}$

The EPR spectra recorded during the oxidation of $[Cr^{III}(S,S\text{-bprolben})L_2]^{n+}$ in DMF by iodosobenzene were dominated by a five-line Cr(V) signal, g_{iso} = 1.9821 (Figure 4.8). A weaker Cr(V) signal, that also displayed superhyperfine coupling, was present at a higher g_{iso} value, but it partially overlapped the major five-line signal so the g_{iso} value was not determined precisely. The intensity of these two Cr(V) signals

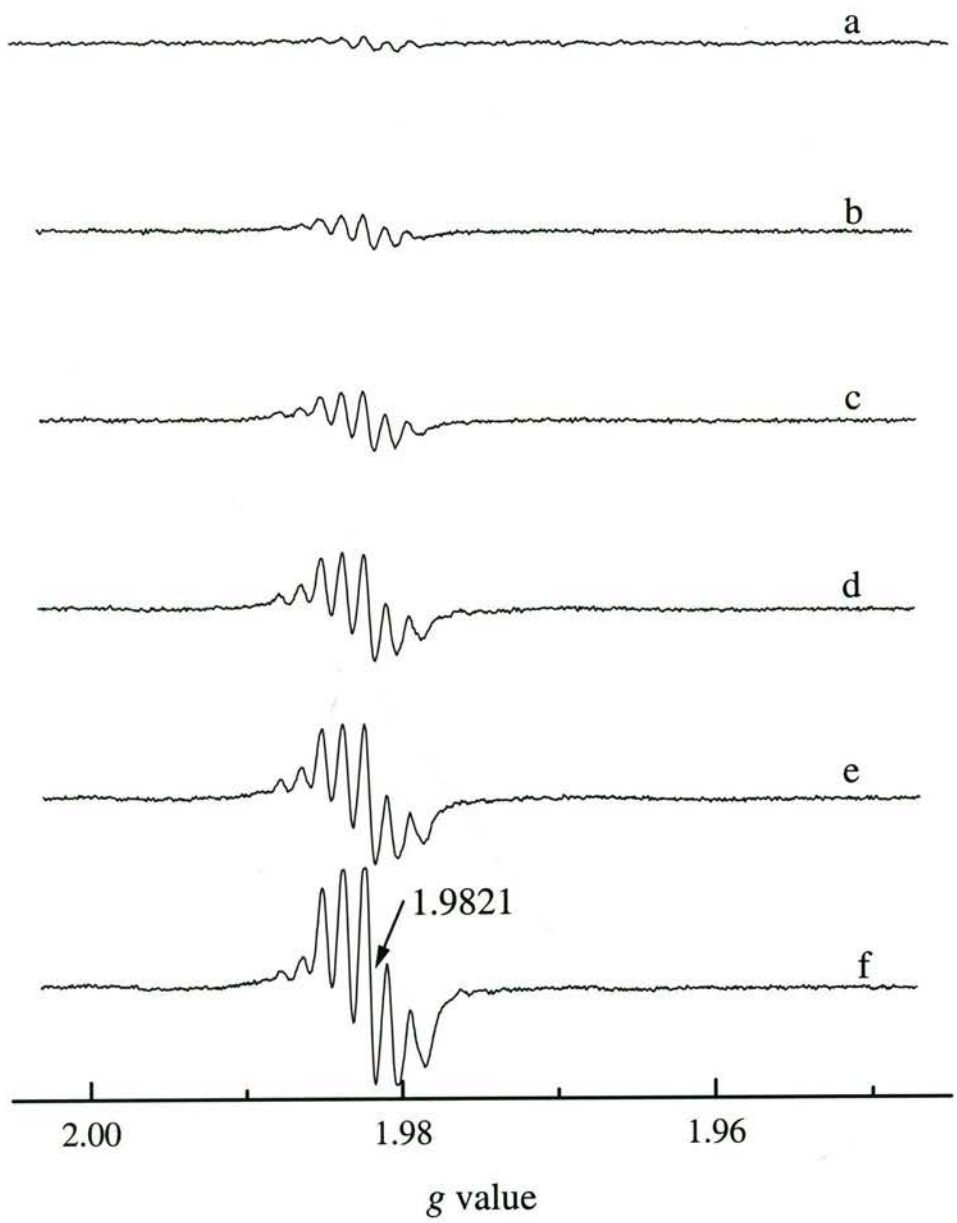

Figure 4.8 EPR spectra of the Cr(V) species generated during the iodosobenzene oxidation of $[Cr^{III}(S,S\text{-bprolben})L_2]^{n+}$ in DMF recorded at: (a) 5 min, (b) 10 min, (c) 20 min, (d) 40 min, (e) 90 min, and (f) 22 h after the addition of the oxidant. Parameters: receiver gain, 6.32×10^5; sweep width, 100 G; power, 20.12 mW; modulation amplitude, 1.00 G; time constant, 20.48 msec; conversion time, 20.48 msec; scans, 5.

increased over the first 90 min after the addition of iodosobenzene, and had increased even further in the EPR spectrum of the 1-day-old solution. The increase in intensity of the Cr(V) signals between 90 min and 22 h showed that the species formed were

extremely stable. This was in contrast to the oxidations of *trans*-[Cr^{III}(bpb)Cl(OH_2)] and [Cr^{III}(bpen)Cl(OH_2)].$2H_2O$.$2CH_3OH$ where the Cr(V) signals in the 1-day-old solutions were considerably weaker than those in freshly oxidised solutions. The *S,S*-bprolben ligand was considerably more effective at stabilising Cr(V) under these conditions than the bpb and bpen ligands. The increase in the intensity of Cr(V) signals between 90 min and 22 h also indicated that the oxidation of [Cr^{III}(*S,S*-bprolben)L_2]$^{n+}$ to Cr(V) was a slow process. This was possibly due to the very limited solubility of iodosobenzene in DMF; after 90 min a large proportion of the iodosobenzene was still undissolved.

In the EPR spectra recorded at the later points in the oxidation reaction, the lines due to superhyperfine coupling at lower g_{iso} values of the major Cr(V) species were broader than the superhyperfine lines at higher g_{iso} values. A spectrum was recorded using a smaller modulation amplitude and a greater number of scans 22 h after the addition of iodosobenzene to try and elucidate the cause of this broadening (Figure 4.9(a)). It showed that there was another weak Cr(V) species with superhyperfine couplings that overlapped with the major Cr(V) species in the lower g_{iso} region. Endeavours were made to resolve the overlapping signals by recording the Q-band EPR spectra, but they were unsuccessful due to the difficulty of generating concentrated Cr(V) solutions. Simulation of this spectrum as three five-line species (Figure 4.9(b)) gave excellent agreement between the experimental and simulated spectra (correlation coefficient = 0.990). The EPR parameters used to simulate the spectrum are listed in Table 4.10. The magnitude of the superhyperfine splittings showed that they arose from coupling to ^{14}N.[45] The five-line species were due to coupling to two equivalent ^{14}N atoms, and the A_N values of 2.2-2.3 $\times$ 10^{-4} cm^{-1} denoted that the coupling was to amide N atoms.[45] No coupling to the amine N atoms were observed in the EPR spectra, but this does not preclude amine N coordination in the Cr(V) complexes, the couplings may just be too small to be resolved.

The oxidation of [Cr^{III}(*S,S*-bprolben)L_2]$^{n+}$ by iodosobenzene produced three Cr(V)-(*S,S*-bprolben) complexes that had similar g_{iso} values and displayed superhyperfine coupling to two amide N atoms. The very small differences in the

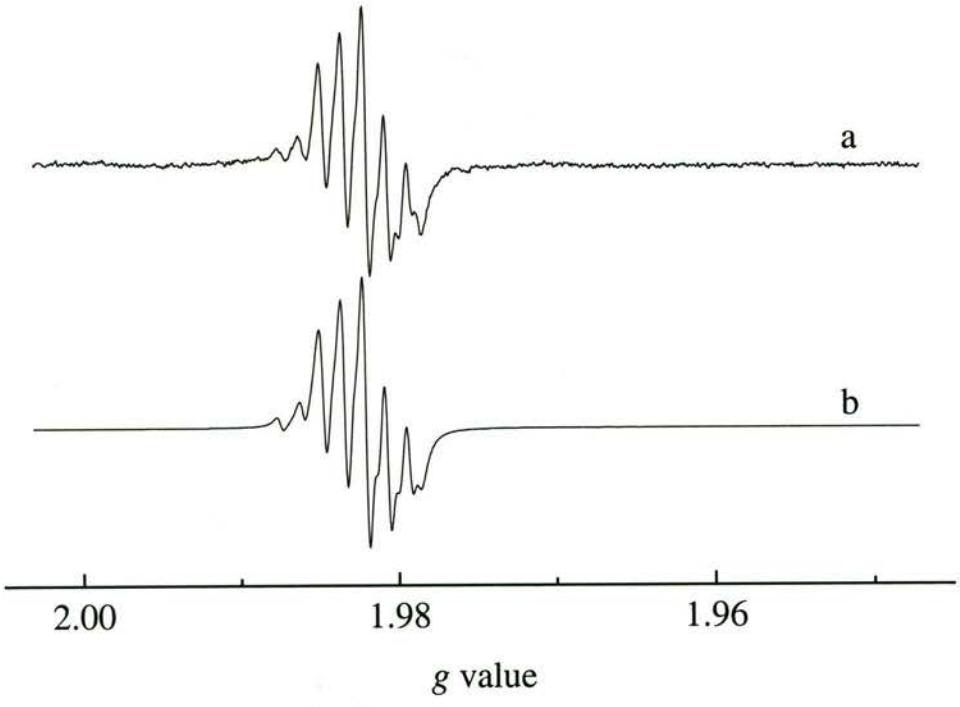

Figure 4.9 (a) Experimental and (b) simulated spectra of the Cr(V) species generated during the iodosobenzene oxidation of $[Cr^{III}(S,S\text{-bprolben})L_2]^{n+}$ in DMF, 22 h after the addition of the oxidant. Experimental parameters: receiver gain, 6.32×10^5; sweep width, 100 G; power, 20.12 mW; modulation amplitude, 0.20 G; time constant, 20.48 msec; conversion time, 20.48 msec; scans, 50. The simulation parameters are contained in Table 4.10.

Table 4.10 Chromium(V) EPR parameters obtained from the simulated spectrum of the iodosobenzene oxidation of $[Cr^{III}(S,S\text{-bprolben})L_2]^{n+}$ in DMF

Cr(V) Species	g_{iso} value	relative concentration (%)	A_N ($\times 10^{-4}$ cm^{-1})	Number of N atoms
1	1.9847	4.5	2.33	2
2	1.9821	67.6	2.29	2
3	1.9815	27.9	2.21	2

g_{iso} and A_N values indicated that the three Cr(V) species had the same or very similar donor ligands. The reduction of Cr(VI) in the presence of *S,S*-bprolbenH_2 produced a five-coordinate Cr(V) species that gave a five-line EPR signal with g_{iso} = 1.9824 when dissolved in water (discussed in Section 4.3.3.3 below), so the

Cr(V)-(*S,S*-bprolben) complexes generated by the iodosobenzene oxidation of $[Cr^{III}(S,S\text{-bprolben})L_2]^{n+}$ are predicted to be five-coordinate. The slight differences in the EPR parameters for the Cr(V) species may be due to differences in the conformation but it is not possible to give a definitive explanation or assign them to particular structures.

There was considerable similarity between the results of the iodosobenzene oxidations of $[Cr^{III}(S,S\text{-bprolben})L_2]^{n+}$ and *trans*-$[Cr^{III}(bpb)Cl(OH_2)]$ in DMF. In both reactions, three Cr(V) species with g_{iso} values just above 1.98 and superhyperfine coupling to ^{14}N atoms were formed. This was evidence that the Cr(V) complexes formed with the two ligands had highly similar structures. The bpb and *S,S*-bprolben ligands had central 1,2-benzene units and different terminal donor groups, whereas the bpb and bpen ligands both had pyridyl terminal groups but differed in the linkage between the central amide groups. The close similarity between the Cr(V) complexes with bpb and *S,S*-bprolben, and the quite different Cr(V) species formed with bpen showed that the nature of the amide groups had a greater influence on the structure of the Cr(V) species formed by oxidation of the Cr(III) complexes than the terminal donor groups from these tetradentate ligands.

4.3.3 Reduction of Cr(VI) in the Presence of Tetradentate Diamide Ligands

4.3.3.1 Reduction of Cr(VI) in Acetone/Methanol

The reaction of Cr(VI) with methanol has been reported previously to give rise to two Cr(V) signals in the EPR spectrum at g_{iso} = 1.9765 and 1.9687.[30,46] The reductions of Cr(VI) in the presence of the amide ligands were performed in an acetone/methanol solvent mixture so a control reaction of Cr(VI) in acetone/methanol alone was studied. The Cr(V) species generated from the reaction mixture were monitored by EPR spectroscopy (Figure 4.10), which showed that two Cr(V) species with g_{iso} = 1.9795 and 1.9764 were present. The species with g_{iso} = 1.9764 was also present in the reduction of Cr(VI) by methanol and was assigned as a six-coordinate Cr(V)-oxo species, **I**.[30,46]

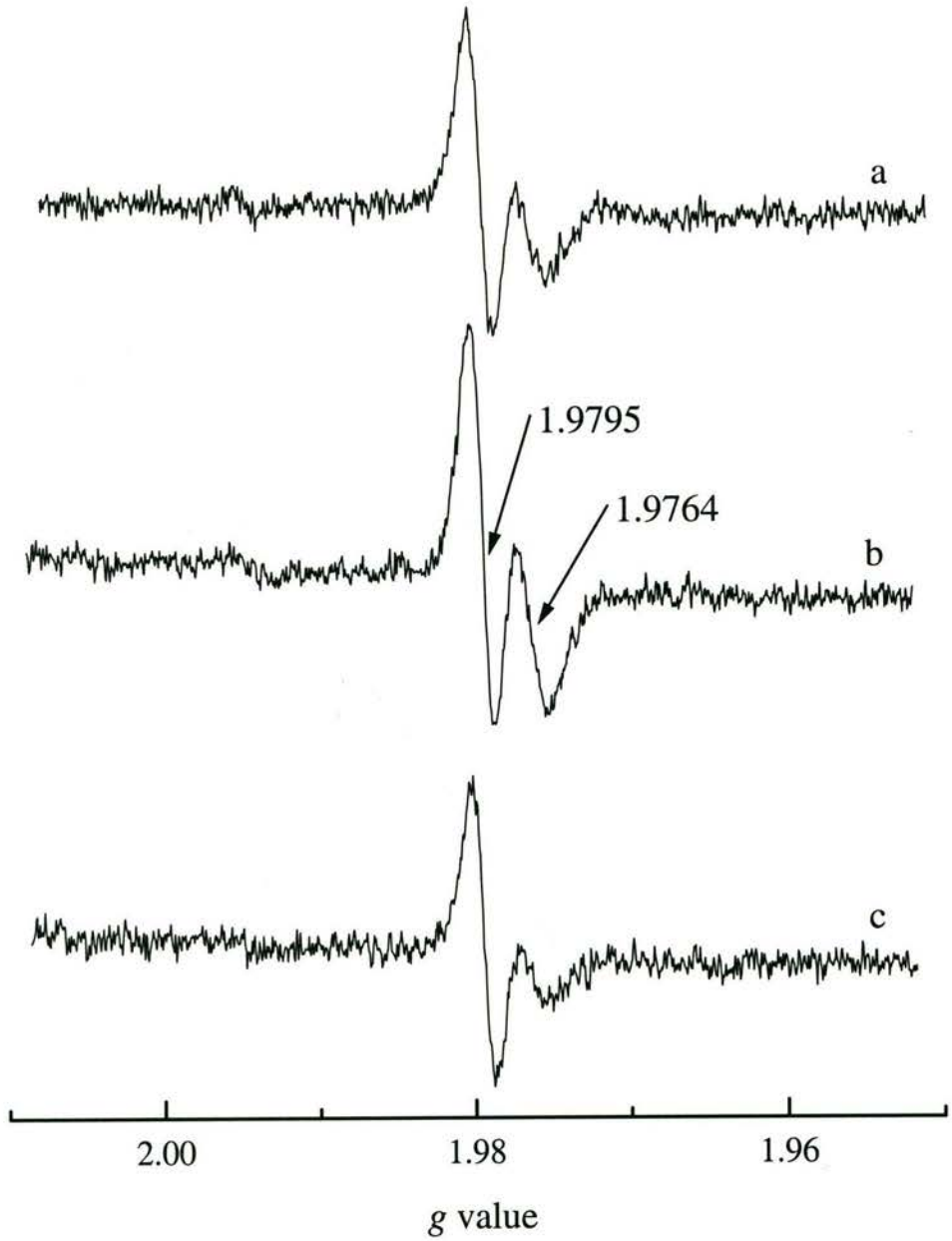

Figure 4.10 EPR spectra of the Cr(V) intermediates generated during the reduction of Cr(VI) in acetone/methanol after: (a) 3 d, (b) 4 d, and (c) 7 d. Parameters: receiver gain, 6.32×10^4; sweep width, 100 G; power, 20.12 mW; modulation amplitude, 1.00 G; time constant, 20.48 msec; conversion time, 20.48 msec; scans, 10.

The second Cr(V) signal at $g_{iso} = 1.9795$ was not observed in the reduction of Cr(VI) by methanol and is consistent with a five-coordinate species **II**, which has a calculated g_{iso} value of 1.9800.[45]

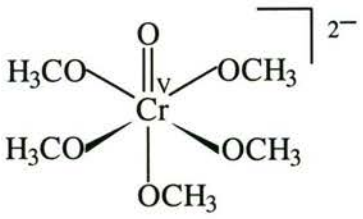

I

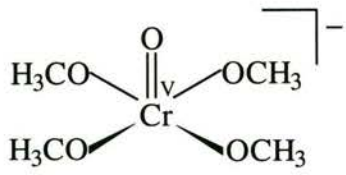

II

4.3.3.2 Reduction of Cr(VI) in the Presence of $bpenH_2$

The initial absence of a colour change using Method 1 indicated that $bpenH_2$ alone does not reduce Cr(VI). When methanol was added to reduce the Cr(VI), a light brown precipitate gradually formed, but IR spectroscopy showed that this contained a large amount of unreacted $bpenH_2$. The different solubilities of the free ligand and the Cr complex in chloroform were used to purify the product; the unreacted $bpenH_2$ dissolved in the chloroform and the insoluble Cr complex was collected by filtration. In Method 2, an acetone/methanol (2:1 v/v) solvent mixture containing much lower concentrations of the reactants was used. The higher dilution conditions prevented the coprecipitation of $bpenH_2$ with the product. The product had poor solubility in all solvents tested; it was insoluble in $CHCl_3$, sparingly soluble in CH_3CN and CH_3CH_2OH, and partially soluble in H_2O, CH_3OH, DMF and DMSO.

The absence of the νN–H band (at 3334 cm^{-1} for $bpenH_2$) from the IR spectrum of the product showed that the ligand was coordinated via deprotonated amide groups to the Cr atoms. The strong peak at 1636 cm^{-1} was due to the amide I band, which occurred at lower frequency than in the free ligand, which is consistent with coordination to Cr through deprotonated amide Ns. The band at 945 cm^{-1}, which was absent from the spectrum of the ligand, was due to a Cr=O stretch.

The elemental analysis of the product led to the molecular formula $C_{16}H_{24}N_4O_{22}Cr_4Na_3$. The greatest weight was given to the C, H and N values because these analyses had the greatest precision. The Cr:ligand ratio was 4:1 but the targeted mode of coordination of bpen to Cr as a tetradentate via two deprotonated amide nitrogens and two pyridyl nitrogens would lead to a Cr:ligand ratio of 1:1. The molecular formula indicated that the product was a polynuclear Cr

complex, or possibly a mixed chromate-dichromate salt of a mononuclear Cr(V) complex.

The assignment of the ES/MS results is in Table 4.11, and the observed and calculated molecular isotope distributions for the more abundant ions are given in Table 4.12. The most abundant adduct was the sodiated adduct of $bpenH_2$, followed by a dinuclear Cr species with a Cr:bpen ratio of 2:1. The higher mass peaks were probably due to multinuclear Cr species, but were difficult to assign unambiguously. It is unclear whether the multinuclear species arose from incomplete dissociation of a $[Cr^{V}]^{+}_{m}[Cr^{VI}]^{-}_{n}$ salt or the decomposition of a $[Cr^{V}_{m}Cr^{VI}_{n}]$ complex.

Table 4.11 Assignment of the +ve ion ES/MS data for the product of the reduction of Cr(VI) in the presence of $bpenH_2$

m/z	Relative Intensity	Molecular Formula	Tentative Assignment
293	100	$C_{14}H_{14}N_4O_2Na$	$[Na(bpenH_2)]^+$
372	24	–	–
563	47	$C_{16}H_{12}N_4O_{11}Cr_2Na$	–
757	11	$C_{14}H_{16}N_4O_{15}Cr_4Na_3$	$[Cr_4(bpen)H_4Na_3O_{13}]^+$
955	27	–	–
1497	15	–	–

Table 4.12 Observed and calculated molecular isotope distributions for the +ve ion ES/MS data for the product of the reduction of Cr(VI) in the presence of $bpenH_2$

Molecular Formula	m/z	Relative Intensity	
		Calculated	Observed
$C_{14}H_{14}N_4O_2Na$	293	100	100
	294	16.8	14
$C_{16}H_{12}N_4O_{11}Cr_2Na$	564	100	100
	565	41.7	40

The product was only partially soluble in DMF and DMSO, so solutions were filtered through 0.45 μm filters prior to recording of the EPR spectra to remove the undissolved product. The EPR spectra of the product showed the presence of Cr(V) species (Figure 4.11). The main Cr(V) species changed over time in the DMF solution. The change in the identity of the main species in DMF may have been due to solvent interaction with the complex, or to partial dissociation of a polynuclear Cr complex. The presence of a Cr(V) signal in a two-day-old DMF solution indicated that the ligand stabilised Cr(V). EPR spectra of DMSO solutions of the product were also recorded; in freshly prepared solutions, there was a single Cr(V) signal with g_{iso} = 1.9780, which gradually decayed and had completely disappeared after 1 d. The EPR spectra of the products obtained from reactions using Methods 1 or 2 were identical.

The g_{iso} value of the Cr(V) species of a freshly dissolved sample of the product in DMF differed from the g_{iso} values observed for the Cr(V) species produced initially in the oxidation of a DMF solution of $[Cr^{III}(bpen)Cl(OH_2)].2H_2O.2CH_3OH$ by iodosobenzene (Section 4.3.2.2). However, the g_{iso} values of the Cr(V) species in the aged solutions were the same, g_{iso} = 1.9826 and 1.9801.

The EPR spectra showed that the product contained Cr(V), but it did not provide conclusive evidence to discriminate between a $[Cr^{V}]^{+}_{m}[Cr^{VI}]^{-}_{n}$ salt or a multinuclear $[Cr^{V}_{m}Cr^{VI}_{n}]$ complex. The presence of an EPR signal from Cr(V) indicated that there was not an even number of closely associated Cr(V) centres, as an EPR signal would not be expected to appear at room temperature due to coupling between the Cr(V) centres. Thus, if the product is a multinuclear species, it contains an odd number of Cr(V) centres, or due to the presence of Cr(VI) centres, the product has a structure in which the Cr(V) centres can not undergo coupling.

The reduction of Cr(VI) in the presence of $bpenH_2$ produced a solid containing a mixture of Cr(V) and Cr(VI), but the intractable nature of the product made it difficult to determine its structure.

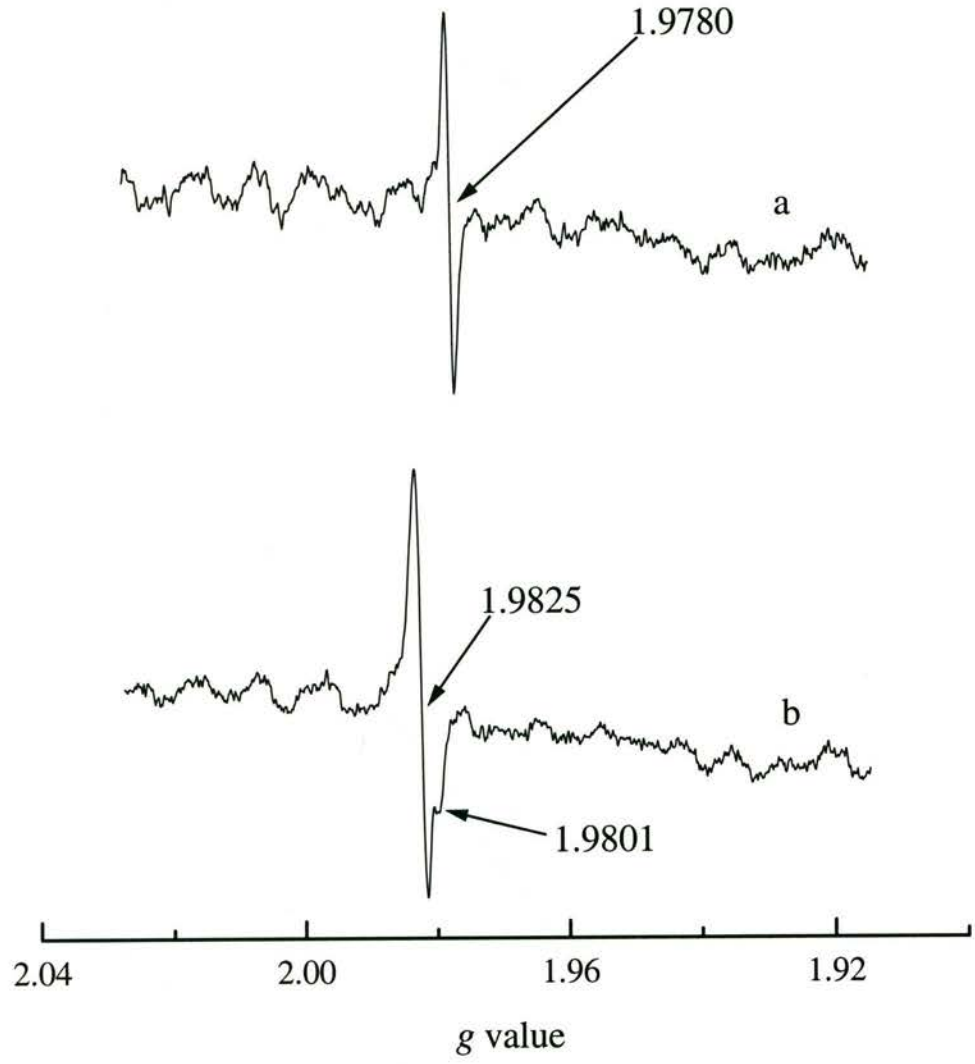

Figure 4.11 EPR spectra of the: (a) freshly prepared, and (b) 2-day-old DMF solutions of the product from the reduction of dichromate in the presence of bpenH_2. Parameters: receiver gain, 6.32×10^4; sweep width, 200 G; power, 63.62 mW; modulation amplitude, 1.07 G; time constant, 20.48 msec; conversion time, 10.24 msec; scans, 200.

4.3.3.3 Reduction of Cr(VI) in the Presence of bpbH_2

The EPR spectra of the reaction mixture (Figure 4.12) showed two Cr(V) signals with g_{iso} values of 1.9795 and 1.9765; these were the Cr(V)-methanol species that were observed in the control reaction of Cr(VI) in acetone/methanol. There was no evidence for the formation of any Cr(V) complexes with bpb.

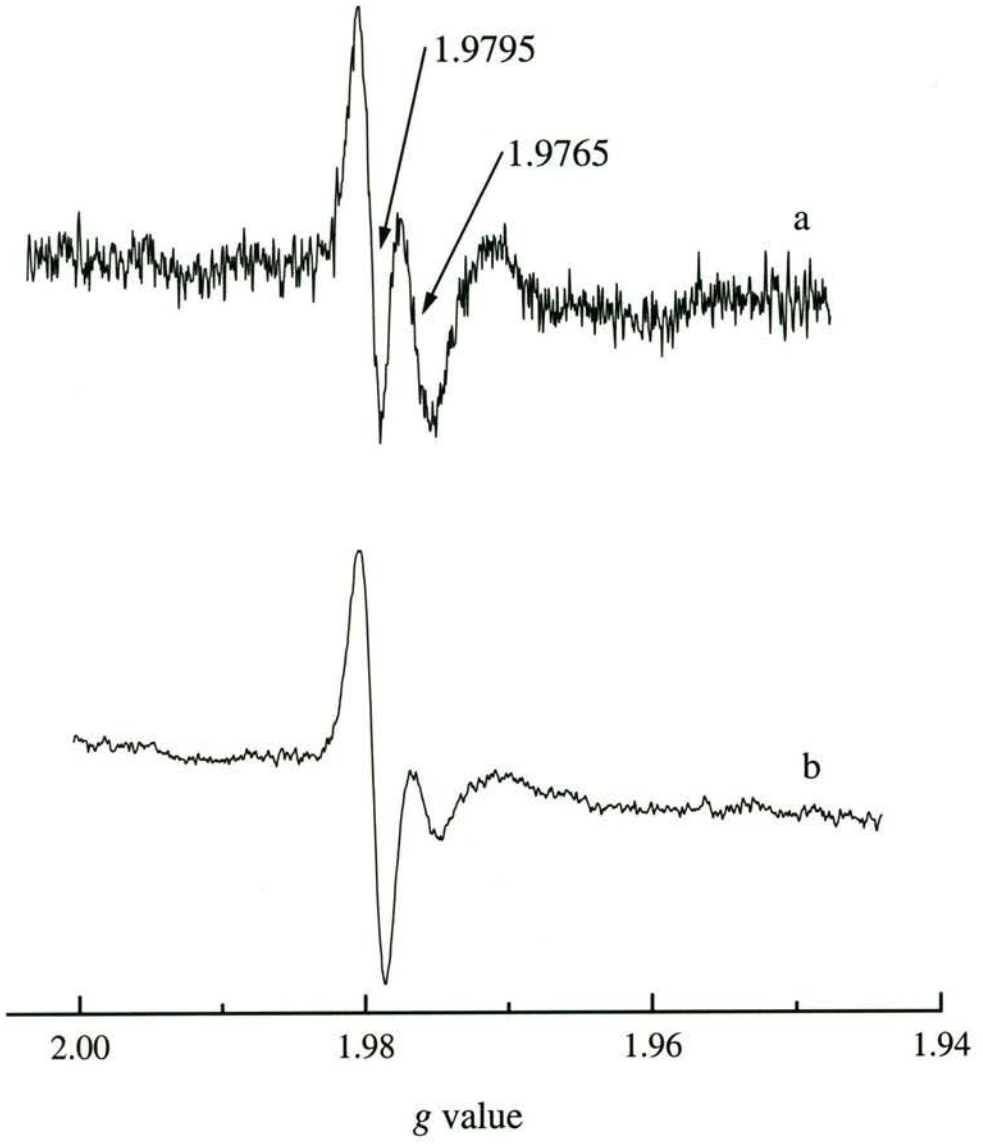

Figure 4.12 EPR spectra of the Cr(V) species generated during the reduction of Cr(VI) in the presence of $bpbH_2$ in acetone/methanol. Reaction mixture after: (a) 1 d, (b) 8 d. Parameters: receiver gain, 6.32×10^4; sweep width, 100 G; power, (a) 2.01 (b) 20.12 mW; modulation amplitude, 1.00 G; time constant, 20.48 msec; conversion time, 20.48 msec; scans, (a) 50, (b) 25.

4.3.3.4 Reduction of Cr(VI) in the Presence of *S,S*-bprolbenH_2

When the reduction of Cr(VI) in the presence of *S,S*-bprolbenH_2 was carried out in the dark (Method 1) only a weak signal due to the six-coordinate Cr(V)-methanol species **I** was observed in the EPR spectra (Figure 4.13). The reaction under a fluorescent lamp (Method 2) showed the signals at g_{iso} = 1.9765 and 1.9796 due to **I**

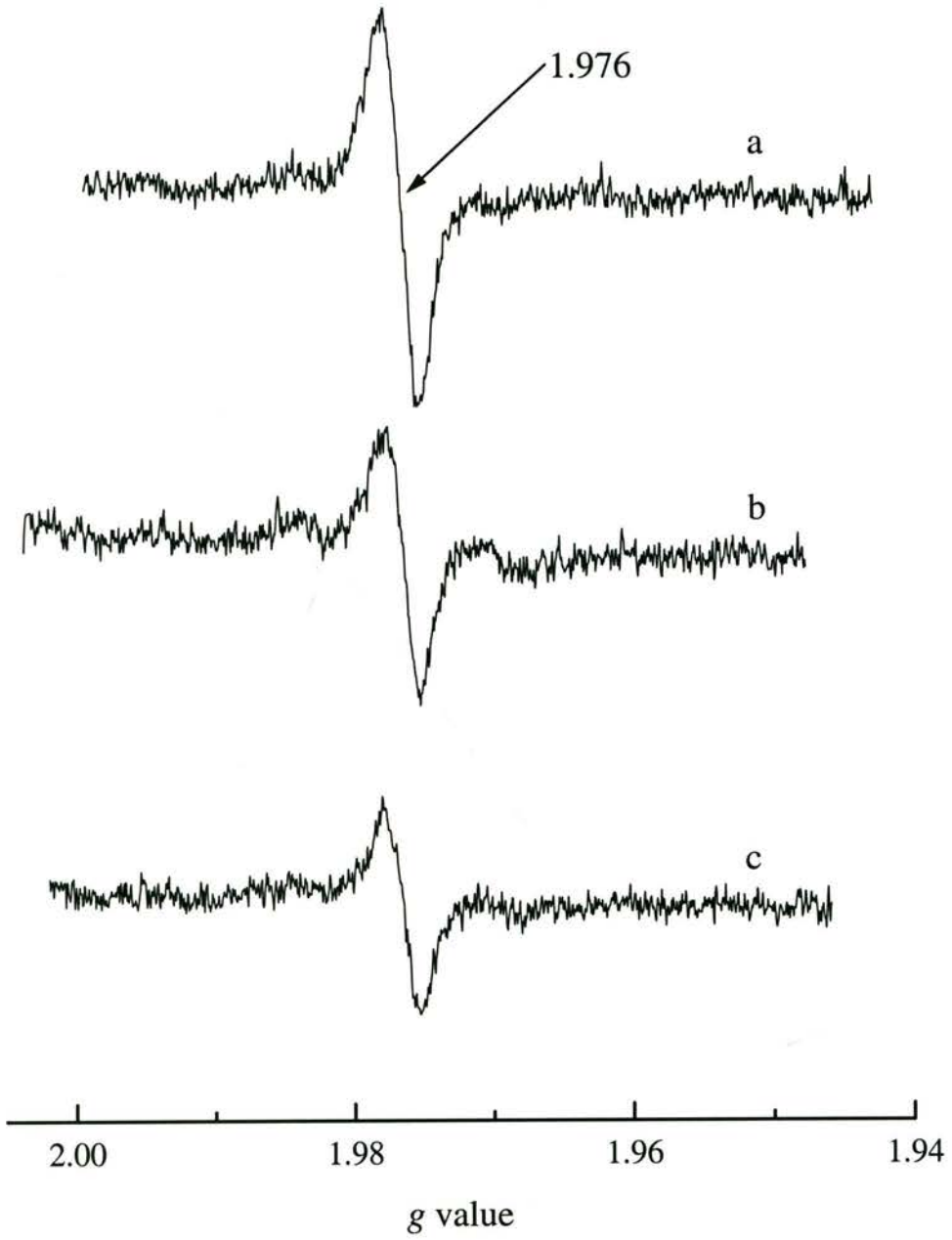

Figure 4.13 EPR spectra of the Cr(V) species generated during the reduction of Cr(VI) in acetone/methanol in the presence of *S,S*-bprolbenH_2. Dark reaction after (a) 1 d, (b) 2 d, and (c) 3 d. Parameters: receiver gain, 6.32×10^4; sweep width, 100 G; power, 20.12 mW; modulation amplitude, 1.00 G; time constant, 20.48 msec; conversion time, 20.48 msec; scans, 20.

and **II**, and an additional Cr(V) signal with g_{iso} value of 1.9823 was observed (Figure 4.14). The new signal showed superhyperfine coupling, but it was partially obscured by the signal from **II**. The superhyperfine coupling indicated that N atoms of the ligand were coordinated to the Cr. Initially the Cr(V)-methanol species were more intense, but the relative amount of the $[Cr^{V}O(S,S\text{-bprolben})]^{+}$ complex increased over time. The concentration of $[Cr^{V}O(S,S\text{-bprolben})]^{+}$ reached a maximum at 3 d, after which it decreased.

In the EPR spectra of the reaction mixture prepared by Method 2 that were recorded after 3 d and 6 d, the superhyperfine peak at highest g_{iso} value of the signal at $g_{iso} = 1.9823$ had a small shoulder, and there was another very small peak at a higher g_{iso} value than the shoulder (Figure 4.14(c) and (d)). The oxidation of $[Cr^{III}(S,S\text{-bprolben})L_2]^{n+}$ in DMF by iodosobenzene resulted in similar features in the EPR spectra. Simulation of the EPR spectrum from the oxidation of $[Cr^{III}(S,S\text{-bprolben})L_2]^{n+}$ with iodosobenzene showed that these features were from a Cr(V) species that had superhyperfine coupling to two amide N atoms. The presence of these features in the EPR spectra of the Cr(VI) reduction in the presence of *S,S*-bprolben means that there was a second minor Cr(V) species with amide N coordinated.

When the reaction mixture that had been kept in the dark was exposed to the light $[Cr^{V}O(S,S\text{-bprolben})]^{+}$ formed and the signal at $g_{iso} = 1.9823$ was observed in the EPR spectrum. Direct irradiation under a fluorescent lamp was not necessary for the formation of $[Cr^{V}O(S,S\text{-bprolben})]^{+}$, since it was still observed when the reaction was carried out under the ambient light in the laboratory.

The brown precipitate that formed during the reaction was too fine to collect by filtration, so it was separated by centrifugation of the reaction mixture. The EPR spectrum of the residue was dominated by a very broad signal with a peak-to-peak width of 450×10^{-4} cm^{-1}, due to Cr(III), and there was only a tiny amount of Cr(V) present. The main EPR active species observed in the spectrum of the supernatant were the Cr(V) species detected in the EPR spectra of the reaction mixture. When the supernatant was chromatographed on a LH20 Sephadex column, two main bands separated. The main Cr(V) species in the faster moving brown band was the

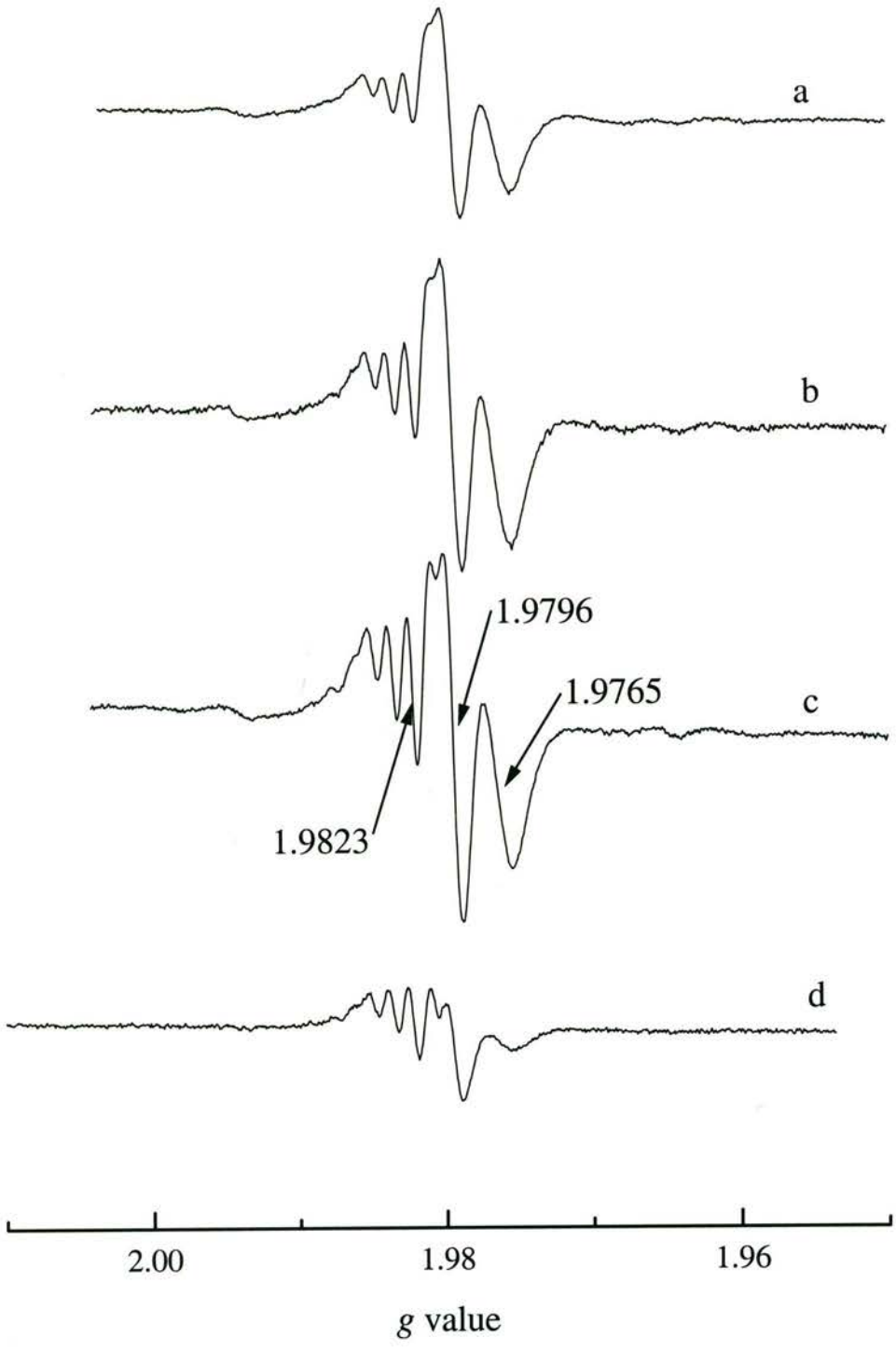

Figure 4.14 EPR spectra of the Cr(V) species generated during the reduction of Cr(VI) in acetone/methanol in the presence of *S,S*-bprolbenH_2. Reaction in the presence of fluorescent light irradiation after (a) 1 d, (b) 2 d, (c) 3 d, and (d) 6 d. Parameters: receiver gain, 6.32×10^4; sweep width, 100 G; power, 20.12 mW; modulation amplitude, 1.00 G; time constant, 20.48 msec; conversion time, 20.48 msec; scans, 20.

Cr(V)-methanol complex, **II**; in the second orange-brown band $[Cr^{V}O(S,S\text{-bprolben})]^{+}$ was the major form of Cr(V). The bands broadened considerably as they moved down the columns and separation was not complete; no fraction contained a single Cr(V) species. When a longer column (25 × 2 cm) was used for the chromatography, the separation of the bands improved and a very small yellow band that moved slower than the orange-brown band was also observed. The main Cr(V) species in the yellow band was the Cr(V)-methanol complex, **I**. Though the separation of the bands had improved it was still incomplete, and none of the fractions contained a single Cr(V) species.

When the solvent was removed from the orange-brown band on a rotary evaporator and the residue was dissolved in water, the Cr(V)-methanol EPR signals disappeared and only the signal due to $[Cr^{V}O(S,S\text{-bprolben})]^{+}$ remained. This signal was quite stable, since it was still present after a week, though the intensity had decreased (Figure 4.15). Hyperfine couplings to the ^{53}Cr nucleus (which has an abundance of 9.5%) were visible in the EPR spectrum recorded after 10 min (Figure 4.15(a)) an expansion of which is shown in Figure 4.16.

The spectrum that exhibited ^{53}Cr hyperfine coupling was simulated as a five-line species due to coupling to two equivalent N atoms, with a second signal that was also coupled to the ^{53}Cr nucleus (spin $^{3}/_{2}$). The experimental and simulated spectra are in Figures 4.17(a) and (b), respectively, and show excellent agreement (correlation coefficient = 0.992). The parameters obtained from the simulation are in Table 4.13. A_{Cr} is smaller for five-coordinate complexes than for six-coordinate complexes[45] and the value of 16.38×10^{-4} cm^{-1} indicated that the complex was five-coordinate. The g_{iso} value of the Cr(V)-(*S,S*-bprolben) complex was the same in aqueous and acetone/methanol solutions, further evidence that there was no solvent coordinated to the Cr. The A_N and A_{Cr} values were similar to those observed for two five-coordinate oxo-Cr(V) complexes with macrocyclic tetraamido ligands,[5,45] for $[Cr^{V}O(mac)]^{-}$ $A_N = 2.4 \times 10^{-4}$ cm^{-1} and $A_{Cr} = 16.6 \times 10^{-4}$ cm^{-1}, for $[Cr^{V}O(mampa)]^{-}$ $A_N = 2.6 \times 10^{-4}$ cm^{-1} and $A_{Cr} = 16.9 \times 10^{-4}$ cm^{-1}. $[Cr^{V}O(mac)]^{-}$ and $[Cr^{V}O(mampa)]^{-}$ had g_{iso} values of 1.999 and 2.006, respectively, the g_{iso} value was lower in the Cr(V)-(*S,S*-bprolben) complex since it contained only two deprotonated

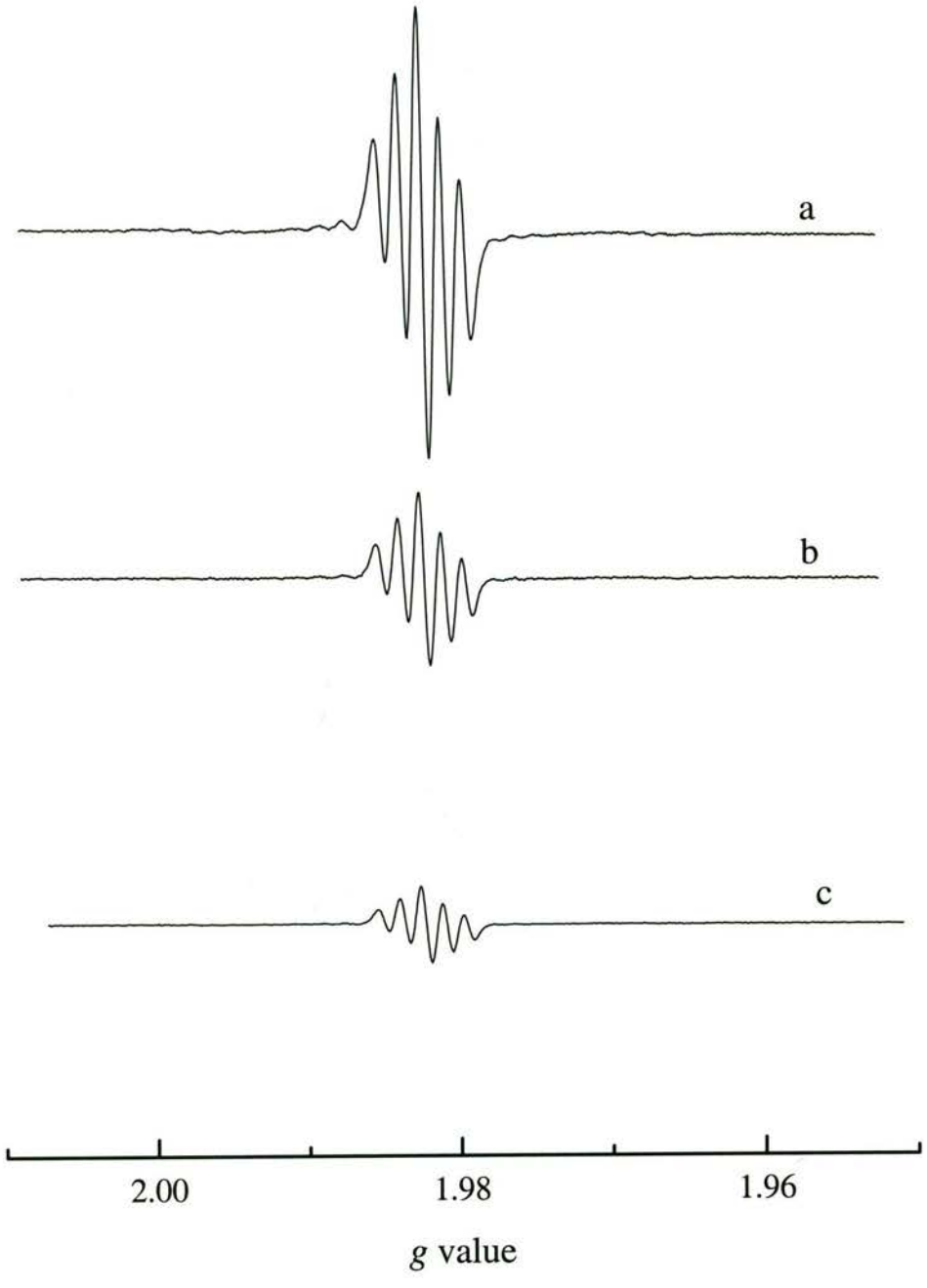

Figure 4.15 EPR spectra of the Cr(V) species in an aqueous solution of the $[Cr^{V}O(S,S\text{-bprolben})]^{+}$ partially purified product (a) 10 min, (b) 1 d, and (c) 7 d after dissolution. Parameters: receiver gain, 6.32×10^{4}; sweep width, 100 G; power, 20.17 mW; modulation amplitude, 1.00 G; time constant, 20.48 msec; conversion time, 20.48 msec; scans, 10.

amide groups while there were four deprotonated amide groups in the macrocyclic ligands. The superhyperfine couplings to the amine N atoms of *S,S*-bprolben were not resolved in the EPR spectra. Since the g_{iso} value was solvent independent, and

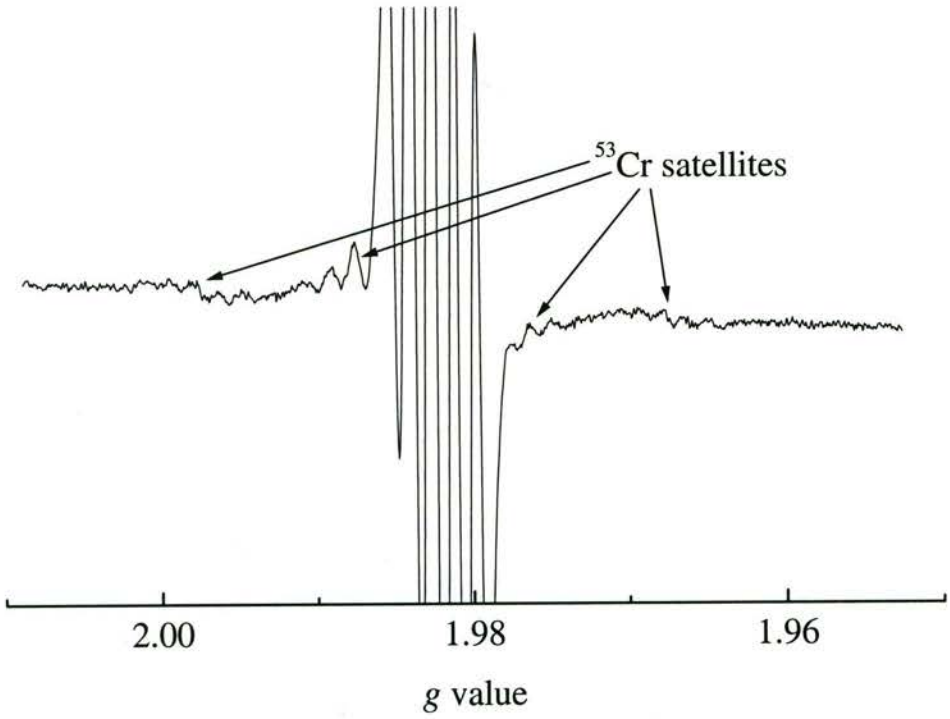

Figure 4.16 ^{53}Cr hyperfine coupling in the EPR spectrum of an aqueous solution of the $[Cr^{V}O(S,S\text{-bprolben})]^{+}$ partially purified product recorded 10 min after dissolution.

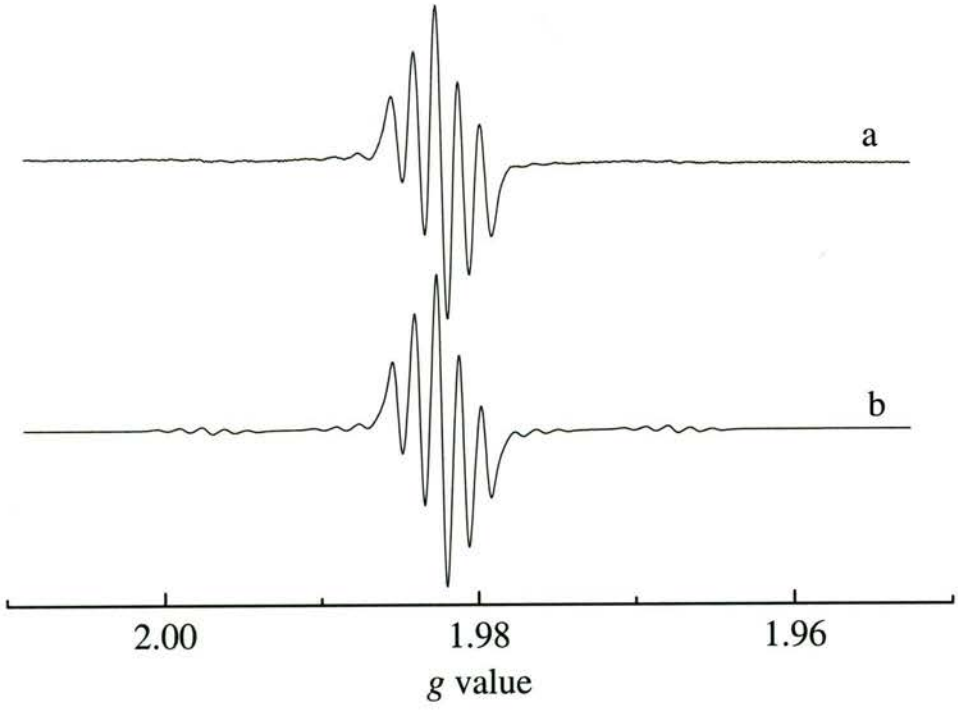

Figure 4.17 (a) Experimental and (b) simulated EPR spectra of an aqueous solution of $[Cr^{V}O(S,S\text{-bprolben})]^{+}$. The parameters used in the simulation are in Table 4.13.

Table 4.13 Chromium(V) EPR parameters obtained from the simulated spectrum of the aqueous solution of $[Cr^{V}O(S,S\text{-bprolben})]^{+}$

Cr(V) Species	g_{iso} value	relative concentration (%)	A_{iso} ($\times 10^{-4}$ cm^{-1})	Number of atoms
1	1.9824	91.7	2.32	2 N
2	1.9824	8.3	2.32 16.38	2 N 2 Cr

the A_{Cr} value showed the Cr(V) complex with *S,S*-bprolben was five-coordinate, the amine N of *S,S*-bprolben were probably coordinated to Cr but their ^{14}N superhyperfine couplings were not resolved. The Cr(V)-phen complex $[Cr^{V}(O)_2(phen)_2]^{+}$ is another example of a Cr(V) complex with N donor atoms where ^{14}N superhyperfine couplings were not resolved in the EPR spectra.[36,47] The g_{iso} = 1.9824 species was assigned as the five-coordinate species **III**.

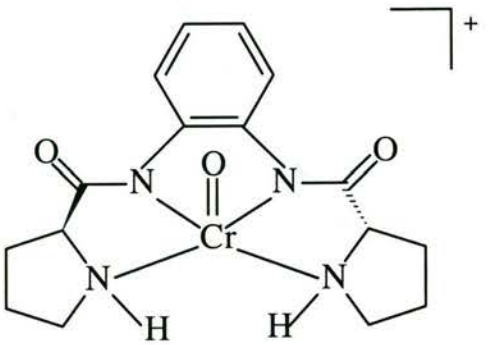

III

The light dependence of the formation of the Cr(V)-(*S,S*-bprolben) complex is similar to that for Cr(V)-amino acid complexes formed by the reduction of Cr(VI) in the presence of glycine and α-aminoisobutyric acid.[30]

4.4 Conclusions

Oxidation of Cr(III) complexes with the tetradentate diamide ligands bpb, bpen, and *S,S*-bprolben produced Cr(V) complexes that were detected by EPR spectroscopy. Several structurally similar complexes that displayed superhyperfine coupling to amide N atoms were generated during the oxidation of the Cr(III) complexes with the

bpb and *S,S*-bprolben ligands. The Cr(V) complexes with bpb were present in significant but somewhat decreased amounts a day after the oxidation was carried out. The concentrations of the Cr(V) complexes with *S,S*-bprolben were greater in the 1-day-old solution than the freshly oxidised solution of $[Cr^{III}(S,S\text{-bprolben})L_2]^{n+}$. This was due to the slow rate of the oxidation reaction and the exceptional stability of the Cr(V)-(*S,S*-bprolben) complexes.

Chromium(V) complexes with bpen and *S,S*-bprolben were also produced by the reduction of Cr(VI) by methanol in the presence of the ligand. The complex with bpen was difficult to characterise due to limited solubility, but it was determined that it contained Cr in both the Cr(VI) and Cr(V) oxidation states. The intractable nature of this product prevented a definite assignment of the structure from being made, but the Cr(V) in it was quite stable. The formation of Cr(V) complexes with *S,S*-bprolben was light dependent; in the absence of light only Cr(V)-methanol species formed. The Cr(V) complex with *S,S*-bprolben was very stable in acetone/methanol and aqueous solutions. The EPR spectra of the complex in aqueous solution exhibited hyperfine coupling to ^{53}Cr and superhyperfine coupling to ^{14}N, and the complex was assigned as a five-coordinate oxo-Cr(V) species. The amide ligands alone did not reduce Cr(VI), but they were able to form complexes with and stabilise Cr(V) formed by the reaction of Cr(VI) with the reductant methanol.

Oxidation of the Cr(III) analogue was an effective method of generating Cr(V) species in solution, but it was difficult to isolate a single Cr(V) species. The reduction of Cr(VI) by methanol in the presence of *S,S*-bprolbenH_2 was the best method for isolating a single Cr(V) species. The insoluble Cr(III) products that formed during the reduction were readily separated from the soluble Cr(V) species, and the small amounts of Cr(V)-methanol complexes that remained after column chromatography decomposed in aqueous solution. Though time did not permit the preparation of the other enantiomer of the bprolben ligand, the procedures developed can be used to prepare enantiomeric Cr(V) species.

The stability of the Cr(V) complexes generated by the reduction of Cr(VI) and the oxidation of Cr(III) with these diamide ligands showed that the deprotonated amide

N was very effective at stabilising the Cr(V) oxidation state. This ability of amide ligands to stabilise the Cr(V) oxidation state in aqueous solution has implications for the *in vivo* metabolism of the carcinogen Cr(VI). The formation of Cr(V)-amide complexes was rather slow, so they are not likely to form in large amounts inside a cell where there are a large number of potential ligands that will coordinate to Cr(V) more rapidly, such as amino acids, sugars, 2-hydroxy acids, and ascorbate. The greater stability of Cr(V)-amide complexes means that though probably only minor species, they may still play a role in Cr(VI)-induced carcinogenesis.

4.5 References

1) M. Krumpolc and J. Roček *J. Am. Chem. Soc.* **1979**, *101*, 3206-3209.

2) M. Krumpolc, B. G. DeBoer and J. Roček *J. Am. Chem. Soc.* **1978**, *100*, 145-153.

3) R. Codd, A. Levina, L. Zhang, T. W. Hambley and P. A. Lay *Inorg. Chem.* **2000**, *39*, 990-997.

4) P. O'Brien, J. Pratt, F. J. Swanson, P. Thornton and G. Wang *Inorg. Chim. Acta* **1990**, *169*, 265-269.

5) T. J. Collins, C. Slebodnick and E. S. Uffelman *Inorg. Chem.* **1990**, *29*, 3433-3436.

6) T. L. Siddall, N. Miyaura, J. C. Huffman and J. K. Kochi *J. Chem. Soc., Chem. Commun.* **1983**, 1185-1186.

7) K. Srinivasan and J. K. Kochi *Inorg. Chem.* **1985**, *24*, 4671-4679.

8) J. T. Groves, T. Takahashi and W. M. Butler *Inorg. Chem.* **1983**, *27*, 884-887.

9) J. Bendix, S. R. Wilson and T. Prussak-Wieckowska *Acta Crystallogr., Sect. C* **1998**, *C54*, 923-925.

10) N. Azuma, Y. Imori, H. Yoshida, K. Tajima, Y. Li and J. Yamauchi *Inorg. Chim. Acta* **1997**, *266*, 29-36.

11) A. Hori, T. Ozawa, H. Yoshida, Y. Imori, Y. Kuribayashi, E. Nakano and N. Azuma *Inorg. Chim. Acta* **1998**, *281*, 207-213.

12) C.-M. Che, J.-X. Ma, W.-T. Wong, T.-F. Lai and C.-K. Poon *Inorg. Chem.* **1988**, *27*, 2547-2548.

13) M. Branca, A. Dessí, H. Kozlowski, G. Micera and J. Swiatek *J. Inorg. Biochem.* **1990**, *39*, 217-226.

14) R. P. Farrell, R. J. Judd, P. A. Lay, R. Bramley and J.-Y. Ji *Inorg. Chem.* **1989**, *28*, 3401-3403.

15) R. Bramley, R. P. Farrell, J.-Y. Ji and P. A. Lay *Aust. J. Chem.* **1990**, *43*, 263-279.

16) R. Stomberg and C. Brosset *Acta Chem. Scand.* **1960**, *14*, 441-452.

17) R. J. Judd, T. W. Hambley and P. A. Lay *J. Chem. Soc., Dalton Trans.* **1989**, 2205-2210.

18) R. P. Farrell and P. A. Lay *Comments Inorg. Chem.* **1992**, *13*, 133-175.

19) M. Kimura, R. Ikawa, Y. Shiota and K. Tsukahara *Bull. Chem. Soc. Jpn.* **1998**, *71*, 893-897.

20) L. Zhang and P. A. Lay *Inorg. Chem.* **1998**, *37*, 1729-1733.

21) F. Chen, J. Ye, X. Zhang, Y. Rojanasakul and X. Shi *Arch. Biochem. Biophys.* **1997**, *338*, 165-172.

22) V. Srinivasan and J. Roček *J. Am. Chem. Soc.* **1974**, *96*, 127-133.

23) R. P. Farrell, P. A. Lay, A. Levina, I. A. Maxwell, R. Bramley, S. Brumby and J.-Y. Ji *Inorg. Chem.* **1998**, *37*, 3159-3166.

24) S. Kitagawa, H. Seki, F. Kametani and H. Sakurai *Inorg. Chim. Acta* **1988**, *152*, 251-255.

25) P. O'Brien and Z. Ozolins *Inorg. Chim. Acta* **1989**, *161*, 261-266.

26) D. I. Pattison, P. A. Lay and M. J. Davies *Inorg. Chem.* **2000**, *39*, 2729-2739.

27) S. Signorella, M. I. Frascaroli, S. Garcia, M. Santoro, J. C. Gonzalez, C. Palopoli, V. Daier, N. Casado and L. F. Sala *J. Chem. Soc., Dalton Trans.* **2000**, 1617-1623.

28) L. Zhang and P. A. Lay *J. Am. Chem. Soc.* **1996**, *118*, 12624-12637.

29) L. Zhang and P. A. Lay *Aust. J. Chem.* **2000**, *53*, 7-13.

30) H. A. Headlam; PhD Thesis, The University of Sydney, 1998.

31) W.-H. Leung, J.-X. Ma, V. W.-W. Yam, C.-M. Che and C.-K. Poon *J. Chem. Soc., Dalton Trans.* **1991**, 1071-1076.

32) R. E. Lenga, Ed. *The Sigma-Aldrich library of chemical safety data*; II ed.; Sigma-Aldrich Corporation: Milwaukee, 1988.

33) R. P. Farrell, R. J. Judd, P. A. Lay, N. E. Dixon, R. S. U. Baker and A. M. Bonin *Chem. Res. Toxicol.* **1989**, *2*, 227-229.

34) C. T. Dillon, P. A. Lay, A. M. Bonin, M. Cholewa, G. J. F. Legge, T. J. Collins and K. L. Kostka *Chem. Res. Toxicol.* **1998**, *11*, 119-129.

35) A. Levina, G. Barr-David, R. Codd, P. A. Lay, N. E. Dixon, A. Hammershøi and P. Hendry *Chem. Res. Toxicol.* **1999**, *12*, 371-381.

36) C. T. Dillon, P. A. Lay, A. M. Bonin, N. E. Dixon and Y. Sulfab *Aust. J. Chem.* **2000**, *53*, 411-424.

37) D. R. Duling *J. Magnet. Reson. Series B* **1994**, *104*, 105-110.

38) L. J. Bellamy *The Infra-red Spectra of Complex Molecules*; 2nd ed.; Methuen and Co. Ltd.: London, **1959**.

39) J. R. Ferraro *Low-frequency vibrations of inorganic and coordination compounds*; Plenum Press: New York, **1971**.

40) J. J. Manura *Molecular Isotope Distribution Calculator Program*; **1996**, Scientific Instrument Services.

41) O. Clement, B. M. Rapko and B. P. Hay *Coord. Chem. Rev.* **1998**, *170*, 203-243.

42) A. E. Ceniceros-Gómez, N. Barba-Behrens, M. E. Quiroz-Castro, S. Bernes, H. Nöth and S. E. Castillo-Blum *Polyhedron* **2000**, *19*, 1821-1827.

43) K. Nakamoto *Infrared and Raman Spectra of Inorganic and Coordination Compounds*; 5th ed.; John Wiley and Sons: New York, **1997**.

44) K. Kawabe, T. Suekuni, T. Inada, K. Yamoto, M. Tadokoro, Y. Kojima, Y. Fujisawa and H. Sakurai *Chem. Lett.* **1998**, 1155-1156.

45) G. Barr-David, M. Charara, R. Codd, R. P. Farrell, J. A. Irwin, P. A. Lay, R. Bramley, S. Brumby, J.-Y. Ji and G. R. Hanson *J. Chem. Soc., Faraday Trans.* **1995**, *91*, 1207-1216.

46) H. A. Headlam and P. A. Lay *Inorg. Chem.* **2001**, *40*, 78-86.

47) Y. Sulfab and M. Nasreldin *Trans. Met. Chem.* **2001**, *26*, 147-149.

Chapter 5

X-Ray Absorption Spectroscopy of Chromium Complexes

5.1 Introduction

5.1.1 X-ray Absorption Spectroscopy

A typical X-ray absorption spectrum is shown in Figure 5.1. The increase in the absorption, known as an absorption edge, is due to the photon having just enough energy to excite an electron from a core orbital to an unoccupied or partially filled orbital, XANES (X-ray absorption near-edge structure), or to the continuum, XAFS (X-ray absorption fine structure) (Figure 5.2).[1] The core hole created decays by the emission of a fluorescent X-ray photon or the emission of an Auger electron. These edges occur at characteristic positions for each element and are labelled according to the core orbital from which the electron is excited; a *K* edge is due to excitation of a 1*s* electron, while *L* edges are due to excitation of 2*s* or 2*p* electrons, etc.

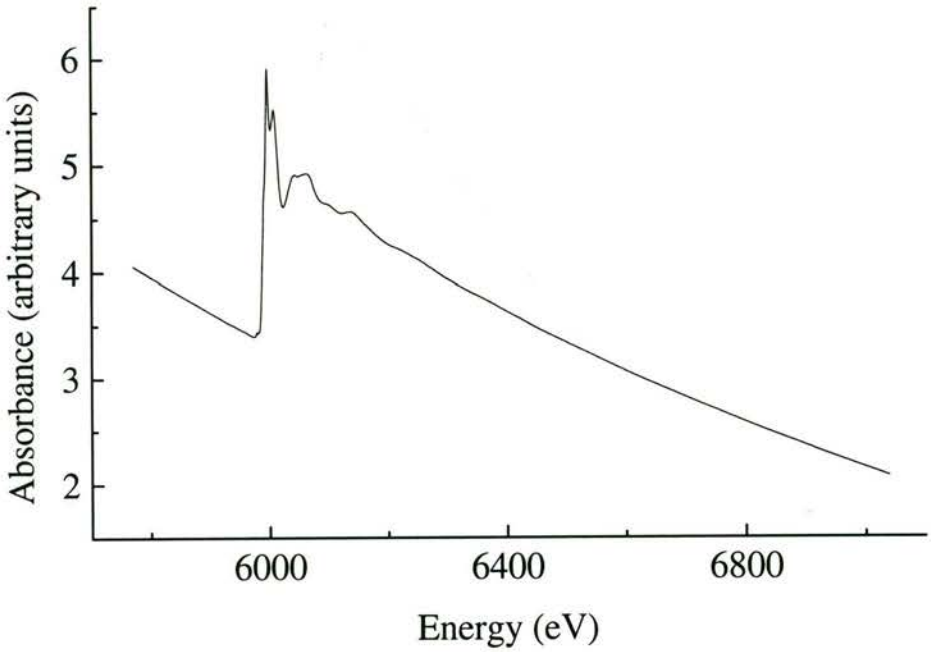

Figure 5.1 Transmission-mode X-ray absorption spectrum of *cis*-$[Cr^{III}(phen)_2(OH_2)_2](NO_3)_3.2.5H_2O$

The oscillations in the spectrum (Figure 5.1) around the absorption edge continue for up to several hundred eV above the absorption edge, though the amplitude decreases rapidly with increasing energy. It is from these features of the X-ray absorption spectrum that a great deal of structural information can be obtained. Most of the features within about 25 eV of the edge are ascribed to bound-state transitions.[1] This is the XANES and can yield information about the oxidation state, coordination

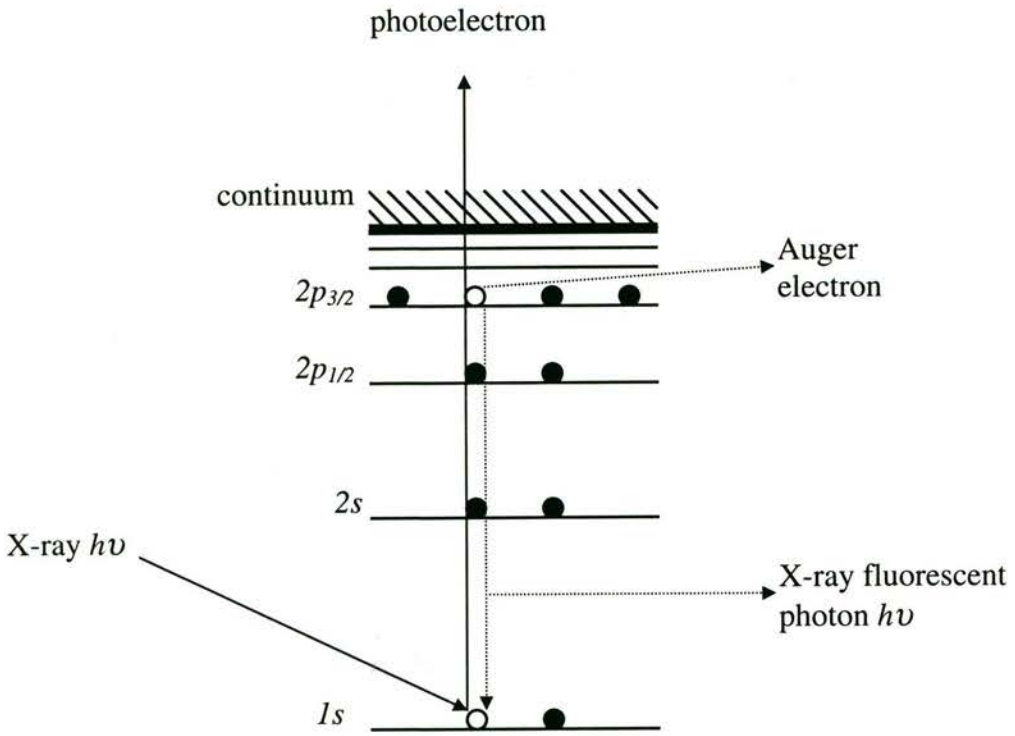

Figure 5.2 XAFS processes

geometry and the nature of the atoms surrounding the absorbing atom.[1] The oscillations that continue for several hundred eV beyond the absorption edge, XAFS, is the modulation of the absorption coefficient μ compared to the smooth background coefficient μ_s. This is normalised by the absorption coefficient for the free atom μ_0.[1]

$$\chi = (\mu+\mu_s)/\mu_0 \qquad (5.1)$$

Since $\mu_s = \mu_0$, the XAFS can instead be defined as:

$$\chi = (\mu+\mu_0)/\mu_0 \qquad (5.2)$$

5.1.2 XAFS

XAFS results from interference between the outgoing photoelectron wave from the absorbing atom and the photoelectron waves backscattered from the surrounding atoms (Figure 5.3).[1-4] The backscattered wave modifies the final-state wavefunction at the absorbing atom.[2,3]

If the absorption of an X-ray photon of energy E excites a core electron with binding energy E_0 ($E > E_0$), the photoelectron generated has energy $E - E_0$.[2] The de Broglie

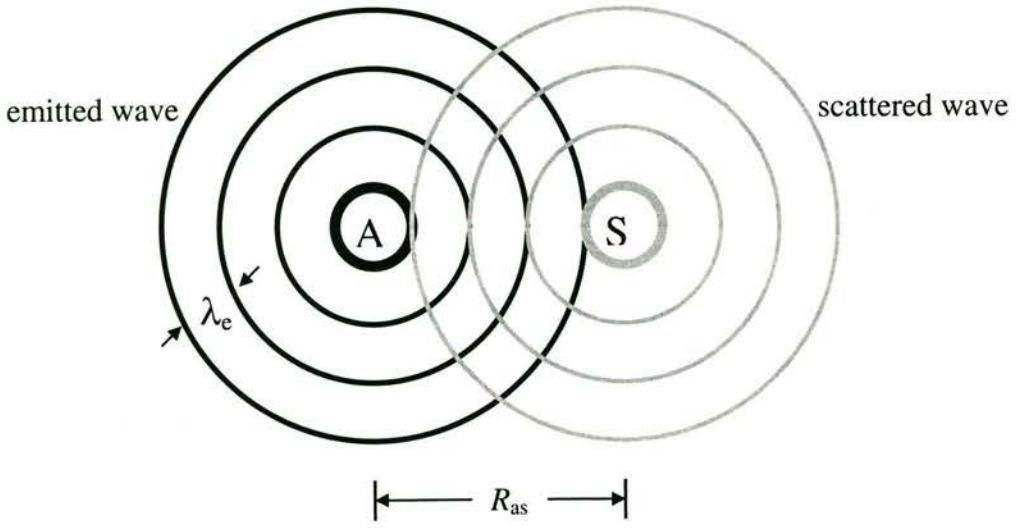

Figure 5.3 The photoelectron emitted from the absorbing atom A is backscattered by the atom S at a distance of R_{as}

relation gives the wavelength of the photoelectron as:

$$\lambda_e = h/p_e \tag{5.3}$$

where h is Planck's constant and p_e is the photoelectron momentum. The energy of the photoelectron in terms of the momentum is:

$$E_e = p_e^2/2m_e \tag{5.4}$$

where m_e is the mass of the electron. Combining Equations 5.3 and 5.4, the wavelength of the photoelectron is:

$$\lambda_e = h/(2m_eE_e) = h/\sqrt{2m_e(E-E_0)} \tag{5.5}$$

Figure 5.3 shows an absorbing atom emitting a photoelectron wave of wavelength λ_e. The photoelectron wave is scattered from another atom at a distance R_{as} and returns to the absorbing atom. The total distance travelled by the photoelectron wave is $2R_{as}$. This corresponds to $2R_{as}/\lambda_e$ wavelengths or a change in phase of:

$$\Delta_{phase} = 2\pi(2R_{as}/\lambda_e) \tag{5.6}$$

In XAFS, the quantity $2\pi/\lambda_e$ is known as the photoelectron wave vector, k:

$$k = 2\pi/\lambda_e = \hbar^{-1}\sqrt{2m_e(E-E_0)} \tag{5.7}$$

where $\hbar = h/2\pi$.

Thus the phase change of the photoelectron due to the distance travelled is:

$$\Delta_{phase} = 2kR_{as} \tag{5.8}$$

The phase of the photoelectron wave is also altered when it passes through the potentials of the absorbing and scattering atoms.[1,5] A correction $\alpha_{as}(k)$ must be added to take this effect into account. The corrected expression for the change in phase is:

$$\Delta_{phase} = 2kR_{as} + \alpha_{as}(k) \qquad (5.9)$$

The absorbance is increased when the waves are in phase and decreased when the waves are out of phase. The dipole-coupled absorption cross-section is:

$$\sigma = \left| \hat{e} \int \psi^*_i . \hat{r} . \psi_f \, d\tau \right|^2 \qquad (5.10)$$

where $\hat{e}$ is the electric field polarisation vector of the X-ray photon, ψ_i is the initial-state wavefunction and ψ_f is the final-state wavefunction. The absorbance varies with the magnitude of ψ_f near the absorbing atom. The magnitude of ψ_f is increased by constructive interference when the waves are in phase, and decreased by destructive interference when they are out of phase. Analysis of the amplitude, phase and frequency of the XAFS oscillations can provide information about the number, type and distances of atoms near the absorber.

5.1.3 Multiple-Scattering Processes

Multiple-scattering (MS) processes involve three or more atoms, the absorber and at least two backscatters. The effective path length of the photoelectron in MS processes is the sum of the pathlengths of the individual legs the photoelectron travels.[3] This makes the effective path length relatively long for MS processes. The XAFS from an atom decreases as the distance from the absorber increases.[6] This changes when the absorbing atom and the neighbouring atoms are arranged in a linear or nearly collinear fashion.[3,6,7] The amplitude of the photoelectron scattered from the distant atom is increased and this is known as the focusing effect or forward scattering.[6,7] These MS contributions are quite small except when the angle between the atoms is 150° or greater.[6,7] MS processes are usually significant only for atoms within 4-5 Å of the absorber but there are reports of effects observed for atoms up to 10 Å from the absorber.[5]

The three types of photoelectron paths for a system with an absorbing atom and two backscattering atoms are shown in Figure 5.4. Atom B1 is directly bonded to the absorbing atom and atom B2 is further away. The number of legs in the

backscattering path, n, is given for the three backscattering paths. The calculations of the XAFS due to the MS paths also include the $n = 2$ paths involving atoms B1 and B2, which are single scattering (SS) processes (only the path involving B2 is shown in Figure 5.4). The XAFS due to the MS pathways can be up to an order of magnitude stronger than those due to the SS pathways for the backscattering atoms further away from the absorber. For the $n = 3$ process, it does not matter whether the photoelectron is scattered by B1 or B2 first; the two paths, absorber→B1→B2→absorber and absorber→B2→B1→absorber are equivalent.

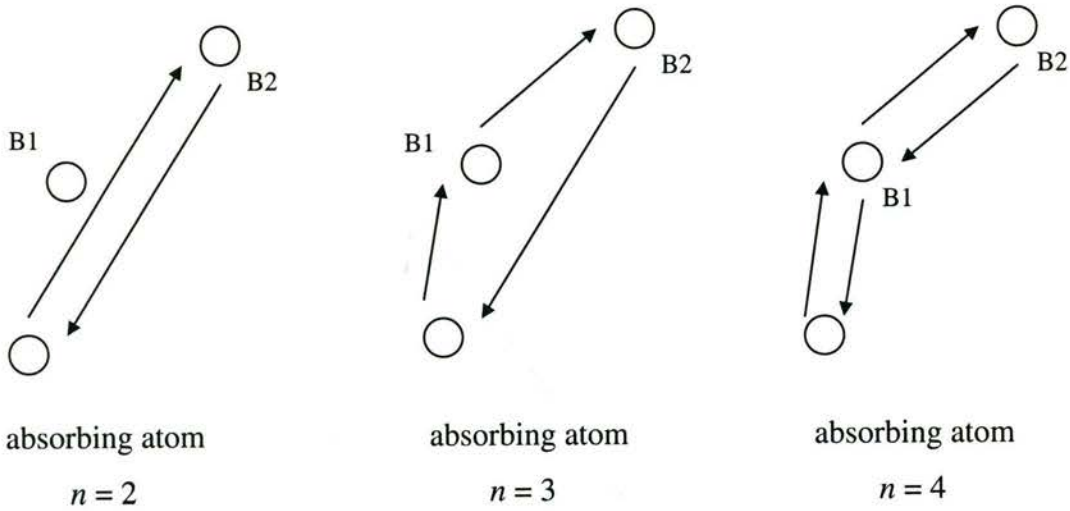

Figure 5.4 The SS ($n = 2$) and MS ($n \geq 3$) processes for a photoelectron in a three-atom system

The MS contributions to the XAFS are of interest because they can provide three-dimensional information about the molecular structure that is not available from SS calculations. Where the MS contributions to the XAFS are strong, they can provide more accurate information about the distances to atoms that are further away from the absorber than is available from SS.[5] The angular dependence of the MS contributions to the XAFS means that XAFS can be used to calculate the bond angles within the molecule or complex.[5-7]

5.1.4 Data Collection

5.1.4.1 Synchrotron Radiation Sources

The development of powerful synchrotron X-ray sources has provided a source of X-rays with a continuous energy distribution and a flux several orders of magnitude

greater than other sources of continuous X-rays.[1-3] Since the first report of XAFS data collection at a synchrotron by Kincaid and Eisenberger in 1975,[8] 99% of XAFS experiments have come to be conducted at synchrotron facilities.[2]

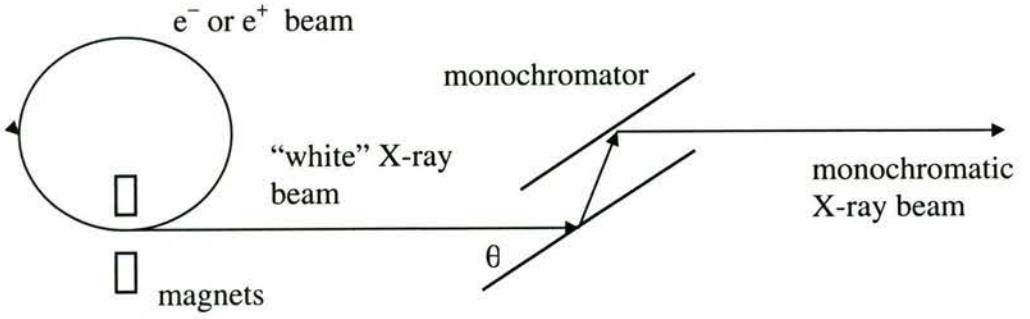

Figure 5.5 The generation of a monochromatic X-ray beam from a synchrotron

The high-flux X-ray radiation from a synchrotron is produced when electrons or positrons are accelerated by a magnetic field (Figure 5.5). The electrons or positrons travel in a ring at close to the speed of light; they are accelerated by magnets around the ring and X-rays are emitted at a tangent to the ring. The X-rays generated have a continuous energy distribution over a wide range of energies. To obtain the energy resolution required for XAFS experiments, the X-rays must be made monochromatic.

5.1.4.2 X-ray Monochromators and Detectors

The monochromator used commonly consists of two crystals cut parallel to the same lattice plane, separated by a small distance, with the two faces parallel to each other. The only X-rays that can pass through the monochromator are those that satisfy the Bragg equation:

$$n\lambda = 2d\sin\theta \qquad (5.11)$$

(n = 1, 2, 3...) where d is the spacing of the crystal plane. The energy of the X-rays coming through the monochromator can be varied by changing the angle θ. The higher harmonics (n > 1) will also come through the monochromator, but they can be removed in a couple of ways. A mirror can be used to reflect only X-rays below a certain energy[3] or the two crystals in the monochromator can be slightly mistuned by tilting one slightly out of parallel, which has a greater effect on the shorter wavelength X-rays.

Several methods of detection are used to collect the X-ray absorption data. The most common are X-ray transmission and fluorescence;[1,3] but the Auger electron yield can also be used.[3] A schematic diagram of the set up for transmission detection is shown below in Figure 5.6. The first detector measures the incident intensity, I_0, while the second detector measures the intensity after passing through the sample, I. The absorbance measured in XAFS is the relative absorbance, which is given by:

$$A = \log I_0/I \qquad (5.12)$$

The third detector measures the XAFS of a standard, eg., a metal foil, so that accurate energy calibration can be carried out. Transmission measurements normally use ionisation chambers for all the detectors. Transmission detection is best for measurements on solid samples and concentrated solutions;[3] fluorescence detection is preferred when working with dilute solutions or thin layers on surfaces.[1,3,9]

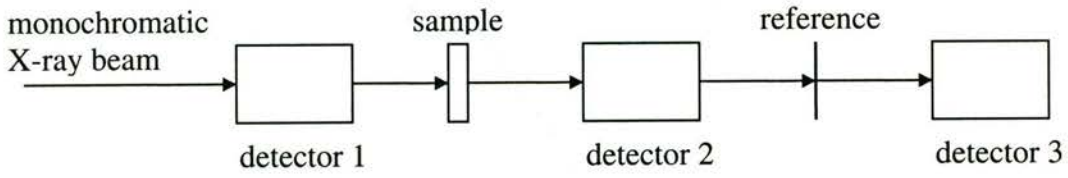

Figure 5.6 Detector arrangement for transmission XAFS measurements

5.1.5 Data Analysis

The extraction of the XAFS data from the X-ray absorption spectra and the analysis of the data were performed using the program XFIT.[10-12] XFIT includes *ab initio* calculation of the XAFS by the programs *FEFF* 4.06 (SS) and *FEFF* 6.01 (MS).[13-15]

5.1.5.1 Extraction of the XAFS from the X-ray Absorption Spectrum

The first step of data reduction is to subtract the underlying background absorbance, which is the absorbance that would be observed in the absence of an edge. The background (or pre-edge) absorbance is estimated by fitting a polynomial curve to the pre-edge region and extrapolating it to the end of the data. In Figure 5.7, the estimated background curve for *cis*-$[Cr^{III}(phen)_2(OH_2)_2](NO_3)_3.2.5H_2O$ is shown along with the X-ray absorption spectrum. The curve is fitted to the pre-edge

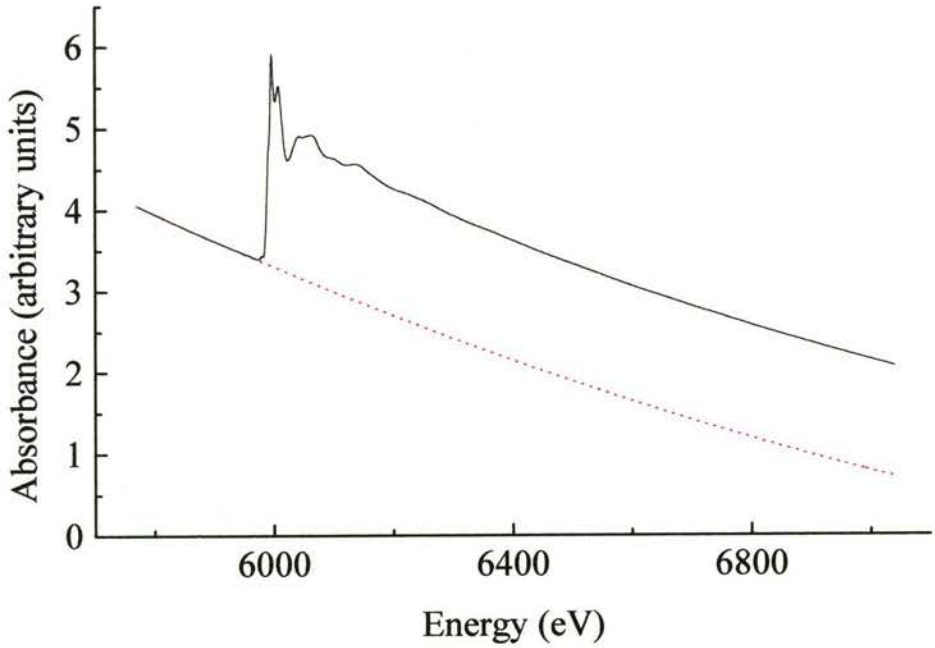

Figure 5.7 Subtraction of the underlying background absorbance (dashed line) from the X-ray absorption spectrum (solid line) of *cis*-$[Cr^{III}(phen)_2(OH_2)_2](NO_3)_3.2.5H_2O$

region, but it is chosen so that it also matches the general slope of the region above the edge.

Once the underlying absorbance has been removed, the absorbance is normalised so that the edge step is 1.0. This makes the final XAFS relative to the edge (μ_0), (Equation 5.2). The XAFS is then extracted by fitting a hypothetical smooth background, called the spline curve, to the normalised absorbance above the edge. The region above the edge is divided into segments and polynomial functions are fitted to each segment. The polynomials are constrained to have equal first derivatives at the points where the segments join. The normalised absorption spectrum and the spline curve for *cis*-$[Cr^{III}(phen)_2(OH_2)_2](NO_3)_3.2.5H_2O$ are shown in Figure 5.8. The subtraction of the spline curve from the normalised absorption spectrum gives the XAFS.

The XAFS is rapidly attenuated with increasing energy, as can be seen in Figure 5.9. To compensate for the attenuation at increasing energy, the XAFS is multiplied by k^3. The result of multiplying the XAFS of *cis*-$[Cr^{III}(phen)_2(OH_2)_2](NO_3)_3.2.5H_2O$ by

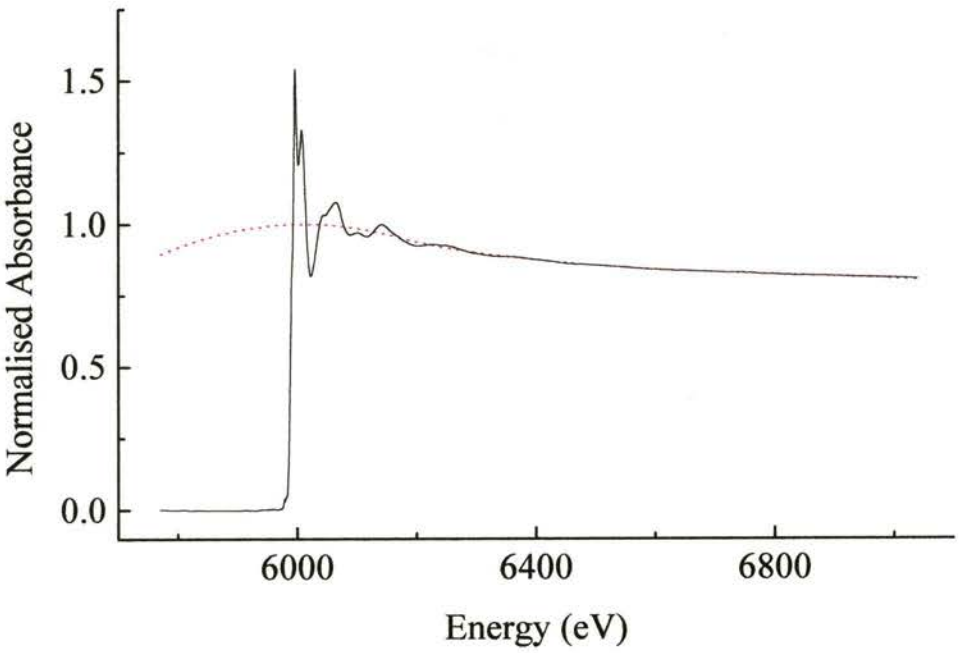

Figure 5.8 Subtraction of the spline function (dashed line) from the normalised absorption spectrum (solid line) of *cis*-$[Cr^{III}(phen)_2(OH_2)_2](NO_3)_3.2.5H_2O$

k^3 plotted as a function of k is shown in Figure 5.10.

5.1.5.2 Fourier Filtering

The XAFS is also displayed as the Fourier transform. This gives a type of radial distribution function as a function of k^{-1} (Å). It does not correspond directly to the absorber-scatterer distances due to a 'phase' correction,[3,11] but the peaks do correspond to the scatterer shells. The inverse transform of the Fourier transform generates the original XAFS. This process of applying a Fourier transform, followed by an inverse Fourier transform is used to remove noise from the XAFS and is described as Fourier filtering.[3]

5.1.5.3 Window Functions

Window functions are used with XAFS and Fourier transform curves to remove the parts of the curves that are noisy or otherwise unwanted. The curves are multiplied by the window functions. The window functions in XFIT have an edge rising from 0 to 1, a region of magnitude 1, and then an edge falling from 1 to 0. The width,

position and function form of each of the edge regions can be varied. This enables the level of importance attached to the data to be changed gradually.

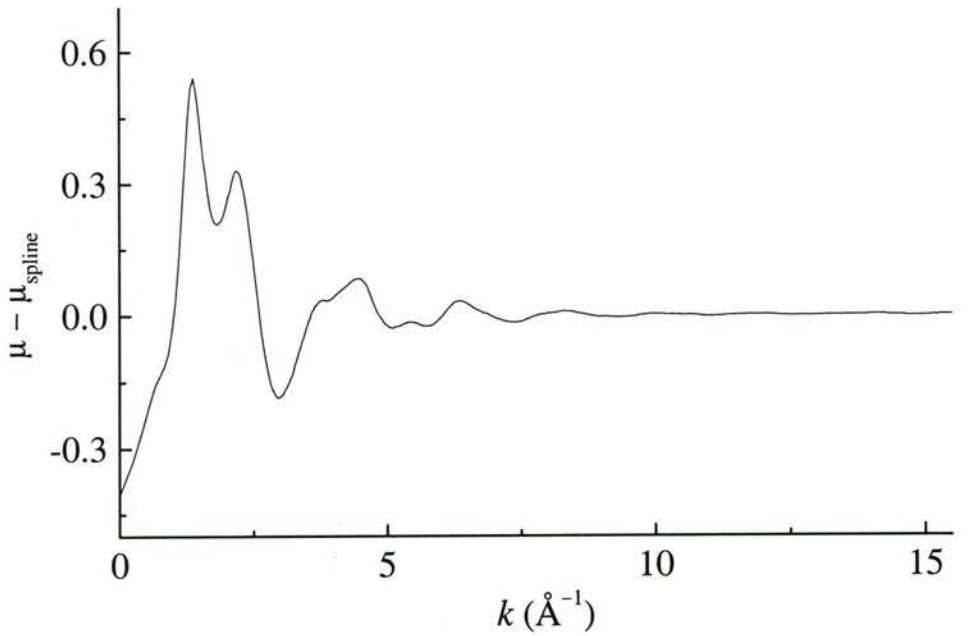

Figure 5.9 The XAFS of *cis*-$[Cr^{III}(phen)_2(OH_2)_2](NO_3)_3.2.5H_2O$ plotted as a function of k

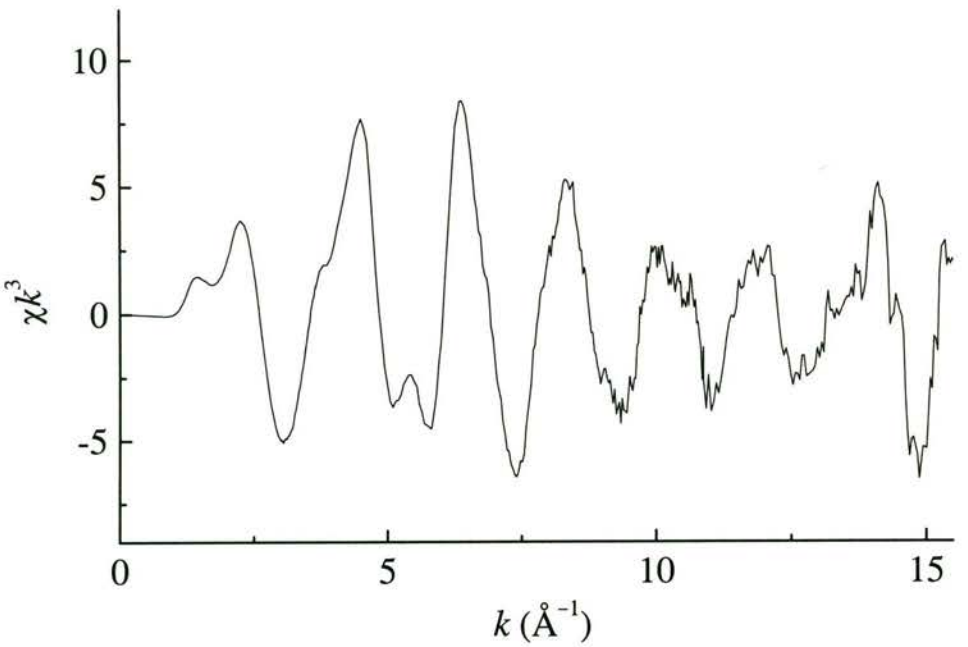

Figure 5.10 The XAFS of *cis*-$[Cr^{III}(phen)_2(OH_2)_2](NO_3)_3.2.5H_2O$ multiplied by k^3 and plotted as a function of k

5.1.5.4 Calculation of the Theoretical XAFS

A model of the absorber site is constructed, and the aim is to minimise the difference between the observed XAFS spectrum χ_{obs} and the XAFS calculated from the model χ_{calc}. XFIT optimises the fit between the observed and calculated XAFS by minimising the X^2, which is defined as:[10,11]

$$X^2_{XAFS} = \int_{k=0}^{\infty} [w(\chi_{obs}(k) - \chi_{calc}(k))]^2 dk \qquad (5.13)$$

where w is the weighting factor;

$\chi_{obs}(k)$ is the filtered observed XAFS curve; and

$\chi_{calc}(k)$ is the filtered calculated XAFS curve.

The theoretical XAFS are calculated *ab initio* by *FEFF* 4.06 and *FEFF* 6.01[13-15] using the expression:

$$\chi(k) = \sum_{\Gamma} N_\Gamma A(k)[f_{eff\Gamma}(\pi,k,R)/kR_\Gamma^2]\sin[2kR_\Gamma + 2\mathrm{Re}(\delta_\Gamma^c(k)) + \phi_{eff\Gamma}(k)]$$

$$\times\exp[-2\sigma_\Gamma^2 k^2]\exp[-2R_\Gamma/\lambda_\Gamma(k)] \qquad (5.14)$$

where $A(k) = S_0^2\exp[-\mathrm{Im}(\delta_\Gamma^c(k))]$ (5.15)

Γ is a scattering path;

N_Γ is the multiplicity of the scattering path;

R_Γ is the effective path length;

σ_Γ^2 is the mean-square deviation in R_Γ;

$\delta_\Gamma^c(k)$ is the final-state central-atom phase shift;

$f_{eff\Gamma}(\pi,k,R) = |f_{eff\Gamma}(\pi,k,R)|\exp[i\phi_{eff\Gamma}(k)]$ is the effective curved-wave backscattering amplitude

$\lambda_\Gamma(k)$ is the photoelectron mean-free path;

$A(k)$ is a factor combining intrinsic losses, final state interference effects, and central-atom losses;

S_0^2 is a many-body amplitude reduction factor; and

Re and Im refer to the real and imaginary parts of a number, respectively.

5.1.5.5 Restraints and Constraints

The XAFS contains insufficient data to determine all of the model parameters, except in very simple systems. In MS analysis, like those in this work, the models consist of a large number or atoms each requiring three positional parameters. When there are fewer independent data points in the XAFS than the number of independent parameters in the model, the model parameters are underdetermined and hence it is not possible to fit the data to a model with confidence that it corresponds to the structure.[16] Constraints and restraints are used to reduce the number of independent parameters in the model.

Constraints specify a precise relationship between two parameters, restraints specify target relationships between parameters. Constraints and restraints are used to include prior knowledge of the structure of the absorber site in the model. A value like a standard deviation (σ) can be included in the restraint expression.

The restraints are refined by including them as an extra term in the expression for X^2:

$$X^2 = X^2_{XAFS} + \sum_{\text{restraint}} X^2_{\text{restraint}} \qquad (5.16)$$

where $X^2_{\text{restraint}} = [\Delta_{\text{restraint}}/\sigma_{\text{restraint}}]^2$ (5.17)

and $\Delta_{\text{restraint}} = 0$ when the restraint is satisfied

$\Delta_{\text{restraint}}$ = the difference between the two sides of the restraint expression if the restraint is not satisfied.

5.1.5.6 Monte-Carlo Error Analysis

XFIT[10,11] estimates the standard deviations in refined parameters and the relationships between refined parameters by a Monte-Carlo calculation. XFIT smooths the XAFS by Fourier filtering, and generates a series of simulated XAFS data sets by adding randomly generated noise to the smoothed XAFS. The simulated XAFS data sets are used to fit the model, and the sets of fitted parameters are generated for each refinement. The series of values for each fitted parameter are used to estimate the standard deviations in the fitted parameters and to estimate the uncertainty in the standard deviations.

5.2 Experimental

5.2.1 Synthesis of Cr complexes

5.2.1.1 $[Cr^{V}(O)_2(phen)_2]ClO_4$

The complex was prepared by a modification of the method of Dillon *et al.*[17] Excess PbO_2 (Merck, pure) was added to a solution of *cis*-$[Cr^{III}(phen)_2(OH_2)_2](NO_3)_3.2{\cdot}5H_2O$[18] (129 mg) in acetate buffer (~10 mL, pH 4.4) and the mixture was stirred for 30 min. The mixture was filtered at the pump and a concentrated solution of $LiClO_4$ was gradually added to the filtrate until a dark red precipitate formed. The precipitate was collected at the pump and dried over silica gel. Yield 7.6 mg.

5.2.1.2 $[Cr^{V}O(salen)]CF_3SO_3$

The complex was synthesised by the method of Srinivasan and Kochi.[19] Iodosobenzene (53 mg) was added to a solution of *trans*-$[Cr^{III}(salen)(OH_2)_2](CF_3SO_3)$ (98 mg) in acetonitrile (15 mL, BDH, 99.5%) and the mixture was stirred for 25 min. The colour changed from orange to dark green and the mixture was filtered to remove unreacted iodosobenzene. The filtrate was reduced to ~10 mL in volume on a rotary evaporator (water bath temperature ~20 °C) and diethyl ether (100 mL) was added. The blackish precipitate was collected at the pump and dried over silica gel. Yield 38.5 mg (41%).

5.2.2 XAFS Data Collection

XAFS data were collected on beamline 20B at the Australian National Beamline Facility (ANBF) at the Photon Factory in Tsukuba, Japan. The ring energy was 2.5 GeV and the ring current was 200-400 mA. The monochromator was a silicon crystal channel cut along the 111 face. Harmonic rejection was carried out by bending the second crystal in the monochromator until the incident beam intensity was half the intensity of the completely tuned beam.

The Cr complexes were prepared as finely ground powders and were placed in 0.5 mm thick Al holders with a 1.0 cm diameter sample window. The samples were sealed with KAPTON™ tape on both sides. The samples were pre-chilled in liquid

nitrogen then transferred to a Cryo Industries cryostat (model number REF-1577-D22) for recording of the XAFS data. A Neocera LTC-11 temperature controller was used to regulate the temperature of the cryostat. The position of the sample was changed after each run so that a fresh area of the sample was exposed to the beam for each scan.

The XAFS data for the Cr solids were recorded using the transmission mode. Three N_2-ionisation chambers were used as X-ray detectors. The signal from the ionisation chambers went to Keithley 428 current amplifiers. The energy was calibrated against Cr (16% Cr in stainless steel foil), assigning the first peak in the first derivative to 5989.0 eV,[20] or the strongest inflection point at the edge to an energy of 6005.0 eV.[12,21] The choice of reference point did not affect the value of the refined parameters or the goodness-of-fit values, except the value of the correction to the edge position, E_0.

5.2.2.1 $Na_2[Cr^V_2O_4(S\text{-ala})_2(OCH_3)_2].0{\cdot}5CH_3OH.0{\cdot}5(S\text{-alaH})$

A ground mixture of $Na_2[Cr^V_2O_4(S\text{-ala})_2(OCH_3)_2].0{\cdot}5CH_3OH.0{\cdot}5(S\text{-alaH})$[22] (22.6 mg) provided by Dr Henrietta Headlam and BN (30.7 mg) were ground together in a mortar and pestle before the XAFS data were recorded (3 scans). The temperature of the sample during data collection was 14 K.

Table 5.1 Regions program for $Na_2[Cr^V_2O_4(S\text{-ala})_2(OCH_3)_2].0{\cdot}5CH_3OH.0{\cdot}5(S\text{-alaH})$

region	start (keV)	finish (keV)	No. of points	No. of counts/point
1	5.77	5.97	20	200,000
2	5.97	6.05	160	200,000
3	6.05	6.45	200	500,000
4	6.45	7.05	150	1,000,000

5.2.2.2 *cis*-$[Cr^{III}(phen)_2(OH_2)_2](NO_3)_3.2{\cdot}5H_2O$

Neat *cis*-$[Cr^{III}(phen)_2(OH_2)_2](NO_3)_3.2{\cdot}5H_2O$[18] provided by Dr Carolyn Dillon was used to record the XAFS data (3 scans). The temperature of the sample during data

collection was 14 K.

Table 5.2 Regions program for *cis*-$[Cr^{III}(phen)_2(OH_2)_2](NO_3)_3.2{\cdot}5H_2O$

region	start (keV)	finish (keV)	No. of points	No. of counts/point
1	5.77	5.97	20	200,000
2	5.97	6.05	160	200,000
3	6.05	6.45	200	500,000
4	6.45	7.05	150	1,000,000

5.2.2.3 $[Cr^{V}(O)_2(phen)_2]ClO_4$

A ground mixture of $[Cr^{V}(O)_2(phen)_2]ClO_4$ (15 mg) and BN (28 mg) was used to record the XAFS data (8 scans). The temperature of the sample during data collection was 9 K.

Table 5.3 Regions program for $[Cr^{V}(O)_2(phen)_2]ClO_4$

region	start (keV)	finish (keV)	No. of points	No. of counts/point
1	5.78	5.98	20	132,000
2	5.98	6.02	200	132,000
3	6.02	k range 16 $Å^{-1}$	k step size 0.05 $Å^{-1}$	660,000

5.2.2.4 *trans*-$[Cr^{III}(salen)(OH_2)_2]CF_3SO_3$

Neat *trans*-$[Cr^{III}(salen)(OH_2)_2]CF_3SO_3$[19] provided by Dr Carolyn Dillon was used to record the XAFS data (3 scans). The temperature of the sample during data collection was 14 K.

Table 5.4 Regions program for *trans*-$[Cr^{III}(salen)(OH_2)_2]CF_3SO_3$

region	start (keV)	finish (keV)	No. of points	No. of counts/point
1	5.77	5.97	20	200,000
2	5.97	6.05	160	200,000
3	6.05	6.45	200	500,000
4	6.45	7.05	150	1,000,000

5.2.2.5 $[Cr^{V}O(salen)]CF_3SO_3$

A ground mixture of $[Cr^{V}O(salen)]CF_3SO_3$ (38 mg) and BN (29 mg) was used to record the XAFS data (2 scans). The temperature of the sample during data collection was 9 K.

Table 5.5 Regions program for $[Cr^{V}O(salen)]CF_3SO_3$

region	start (keV)	finish (keV)	No. of points	No. of counts/point
1	5.78	5.98	20	132,000
2	5.98	6.02	200	132,000
3	6.02	k range 16 $Å^{-1}$	k step size 0.05 $Å^{-1}$	660,000

5.2.2.6 *trans*-$[Cr^{III}(bpb)(OH_2)_2]ClO_4.H_2O$

A ground mixture of *trans*-$[Cr^{III}(bpb)(OH_2)_2]ClO_4.H_2O$ (22 mg) and BN (22 mg) was used to record the XAFS data (2 scans). The temperature of the sample during data collection was 10 K.

Table 5.6 Regions program for *trans*-$[Cr^{III}(bpb)(OH_2)_2]ClO_4.H_2O$

region	start (keV)	finish (keV)	No. of points	Count time (s)
1	5.78	5.98	20	1
2	5.98	6.02	200	1
3	6.02	k range 16 $Å^{-1}$	k step size 0.05 $Å^{-1}$	1 increasing to 5

5.2.2.7 *trans*-[Cr^{III}(bpb)Cl(OH_2)].DMF

A ground mixture of *trans*-[Cr^{III}(bpb)Cl(OH_2)].DMF and BN with a ~1:2 ratio of *trans*-[Cr^{III}(bpb)Cl(OH_2)].DMF:BN was used to record the XAFS data (2 scans). The temperature of the sample was 50 K during data collection.

Table 5.7 Regions program for *trans*-[Cr^{III}(bpb)Cl(OH_2)].DMF

region	start (keV)	finish (keV)	No. of points	No. of counts/point
1	5.77	5.97	20	200,000
2	5.97	6.05	160	200,000
3	6.05	6.45	200	500,000
4	6.45	7.05	150	1,000,000

5.2.3 XAFS Data Analysis

The XAFS spectra were extracted from the raw data of all experiments using the program XFIT.[10-12] The X-ray absorption spectra were averaged and monochromator glitches were removed. The pre-edge background subtraction used polynomial functions of order two for all the spectra. Three spline segments were used, the first was fitted with a polynomial of order two and the second and third were fitted with a polynomial of order three for all the spectra analysed. The region that the pre-edge background was fitted to, and the spline segments used to extract the XAFS data, are listed in Table 5.8. A k^3 weighting was applied to the XAFS data in all experiments. The XAFS and Fourier transform window functions used in the refinements are shown in Table 5.9.

Model structures were refined to optimise the fit of the calculated to the observed XAFS. The parameters varied in the refinements were: the x, y, z coordinates in Cartesian axes for each atom in the model, the Debye-Waller factor, σ^2, of every atom in the model (except the absorbing atom), a scale factor S_0^2, and E_0.

Table 5.8 Spline parameters used to extract XAFS data

Complex	Pre-edge Background (eV)	Spline Segments (eV)
$Na_2[Cr^{V}_2O_4(S\text{-ala})_2(OCH_3)_2]$ .0·5CH_3OH.0·5(*S*-alaH)	5792.8-5989.6	6006.0-6096.2 6096.2-6780.0 6780.0-7092.4
cis-$[Cr^{III}(phen)_2(OH_2)_2](NO_3)_3$ .2·5H_2O	5802.7-5966.7	5989.4-6163.9 6163.9-6418.8 6418.8-6935.4
trans-$[Cr^{III}(bpb)(OH_2)_2]ClO_4.H_2O$	5787.8-5948.8	5991.8-6095.6 6095.6-6532.9 6532.9-6838.6
trans-$[Cr^{III}(bpb)Cl(OH_2)]$.DMF	5793.0-5980.9	5995.3-6156.3 6156.3-6720.4 6720.4-7004.1

Table 5.9 XAFS and Fourier transform window functions

Complex	XAFS Window ($Å^{-1}$)		Fourier Transform Window (Å)	
	Range	Edge Width	Range	Edge Width
$Na_2[Cr^{V}_2O_4(S\text{-ala})_2(OCH_3)_2]$ .0·5CH_3OH.0·5(*S*-alaH)	0.5-13.6	0.1	1.1-4.7	0.1
cis-$[Cr^{III}(phen)_2(OH_2)_2]$ $(NO_3)_3$.2·5H_2O	1.0-13.2	0.1	1.0-5.0	0.1
trans-$[Cr^{III}(bpb)(OH_2)_2]ClO_4$ .H_2O	2.0-13.7	0.1	1.0-5.0	0.1
trans-$[Cr^{III}(bpb)Cl(OH_2)]$ .DMF	1.5-13.0	0.1	1.0-5.0	0.1

Restraints on S_0^2, the Debye-Waller factors, some bond lengths and some bond angles were included in the refinements. Symmetry constraints were used to reduce the number of parameters refined so that the refinements were overdetermined.[16] The restraints and constraints on the models that gave the best fit between the

observed and calculated XAFS are listed in Appendix 3. In the MS analysis, the plane-wave and curved-wave path filter thresholds were set at 2% and 3% of the strongest SS path, respectively. The significant MS pathways for the best model of each complex are tabulated in Appendix 3.

The goodness of fit parameter, R, was calculated by the method of Ellis and Freeman.[10,11] The errors in the bond lengths and some of the bond angles due to the noise in the XAFS data were estimated by the Monte-Carlo method included in the XFIT program.[10,11] They were combined with conservative systematic errors[2,5,23] to produce the probable errors.

5.2.3.1 $Na_2[Cr^V_2O_4(S\text{-ala})_2(OCH_3)_2].0{\cdot}5CH_3OH.0{\cdot}5(S\text{-alaH})$

The restraints on the bond lengths and angles of the alanine ligand were estimated from the crystal structure of the Cr(III) dimer $[Cr_2(OH)_2(S\text{-ala})_4]$.[24] In the dinuclear models, one of the Cr atoms was defined as the absorber and the second was treated only as a backscatterer. Symmetry constraints were used in the dinuclear models to reduce the number of parameters refined so that the refinements were overdetermined.[16] The x, y, and z coordinates of atoms in the half of the molecule containing the "backscattering" Cr atom were constrained to be equivalent to the coordinates of the atoms about the "absorbing" Cr atom. The R_{max} value was 5.50 Å for all the refinements.

5.2.3.2 *cis*-$[Cr^{III}(phen)_2(OH_2)_2](NO_3)_3.2{\cdot}5H_2O$

The restraints on the bond lengths and angles were taken from the crystal structure.[25] The Cr atom was placed at the origin, the Cartesian axes bisected the angles between the two phen ligands, and symmetry constraints about the axes were imposed to make the two ligands equivalent. Symmetry constraints were also placed on the O atoms from the aqua ligands. The R_{max} value was 5.50 Å for all the refinements.

5.2.3.3 *trans*-$[Cr^{III}(bpb)(OH_2)_2]ClO_4.H_2O$

The restraints on the ligand bond lengths and angles were based on the structure of the ligand in crystal structures of its Cr(V),[26] Ni(II),[27] Rh(III)[28] and Cu(II)[29] complexes. The Cr atom was placed at the origin and the bpb ligand in the

horizontal plane, with the aqua ligands in the axial positions; the x, y, z coordinates of the atoms in the two halves of bpb were constrained by symmetry to be equivalent and the Debye-Waller factors were also constrained to be equal. The O atoms from the aqua ligands were allowed to move independently or constrained to be symmetry equivalent. The R_{max} value was 5.50 Å for all the refinements.

5.2.3.4 *trans*-[Cr^{III}(bpb)Cl(OH_2)].DMF

The restraints on the ligand bond lengths and angles were the same as those for Model **XA** of *trans*-[Cr^{III}(bpb)(OH_2)$_2$]ClO_4. The constraints on the x, y and z coordinates of the bpb ligand and the Debye-Waller factors of the bpb atoms were the same as those for Model **XA** of *trans*-[Cr^{III}(bpb)(OH_2)$_2$]ClO_4. The parameters of the axial ligands in the two models refined were allowed to vary independently. The R_{max} value was 5.50 Å for all the refinements.

5.2.4 Bond Valence Sum Calculation

The bond valence sum (BVS) of the Cr in the Cr(V)-alanine complex was calculated according to Wood *et al.*[30] using Equation 5.18:

$$\text{BVS} = \sum_j s_{ij} \tag{5.18}$$

where $s_{ij} = \exp[(R_0 - R_{ij})/0.37]$ (5.19)

R_0 is a bond length of unit valence

R_{ij} is the observed bond length

The value of R_0 is dependent upon the nature of the atoms i and j. An average value of R_0 = 1.724 Å after Wood *et al.*[30] was used for the Cr–O bonds. There has been no report of a value of R_0 for Cr–N bonds in the literature, so an average value of R_0 = 1.83 Å (s.d. = 0.06Å), calculated from the crystal structures of 15 Cr(III) and Cr(V) complexes that contained either N or mixed N/O donor ligands,[19,24-26,31-37] was used. The complexes contained a range of N donor groups: nitrido, amido, imine, amine, imidazole and porphyrin.

5.3 Results and Discussion

5.3.1 XANES

The XANES spectra of $Na_2CrO_4.4H_2O$, and the Cr(V) complexes $Na[Cr^VO(ehba)_2].H_2O$, $Na_2[Cr^V_2O_4(S\text{-ala})_2(OCH_3)_2].0{\cdot}5CH_3OH.0{\cdot}5(S\text{-alaH})$, $[Cr^V(O)_2(phen)_2]ClO_4$, and $[Cr^VO(salen)]CF_3SO_3$ are shown in Figure 5.11. The XANES spectra of the Cr(III) complexes *cis*-$[Cr^{III}(phen)_2(OH_2)_2](NO_3)_3.2{\cdot}5H_2O$, *trans*-$[Cr^{III}(salen)(OH_2)_2]CF_3SO_3$, *trans*-$[Cr^{III}(bpb)(OH_2)_2]ClO_4.H_2O$, and *trans*-$[Cr^{III}(bpb)Cl(OH_2)].DMF$ are shown in Figure 5.12. The XANES data for $Na_2CrO_4.4H_2O$ and $Na[Cr^VO(ehba)_2].H_2O$ were provided by Dr Aviva Levina. The XANES data are summarised in Table 5.10. The XANES spectra of compounds of known oxidation state: $Na_2CrO_4.4H_2O$, $Na[Cr^VO(ehba)_2].H_2O$, $[Cr^VO(salen)]CF_3SO_3$, *cis*-$[Cr^{III}(phen)_2(OH_2)_2](NO_3)_3.2{\cdot}5H_2O$ and *trans*-$[Cr^{III}(salen)(OH_2)_2]CF_3SO_3$ were included as standards.

The position of the Cr *K* edge is shifted to higher energy as the oxidation state of the Cr increases. This is because the 1*s* electrons are more strongly bound as the charge on the Cr increases. The position of the pre-edge peak, which arises from the excitation of an electron from the 1*s* orbital to an unfilled or partially filled 3*d* orbital,[21,38] is also shifted to higher energy by an increase in the Cr oxidation state.

The variations in the intensities of the pre-edge peaks also provide information on the oxidation state. This $1s \rightarrow 3d$ transition is symmetry-forbidden, but the intensity of the band corresponding to this transition increases when there is a decrease in the symmetry of complex from octahedral geometry, and/or an increase in Cr-ligand π bonding. The increasing hybridisation of the Cr 3*d* orbitals with metal and/or ligand *p* orbitals makes the $1s \rightarrow 3d$ transition more allowed.[38]

The very intense pre-edge peak in the XANES of chromate (Figure 5.11(a)), almost as strong as the edge jump, is typical of Cr(VI) compounds.[21,39] Chromate has a strong pre-edge peak due to the tetrahedral coordination geometry of the Cr atom, and the strong π bonding between the Cr and the four oxo groups.

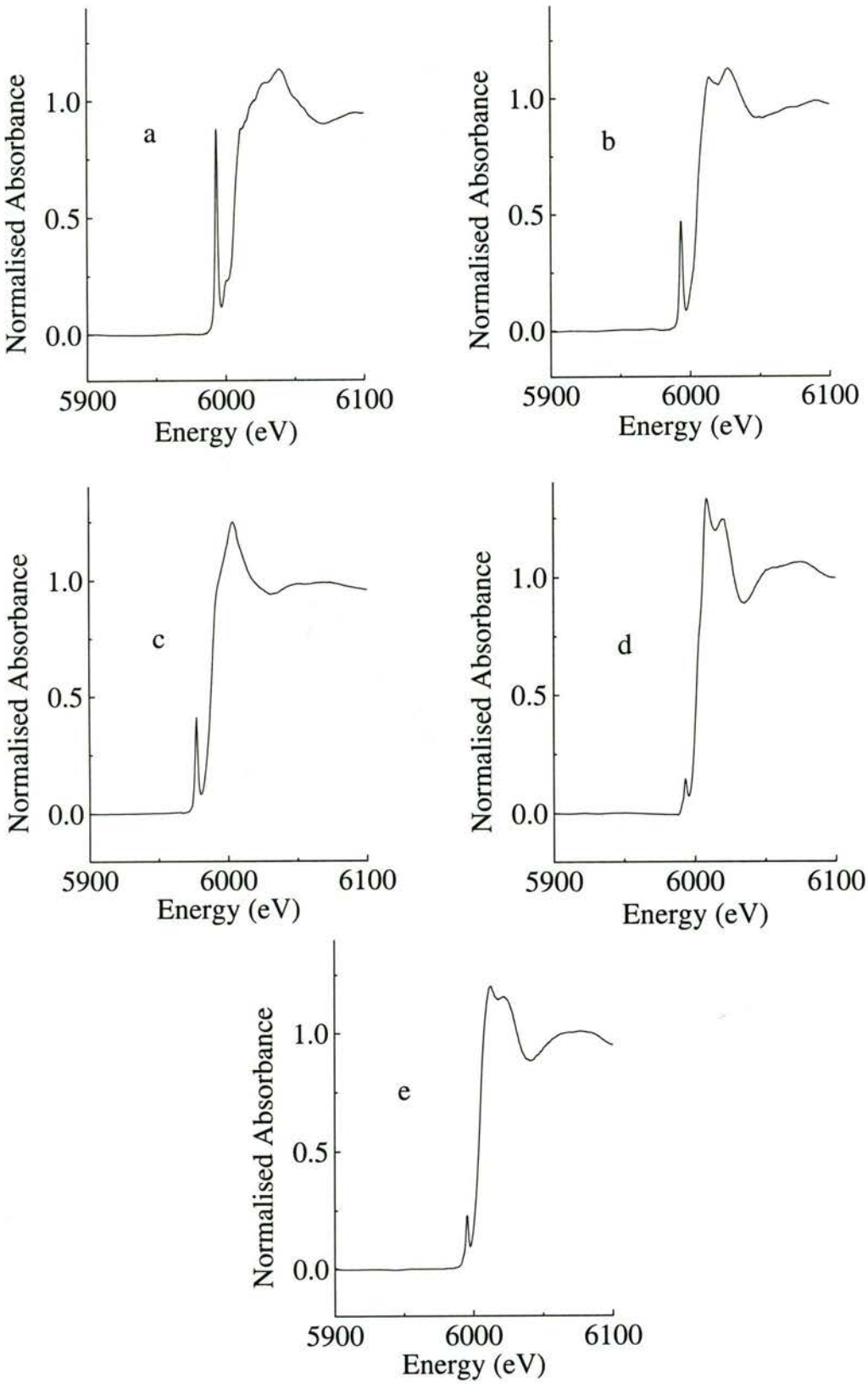

Figure 5.11 XANES spectra of (a) $Na_2CrO_4.4H_2O$, (b) $Na[Cr^VO(ehba)_2].H_2O$, (c) $[Cr^VO(salen)]CF_3SO_3$, (d) $[Cr^V(O)_2(phen)_2]ClO_4$, and (e) $Na_2[Cr^V{}_2O_4(S\text{-ala})_2(OCH_3)_2].0{\cdot}5CH_3OH.0{\cdot}5(S\text{-alaH})$

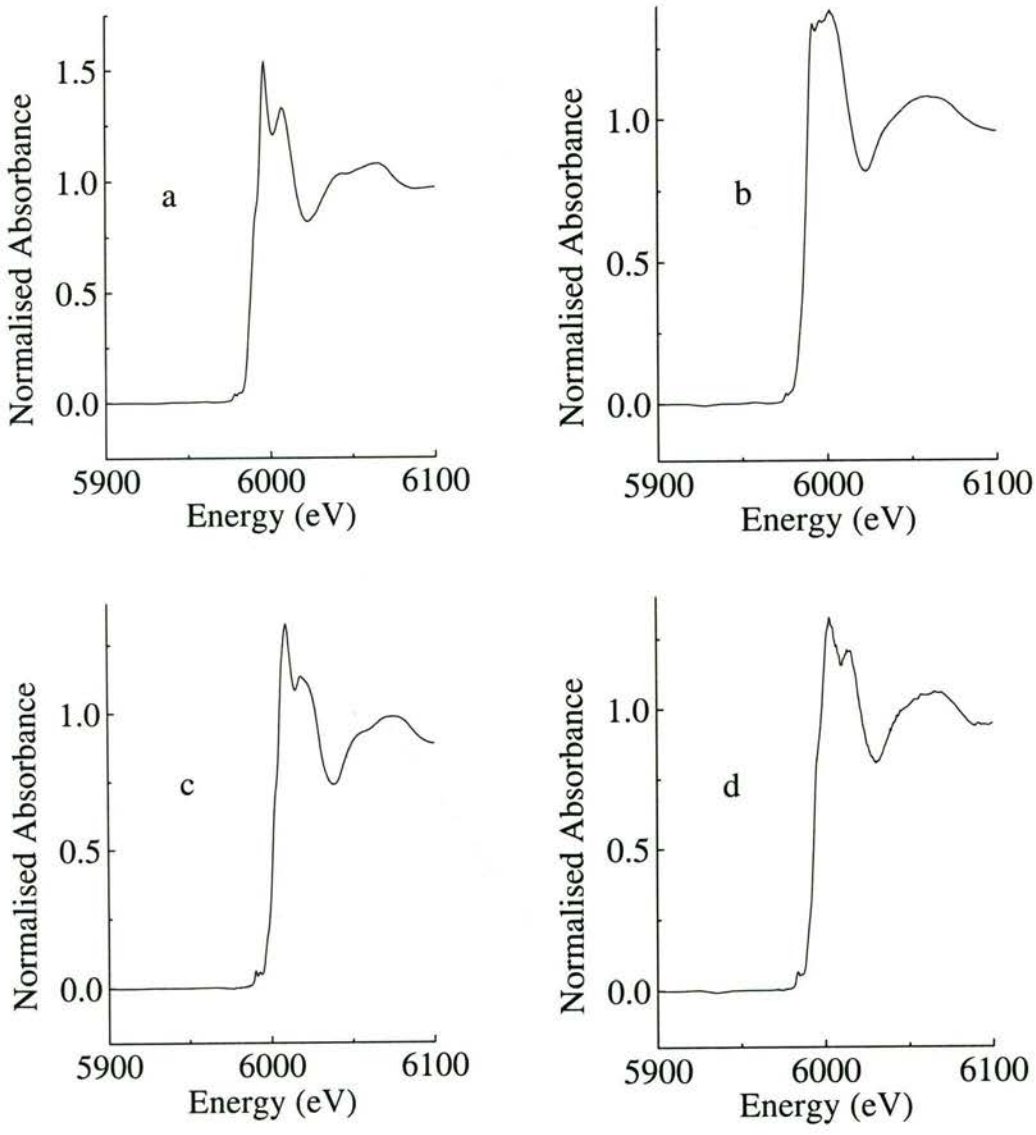

Figure 5.12 XANES spectra of (a) *cis*-$[Cr^{III}(phen)_2(OH_2)_2](NO_3)_3.2{\cdot}5H_2O$,
(b) *trans*-$[Cr^{III}(salen)(OH_2)_2]CF_3SO_3$,
(c) *trans*-$[Cr^{III}(bpb)(OH_2)_2]ClO_4.H_2O$, and
(d) *trans*-$[Cr^{III}(bpb)Cl(OH_2)].DMF$

The XANES spectra of the Cr(V/IV/III)-ehba complexes have been previously reported.[38] The pre-edge peak in the XANES spectrum of $Na[Cr^{V}O(ehba)_2].H_2O$ (Figure 5.11(b)) is quite strong, though not as strong as that in the spectrum of chromate. $Na[Cr^{V}O(ehba)_2].H_2O$ is five-coordinate and the geometry about the Cr is intermediate between trigonal bipyramidal and square pyramidal,[40] a large distortion from octahedral geometry. There is also strong π bonding between the Cr atom and the oxo group, and to a lesser extent the alcoholate and carboxylate groups.

Table 5.10 Summary of XANES data for Cr compounds

Compound	Energy (eV)		Pre-edge Peak (normalised absorbance)
	Edge	Pre-edge Peak	
$Na_2CrO_4.4H_2O$	6009	5996	0.88
$Na[Cr^{V}O(ehba)_2].H_2O$	6001	5989	0.47
$[Cr^{V}O(salen)]CF_3SO_3$	6002	5990	0.41
$[Cr^{V}(O)_2(phen)_2]ClO_4$	5999	5991	0.15
$Na_2[Cr^{V}_2O_4(S\text{-}ala)_2(OCH_3)_2]$ .0·5CH_3OH.0·5(S-alaH)	5999	5990	0.23
cis-$[Cr^{III}(phen)_2(OH_2)_2](NO_3)_3$ .2·5H_2O	5998	5987	0.04
trans-$[Cr^{III}(salen)(OH_2)_2]CF_3SO_3$	5995	5987	0.04
trans-$[Cr^{III}(bpb)(OH_2)_2]ClO_4.H_2O$	5997	5986	0.06
trans-$[Cr^{III}(bpb)Cl(OH_2)]$.DMF	5997	5987	0.06

The XANES spectrum of $[Cr^{V}O(salen)]CF_3SO_3$ also has a quite strong pre-edge peak (Figure 5.11 (c)). The crystal structure of $[Cr^{V}O(salen)]PF_6.CH_3CN$ showed that the coordination geometry of Cr was approximately square pyramidal.[41] The Cr is five-coordinate and there is a large distortion from octahedral coordination geometry. There is also strong π bonding to the oxo group, and to a lesser extent the phenoxide groups.

The structure of the Cr(V)-phen complex is of interest as the Cr(V) complex is readily generated from the Cr(III)-phen complex and is genotoxic and mutagenic.[17,42] The Cr(V)-phen complex was postulated to be the six-coordinate species $[Cr^{V}(O)_2(phen)_2]^{+}$.[17,43] The energies of the edge and the pre-edge peak were close to the energies of these features in the XANES spectra of $Na[Cr^{V}O(ehba)_2].H_2O$ and $[Cr^{V}O(salen)]CF_3SO_3$, which showed that the assignment of the oxidation state as Cr(V) was correct. The intensity of the pre-edge peak in the XANES spectrum of $[Cr^{V}(O)_2(phen)_2]ClO_4$ (Figure 5.11(d)) was about a third the intensity of the pre-edge peaks in the spectra of $Na[Cr^{V}O(ehba)_2].H_2O$ and $[Cr^{V}O(salen)]CF_3SO_3$. The significantly weaker intensity of the pre-edge peak in the spectrum of

$[Cr^{V}(O)_2(phen)_2]ClO_4$ was consistent with the approximately octahedral coordination geometry that was postulated. The similarity of the shape of the XANES to the XANES regions of the octahedral Cr(III) complexes (Figure 5.12) also indicated that the Cr(V)-phen complex was six-coordinate.

The energies of the edge and the pre-edge peak in the spectrum of the Cr(V)-alanine complex (Figure 5.11(e)) were similar to the energies of these features in the XANES spectra of the Cr(V) standards, which demonstrated that the oxidation state was Cr(V). The intensity of the pre-edge peak was approximately half that of the pre-edge peak in the spectra of $Na[Cr^{V}O(ehba)_2].H_2O$ and $[Cr^{V}O(salen)]CF_3SO_3$. The lower intensity of the pre-edge peak in the spectrum of the Cr(V)-alanine complex was evidence that the coordination environment of the Cr was closer to octahedral than in $Na[Cr^{V}O(ehba)_2].H_2O$ and $[Cr^{V}O(salen)]CF_3SO_3$. The shape of the XANES region for the Cr(V)-alanine complex was much closer to the shape of the XANES for $[Cr^{V}(O)_2(phen)_2]ClO_4$, which was expected to be six-coordinate, and the XANES of the octahedral Cr(III) complexes than the shape of the XANES for the five-coordinate complexes $Na[Cr^{V}O(ehba)_2].H_2O$ and $[Cr^{V}O(salen)]CF_3SO_3$. This indicated that the Cr in the Cr(V)-alanine complex was six-coordinate.

The pre-edge peaks in the XANES of the Cr(III) complexes (Figure 5.12 (a)-(d)) were very weak. This was because the Cr(III) complexes were six-coordinate, with only slight distortions from octahedral coordination geometry. Also, the Cr(III) complexes did not have the oxo groups, which were present in the higher oxidation state complexes, and formed strong π bonds. They are typical of Cr(III) complexes.[21,44,45]

5.3.2 XAFS

5.3.2.1 XAFS Structure of $Na_2[Cr^{V}_2O_4(S\text{-ala})_2(OCH_3)_2].0{\cdot}5CH_3OH.0{\cdot}5(S\text{-alaH})$

The lack of a Cr(V) EPR signal from the solid product combined with the dinuclear ions observed in the ES/MS spectrum indicated that the solid product had a dimeric structure.[22] The EPR spectrum of the mononuclear Cr(V) intermediate was assigned to a six-coordinate species,[22] and the XANES region was consistent with a six-

coordinate complex so **I, III, IV** and **VI** were used as models in the MS XAFS refinement (Figure 5.13). Mononuclear, **II**, and five-coordinate, **V**, models were also examined. Fitting of the XAFS data to Model **I** was initially carried out with R_{max} of 6.50 Å, but there was no significant backscattering of the photoelectron from the carbon backbone of the alanine ligand further from the absorber, Cr0. The lack of contributions to the XAFS from these atoms was consistent with the fact that usually only scattering from atoms within 4-5 Å of the absorber affects the XAFS.[10,11] Only the O and N atoms of the alanine ligand coordinated to the second Cr atom made significant contributions to the XAFS, so the remaining atoms were removed from **I** to give Model **III** and the R_{max} value was decreased to 5.50 Å.

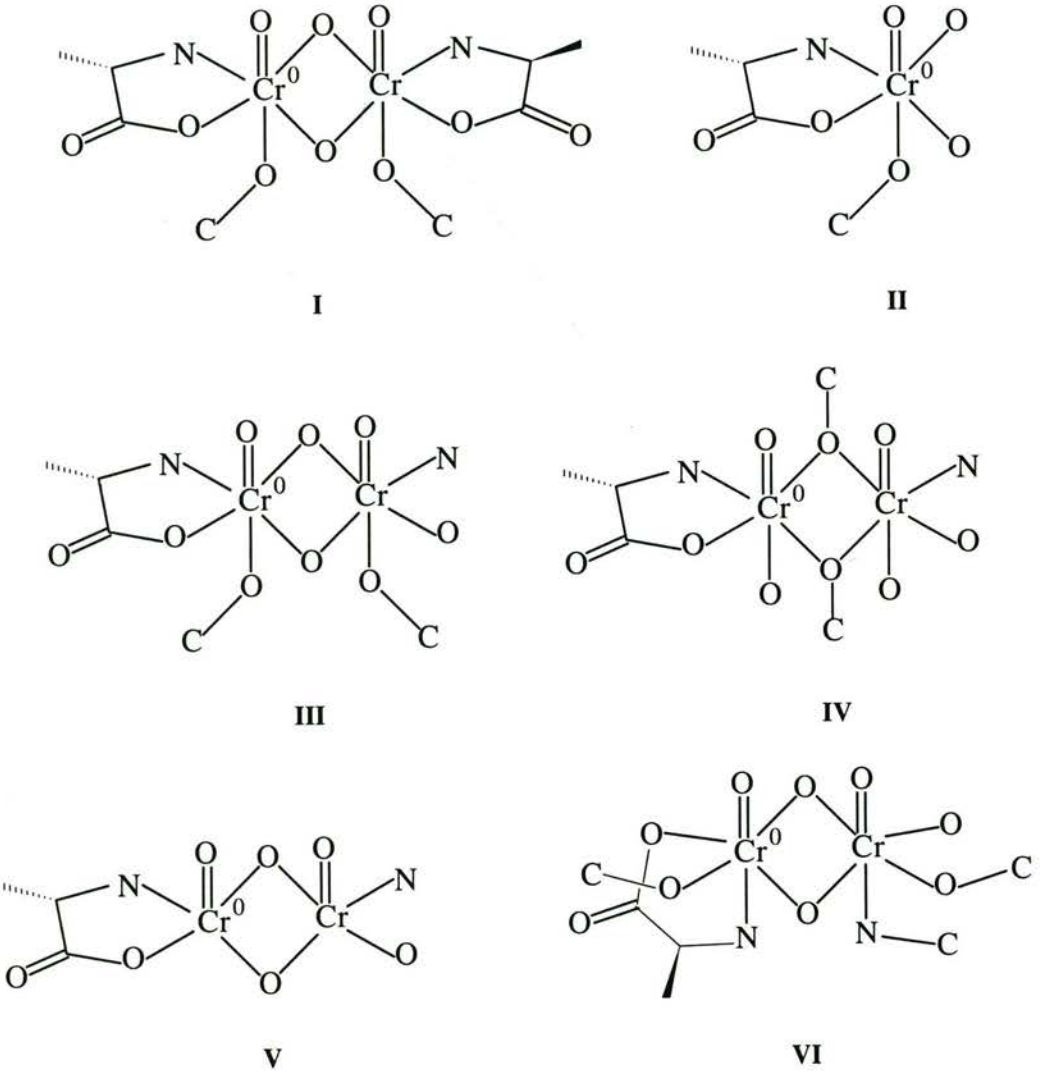

Figure 5.13 Models used in the MS fitting to the XAFS data for $Na_2[Cr^{V}_2O_4(S\text{-ala})_2(OCH_3)_2].0{\cdot}5CH_3OH.0{\cdot}5(S\text{-alaH})$

Mononuclear and dinuclear models with both five- and six-coordinate Cr atoms were compared in preliminary refinements. The XAFS calculated for six-coordinate dinuclear models gave the best fits to the observed XAFS (Table 5.11). The best fit between the calculated and the observed XAFS was obtained with **III** (restraints and constraints for **III** are included in Appendix 3, Tables A3.1 and A3.2). Model **III** gave a slightly better fit than Model **I** because the restraints for the extra shells of **I** are included in the goodness-of-fit parameters, but there was no significant contribution of the extra shells to the XAFS. The mononuclear Model **II** resulted in a much poorer fit between the calculated and the observed XAFS and the higher values of R for **II** as opposed to **III** indicated that the complex was dinuclear. The dinuclear structure of the complex was confirmed by the presence of significant scattering pathways involving the second Cr atom in the refined Model **III** (Appendix 3, Table A3.3, Paths 11 and 28). Model **IV** (a truncated model like **III**) is just as consistent with the ES/MS and microanalytical data as **III**, but it gave a significantly worse fit to the observed XAFS data. This showed that the methoxo ligands are unlikely to act as bridging ligands between the two Cr atoms but are coordinated *trans* to the oxo groups. The truncated five-coordinate Model **V** had a significantly higher R_{XAFS} value than **III**, which indicated that the Cr was six-coordinate. The coordination of the alanine with the amine *trans* to the oxo group

Table 5.11 Goodness-of-fit parameters for refined models **I-VI** of $Na_2[Cr^{V}{}_2O_4(S\text{-ala})_2(OCH_3)_2].0{\cdot}5CH_3OH.0{\cdot}5(S\text{-alaH})$

Model	R	R_{XAFS}	Determinancy
I	15.38 %	13.32 %	1.11
II	20.43 %	17.57 %	1.26
III	14.24 %	12.24 %	1.21
IV	16.30 %	14.40 %	1.18
V	21.56 %	20.69 %	1.37
VI	18.65 %	14.90 %	1.18

and *cis* to the two bridging oxygen atoms was examined in model **VI** (again a truncated model). The value of R_{XAFS} was significantly increased; therefore, both the amine and carboxylate groups of alanine are likely to be coordinated *cis* to the oxo and methoxide groups.

Other possible isomers of the complex are harder to distinguish by XAFS. The two oxo groups can be *syn* or *anti* to each other; the *syn* isomer had somewhat lower goodness-of-fit values, but there was little difference between the XAFS calculated from the two models. In **I,** the alanine ligands were arbitrarily arranged in a *cis* geometry. When the alanine ligands were *trans* to each other, the R_{XAFS} value increased slightly. Distinguishing between N and O atoms by XAFS is very difficult, and often impossible because their backscattering amplitudes and phases are similar,[10,11] so a distinction relies on differences in MS pathways involving the non-coordinating atoms of the *trans* and *cis* isomers. The bond distances to the O and N atoms of the alanine ligand coordinated to Cr0 could be accurately distinguished because there were strong MS paths involving the C atom and the three atoms of the carboxylate group from the alanine ligand (Appendix 3, Table A3.3, Paths 14, 54, 56, 58, 60, and 66). However, since the O and N atoms of the second alanine ligand were so far away from the absorber, the difference in the distant Cr–O and Cr–N bond lengths has little effect on the XAFS.

The XAFS and Fourier transform curves calculated for **III** are in Figures 5.14(a) and 5.15(a), respectively. To show the difference between the dinuclear and the mononuclear models, the XAFS and Fourier transform curves calculated for **II** are in Figures 5.14(b) and 5.15(b), respectively. There is a better match between the calculated and the observed XAFS for the dinuclear model, especially in the low k region where MS effects are most important. The difference between the dinuclear and the mononuclear models is also evident in the Fourier transforms; the calculations based on the mononuclear model significantly underestimated the magnitude of the Fourier transform for all the shells above 2 Å. Selected bond lengths, interatomic distances and bond angles for **III** are contained in Table 5.12, with the atom numbering scheme shown in Figure 5.16.

There have been few reports of isolated and structurally characterised dinuclear Cr(V) complexes. Crystal structures have been reported for an azide-bridged,[46] a bis(μ-imido),[47] and two bis(μ-oxo)[48,49] dinuclear Cr(V) complexes. The average Cr–(μ-O) bond length in $Li_2\{[Cr^VO(PFP)(\mu\text{-}O)]_2\}.2H_2O.2py$[48] (PFP = perfluoropinacolate(2–), py = pyridine) was 1.812 Å. The average Cr–(μ-O) bond length in $\{[Cr^VO(CpMe_5)(\mu\text{-}O)]_2\}$[49] (where $CpMe_5$ is the pentamethylcyclopentadienyl ligand) was 1.815 Å. The Cr–(μ-O) bond lengths in

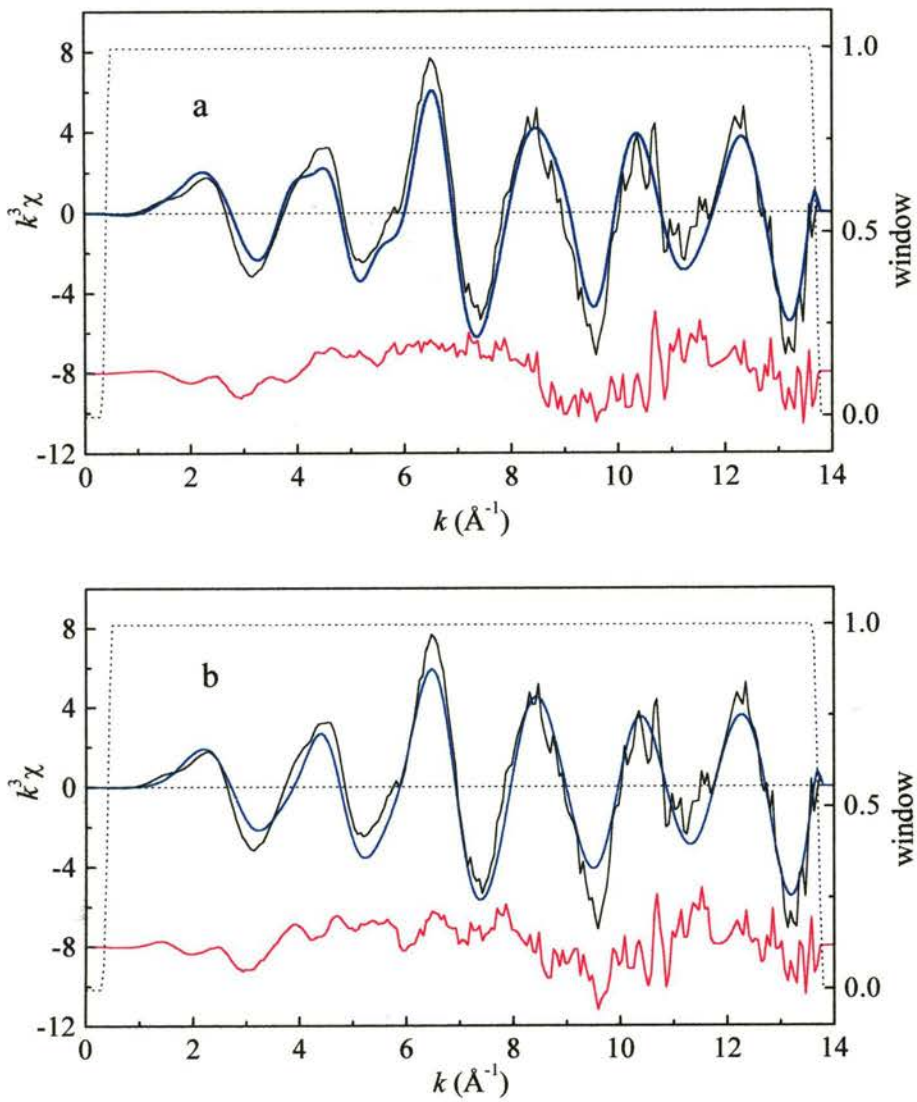

Figure 5.14 Observed (black), calculated (blue) and residual (red) XAFS curves and the window function (dotted line) for Models (a) **III** and (b) **II** of $Na_2[Cr^V_2O_4(S\text{-ala})_2(OCH_3)_2].0{\cdot}5CH_3OH.0{\cdot}5(S\text{-alaH})$

III are approximately 0.13 Å longer than the Cr–(μ-O) bond lengths in these complexes. This large increase in the Cr–(μ-O) bond lengths in **III** could be attributed to a couple of factors. The Cr atoms in **III** were six-coordinate while in $Li_2\{[CrO(PFP)(\mu\text{-}O)]_2\}.2H_2O.2py$ each Cr atom was five-coordinate and was coordinated to two μ-oxo ligands, an oxo group and the bidentate PFP^{2-} in a square pyramidal environment, and in $\{[Cr^{V}O(CpMe_5)(\mu\text{-}O)]_2\}$ each Cr atom was coordinated to two μ-oxo ligands, an oxo group and a $CpMe_5$ ligand in a distorted

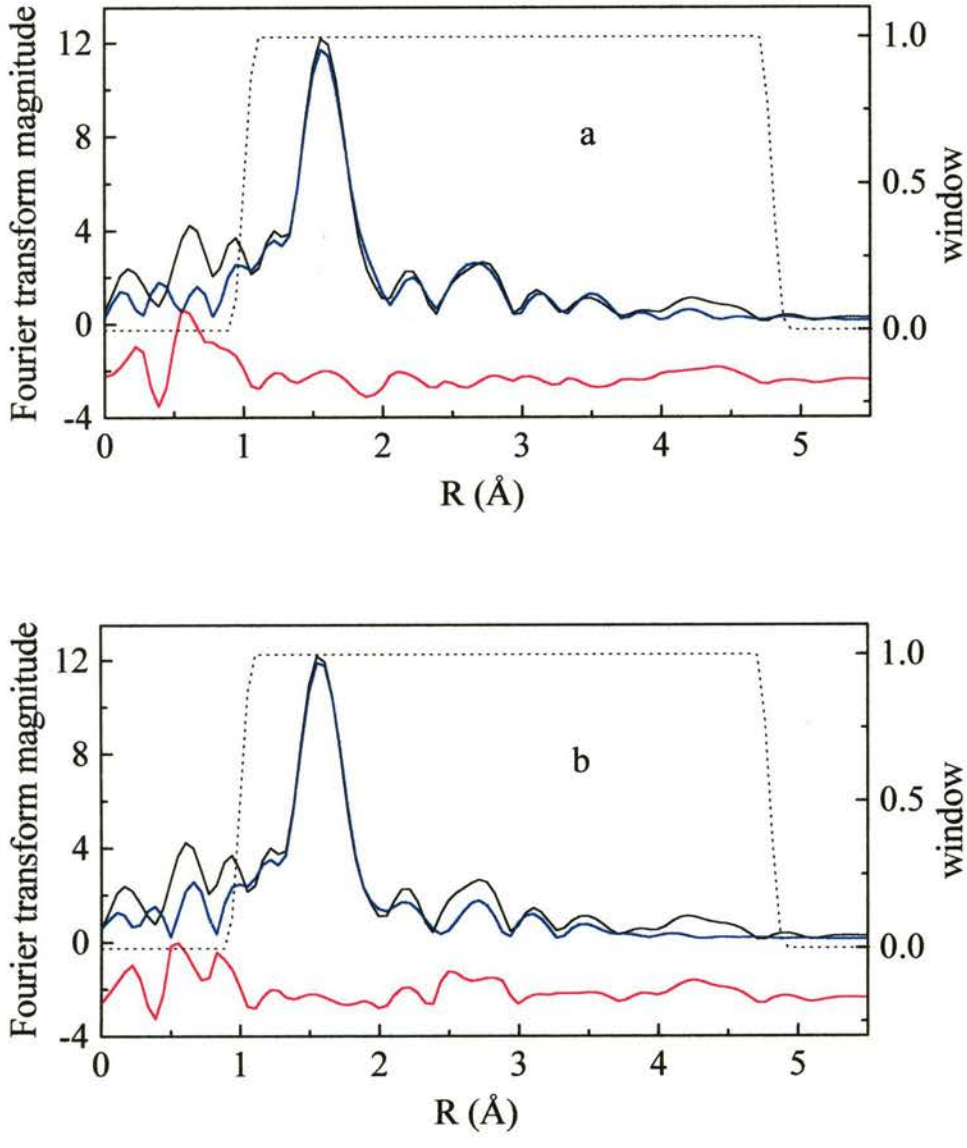

Figure 5.15 Observed (black), calculated (blue) and residual (red) Fourier transform curves and the window function (dotted line) for Models (a) **III** and (b) **II** of $Na_2[Cr^{V}_2O_4(S\text{-ala})_2(OCH_3)_2].0{\cdot}5CH_3OH.0{\cdot}5(S\text{-alaH})$

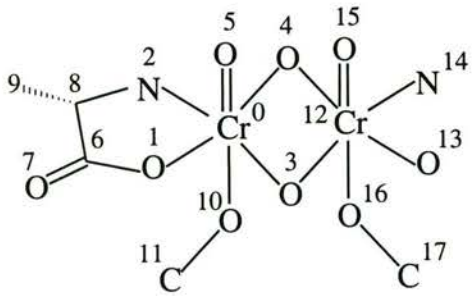

Figure 5.16 Atom numbering scheme for Model **III** of $Na_2[Cr^V_2O_4(S\text{-ala})_2(OCH_3)_2].0{\cdot}5CH_3OH.0{\cdot}5(S\text{-alaH})$

Table 5.12 Selected bond lengths, interatomic distances and bond angles from Model **III** of $Na_2[Cr^V_2O_4(S\text{-ala})_2(OCH_3)_2].0{\cdot}5CH_3OH.0{\cdot}5(S\text{-alaH})$[a]

atom–atom	distance (Å)	atom–atom–atom	angle(°)
Bond Lengths			
Cr0–O1	1.96(2)	O1–Cr0–O4	168(5)
Cr0–N2	2.03(2)	N2–Cr0–O3	167(5)
Cr0–O3	1.94(2)	O3–Cr0–O4	78(1)
Cr0–O4	1.94(2)	O5–Cr0–O10	166(4)
Cr0–O5	1.56(2)	O3–Cr12–O4	78(1)
Cr0–O10	1.74(2)	Cr0–O3–Cr12	99(1)
O10–C11	1.36(2)	Cr0–O4–Cr12	99(1)
Interatomic Distances			
Cr0–Cr1	2.95(2)		
O3–O4	2.45(2)		

[a] The estimated error in the last significant figure is shown in parentheses. The errors in the bond lengths and interatomic distances are the root-mean-square (rms) combination of the conservative systematic error[2,5,23] with the error determined by Monte-Carlo analyses.[10,11] The errors in the bond angles are the rms combination of the Monte Carlo error and the error in the bond angle due to the Monte-Carlo error in the bond lengths.[50]

tetrahedral environment (μ-O–Cr–μ-O = 92.7(2)°). The higher coordination number for the Cr atoms in **III** may lead to a weaker interaction with the μ-O groups and longer bond lengths. The other explanation is that the Cr atoms in **III** are already

coordinated by two short, strong bonds to the single oxo group and the methoxo oxygen, this leads to a lengthening of the Cr–(μ-O) bond lengths. Since hydrogen atoms are not normally significant contributors to the XAFS, it is possible that the two bridging ligands in **III** are hydroxo groups rather than oxo groups. This could be the reason that the Cr–(μ-O) bond lengths are longer for **III** than in the crystal structures of the complexes with μ-oxo bridging ligands, but this would require that the complex is a dinuclear Cr(IV) species rather than Cr(V).

The Cr–O(methoxo) distance in **III**, 1.74(2) Å is similar to, but a little shorter than the Cr–O(alkoxo) distances of 1.767-1.798 Å in the Cr(V) complexes $Na[Cr^{V}O(ehba)_2].1.5H_2O$[40] and $K[Cr^{V}O(hmba)_2].H_2O$[51] and 1.861-1.905 Å in $Li_2\{[CrO(PFP)(\mu\text{-}O)]_2\}.2H_2O.2py$ and $\{[(py)_2H][CrO(PFP)_2]\}$.[48] This is unusual, especially considering the strong *trans* influence of the oxo ligand. The short Cr–O(methoxo) bond appears to be real because the Cr–O or Cr–N bond lengths *trans* to the oxo group were in the range 1.72-1.74 Å in all the models refined. There are also examples of short M–O(methoxo) bonds in crystal structures of V(V) complexes; values of 1.723 Å,[52] 1.760 Å and 1.783 Å[53] have been reported. The Cr–O(oxo) length of 1.56(2) Å is typical for Cr(V) complexes, and the Cr–O(carboxylate) bond length of 1.96(2) Å is slightly longer than the values of 1.90-1.92 Å reported in crystal structures.[40,48,49,51]

The BVS analysis of the complex gave a value of 4.74 for the Cr oxidation state, which was in good agreement with the expected value of 5. Wood, *et al.* in their study on BVS analysis of Cr complexes with O donor ligands considered values within 0.30 of the integer value as acceptable.[30] They also noted that the use of an average value for R_0 tended to result in an underestimation of the BVS for Cr(V) complexes. The BVS analysis confirmed the interpretation of the XANES spectrum and indicated that the Cr–ligand bond lengths determined by XAFS were reasonable.

The close match between the experimental and observed curves in the 2-4 Å region of the Fourier transform indicates that MS scattering analysis can accurately determine structural details further away than the first coordination shell of the absorber. The results of the XAFS analysis of the Cr(V)-alanine complex indicated

that the structure, **I** (of which the best model, **III**, was a truncated version), was correct.

5.3.2.2 XAFS Structure of *cis*-$[Cr^{III}(phen)_2(OH_2)_2](NO_3)_3.2{\cdot}5H_2O$

The XAFS of *cis*-$[Cr^{III}(phen)_2(OH_2)_2](NO_3)_3.2{\cdot}5H_2O$ was analysed as a prelude to analysing the data for the Cr(V) analogue. The refinement of the XAFS data for *cis*-$[Cr^{III}(phen)_2(OH_2)_2](NO_3)_3.2{\cdot}5H_2O$ was also used to determine the importance of outer-sphere effects.

Three different models, **VII-IX** (Figure 5.17), were refined in the MS analysis of *cis*-$[Cr^{III}(phen)_2(OH_2)_2](NO_3)_3.2{\cdot}5H_2O$. They were based on the crystal structure of *cis*-$[Cr^{III}(phen)_2(OH_2)_2](NO_3)_3.2{\cdot}5H_2O$ determined by Dr Peter Turner.[25] The phen ligands and the aqua ligands were constrained by symmetry to be equivalent in all the models, as the differences between the two ligands in the crystal structure were less than the systematic errors in the XAFS bond lengths. Model **VII** included the non-hydrogen atoms in the phen ligands and the O atoms of the aqua ligands. In **VIII** four O atoms that were hydrogen-bonded to the aqua ligands were included in the model. An additional five atoms from the nitrate counterions that were within 5 Å of Cr were included in **IX**.

The goodness-of-fit parameters are summarised in Table 5.13; the XAFS calculated for **VIII** gave the best fit to the observed XAFS (restraints and constraints for **VIII** are included in Appendix 3, Tables A3.5 and A3.6). The inclusion of the four O atoms H-bonded to the aqua ligands significantly improved the R_{XAFS} and overall R values compared to **VII**. The inclusion of five additional atoms from the nitrate counterions in **IX** did not improve the fit of the calculated XAFS compared to **VII**, which indicated that the additional atoms did not contribute significantly to the XAFS.

The XAFS and Fourier transform curves calculated for **VIII** are in Figures 5.18(a) and 5.19(a), respectively. The XAFS and Fourier transform curve calculated for **VII** are shown for comparison in Figures 5.18(b) and 5.19(b), respectively. Figure 5.18

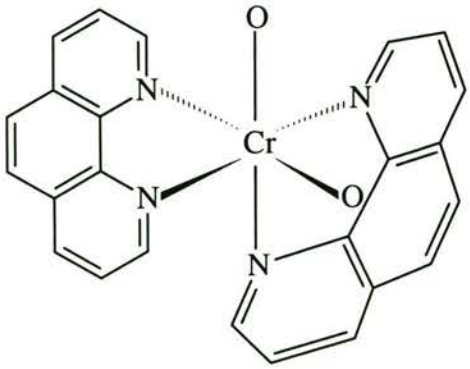

VII

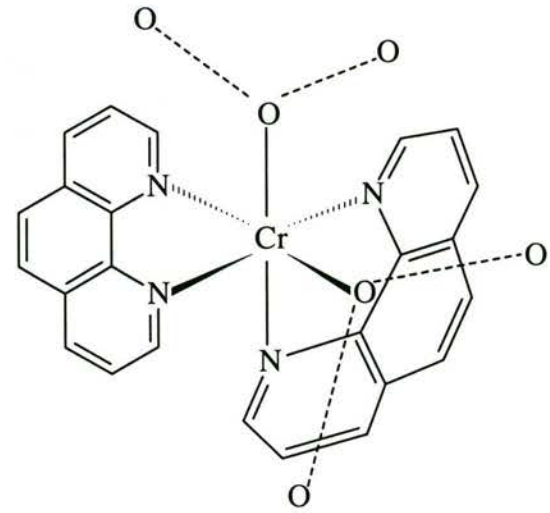

VIII

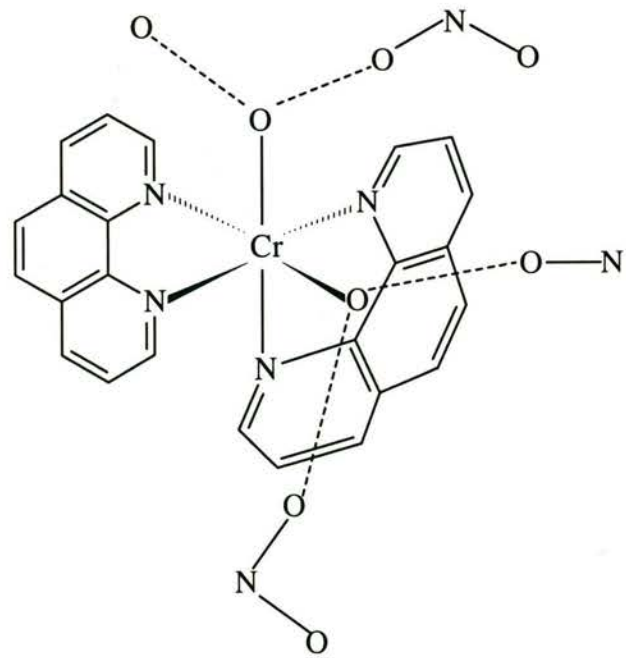

IX

Figure 5.17 Models used in the MS fits to the XAFS data for *cis*-$[Cr^{III}(phen)_2(OH_2)_2](NO_3)_3.2{\cdot}5H_2O$

shows that the agreement between the calculated and observed XAFS is better for **VIII**, the difference is mainly in the 4-7 $Å^{-1}$ region. The contribution of the extra atoms in **VIII** is observed in the 3-4 Å region of the Fourier transform curves (Figure 5.19). The intensity of the calculated Fourier transform for **VIII** was close to the observed Fourier transform, but the intensity of the Fourier transform calculated for

Table 5.13 Goodness-of-fit parameters for refined Models **VII-IX** of *cis*-$[Cr^{III}(phen)_2(OH_2)_2](NO_3)_3.2{\cdot}5H_2O$

Model	R	R_{XAFS}	Determinancy
VII	20.03 %	17.07 %	1.33
VIII	18.39 %	14.86 %	1.13
IX	18.90 %	15.60 %	1.05

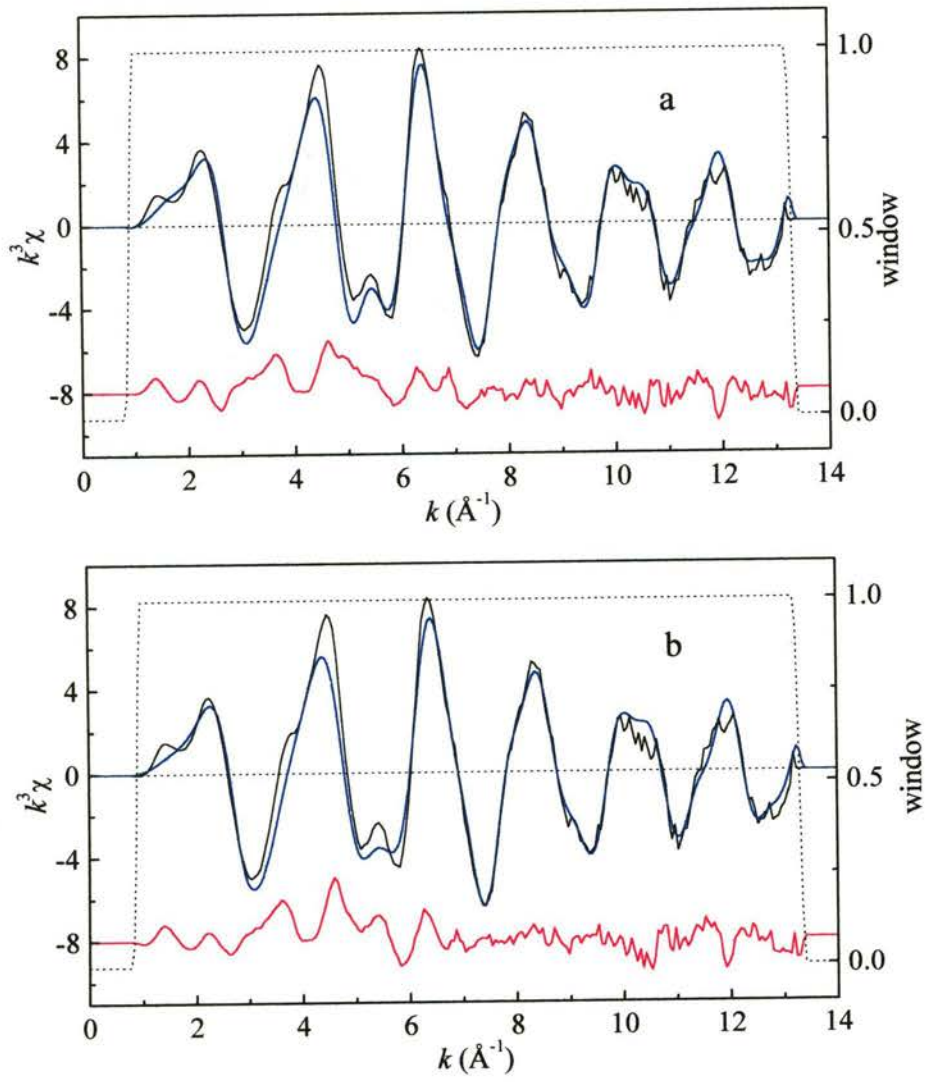

Figure 5.18 Observed (black), calculated (blue) and residual (red) XAFS curves and the window function (dotted line) for Models (a) **VIII** and (b) **VII** of *cis*-$[Cr^{III}(phen)_2(OH_2)_2](NO_3)_3.2{\cdot}5H_2O$

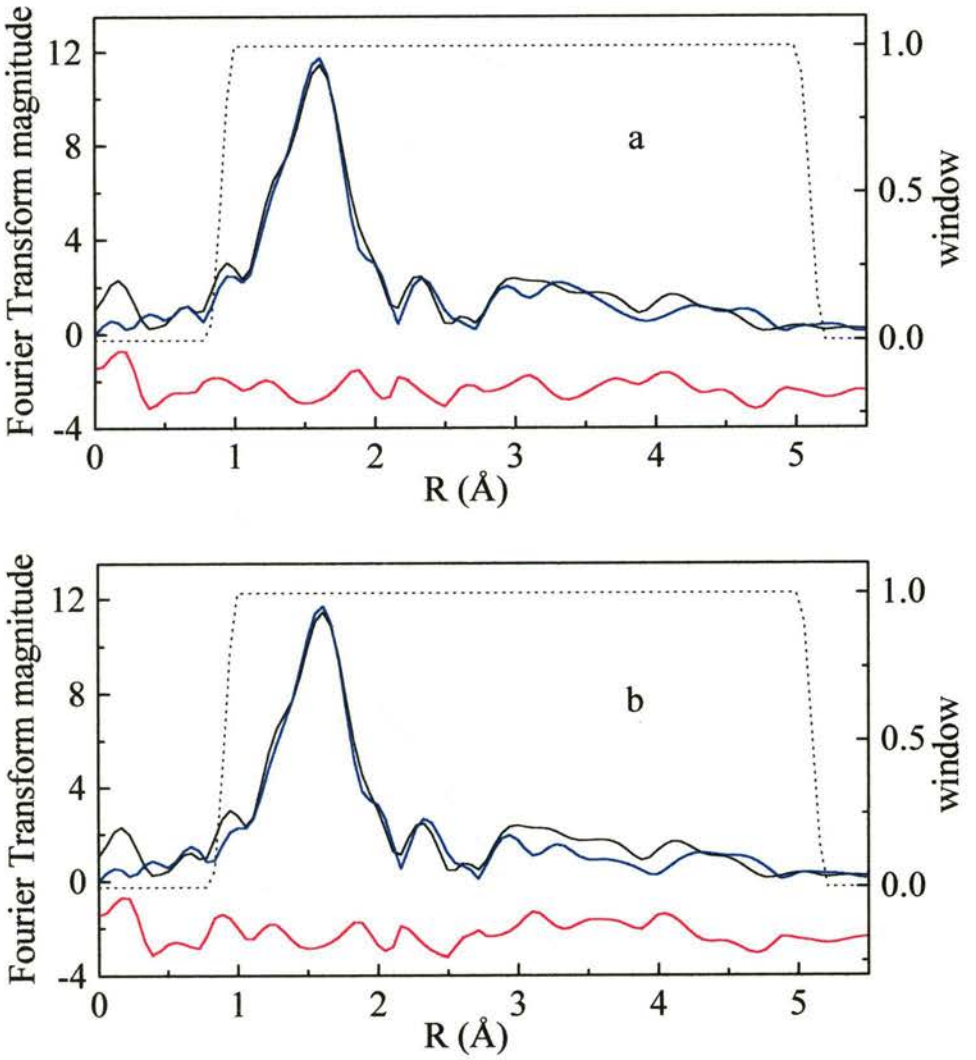

Figure 5.19 Observed (black), calculated (blue) and residual (red) Fourier transform curves and the window function (dotted line) for Models (a) **VIII** and (b) **VII** of *cis*-$[Cr^{III}(phen)_2(OH_2)_2](NO_3)_3.2{\cdot}5H_2O$

VII was too low in the 3-4 Å region. (The MS paths and Debye-Waller factors for **VIII** are in Appendix 3, in Table A3.7 and Table A3.8, respectively).

Selected bond lengths and interatomic distances for **VIII** are listed in Table 5.14 and selected bond angles are listed in Table 5.15, with the atom numbering scheme for **VIII** in Figure 5.20. The agreement between the values determined by MS XAFS analysis and X-ray crystallography was excellent. The difference for the Cr0–O1 bond length is greater than the cumulative errors by 0.001 Å, which is not significant. The differences for the O1–Cr0–N6 and N3–Cr0–N5 angles were 1° greater than the cumulative error, which is not surprising as these angles are considerably less than

Table 5.14 Selected bond lengths and interatomic distances for *cis*-$[Cr^{III}(phen)_2(OH_2)_2](NO_3)_3.2{\cdot}5H_2O$

atom–atom	XAFS[a]	Crystal Structure[b]	
Bond Lengths (Å)			
Cr0–O1	1.93(2)	1.953(2)	1.959(2)
Cr0–N3	2.05(2)	2.063(2)	2.064(2)
Cr0–N4	2.05(2)	2.067(2)	2.059(2)
N3–C7	1.33(2)	1.332(3)	1.341(3)
N3–C13	1.37(2)	1.364(3)	1.365(3)
N4–C10	1.33(2)	1.327(3)	1.328(3)
N4–C14	1.37(2)	1.367(3)	1.374(3)
C7–C8	1.40(2)	1.398(4)	1.398(4)
C8–C9	1.36(2)	1.378(4)	1.364(4)
C9–C18	1.40(2)	1.403(4)	1.405(4)
C10–C11	1.40(2)	1.401(4)	1.392(3)
C11–C12	1.36(2)	1.360(4)	1.359(4)
C12–C15	1.40(2)	1.407(4)	1.405(4)
C13–C14	1.42(2)	1.420(4)	1.415(3)
C13–C18	1.41(2)	1.408(3)	1.417(3)
C14–C15	1.41(2)	1.407(3)	1.412(3)
C15–C16	1.43(2)	1.440(4)	1.438(4)
C16–C17	1.34(2)	1.350(4)	1.336(6)
C17–C18	1.43(2)	1.439(4)	1.431(4)
Interatomic Distances (Å)			
O1–O31	2.56(2)	2.562(3)	
O1–O32	2.66(2)	2.664(3)	
O2–O33	2.63(2)	2.633(3)	
O2–O34	2.63(2)	2.633(3)	

[a] The estimated error in the last significant figure is shown in parentheses. The errors in the bond lengths and interatomic distances are the rms combination of the conservative systematic error[2,5,23] with the error determined by Monte-Carlo analyses.[10,11] [b] Two distances are reported for the bond lengths involving the phen ligands and the aqua ligands as they were independent in the crystal structure.[25] The estimated error in the last significant figure is in parentheses.

150°, below which value the intensity of MS processes is weak.[6,7] The agreement of the structural parameters determined by the two different methods was partially due to the restraints used in the XAFS refinement based on the values from the crystal

structure. However, the deviation of the values determined by XAFS from the crystal structure values were in all cases much smaller than the variation allowed by the restraints (Appendix 3, Table A3.5). This indicates that the agreement observed was not merely forced by the restraints.

Table 5.15 Selected bond angles for *cis*-$[Cr^{III}(phen)_2(OH_2)_2](NO_3)_3.2{\cdot}5H_2O$

atom–atom–atom(°)	XAFS[a]	Crystal Structure[25]
O1–Cr0–O2	89(1)	88.62(9)
O1–Cr0–N3	92(1)	92.48(8)
O1–Cr0–N4	172(1)	172.22(8)
O1–Cr0–N5	91(1)	91.90(8)
O1–Cr0–N6	93(1)	91.04(8)
N3–Cr0–N4	80(1)	80.17(8)
N3–Cr0–N5	95(1)	93.12(8)
N3–Cr0–N6	173(2)	172.67(8)
N4–Cr0–N5	91(1)	91.08(7)

[a] The estimated error in the last significant figure are in parentheses. The errors in the bond angles are the rms combination of the Monte Carlo error and the error in the bond angle due to the Monte-Carlo error in the bond lengths.[50]

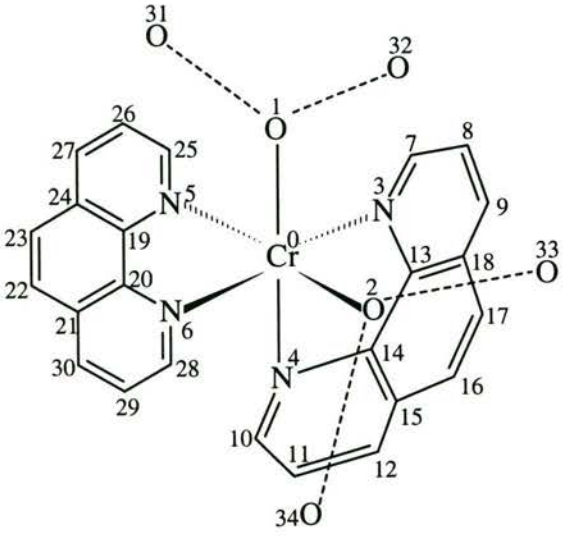

Figure 5.20 Atom numbering scheme for Model **VIII** of *cis*-$[Cr^{III}(phen)_2(OH_2)_2](NO_3)_3.2{\cdot}5H_2O$

The crystal structure of *cis*-$[Cr^{III}(phen)_2(OH_2)_2]^{3+}$ has not been reported previously, but the X-ray powder diffraction data for *cis*-$[Cr^{III}(phen)_2(OH_2)_2](NO_3)_3.2H_2O$ was reported by Andersen and Josephsen,[54] who concluded that the aqua ligands were *cis*. This was confirmed in the crystal structure determined by Dillon and Turner.[25] The crystal structure of the dinuclear complex $[Cr^{III}(phen)_2(\mu\text{-}OH)]_2Cl_4.6H_2O$[55] has the two bridging hydroxo groups in the *cis* arrangement. The structural parameters of the phen ligands in the mononuclear and dinuclear complexes were very similar. The Cr–N bond lengths in the crystal structure of the dinuclear complex ranged from 2.031-2.072 Å with an average of 2.052 Å,[55] and the values in the mononuclear complex fell within this range.[25]

The agreement between the structural parameters determined by MS fitting to the XAFS data and X-ray crystallography of *cis*-$[Cr^{III}(phen)_2(OH_2)_2](NO_3)_3.2{\cdot}5H_2O$ showed that MS XAFS can provide accurate structural information for atoms beyond those directly bound to the absorber. For large ligands the number of parameters necessary can lead to underdeterminancy, but where the structure of the ligand is well defined, as was the case for phen, the determinancy is increased by including this information.[16]

The MS XAFS analysis of the different models showed that atoms hydrogen-bonded to ligands can also make significant contributions to the XAFS of metal complexes. In the MS XAFS analysis of *cis*-$[Cr^{III}(phen)_2(OH_2)_2](NO_3)_3.2{\cdot}5H_2O$, it was only possible to include the atoms hydrogen-bonded to the aqua ligands in **VIII** because the crystal structure had been determined. The position of atoms in a ligand may be approximately known from analogous structures, or can at least be estimated, but it is extremely difficult to know whether there are any atoms hydrogen-bonded to the ligand, let alone their approximate position, without a crystal structure. The majority of XAFS analyses, involve compounds that have not been characterised by X-ray crystallography (which is one of the main advantages of the technique). Besides the difficulty in knowing whether to add atoms hydrogen-bonded to ligands to a refinement model and where to position them, the extra atoms increase the number of parameters refined, and may cause the refinement to be underdetermined. The inclusion of restraints based on a crystal structure to overcome this problem, as for

cis-$[Cr^{III}(phen)_2(OH_2)_2](NO_3)_3.2{\cdot}5H_2O$, is not always possible.

The results on the Cr(III)-phen complex show that contributions to XAFS by atoms hydrogen-bonded to the ligands of a complex can be significant, and, where the crystal structure is not known, very difficult to take into account. This will reduce the goodness-of-fit between the observed and calculated XAFS and may reduce the accuracy with which other shells outside the first coordination sphere are determined. These limitations should be considered when analysing the XAFS of complexes with ligands capable of forming hydrogen-bonds with other components of the system, where that would bring extra atoms within ~5 Å of the absorber.

The contribution of backscattering from atoms other than those in the ligands to the XAFS may be responsible in some cases for the difficulties encountered in fitting the positions of atoms outside the first coordination shell. However, in the absence of other evidence, it is not possible to distinguish whether the difficulties in refining a model are due to the failure to include non-ligand atoms near the absorber or to other inherent faults in the model. This is one of the disadvantages of using XAFS on solid samples compared to solutions, where second and subsequent coordination spheres due to solvent and counterion are less organised.

The XAFS data for the Cr(V) analogue,$[Cr^{V}(O)_2(phen)_2]ClO_4$, were fitted using both *cis* and *trans* models. The restraints on the phen ligands were the same as those used in the fits to the data of the Cr(III) complex and the symmetry constraints were similar. The refinement of the XAFS data did not give a satisfactory fit between observed and calculated XAFS ($R > 25\%$ for all models), consequently the results are not reported. The inability to fit the experimental XAFS was possibly due to the precipitation of impurities along with the Cr(V)-phen complex when the perchlorate counterion was added.

5.3.2.3 XAFS Structure of *trans*-$[Cr^{III}(bpb)(OH_2)_2]ClO_4.H_2O$

Model **X**, refined in the MS analysis of *trans*-$[Cr^{III}(bpb)(OH_2)_2]ClO_4.H_2O$ (Figure 5.21) included all the non-hydrogen atoms of bpb and the O atoms of the aqua ligands. The model where the Cr–O distances and angles involving the aqua ligands

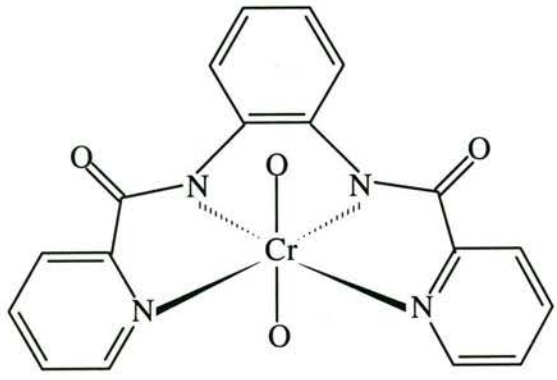

X

Figure 5.21 Model used in the MS refinement of the XAFS data for *trans*-$[Cr^{III}(bpb)(OH_2)_2]ClO_4.H_2O$

were allowed to vary independently is designated as **XA**, the model with the O atoms of the aqua ligands constrained to be equivalent is designated as **XB**.

The goodness-of-fit parameters for models **XA** and **XB** are summarised in Table 5.16. The XAFS and Fourier transform curves for **XA** are in Figure 5.22. The bond lengths involving the non-hydrogen atoms for **XA** are in Table 5.17 and selected bond angles for **XA** are in Table 5.18. The atom numbering scheme for **XA** is in Figure 5.23.

Table 5.16 Goodness-of-fit parameters for refined models **XA** and **XB** of *trans*-$[Cr^{III}(bpb)(OH_2)_2]ClO_4.H_2O$

Model	R	R_{XAFS}	Determinancy
XA	19.85 %	18.94 %	1.10
XB	20.17 %	19.11 %	1.19

There was little difference between the goodness of fit parameters for **XA** and **XB**, the fit between the calculated and observed XAFS was slightly better for model **XA**, but not significantly so (restraints and constraints for **XA** are included in Appendix 3, Tables A3.9 and A3.10). The values of R and R_{XAFS} are below 20%, so the fit was acceptable, but not exceptionally good. Given the results with the phen complex, it

is probable that a major contributing factor to this higher *R* value is the omission of outer-sphere interactions with the aqua ligands.

The complex analysed by XAFS had perchlorate as the counterion and one water of crystallisation per complex molecule, which can hydrogen bond to the aqua ligands of metal complexes. The fit between the calculated and observed XAFS in the low *k* region was poor (Figure 5.22 (a)); and there was little agreement between the observed and calculated Fourier transforms (Figure 5.22(b)) above 4 Å.

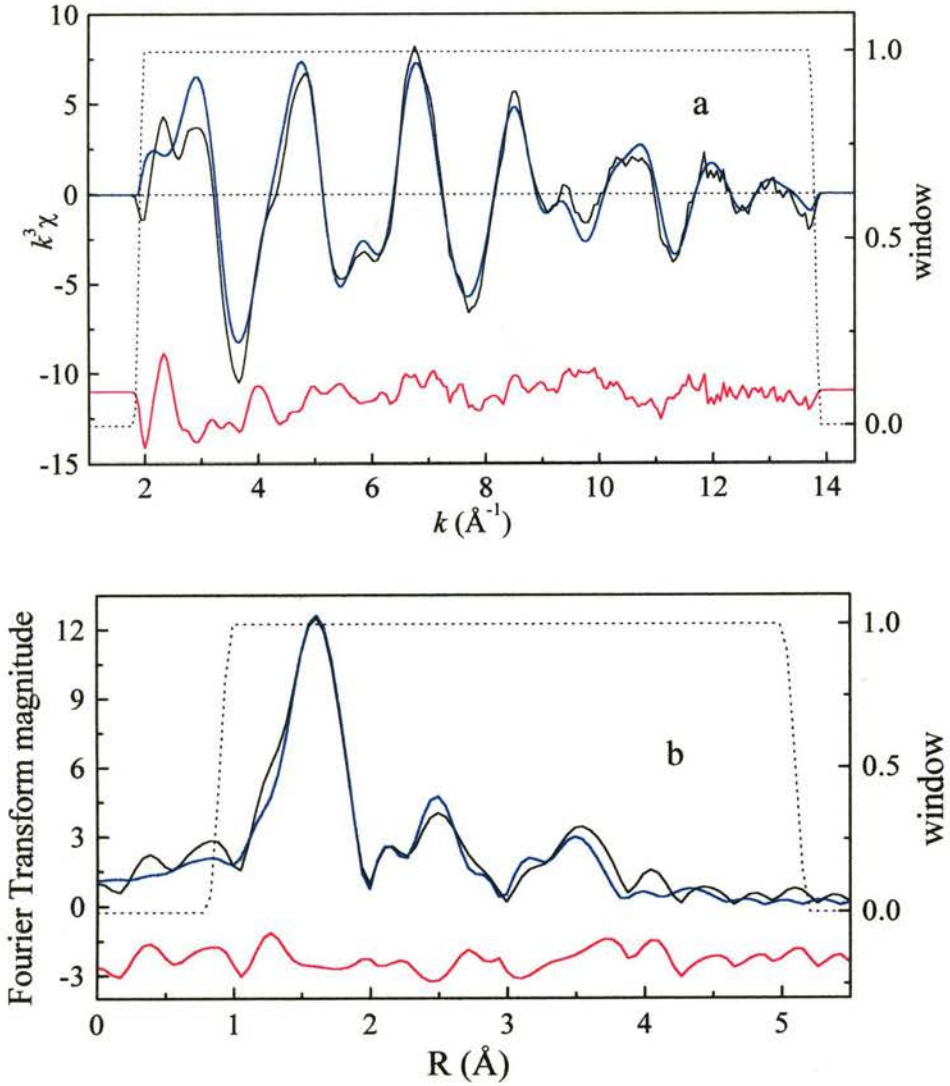

Figure 5.22 (a) XAFS and (b) Fourier transforms for model **XA** of *trans*-[Cr^{III}(bpb)$(OH_2)_2$]$ClO_4.H_2O$. Observed (black), calculated (blue) and residual (red) curves, along with the window function (dotted line).

Table 5.17 Bond lengths from the best fit to the XAFS data using Model **XA** for *trans*-$[Cr^{III}(bpb)(OH_2)_2]ClO_4.H_2O$[a]

atom–atom	distance (Å)	atom–atom	distance (Å)
Cr0–N1	2.07(2)	C7–C13	1.39(2)
Cr0–N2	1.94(2)	C13–C14	1.38(2)
Cr0–O5	1.95(2)	C14–C15	1.38(2)
Cr0–O6	2.03(2)	C9–O11	1.24(2)
N1–C17	1.35(2)	C9–C17	1.50(2)
N1–C21	1.35(2)	C17–C18	1.38(2)
N2–C7	1.41(2)	C18–C19	1.38(2)
N2–C9	1.35(2)	C19–C20	1.36(2)
C7–C8	1.42(2)	C20–C21	1.37(2)

[a] The estimated error in the last significant figure is shown in parentheses. The errors in the bond lengths and interatomic distances are the root-mean-square (rms) combination of the conservative systematic error[2,5,23] with the error determined by Monte-Carlo analyses.[10,11]

Table 5.18 Selected bond angles from the best fit to the XAFS data using Model **XA** for *trans*-$[Cr^{III}(bpb)(OH_2)_2]ClO_4.H_2O$[a]

atom–atom–atom	angle (°)
N1–Cr0–N2	79(1)
N1–Cr0–N3	155(1)
N1–Cr0–N4	112(1)
N2–Cr0–N3	84(1)
O5–Cr0–O6	158(3)

[a] The errors in the bond angles are the rms combination of the Monte Carlo error and the error in the bond angle due to the Monte-Carlo error in the bond lengths.[50]

The average Cr–N(amide) bond length of 1.961(4) Å and the average Cr–N(pyridyl) bond length of 2.080(5) Å in the crystal structure of the nitrido-Cr(V) complex of bpb[26] differ slightly from the bond lengths in the Cr(III) complex, but the differences are within the limits of the cumulative uncertainty. The Cr–N(amide) bond length was within the range 1.910-2.030 Å reported in crystal structures of Cr

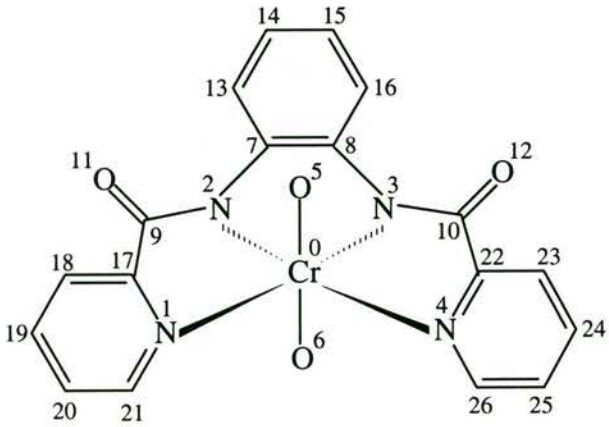

Figure 5.23 Atom numbering scheme for Model **XA** of *trans*-$[Cr^{III}(bpb)(OH_2)_2]ClO_4.H_2O$

complexes.[26,31,32,34,36,56,57] The Cr–N(pyridyl) bond length was also within the range 1.961-2.145 Å reported in crystal structures of Cr complexes.[26,36,58-64] As expected, the Cr–N(amide) bond lengths were shorter than the Cr–N(pyridyl) bond lengths in the XAFS structure of *trans*-$[Cr^{III}(bpb)(OH_2)_2]^+$. No restraints were placed on the Cr–N bond lengths fitting in the XAFS.

The only bond lengths in **XB** that differed significantly from their values in **XA** were Cr0–O5 and Cr0–O6, which were 2.00 Å. This value is not significantly different from the average of the Cr0–O5 and Cr0–O6 bond lengths in **XA**, which was 1.99 Å.

The resolution achievable for bond lengths in SS XAFS is given by:[5]

$$\Delta R \geq \pi/2\Delta k \qquad (5.20)$$

Thus for *trans*-$[Cr^{III}(bpb)(OH_2)_2]ClO_4.H_2O$, $\Delta R \geq 0.13$ Å. The only strong scattering paths involving the O atoms of the two aqua ligands were the SS paths and the MS paths involving both the O atoms of the aqua ligands (Appendix 3, Table A3.11). As there were no strong MS paths involving other atoms, it is difficult to discriminate between two different aqua ligands at distances of 1.95(2) Å and 2.03(2) Å and two equivalent aqua ligands at distances of 2.00(2) Å. In crystal structures of Cr(III) complexes with aqua ligands, the Cr–O(water) distance is commonly about 2.00 Å,[60,65,66] though a wider range of Cr–O(water) distances were observed in the crystal structures of *cis*-$[Cr^{III}(phen)_2(OH_2)_2](NO_3)_3.2{\cdot}5H_2O$, 1.953(2) Å and

1.959(2) Å;[25] *cis*-$[Cr^{III}(phen)_2(OP(O)(OC_6H_5)_2)(OH_2)](NO_3)_2$, 1.947(4) Å;[67] *trans*-$[Cr^{III}(salen)(OH_2)_2]Cl$, 1.923(10) Å and 2.085(9) Å;[68] and *trans*-$[Cr^{III}(tpp)Cl(OH_2)]$, 2.239(3) Å.[69] This shows that both **XA** and **XB** are chemically reasonable structures for $[Cr^{III}(bpb)(OH_2)_2]^+$. The difference between the Cr–N(amide) and the Cr–N(pyridyl) bond lengths, 0.13 Å, was on the limit of SS resolution, but as there were strong MS paths involving other atoms in the benzene and pyridyl rings it was clear that this difference was real and consistent with the typical bond lengths of the respective types.

5.3.2.4 XAFS Structure of *trans*-$[Cr^{III}(bpb)Cl(OH_2)]$.DMF

Two models with different axial ligands, **XI** and **XII** (Figure 5.24), were refined to fit the XAFS data from *trans*-$[Cr^{III}(bpb)Cl(OH_2)]$.DMF. All the non-hydrogen atoms in the bpb ligand were included in the models. The IR spectrum of the complex indicated that one of the axial ligands was a water molecule (Chapter 4, Section 4.3.1.1) so the models refined had at least one O atom coordinated in the axial positions. Structure **XI** was used as a model for the complex with water and DMF as the axial ligands. Only the O atom of the DMF ligand was included in the model because the inclusion of the parameters for the other DMF atoms would have made the refinement underdetermined. In **XII** one of the axial O atoms was replaced by Cl^- as a model for the complex with water and Cl^- as the axial ligands. The goodness-of-fit parameters for the refined models are in Table 5.19. The XAFS and Fourier transform curves calculated for **XII** are in Figure 5.25 (restraints and constraints used in the refinement of **XII** are in Appendix 3, Tables A3.13 and A3.14, respectively). The bond lengths involving the non-hydrogen atoms of **XII** are in Table 5.20 and selected bond angles in Table 5.21. The atom numbering scheme is given in Figure 5.26.

The fit between the calculated and observed XAFS was considerably better for **XII** than for **XI**. This demonstrated that there was an aqua or DMF ligand and Cl^- coordinated in the axial positions of the complex. The R_{XAFS} value for **XII** was just below 20%, and though the overall R value was slightly above 20% the fit between the calculated and observed XAFS is reasonable. The fit between the calculated and observed XAFS was poor in the low k region (Figure 5.25(a)), which is where MS

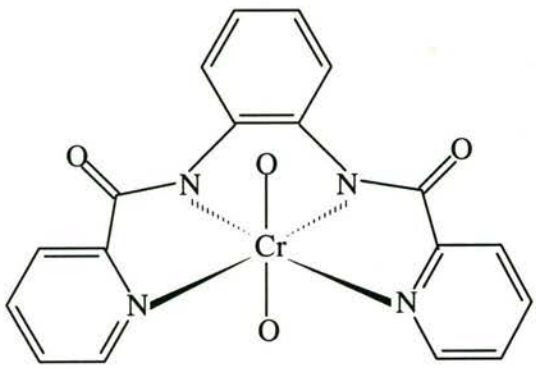

XI

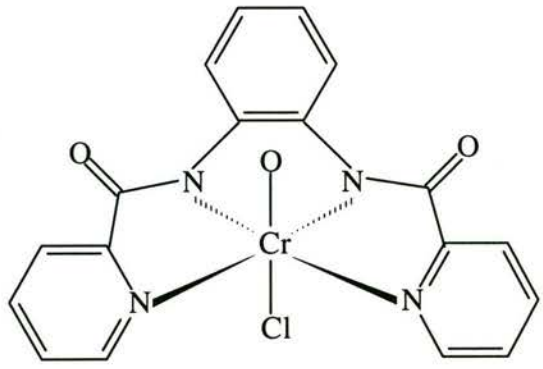

XII

Figure 5.24 Models used in the MS refinement of the XAFS data for *trans*-[Cr^{III}(bpb)Cl(OH_2)].DMF

Table 5.19 Goodness-of-fit parameters for refined models of *trans*-[Cr^{III}(bpb)Cl(OH_2)].DMF

Model	*R*	R_{XAFS}	Determinancy
XI	27.61%	26.28%	1.09
XII	21.02%	19.87%	1.09

effects are greatest. The failure to obtain a R_{XAFS} value significantly below 20% may be due to an inability to take into account MS to atoms hydrogen-bonded to the aqua ligand, as indicated previously, or possibly, the other atoms of the DMF molecule.

The bond lengths within the bpb ligand in **XI** were not significantly different to those determined for **XII**, nor did the bond lengths of 1.99(2) Å for Cr–N(amide) and 2.08(2) Å for Cr–N(pyridyl) in **XI** differ significantly from the values determined for **XII**. In **XI**, the Cr0–O5 bond length was 1.95(2) Å and the Cr0–O6 bond length was 2.16(2) Å. The difference between the Cr0–O5 bond lengths in **XI** and **XII** was equal to the cumulative uncertainty, but the Cr0–O6 bond length in **XI** was considerably shorter than the Cr0–Cl6 distance in **XII**. The Cr0–O6 bond length in **XI** was considerably longer than the Cr–O(DMF) distance of 1.91(2) Å in the complex [$Cr^{III}Cl_3$(DMF)(phen)].[70] The Cr0–O6 bond length in **XI** was within the range 1.923-2.239 Å observed for Cr^{III}–O(water) distances in crystal structures,[25,60,65-69] but it was considerably greater than the Cr0–O(water) bond

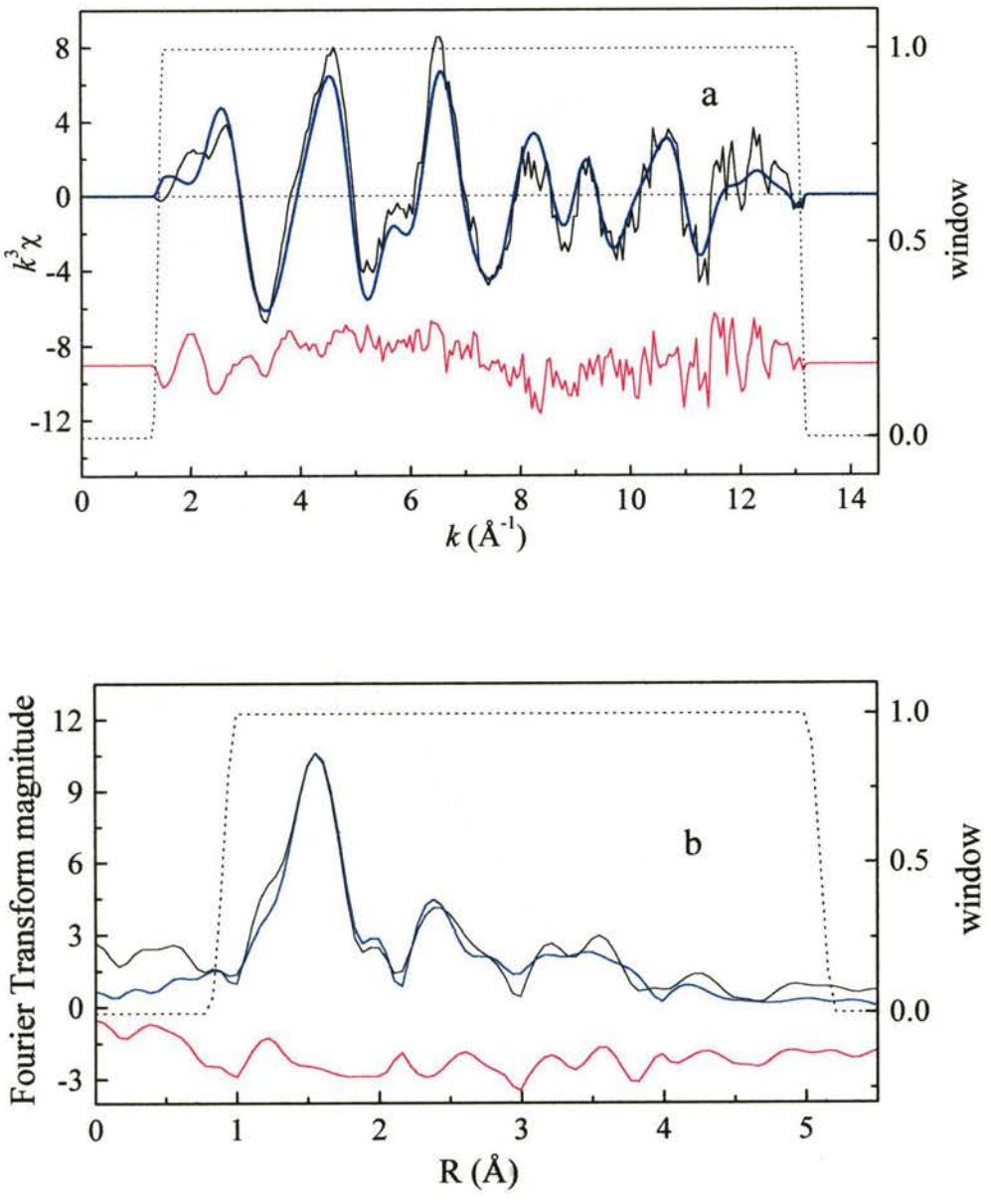

Figure 5.25 (a) XAFS and (b) Fourier transform curves for Model **XII** of *trans*-[Cr^{III}(bpb)Cl(OH_2)].DMF. Observed (black), calculated (blue) and residual (red) curves, along with the window function (dotted line).

lengths in Model **XA** of the diaqua complex (Section 5.3.2.3). The Cr0–Cl6 distance in **XII** of 2.32(2) Å was in the range 2.242-2.35 Å reported for Cr–Cl bond lengths in the crystal structures of Cr(III) complexes.[69-72] The Cr0–O5 bond length in **XII** was quite short for a Cr–O(water) bond, but it was within experimental error of the value reported for one of the aqua ligands in the crystal structure of *trans*-[Cr^{III}(salen)(OH_2)$_2$]$^+$.[68]

Table 5.20 Bond lengths involving the non-hydrogen atoms in Model **XII** of *trans*-[Cr^{III}(bpb)Cl(OH_2)].DMF[a]

atom–atom	distance (Å)	atom–atom	distance (Å)
Cr0–N1	2.07(2)	C7–C13	1.38(2)
Cr0–N2	1.98(2)	C13–C14	1.38(2)
Cr0–O5	1.91(2)	C14–C15	1.38(2)
Cr0–Cl6	2.32(2)	C9–O11	1.23(2)
N1–C17	1.35(2)	C9–C17	1.50(2)
N1–C21	1.34(2)	C17–C18	1.38(2)
N2–C7	1.42(2)	C18–C19	1.38(2)
N2–C9	1.34(2)	C19–C20	1.36(2)
C7–C8	1.42(2)	C20–C21	1.37(2)

[a] The estimated error in the last significant figure is shown in parentheses. The errors in the bond lengths and interatomic distances are the root-mean-square (rms) combination of the conservative systematic error[2,5,23] with the error determined by Monte-Carlo analyses.[10,11]

Table 5.21 Selected bond angles from the refinement of Model **XII** of *trans*-[Cr^{III}(bpb)Cl(OH_2)].DMF[a]

atom–atom–atom	angle (°)
N1–Cr0–N2	79(1)
N1–Cr0–N3	154(2)
N1–Cr0–N4	113(1)
N2–Cr0–N3	82(1)
O5–Cr0–Cl6	161(4)

[a] The errors in the bond angles are the rms combination of the Monte Carlo error and the error in the bond angle due to the Monte-Carlo error in the bond lengths.[50]

The Cr–N(amide) bond length of 1.98(2) Å in **XII** was 0.04 Å longer than the distance in the diaqua complex **XA**. The difference in the Cr–N(amide) bond lengths was equal to the sum of the uncertainties in the bond lengths, so it cannot be considered to be significant. The Cr–N(pyridyl) bond length of 2.07(2) Å in **XII** was

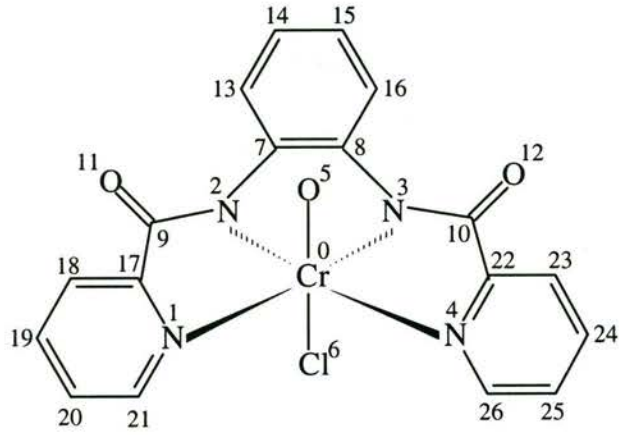

Figure 5.26 Atom numbering scheme for Model **XII** of *trans*-[Cr^{III}(bpb)Cl(OH_2)].DMF

identical to the value determined for the diaqua complex **XA**. The Cr–(bpb) bond lengths for **XI** and **XII** agreed with those determined for **XA**, which had known axial ligands. This demonstrated that the refinement of models with different axial ligands did not inhibit the determination of the core Cr–(bpb) structure by MS XAFS analysis and that the differences in the goodness-of-fit parameters between **XI** and **XII** were due to the axial ligands.

5.4 Conclusions

The XANES region of the X-ray absorption spectra provided information about the oxidation state of the Cr complexes and gave an indication of the coordination geometry about the Cr atom.

MS XAFS analysis provided accurate structural information about atoms beyond the first coordination sphere of the absorbing atom. This makes it an important tool in the study of Cr complexes, many of which cannot be obtained as single crystals suitable for X-ray crystallography. This is especially true for the Cr(V) complexes, due to their inherent instability.

The determination of the structure the Cr(V)-alanine complex by XAFS is significant because it is the first structural characterisation of a Cr(V) amino acid complex. Also there are very few dinuclear Cr(V) complexes that have been characterised.

The XAFS analysis of the Cr(III)-phen complex showed that outer-sphere atoms can make significant contributions to the XAFS of a metal complex in the solid state. This factor, which is very difficult to take into account in most XAFS analyses of solids, may limit the accuracy with which the XAFS simulated from a model fits the observed data.

The structures of two Cr(III) complexes of the ligand bpb have been determined by XAFS for the first time. As expected, Cr–N(amide) bonds were shorter and stronger than the Cr–N(pyridyl) bonds. The MS analysis of the XAFS data for *trans*-$[Cr^{III}(bpb)(OH_2)_2]ClO_4.H_2O$ and *trans*-$[Cr^{III}(bpb)Cl(OH_2)]$.DMF was used to determine that axial coordination sites in the latter were occupied by an aqua ligand and Cl^-.

5.5 References

1) S. P. Cramer and K. O. Hodgson *Prog. Inorg. Chem.* **1979**, *25*, 1-39.

2) S. J. Gurman *J. Synchrotron Rad.* **1995**, *2*, 56-63.

3) P. A. Lee, P. H. Citrin, P. Eisenberger and B. M. Kincaid *Rev. Mod. Phys.* **1981**, *53*, 769-806.

4) S. J. Gurman In *Synchrotron Radiation and Biophysics*; 1st ed.; S. S. Hasnain, Ed.; Ellis Horwood Limited: Chichester, **1990** pp 9-42.

5) P. Riggs-Gelasco, T. L. Stemmler and J. E. Penner-Hahn *Coord. Chem. Rev.* **1995**, *144*, 245-286.

6) B.-K. Teo *J. Am. Chem. Soc.* **1981**, *103*, 3990-4001.

7) B.-K. Teo In *EXAFS and Near Edge Structure*; A. Bianconi, L. Incoccia and S. Stipcich, Eds.; Springer-Verlag: Berlin, **1983** pp 11-21.

8) B. M. Kincaid and P. Eisenberger *Phys. Rev. Lett.* **1975**, *34*, 1361-1364.

9) J. Jaklevic, J. A. Kirby, M. P. Klein, A. S. Robertson, G. S. Brown and P. Eisenberger *Solid State Commun.* **1977**, *23*, 679-682.

10) P. J. Ellis; PhD Thesis, The University of Sydney, 1995.

11) P. J. Ellis and H. C. Freeman *J. Synchrotron Rad.* **1995**, *2*, 190-195.

12) P. J. Ellis *XFIT for Windows '95*; **1996**, Australian Synchrotron Research Program: Sydney.

13) J. J. Rehr, J. M. de Leon, S. I. Labinsky and R. C. Albers *J. Am. Chem. Soc.* **1991**, *113*, 5135-5140.

14) J. M. de Leon, J. J. Rehr, S. I. Zabinsky and R. C. Albers *Phys. Rev. B* **1991**, *44*, 4146-4156.

15) J. J. Rehr and R. C. Albers *Phys. Rev. B* **1990**, *41*, 8139-8149.

16) N. Binsted, R. W. Strange and S. S. Hasnain *Biochemistry* **1992**, *31*, 12117-12125.

17) C. T. Dillon, P. A. Lay, A. M. Bonin, N. E. Dixon and Y. Sulfab *Aust. J. Chem.* **2000**, *53*, 411-424.

18) R. G. Inskeep and J. Bjerrum *Acta Chem. Scand.* **1961**, *15*, 62-68.

19) K. Srinivasan and J. K. Kochi *Inorg. Chem.* **1985**, *24*, 4671-4679.

20) G. N. George *Centre for X-ray Optics X-ray Data Booklet*; SSRL: Berkeley, **1993**.

21) P. J. Ellis, R. W. Joyner, T. Maschmeyer, A. F. Masters, D. A. Niles and A. K. Smith *J. Mol. Catal. A* **1996**, *111*, 297-305.

22) H. A. Headlam; PhD Thesis, The University of Sydney, 1998.

23) C. D. Garner *Adv. Inorg. Chem.* **1991**, *36*, 303-339.

24) G. Ranger and A. L. Beauchamp *Acta Crystallogr. Sect. B* **1981**, *B37*, 1063-1067.

25) C. T. Dillon and P. Turner, personal communication, **2000**.

26) C.-M. Che, J.-X. Ma, W.-T. Wong, T.-F. Lai and C.-K. Poon *Inorg. Chem.* **1988**, *27*, 2547-2548.

27) F. S. Stephens and R. S. Vagg *Inorg. Chim. Acta* **1986**, *120*, 165-171.

28) S.-T. Mak, V. W.-W. Yam, C.-M. Che and T. C. W. Mak *J. Chem. Soc., Dalton Trans.* **1990**, 2555-2654.

29) R. L. Chapman, F. S. Stephens and R. S. Vagg *Inorg. Chim. Acta* **1980**, *43*, 29-33.

30) R. M. Wood, K. A. Abboud, R. C. Palenik and G. J. Palenik *Inorg. Chem.* **2000**, *39*, 2065-2068.

31) T. J. Collins, C. Slebodnick and E. S. Uffelman *Inorg. Chem.* **1990**, *29*, 3433-3436.

32) C. M. Murdoch, M. K. Cooper, T. W. Hambley, W. N. Hunter and H. C. Freeman *J. Chem. Soc., Chem. Commun.* **1986**, 1329-1331.

33) N. Azuma, Y. Imori, H. Yoshida, K. Tajima, Y. Li and J. Yamauchi *Inorg. Chim. Acta* **1997**, *266*, 29-36.

34) J.-H. Choi, I.-H. Suh and S.-H. Kwak *Acta Crystallogr. Sect. C* **1995**, *C51*, 1745-1748.

35) J. T. Groves, T. Takahashi and W. M. Butler *Inorg. Chem.* **1983**, *27*, 884-887.

36) T. J. Collins, B. D. Santarsiero and G. H. Spies *J. Chem. Soc., Chem. Commun.* **1983**, 681-682.

37) H. Oki and H. Yoneda *Inorg. Chem.* **1981**, *20*, 3875-3879.

38) A. Levina, G. J. Foran and P. A. Lay *J. Chem. Soc., Chem. Commun.* **1999**, 2339-2340.

39) C. T. Dillon, P. A. Lay, M. Cholewa, G. J. F. Legge, A. M. Bonin, T. J. Collins, K. L. Kostka and G. Shea-McCarthy *Chem. Res. Toxicol.* **1997**, *10*, 533-535.

40) R. J. Judd, T. W. Hambley and P. A. Lay *J. Chem. Soc., Dalton Trans.* **1989**, 2205-2210.

41) T. L. Siddall, N. Miyaura, J. C. Huffman and J. K. Kochi *J. Chem. Soc., Chem. Commun.* **1983**, 1185-1186.

42) C. T. Dillon, P. A. Lay, A. M. Bonin, M. Cholewa and G. J. F. Legge *Chem. Res. Toxicol.* **2000**, *13*, 742-748.

43) Y. Sulfab and M. Nasreldin *Trans. Met. Chem.* **2001**, *26*, 147-149.

44) Y. Izumi and H. Nagamori *Bull. Chem. Soc. Jpn.* **2000**, *73*, 1581-1587.

45) S. Díaz-Moreno, A. Muñoz-Páez, J. M. Martínez, R. R. Pappalardo and E. S. Marcos *J. Am. Chem. Soc.* **1996**, *118*, 12654-12664.

46) K. Meyer, J. Bendix, E. Bill, T. Weyhermüller and K. Wieghardt *Inorg. Chem.* **1998**, *37*, 5180-5188.

47) A. A. Danopoulos, G. Wilkinson, T. K. N. Sweet and M. B. Hursthouse *J. Chem. Soc., Dalton Trans.* **1995**, 2111-2123.

48) H. Nishino and J. K. Kochi *Inorg. Chim. Acta* **1990**, *174*, 93-102.

49) M. Herberhold, W. Kremnitz, A. Razavi, H. Schöllhorn and U. Thewalt *Angew. Chem. Int. Ed. Engl.* **1985**, *24*, 601-602.

50) A. M. Rich, R. S. Armstrong, P. J. Ellis, H. C. Freeman and P. A. Lay *Inorg. Chem.* **1998**, *37*, 5743-5753.

51) M. Krumpolc, B. G. DeBoer and J. Roček *J. Am. Chem. Soc.* **1978**, *100*, 145-153.

52) S. K. Dutta, S. B. Kumar, S. Bhattacharyya, E. R. T. Tiekink and M. Chaudhury *Inorg. Chem.* **1997**, *36*, 4954-4960.

53) F. Jiang, O. P. Anderson, S. M. Miller, J. Chen, M. Mahroof-Tahir and D. C. Crans *Inorg. Chem.* **1998**, *37*, 5439-5451.

54) P. Andersen and J. Josephsen *Acta Chem. Scand.* **1971**, *25*, 3255-3260.

55) J. T. Veal, W. E. Hatfield and D. J. Hodgson *Acta Crystallogr. Sect. B* **1973**, *B29*, 12-20.

56) V. Subramaniam, K.-W. Lee, R. G. Garvey and P. E. Hoggard *Polyhedron* **1988**, *7*, 523-527.

57) T. Weyhermüller, K. Weighardt and P. Chaudhuri *J. Chem. Soc., Dalton Trans.* **1998**, 3805-3813.

58) B. G. Gafford and R. A. Holwerda *Inorg. Chem.* **1989**, *28*, 60-66.

59) B. G. Gafford, R. E. Marsh, W. P. Schaefer, J. H. Zhang, C. J. O'Connor and R. A. Holwerda *Inorg. Chem.* **1990**, *29*, 4652-4657.

60) U. Casellato, R. Graziani, G. Maccarrone and A. J. D. Bilio *J. Crystallogr. Spectrosc. Res.* **1986**, *16*, 695-702.

61) U. Casellato, R. Graziani, R. P. Bonomo and A. J. D. Bilio *J. Chem. Soc., Dalton Trans.* **1991**, 23-31.

62) M. Ardon and A. Bino *Inorg. Chem.* **1985**, *24*, 1343-1347.

63) P. A. Goodson, J. Glerup, D. J. Hodgson, K. Michelsen and U. Rychlewska *Inorg. Chem.* **1994**, *33*, 359-366.

64) R. L. Lieberman, A. Bino, N. Mirsky, D. A. Summers and R. C. Thompson *Inorg. Chim. Acta* **2000**, *297*, 1-5.

65) S. J. Brudenell, S. J. Crimp, J. K. E. Higgs, B. Moubaraki, K. S. Murray and L. Spiccia *Inorg. Chim. Acta* **1996**, *247*, 35-41.

66) D. A. House and J. Svensson *Inorg. Chim. Acta* **1998**, *278*, 24-31.

67) A. D. Q. Ferreira, A. Bino and D. Gibson *Inorg. Chem.* **1998**, *37*, 6560-6561.

68) P. Coggon, A. T. McPhail, F. E. Mabbs, A. Richards and A. S. Thornley *J. Chem. Soc. A* **1970**, 3296-3303.

69) M. Inamo, M. Hoshino, K. Nakajima, S.-i. Aizawa and S. Funahashi *Bull. Chem. Soc. Jpn.* **1995**, *68*, 2293-2303.

70) J. A. Broomhead, J. Evans, W. D. Grumley and M. Sterns *J. Chem. Soc., Dalton Trans.* **1977**, 173-176.

71) D. J. Ayres, D. A. House and W. T. Robinson *Inorg. Chim. Acta* **1998**, *277*, 177-185.

72) A. Derwahl, W. T. Robinson and D. A. House *Inorg. Chim. Acta* **1996**, *247*, 19-28.

Chapter 6

DNA Cleavage and Biological Implications

6.1 Introduction

6.1.1 Plasmid DNA Cleavage Assay

Gel electrophoresis was used to assay supercoiled plasmid DNA relaxation as a way to assess the ability of $[Cr^{V}O(S,S\text{-bprolben})]^{+}$ to cleave DNA. The pUC9 plasmid (2.67×10^{3} base pairs) from an *Escherichia coli* strain[1] was used in the assay. The natural state of the pUC9 DNA is the negatively supercoiled form I (Figure 6.1(a)). A single DNA strand break results in the relaxation of form I to form II, nicked circular plasmid DNA (Figure 6.1(b)). Two strand breaks close together on opposite strands of the DNA results in complete cleavage of the DNA and the formation of form III, linear DNA (Figure 6.1(c)).[1]

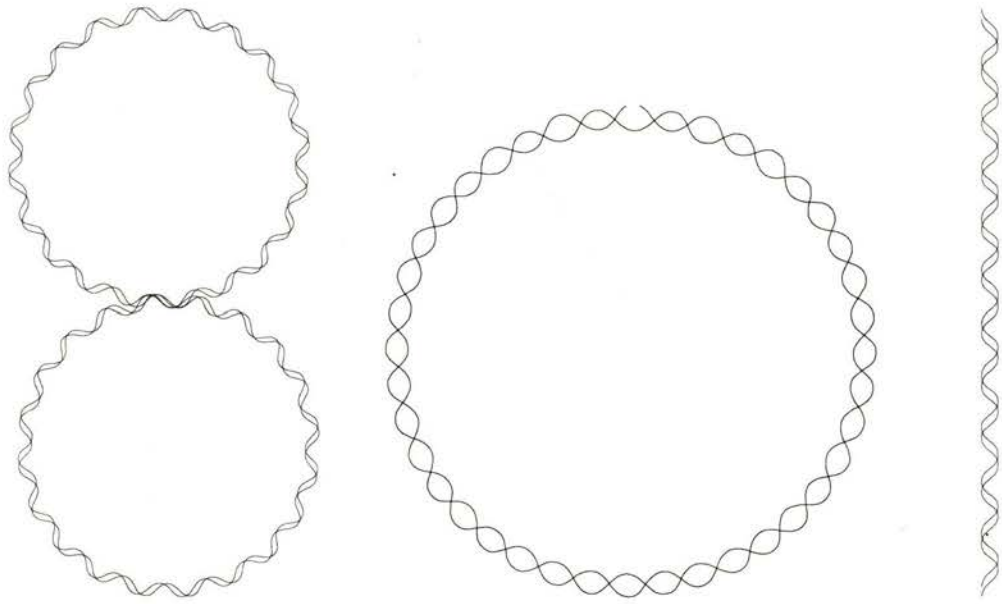

(a) (b) (c)

Figure 6.1 Diagrammatic representations of (a) supercoiled (form I), (b) open circular (form II), and (c) linear (form III) plasmid DNA

The three types of plasmid DNA are separated by DNA gel electrophoresis. The negatively supercoiled form I is the most compact and mobile, migrating fastest through the gel. Form II DNA migrates the slowest through the gel due to its much larger size. Form III DNA has a mobility that is intermediate between those of form I and form II DNA, as it can snake through the pores in the gel and migrates a little way ahead of form II DNA. The increase in the amount of form II and form III after

reaction of the plasmid with a suspected DNA damaging agent is a measure of the extent of DNA cleavage.

6.1.2 DNA Cleavage by Cr(V)-Amide Complexes

There have been few studies on the potential of Cr(V)-amide complexes to cause DNA damage, most studies to date have concentrated on the effect of Cr(V) complexes with 2-hydroxy acids, and the reduction of Cr(VI) by various biological reductants in the presence of DNA. The Cr(V) complex with a macrocyclic tetraamido ligand, $[Cr^{V}O(mampa)]^{-}$, caused DNA cleavage at pH 3.8 and 7.4.[2] There was little difference in the amount of DNA cleavage at the different pH values, with slightly more cleavage observed at the lower pH value. The level of DNA cleavage was fairly low, form I DNA predominated over form II DNA in all reactions, even for $[Cr^{V}O(mampa)]^{-}$ concentrations of 2 mM and incubation times of 48 h.

Chromium(V) complexes with tetraglycine and pentaglycine at pH 3.85 and 5.6 caused similar levels of DNA cleavage to $[Cr^{V}O(mampa)]^{-}$. Incubation of DNA with Cr(V)-triglycine at pH 3.85 caused more extensive DNA cleavage, though no cleavage was observed at higher pH. Reaction of Cr(V)-trialanine with DNA at pH 7.4 also caused significant amounts of DNA cleavage. Incubation of Cr(V)-triglycine at pH 3.85 and Cr(V)-trialanine at pH 7.4 with DNA for 24 h or longer caused precipitation of the DNA.[3]

6.2 Experimental

6.2.1 Preparation of an Aqueous Solution of $[Cr^{V}O(S,S\text{-bprolben})]^{+}$

A solution of *S,S*-bprolbenH_2 (0.255 g) in acetone (40 mL) and a solution of $Na_2Cr_2O_7.2H_2O$ (0.122 g, Ajax, 99%) in methanol (10 mL) were mixed. Acetone (20 mL) was added and the mixture was stirred under a fluorescent desk lamp (~20 cm away, Norax brand fitted with a 45 × 2.5 cm 15 W tube) for 3 d. The reaction mixture was filtered through a celite pad and the solvent was removed from the filtrate on a rotary evaporator (water bath temperature ~20 °C). The residue thus

obtained was dissolved in methanol (5 mL) and loaded onto a lipophilic LH20 Sephadex column (25 × 2 cm). The column was eluted with methanol and three bands eluted, a fast moving grey-brown band, then an orange-brown band, and finally a tiny yellow band. The solvent was removed from the fraction containing the orange-brown band on a rotary evaporator with the water bath at ~20 °C and the resultant residue was dissolved in 5 mL of Milli-Q water. The approximate concentration of $[Cr^{V}O(S,S\text{-bprolben})]^{+}$ was determined immediately prior to its use in the DNA cleavage assay by EPR spin quantitation against a $Na[Cr^{V}O(ehba)_2]$ standard.[4]

6.2.2 Plasmid DNA Cleavage Assays

All solutions were prepared in water purified by a Milli-Q system and buffer solutions were treated overnight with Chelex 100 resin to remove residual trace metal ions. Stock solutions of buffer were freshly prepared by adjusting the pH value to that required with 1 M NaOH or 1 M HCl and diluting to give a concentration of 0.500 M. DNA cleavage reactions at pH 4.0 and 5.0 were carried out in acetate buffer, reactions at pH 6.0 and 7.0 were carried out in cacodylate buffer, and pH 7.4 reactions were performed in phosphate buffer. Control reactions were run using stock solutions of Cr(VI) (as $Na_2Cr_2O_7.2H_2O$, Ajax, 99%), Cr(III) (as $CrCl_3.6H_2O$, Merck, 95%), and *S,S*-bprolbenH_2 (purified by flash chromatography). *Hin*dIII restriction enzyme (Sigma, 10 units μL^{-1}) in SB buffer for endonucleases (Sigma) was used as a positive control to generate form III DNA. For a typical DNA reaction with $[Cr^{V}O(S,S\text{-bprolben})]^{+}$: [DNA] = 25 mg L^{-1}, [Cr(V)] = 2 μM, [buffer] = 0.100 M (pH 4.0); an aqueous solution of pUC9 DNA (1 μL, 375 mg L^{-1}) was mixed with acetate buffer (3 μL, 0.500 mM, pH 4.0) and water (5 μL), followed by the addition of an aqueous solution of $[Cr^{V}O(S,S\text{-bprolben})]^{+}$ (6 μL, 5 μM). The mixture was incubated at 37 °C for 1 h (protected from light) and then cooled to 0 °C and the loading solution (5 μL, 0.25% bromophenol blue, 40% sucrose, cooled to 0 °C) was added. The mixture was loaded onto a 1.25% agarose gel in TBE buffer (45 mM Tris, 45 mM borate, 1.0 mM Na_2edta, and 0.5 mg L^{-1} ethidium bromide), and electrophoresis was performed for 18 h at ~1 V cm^{-1}.

To examine the pH dependence of the interaction of $[Cr^{V}O(S,S\text{-bprolben})]^{+}$ with DNA, reactions were run at pH 4.0, 5.0, 6.0, or 7.0. A second set of reactions over a wider range of $[Cr^{V}O(S,S\text{-bprolben})]^{+}$ concentrations were performed at pH 4.0 and 5.0.

The gels were photographed under UV light using a Chromato-Vue TM-20 transilluminator and a Polaroid camera with Type 55 positive/negative Polaroid film. The positive images were scanned into an IBM-compatible computer using a Microtek ScanMaker IIsp scanner. The scans were processed by Adobe Photoshop.[5] The intensities of the bands of form I-III DNA were calculated by multiplying the mean density and area (in pixels) for each band. The higher fluorescence of the ethidium bromide adducts of form II and form III DNA compared to form I DNA was accounted for by multiplying the intensity of the form II and III bands by 0.8.[6]

6.3 Results and Discussion

6.3.1 Preparation of an Aqueous Solution of $[Cr^{V}O(S,S\text{-bprolben})]^{+}$

A detailed discussion of the synthesis of $[Cr^{V}O(S,S\text{-bprolben})]^{+}$ is given in Chapter 4, Section 4.3.3.3. The reaction mixture was filtered through a celite pad to remove the very fine Cr(III) precipitate. EPR spectroscopy of the fractions eluted from the LH20 Sephadex column showed that the main Cr(V) species in the grey-brown and yellow bands were Cr(V)-methanol complexes, while the main Cr(V) complex in the orange-brown band was $[Cr^{V}O(S,S\text{-bprolben})]^{+}$. When the residue of the fraction containing the orange-brown band was dissolved in water, EPR spectroscopy showed only a single Cr(V) signal, from $[Cr^{V}O(S,S\text{-bprolben})]^{+}$; the small amounts of the Cr(V)-methanol species present had decomposed.

6.3.2 Plasmid DNA Cleavage Assays

Preliminary experiments at pH 4.0 and 7.4 exhibited significant DNA cleavage by $[Cr^{V}O(S,S\text{-bprolben})]^{+}$ only at the lower pH value. The DNA cleavage reactions at pH 4.0, 5.0, 6.0, and 7.0 were carried out to examine the pH dependence of the reaction and the results are in shown Figure 6.2, with the conditions for each lane

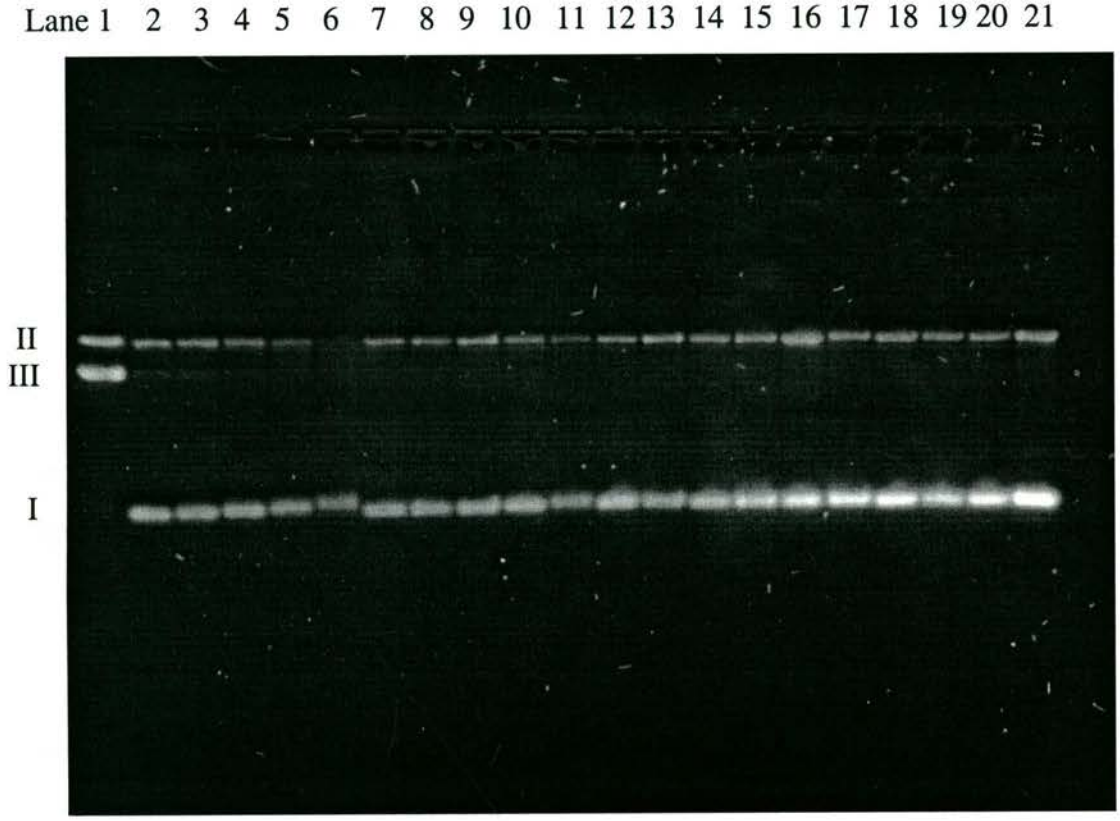

Figure 6.2 Electrophoresis gel of pUC9 plasmid DNA cleavage reactions at pH 4.0 (lanes 2-6), pH 5.0 (lanes7-11), pH 6.0 (lanes 12-16), and pH 7.0 (lanes 17-21). Lane 1, DNA + *Hin*dIII; lanes 2, 7, 12, and 17, DNA alone; lanes 3, 8, 13, and 18, DNA + Cr(VI) (1.0 mM); lanes 4, 9, 14, and 19, DNA + $[Cr^{V}O(S,S\text{-bprolben})]^{+}$ (1.0 μM); lanes 5, 10, 15, and 20, DNA + $[Cr^{V}O(S,S\text{-bprolben})]^{+}$ (2.0 μM); lanes 6, 11, 16, and 21, DNA + $[Cr^{V}O(S,S\text{-bprolben})]^{+}$ (4.0 μM).

listed in the figure caption. The reactions were only performed over a narrow range of $[Cr^{V}O(S,S\text{-bprolben})]^{+}$ concentrations to ensure that form I and form II DNA could be detected in the pH 4.0 reactions, as higher concentrations led to the disappearance of all three forms in the preliminary reactions at that pH value.

The restriction enzyme *Hin*dIII (lane 1) was used to completely cleave the pUC9 DNA to mark the position of form III DNA on the gel. At all pH values, Cr(VI) by itself (lanes 3, 8, 13, and 18) caused no significant change in the ratio form II to form I DNA, in agreement with previous reports of the inability of Cr(VI) to directly damage DNA.[1,7-10] At pH 4.0 migration of the form I DNA was increasingly

retarded as the concentration of $[Cr^{V}O(S,S\text{-bprolben})]^{+}$ increased (lanes 5 and 6). A slight retardation of form I DNA migration was also caused by 4 μM $[Cr^{V}O(S,S\text{-bprolben})]^{+}$ at pH 5.0 (lane 11).

The amounts of both form I and form II DNA decreased as the concentration of $[Cr^{V}O(S,S\text{-bprolben})]^{+}$ increased at pH 4.0, with the effect on form II being more significant than form I. At 4.0 μM $[Cr^{V}O(S,S\text{-bprolben})]^{+}$, form II DNA had disappeared completely. There was also a decrease in the amounts of both form I and form II DNA at 4 μM $[Cr^{V}O(S,S\text{-bprolben})]^{+}$ (pH 5.0). There were no significant changes in the ratio of form II to form I DNA in the reactions carried out at pH 6.0 and 7.0, neither was there any retardation of the migration of the form I DNA at these pH values.

The total amount of DNA in the control lanes with DNA + buffer increased as the pH value increased from 4.0 to 7.0. The total amounts of DNA in the reactions containing DNA + Cr(VI), and DNA + $[Cr^{V}O(S,S\text{-bprolben})]^{+}$ at pH 6.0 and 7.0 were similar to the DNA + buffer control reaction and considerably higher than in the corresponding reactions at pH 4.0 and 5.0. The total amount of DNA was lower at more acidic pH because heating in acetate buffer causes denaturation of DNA, with the effect greater at lower pH values.[11,12]

The interaction of $[Cr^{V}O(S,S\text{-bprolben})]^{+}$ with DNA was examined over a wider range of concentrations at pH 4.0 and 5.0. The results of these reactions and the control reactions are shown in Figure 6.3. The reaction of DNA with *S,S*-bprolbenH_2 alone at pH 4.0 (lane 3) resulted in a slight increase in the ratio of form II and form III DNA to form I DNA. This relaxation of the form I DNA by *S,S*-bprolbenH_2 at pH 4.0 was inhibited in the reaction of DNA with *S,S*-bprolbenH_2 + Cr(III) (lane 4), though the Cr(III) also caused a tiny amount of DNA to precipitate in the loading well. At pH 5.0 neither *S,S*-bprolbenH_2 alone nor *S,S*-bprolbenH_2 + Cr(III) (lanes 13 and 14, respectively) increased the ratio of form II and form III DNA to form I DNA. The ratio of form II to form I in the reaction of DNA with *S,S*-bprolbenH_2 + Cr(III) actually decreased slightly compared to DNA alone (lane 12).

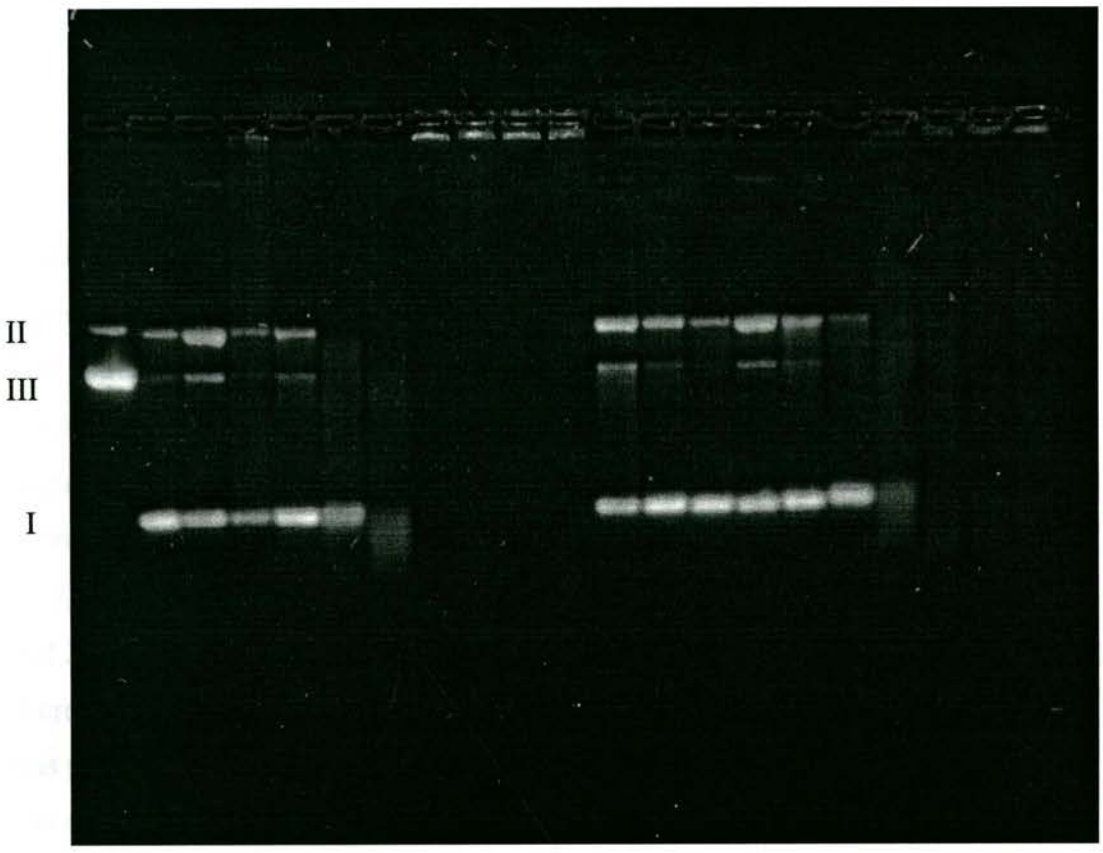

Figure 6.3 Electrophoresis gel of pUC9 plasmid DNA cleavage reactions at pH 4.0 (lanes 2-11) and pH 5.0 (lanes 12-21). Lane 1, DNA + *Hin*dIII; lanes 2 and 12, DNA alone; lanes 3 and 13, DNA + *S,S*-bprolbenH_2 (0.67 mM); lanes 4 and 14, DNA + *S,S*-bprolbenH_2 (0.67 mM) + Cr(III) (0.67 mM); lanes 5 and 15, DNA + Cr(VI) (1.0 mM); lanes 6 and 16, DNA + $[Cr^{V}O(S,S\text{-bprolben})]^{+}$ (1.0 μM); lanes 7 and 17, DNA + $[Cr^{V}O(S,S\text{-bprolben})]^{+}$ (2.0 μM); lanes 8 and 18, DNA + $[Cr^{V}O(S,S\text{-bprolben})]^{+}$ (5.0 μM); lanes 9 and 19, DNA + $[Cr^{V}O(S,S\text{-bprolben})]^{+}$ (10 μM); lanes 10 and 20, DNA + $[Cr^{V}O(S,S\text{-bprolben})]^{+}$ (15 μM); lanes 11 and 21, DNA + $[Cr^{V}O(S,S\text{-bprolben})]^{+}$ (20 μM).

At pH 4.0, 1 μM $[Cr^{V}O(S,S\text{-bprolben})]^{+}$ (lane 6) decreased the amount of form I DNA and there was smearing from the form I band to the approximate position that the form II and form III bands occurred. When the concentration of $[Cr^{V}O(S,S\text{-bprolben})]^{+}$ was increased to 2 μM at pH 4.0 (lane 7) the form I band migrated faster and was smeared out, the band in the position of the form II and

form III bands was also smeared out, and had decreased in intensity compared to the band from the 1 μM $[Cr^{V}O(S,S\text{-bprolben})]^{+}$ reaction. Concentrations of 5 μM $[Cr^{V}O(S,S\text{-bprolben})]^{+}$ and above at pH 4.0 caused precipitation of the DNA in the loading well and consequently no bands were observed in the gel.

At pH 5.0, 1 μM and 2 μM $[Cr^{V}O(S,S\text{-bprolben})]^{+}$ (lanes 16 and 17, respectively) caused a slight retardation in migration of form I DNA that increased with increasing concentration, and a concomitant decrease in the amounts of form II and form III DNA. An increase in the concentration of $[Cr^{V}O(S,S\text{-bprolben})]^{+}$ to 5 μM (lane 18) caused accelerated migration and smearing out of the form I band; no distinct form II or form III bands were observed, but only smearing out of the DNA in that region. At $[Cr^{V}O(S,S\text{-bprolben})]^{+}$ concentrations of 10 μM, 15 μM, and 20 μM (lanes 19, 20, and 21, respectively) there was a complete smearing out of the DNA bands, which decreased in intensity with increasing concentration. A very small amount of DNA was precipitated in the loading wells for $[Cr^{V}O(S,S\text{-bprolben})]^{+}$ concentrations of 5 μM and above, increasing with $[Cr^{V}O(S,S\text{-bprolben})]^{+}$ concentration (lanes 18-21).

The slight increase in the ratio of form II and form III to form I DNA in the control reaction with *S,S*-bprolbenH_2 alone at pH 4.0 indicated that the ligand may be able to cause DNA cleavage by itself. However, this low level of DNA damage by *S,S*-bprolbenH_2 was observed at a concentration more than thirty times that of the highest concentration of $[Cr^{V}O(S,S\text{-bprolben})]^{+}$ used, and there was no DNA damage when Cr(III) was present along with *S,S*-bprolbenH_2. These results show that the DNA cleavage observed in the reactions with $[Cr^{V}O(S,S\text{-bprolben})]^{+}$ was not due to the action of free ligand released by decomposition of the complex. The control reactions with Cr(III) + *S,S*-bprolbenH_2, and Cr(VI) were carried out because Cr(III) and Cr(VI) were likely decomposition products of the Cr(V)-methanol species in the fraction containing $[Cr^{V}O(S,S\text{-bprolben})]^{+}$ when it was dissolved in water. It was not possible to carry out a control reactions with the complexes of the type $[Cr^{III}(S,S\text{-bprolben})L_2]^{n+}$ due to their insolubility in water.

The retardation of the migration of form I DNA by $[Cr^{V}O(S,S\text{-bprolben})]^{+}$ was observed on two different gels, at both pH 4.0 and 5.0, and was concentration

dependent. This was clear evidence that it was not an experimental artefact. The retardation of the migration of form I DNA was due to a change in the supercoiling, the absence of similar retardation of form II showed that it was not simply electrostatic binding.

At pH 4.0 and 5.0, the $[Cr^{V}O(S,S\text{-bprolben})]^{+}$ was able to react with form I and form II DNA, causing extensive DNA cleavage. The reaction with form II was appreciably faster than the rate of reaction with form I, as form II disappeared faster. The very high susceptibility of the relaxed forms of the pUC9 plasmid to cleavage by $[Cr^{V}O(S,S\text{-bprolben})]^{+}$ at low pH value was shown by the almost complete absence of form III in the reactions at pH 4.0 and 5.0; it was only observed in one of the 1 μM $[Cr^{V}O(S,S\text{-bprolben})]^{+}$ reactions at pH 5.0 (Figure 6.3, lane 16). At the higher concentrations of $[Cr^{V}O(S,S\text{-bprolben})]^{+}$, no bands from form I, form II, or form III were observed; the DNA was more extensively degraded, leading to smearing in the gels, and/or precipitation in the loading wells.

The absence of DNA cleavage or retardation of form I DNA migration at pH values of 6.0 and above indicated that there was little or no interaction between the $[Cr^{V}O(S,S\text{-bprolben})]^{+}$ and DNA at these pH values. The observed pH dependence of the DNA cleavage was similar to that observed for Cr(V)-triglycine,[3] but was in contrast to the results obtained with $[Cr^{V}O(mampa)]^{-}$, which caused low levels of DNA cleavage at both pH 3.8 and 7.4.[2] The concentrations of $[Cr^{V}O(S,S\text{-bprolben})]^{+}$ that caused cleavage of DNA were considerably lower than the concentrations used in the reactions of $[Cr^{V}O(mampa)]^{-}$ (50-2000 μM)[2] and Cr(V)-oligopeptide complexes (2000 μM)[3] with DNA. This may be a reflection of the positive charge on the Cr(V)-(*S,S*-bprolben) complex.

6.4 Conclusions

The Cr(V)-amide complex, $[Cr^{V}O(S,S\text{-bprolben})]^{+}$, was a powerful DNA damaging agent, extensive DNA cleavage was observed even a low concentrations (1 μM) of the complex under acidic conditions. No DNA cleavage by $[Cr^{V}O(S,S\text{-bprolben})]^{+}$ was observed at pH values above 6.0, though only very low concentrations were used in these studies and there may well be significant cleavage or other damage at higher

pH values with higher concentrations. The Cr complexes with these ligands can be used to study the chiral selectivity of interactions with DNA, although time did not permit the preparation of the other enantiomer.

Chromium(V) is produced during the reduction of Cr(VI) by the main biological reductants. In this work it was shown that coordination of deprotonated amide N stabilised the Cr(V) formed during the reduction of Cr(VI) by methanol, and the Cr(V) species produced by the oxidation of the Cr(III) complexes with tetradentate diamide ligands were also stable. Hence, the Cr(V) generated *in vivo* could be stabilised by coordination to the amide groups of proteins and smaller peptides. Such Cr(V)-amide complexes are likely to be only minor species *in vivo* due to their slow rate of formation, as there is a vast array of potential ligands for Cr(V) within cells. Though the Cr(V)-amide complexes are likely to be only a small proportion of all Cr(V) formed, their high stability means that they are more likely to reach DNA than most other Cr(V) complexes formed within cells. The extensive DNA damage caused by $[Cr^{V}O(S,S\text{-bprolben})]^{+}$, and the relative stability of Cr(V)-amide complexes indicates that they may play a role in the mechanism of Cr-induced carcinogenesis, this is especially the case since one of the major forms of DNA damage *in vivo* is Cr-protein crosslinks.[13-16]

The Ni complexes with the tetradentate diamide ligands were observed to have relatively low $Ni^{III/II}$ reduction potentials. The oxidative dehydrogenation of the *S,S*-bprolen ligand during the formation of the Ni complex involved O_2, and it is likely that a higher oxidation state of Ni plays a role in the mechanism. These results indicate that formation of Ni-amide complexes is likely to make the Ni(III) oxidation state, which *in vitro* studies suggest can damage DNA, accessible *in vivo*. The oxidising power of the species formed by the reaction of the Ni(II)-amide complex with O_2 indicates that such interactions may produce species capable of damaging DNA *in vivo*. Thus direct damage of DNA mediated by Ni complexes may play a role alongside epigenetic effects in the mechanism of Ni-induced carcinogenesis.

6.5 References

1) R. P. Farrell, R. J. Judd, P. A. Lay, N. E. Dixon, R. S. U. Baker and A. M. Bonin *Chem. Res. Toxicol.* **1989**, *2*, 227-229.

2) C. T. Dillon, P. A. Lay, A. M. Bonin, N. E. Dixon, T. J. Collins and K. L. Kostka *Carcinogenesis* **1993**, *14*, 1875-1880.

3) H. A. Headlam; PhD Thesis, The University of Sydney, 1998.

4) J. Chappell, B. Chiswell and A. Canning *Talanta* **1998**, *46*, 23-38.

5) Adobe. Systems. Inc. *Adobe Photoshop*; version 2.5, **1993**, Adobe Systems Inc.: Mountain View, CA.

6) A. Kortenkamp, M. Casadevall, S. P. Faux, A. Jenner, R. O. J. Shayer, N. Woodbridge and P. O'Brien *Arch. Biochem. Biophys.* **1996**, *329*, 199-207.

7) M. J. Tsapakos and K. E. Wetterhahn *Chem.-Biol. Interact.* **1983**, *46*, 265-277.

8) T. Wolf, R. Kasemann and H. Ottenwälder *Carcinogenesis* **1989**, *10*, 655-659.

9) M. Casadevall and A. Kortenkamp *Carcinogenesis* **1994**, *15*, 407-409.

10) P. da Cruz Fresco and A. Kortenkamp *Carcinogenesis* **1994**, *15*, 1773-1778.

11) G. Barr-David; PhD Thesis, University of Sydney, 1998.

12) C. T. Dillon, P. A. Lay, A. M. Bonin, N. E. Dixon and Y. Sulfab *Aust. J. Chem.* **2000**, *53*, 411-424.

13) J. E. Gruber and K. W. Jennette *Biochem. Biophys. Res. Commun.* **1978**, *82*, 700-706.

14) R. N. Bose, S. Moghaddas, P. A. Mazzer, L. P. Dudones, L. Joudah and D. Stroup *Nucleic Acids Res.* **1999**, *27*, 2219-2226.

15) K. D. Sugden *J. Inorg. Biochem.* **1999**, *77*, 177-183.

16) A. S. Hneihen, A. M. Standeven and K. E. Wetterhahn *Carcinogenesis* **1993**, *14*, 1795-1803.

Appendices

Appendix 1 X-ray Crystallography Data Collection and Structure Solution

$[Ni^{II}(bprolenH_{-4})].H_2O$

A red prismatic crystal having approximate dimensions of $0.20 \times 0.15 \times 0.08$ mm was attached to a thin glass fibre, and mounted on a Rigaku AFC7R diffractometer employing graphite monochromated Cu-Kα radiation from a rotating anode generator. Primitive triclinic cell constants were obtained from a least-squares refinement using the setting angles of 25 reflections in the range $94.25 < 2\theta < 117.35°$. Diffraction data were collected at a temperature of 21 ± 1 °C using ω-2θ scans to a maximum 2θ value of 130.1°. Omega scans of several intense reflections made prior to data collection, had an average width at half-height of 0.20°, and scans of $(1.73 + 0.35 \tan \theta°)$ were made at a speed of 16.0°/min (in omega). The weak reflections ($I < 15.0\sigma(I)$) were rescanned up to 10 times. Stationary background counts were recorded on each side of the reflection, with a 2:1 ratio of peak to background counting time. The intensities of three representative reflections measured every 150 reflections, did not change significantly during the data collection. An empirical absorption correction based on azimuthal scans of three reflections was applied and the data were also corrected for Lorentz and polarization effects.

All calculations were undertaken with the teXsan[1] crystallographic software package. Neutral atom scattering factors were taken from Cromer and Waber.[2] Anomalous dispersion effects were included in F_{calc}[3] and the values for $\Delta f'$ and $\Delta f''$ were those of Creagh and McAuley.[4] The values for the mass attenuation coefficients were those of Creagh and Hubbell.[5] The structure was solved in the space group $P\bar{1}$ (#2) by heavy-atom Patterson methods[6] and expanded using Fourier techniques.[7] Non-hydrogen atoms were modelled with anisotropic thermal parameters. In general the hydrogen atoms were included in the refinement at calculated positions with group thermal parameters. The asymmetic unit includes a water molecule and the water hydrogens were located and refined with isotropic thermal parameters. The full-matrix least-squares converged with the largest parameter shift being 0.03 times its

estimated standard deviation.

Table A1.1 Summary of crystal data, data collection and refinement for $[Ni^{II}(bprolenH_{-4})].H_2O$

Formula of the refinement model	$C_{12}H_{18}N_4NiO_3$
Formula weight	325.00
Crystal colour, habit	red, prismatic
Crystal dimensions	$0.20 \times 0.15 \times 0.08$ mm
Crystal system	triclinic
Lattice type	Primitive
Space group	$P\bar{1}$ (#2)
a	9.748(1) Å
b	9.923(1) Å
c	8.383(1) Å
α	105.53(1)°
β	104.40(1)°
γ	112.37(1)°
V	664.2(2) $Å^3$
D_c	1.625 g cm^{-3}
Z	2
$2\theta_{max}$	130.1°
hkl range	0 11, −11 10, −9 9
N	2250
N_{obs}	1911($I > 3\sigma(I)$)
N_{var}	190
Residuals: R, Rw	0.051, 0.060
GoF	3.33

$[Ni^{II}(S,S\text{-bprolen})].H_2O$

Table A1.2 Summary of crystal data, data collection and refinement for $[Ni^{II}(S,S\text{-bprolen})].H_2O$

Formula of the refinement model	$C_{12}H_{20}N_4NiO_3$
Formula weight	327.03
Crystal colour, habit	yellow, cut prism
Crystal dimensions	$0.40 \times 0.25 \times 0.21$ mm
Crystal system	trigonal
Space group	$P3_221$(#154)
a	8.5856(14) Å
b	8.5856 Å
c	17.3694(18) Å
γ	120.00°
V	1108.8(2) $Å^3$
D_c	1.460 g cm^{-3}
Z	3
$2\theta_{max}$	135.3°
hkl range	–8 8, 0 10, 0 20
N	1514
N_{obs}	1266($I > 2\sigma(I)$)
N_{var}	93
Residuals: R, Rw	0.0389, 0.1093
GoF	1.068

A yellow prismatic fragment cut from a twinned crystal was attached to a thin glass fibre, and mounted on a Rigaku AFC7R diffractometer employing graphite monochromated CuKα radiation generated from a rotating anode. Cell constants were obtained from a least squares refinement against 25 reflections located between 19.40 and 30.90° 2θ. Data were collected at 294(2) K with ω-2θ scans to 135.30° 2θ. The intensities of 3 standard reflections, measured every 150 reflections, did not change significantly during the data collection. Lorentz and polarisation corrections were applied to the data, and an empirical absorption correction based on azimuthal scans of three reflections was also applied to the data.

Processing and calculations were undertaken with TEXSAN.[8] The structure was solved in the space group $P3_221$(#154) by direct methods with SHELXS-97,[9] and extended and refined with SHELXL-97.[10] Anisotropic thermal parameters were refined for the non-hydrogen atoms, and a riding atom model was used for the hydrogen atoms. The complex straddles a two-fold axis passing through the metal centre. The asymmetric unit contains a water molecule (also located on a two-fold axis), and no hydrogens were included in the model for the water molecule. The Flack parameter[11-13] refined to 0.00(5).

[Ni^{II}(*R,R*-(*S,S*)-bprolchxn)].3H_2O

An orange/yellow prismatic crystal was attached to a thin glass fibre and mounted on a Bruker SMART 1000 CCD diffractometer employing graphite monochromated MoKα generated from a sealed tube. Cell constants were obtained from a least-squares refinement against 8192 reflections located between 0.00 and 56.00° 2θ. Data were collected at 293(2) K with ω scans to 56.00° 2θ, and the full-sphere fraction collected was 0.995. The intensities of 75 standard reflections recollected at the end of the experiment did not change significantly during the data collection. An empirical absorption correction determined with SADABS[14] was applied to the data. The data integration and reduction were undertaken with SAINT and XPREP,[15] and subsequent computations were carried out with the teXsan[8] graphical user interface. The structure was solved in the space group $P2_12_12_1$(#19) by direct methods with SIR97,[16] and extended and refined with SHELXL-97.[10] Anisotropic thermal parameters were refined for the 26 non-hydrogen atoms in the asymmetric unit of the structure model. The hydrogen sites of the water solvate molecules were located and refined; the O(5) hydrogen bond lengths were restrained. The rest of the model hydrogen atoms were placed at calculated positions with group thermal parameters and allowed to ride. The absolute structure was established with the Flack parameter[11,12] refining to 0.00(1).

Table A1.3 Summary of crystal data, data collection and refinement for $[Ni^{II}(R,R\text{-}(S,S)\text{-bprolchxn})].3H_2O$

Formula of the refinement model	$C_{16}H_{32}N_4NiO_5$
Formula weight	419.17
Crystal colour, habit	orange/yellow, prism
Crystal dimensions	$0.226 \times 0.224 \times 0.160$ mm
Crystal system	orthorhombic
Space group	$P2_12_12_1$(#19)
a	9.0175(3) Å
b	10.1232(3) Å
c	21.1448(7) Å
V	1930.22(11) $Å^3$
D_c	1.442 g cm^{-3}
Z	4
$2\theta_{max}$	56.00°
hkl range	−11 11, −13 12, −27 27
N	20641
N_{ind}	4587
N_{obs}	4221($I > 2\sigma(I)$)
N_{var}	260
Residuals: R, Rw	0.0303, 0.0795
GoF	1.061

$[Ni^{II}(S,S\text{-bprolben})].CD_3OD.D_2O$

A yellow columnar-like crystal was attached to a thin glass fibre and mounted on a Rigaku AFC7R diffractometer employing graphite monochromated CuKα generated from a rotating anode. Cell constants were obtained from a least squares refinement against 25 reflections located between 85.20 and 100.60° 2θ. Data were collected at 294(2) K with ω-2θ scans to 135.20° 2θ. The intensities of 3 standard reflections measured every 150 reflections did not change significantly during the data collection. The crystal faces were indexed and an analytical absorption correction was applied to the data. The data were also corrected for Lorentz and polarisation effects.

Data processing and calculations were undertaken with TEXSAN.[1] The structure was solved in the space group $P2_12_12_1$(#19) by direct methods with SIR97,[16] and extended and refined with SHELXL-97[10] using the XSHELL interface.[17] Anisotropic thermal parameters were refined for the non-hydrogen atoms in the asymmetric unit of the structure model. A riding atom model was used for the hydrogen atoms which were included in the model at calculated positions with group thermal parameters. The two water hydrogens were located and modelled with isotropic thermal parameters. The absolute structure was established with the Flack parameter[11,12] refining to 0.01(5).

Table A1.4 Summary of crystal data, data collection and refinement for $[Ni^{II}(S,S\text{-bprolben})].CD_3OD.D_2O$

Formula of the refinement model	$C_{17}H_{26}N_4NiO_4$
Formula weight	409.13
Crystal colour, habit	yellow, columnar
Crystal dimensions	$0.200 \times 0.063 \times 0.063$ mm
Crystal system	orthorhombic
Space group	$P2_12_12_1$(#19)
a	11.760(2) Å
b	18.409(3) Å
c	8.571(2) Å
V	1855.6(6) Å^3
D_c	1.464 g cm^{-3}
Z	4
$2\theta_{max}$	135.20°
hkl range	0 14, 0 22, 0 10
N	1931
N_{obs}	1808($I > 2\sigma(I)$)
N_{var}	247
Residuals: R, Rw	0.0339, 0.0967
GoF	0.975

References

1) Molecular Structure Corporation *teXsan: crystal structure analysis package*; **1985 &1992**, Molecular Structure Corporation: 3200 Research Forest Drive, The Woodlands, TX 77381, USA.

2) D. T. Cromer and J. T. Waber *International Tables for X-ray Crystallography*; The Kynoch Press: Birmingham, **1974**, Vol. IV.

3) J. A. Ibers and W. C. Hamilton *Acta Crystallogr.* **1964**, *17*, 781.

4) D. C. Creagh and W. J. McAuley *International Tables for Crystallography*; Kluwer Academic Publishers: Boston, **1992**, Vol. C.

5) D. C. Creagh and J. H. Hubbell *International Tables for Crystallography*; Kluwer Academic Publishers: Boston, **1992**, Vol. C.

6) P. T. Beurskens, G. Admiraal, G. Buerskens, W. P. Bosman, S. Garcia-Granda, R. O. Gould, J. M. M. Smits and C. Smykalla *PATTY. The DIRDIF program system. Technical Report of the Crystallography Laboratory, University of Nijmegen, The Netherlands*; **1992**, University of Nijmegen, The Netherlands.

7) P. T. Beurskens, G. Admiraal, G. Beurskens, W. P. Bosman, R. de Gelder, R. Israel and J. M. M. Smits *DIRDIF94. The DIRDIF-94 program system. Technical Report of the Crystallography Laboratory, University of Nijmegen, The Netherlands*; **1994**, University of Nijmegen, The Netherlands.

8) Molecular Structure Corporation *teXsan for Windows: Single Crystal Structure Analysis Software*; **1997-1998**, Molecular Structure Corporation: 3200 Research Forest Drive, The Woodlands, TX 77381, USA.

9) G. M. Sheldrick *SHELXS97. Program for crystal structure solution*; **1997**, University of Göttingen, Germany.

10) G. M. Sheldrick *SHELXL97. Program for crystal structure refinement*; **1997**, University of Göttingen, Germany.

11) H. D. Flack *Acta Crystallogr., Sect. A* **1983**, *A39*, 876-881.

12) G. Bernadelli and H. D. Flack *Acta Crystallogr., Sect. A* **1985**, *A41*, 500-511.

13) G. Davenport and H. Flack *LSQPL Xtal3.6 System*; S. R. Hall, D. J. du Boulay and R. Olthof-Hazekamp, Eds. **1999**, University of Western Australia.

14) G. M. Sheldrick *SADABS. Empirical absorption correction program for area detector data*; **1996**, University of Göttingen, Germany.

15) Bruker *SMART, SAINT and XPREP. Area detector control and data integration and reduction software*; **1995**, Bruker Analytical X-ray Instruments Inc.: Madison, Wisconsin, USA.

16) A. Altomare, M. Cascarano, C. Giacovazzo and A. Guagliardi *J. Appl. Cryst.* **1993**, *26*, 343.

17) Bruker *XSHELL. Graphical interface for crystal structure refinement*; **1995**, Bruker Analytical X-ray Intruments Inc.: Madison, Wisconsin, USA.

Appendix 2 NMR Spectra of Ni(II) Complexes

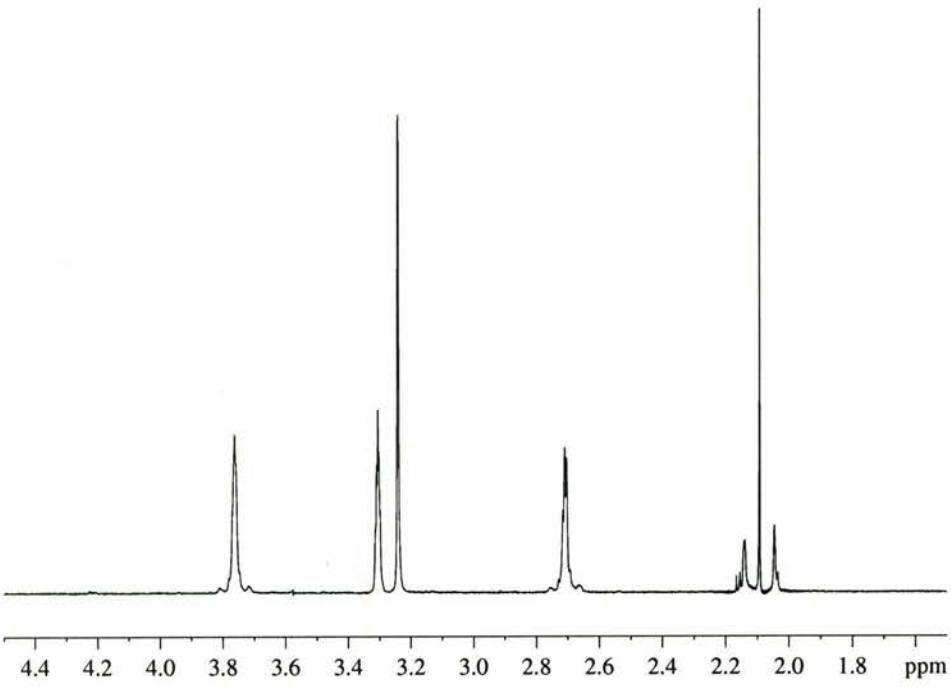

Figure A2.1 1D ^{1}H NMR spectrum of [Ni^{II}(bprolenH$_{-4}$)] in CD_3OD, decoupled at 2.09 ppm

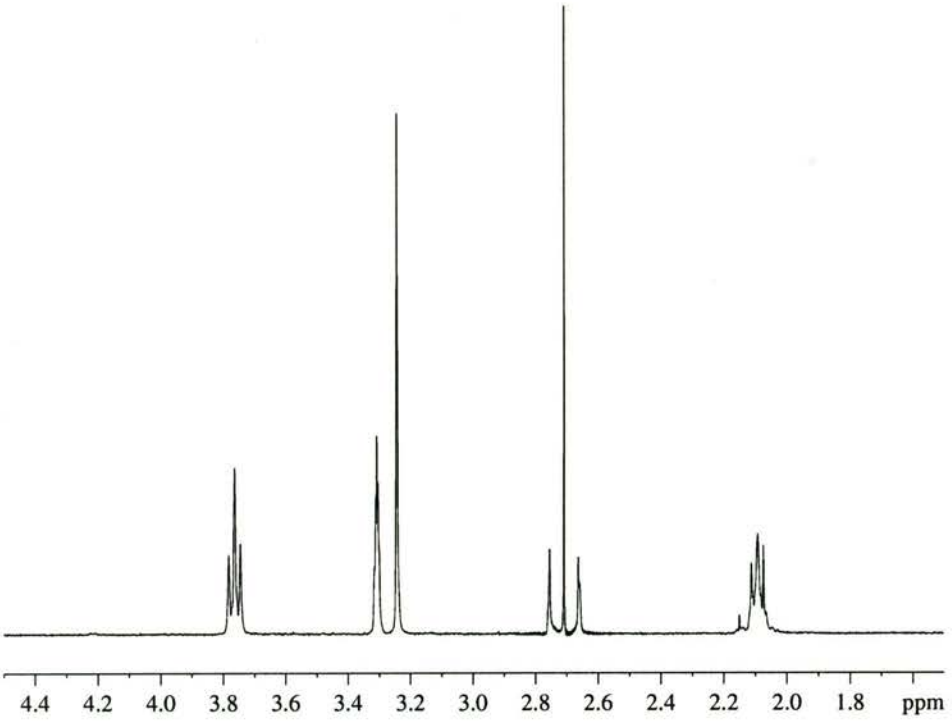

Figure A2.2 1D ^{1}H NMR spectrum of [Ni^{II}(bprolenH$_{-4}$)] in CD_3OD, decoupled at 2.71 ppm

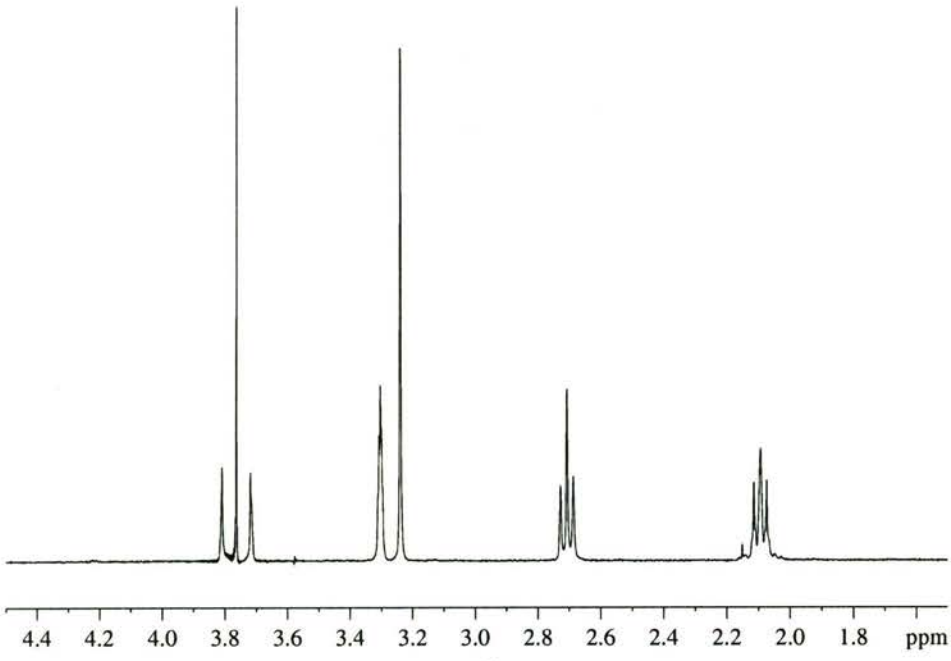

Figure A2.3 1D ^{1}H NMR spectrum of [Ni^{II}(bprolenH$_{-4}$)] in CD_3OD, decoupled at 3.76 ppm

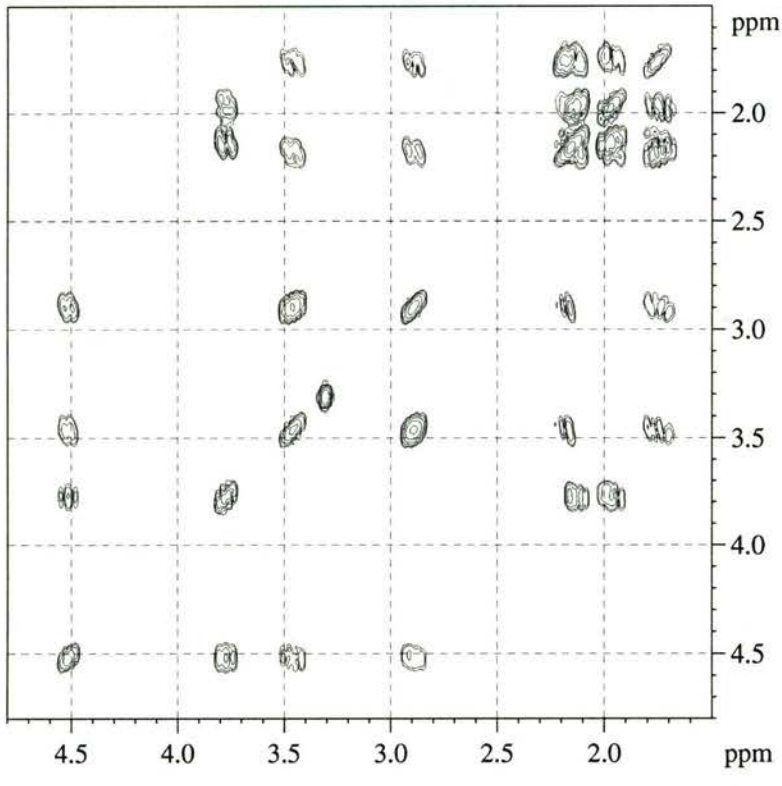

Figure A2.4 Expansion of the 2D COSY ^{1}H NMR spectrum of [Ni^{II}(*S,S*-brolben)] in CD_3OD from 1.5-4.8 ppm

Appendix 3 Supplementary XAFS Data

Table A3.1 Restraints used in the refinement of Model **III** of $Na_2[Cr^{V}_2O_4(S\text{-ala})_2(OCH_3)_2].0{\cdot}5CH_3OH.0{\cdot}5(S\text{-alaH})^a$

Restraints	
$S_0^2 \approx 0.9$ {0.2}	$\sigma^2_1 > 0.001$ {0.0005}
$\sigma^2_2 > 0.001$ {0.0005}	$\sigma^2_3 > 0.001$ {0.0005}
$\sigma^2_4 > 0.001$ {0.0005}	$\sigma^2_5 > 0.001$ {0.0005}
$\sigma^2_6 > 0.001$ {0.0005}	$\sigma^2_7 > 0.001$ {0.0005}
$\sigma^2_8 > 0.001$ {0.0005}	$\sigma^2_9 > 0.001$ {0.0005}
$\sigma^2_{10} > 0.001$ {0.0005}	$\sigma^2_{11} > 0.001$ {0.0005}
$\sigma^2_{12} > 0.001$ {0.0005}	$\sigma^2_{13} > 0.001$ {0.0005}
$\sigma^2_{14} > 0.001$ {0.0005}	$\sigma^2_{15} > 0.001$ {0.0005}
$\sigma^2_{16} > 0.001$ {0.0005}	$\sigma^2_{17} > 0.001$ {0.0005}
$\sigma^2_1 < 0.02$ {0.01}	$\sigma^2_2 < 0.02$ {0.01}
$\sigma^2_3 < 0.02$ {0.01}	$\sigma^2_4 < 0.02$ {0.01}
$\sigma^2_5 < 0.02$ {0.01}	$\sigma^2_6 < 0.03$ {0.01}
$\sigma^2_7 < 0.03$ {0.01}	$\sigma^2_8 < 0.03$ {0.01}
$\sigma^2_9 < 0.03$ {0.01}	$\sigma^2_{10} < 0.02$ {0.01}
$\sigma^2_{11} < 0.02$ {0.01}	$\sigma^2_{12} < 0.02$ {0.01}
$\sigma^2_{13} < 0.03$ {0.01}	$\sigma^2_{14} < 0.03$ {0.01}
$\sigma^2_{15} < 0.02$ {0.01}	$\sigma^2_{16} < 0.03$ {0.01}
$\sigma^2_{17} < 0.03$ {0.01}	$\sigma^2_6 > (\sigma^2_1 + 0.001)$ {0.0005}
$\sigma^2_7 > (\sigma^2_6 + 0.001)$ {0.0005}	$\sigma^2_8 > (\sigma^2_2 + 0.001)$ {0.0005}
$\sigma^2_9 > (\sigma^2_8 + 0.001)$ {0.0005}	$\sigma^2_{11} > (\sigma^2_{10} + 0.001)$ {0.0005}
$\sigma^2_{13} > (\sigma^2_{12} + 0.001)$ {0.0005}	$\sigma^2_{14} > (\sigma^2_{12} + 0.001)$ {0.0005}
$\sigma^2_{17} > (\sigma^2_{16} + 0.001)$ {0.0005}	Cr0–O1 ≈ 1.95 Å {0.2}
Cr0–N2 ≈ 2.05 Å {0.2}	Cr0–O3 ≈ 1.90 Å {0.3}
Cr0–O4 ≈ 1.90 Å {0.3}	Cr0–O5 ≈ 1.55 Å {0.1}
Cr0–O10 ≈ 1.90 Å {0.3}	C10–O11 ≈ 1.35 Å {0.2}
O1–C6 ≈ 1.30 Å {0.1}	N2–C8 ≈ 1.48 Å {0.1}
C6–O7 ≈ 1.22 Å {0.1}	C6–C8 ≈ 1.53 Å {0.05}
C8–C9 ≈ 1.50 Å {0.05}	Cr12–O13 ≈ Cr0–O1 {0.02}
Cr12–N14 ≈ Cr0–N2 {0.02}	Cr0–O4 ≈ Cr0–O3 {0.02}
Cr12–O3 ≈ Cr0–O3 {0.02}	Cr12–O4 ≈ Cr0–O3 {0.02}
Cr12–O15 ≈ Cr0–O5 {0.02}	Cr12–O16 ≈ Cr0–O10 {0.02}
C17–O10 ≈ C11–O10 {0.02}	Cr12–O10 ≈ Cr0–O16 {0.05}
Cr12–C11 ≈ Cr0–C17 {0.05}	Cr12–O5 ≈ Cr0–O15 {0.05}
O15–O13 ≈ O5–O1 {0.05}	O15–N14 ≈ O5–N2 {0.05}
O1–Cr0–N2 ≈ 81° {10}	O13–Cr12–N14 ≈ 81° {10}
O1–C6–O7 ≈ 124° {5}	N2–C8–C9 ≈ 114° {5}
O1–C6–C8 ≈ 116° {5}	N2–C8–C6 ≈ 109° {5}
O7–C6–C8 ≈ 120° {5}	C6–C8–O9 ≈ 113° {5}
Cr0–O10–C11 ≈ 120° {20}	Cr12–O16–C17 ≈ 120° {20}
N2–Cr0–O5 > 80° {2}	N14–Cr12–O15 > 80° {2}
O3–Cr0–O5 > 80° {2}	O3–Cr12–O15 > 80° {2}

O1–Cr0–O5 > 80° {2}	O13–Cr12–O15 > 80° {2}
O3–Cr12–O15 ≈ O3–Cr0–O5 {2}	O4–Cr12–O15 ≈ O4–Cr0–O5 {2}
O15–Cr12–O16 ≈ O5–Cr0–O10 {2}	Cr12–O16–C17 ≈ Cr0–O10–C11 {2}

[a] The ranges of the restraints are given in parentheses.

Table A3.2 Constraints used in the refinement of Model **III** of $Na_2[Cr^{V}{}_2O_4(S\text{-ala})_2(OCH_3)_2].0{\cdot}5CH_3OH.0{\cdot}5(S\text{-alaH})$

Constraints	
$-x0 = x12$	$y0 = y12$
$y0 = 0$	$z0 = z12$
$z0 = 0$	$-x1 = x13$
$y1 = y13$	$-x2 = x14$
$y2 = y14$	$x3 = x4$
$x3 = 0$	$-y3 = y4$
$z3 = z4$	$-x5 = x15$
$-y5 = y15$	$z5 = z15$
$-x10 = x16$	$-y10 = y16$
$z10 = z16$	$-x11 = x17$
$-y11 = y17$	$z11 = z17$
$\sigma^2{}_3 = \sigma^2{}_4$	

Table A3.3 Details of the SS and MS paths for Model **III** of $Na_2[Cr^{V}_2O_4(S\text{-ala})_2(OCH_3)_2].0{\cdot}5CH_3OH.0{\cdot}5(S\text{-alaH})$

Path No.	Atoms in MS pathway[a]	Degeneracy	R[b] (Å)	Importance factor[c]
1	Cr0→O5→Cr0	1	1.56	100
2	Cr0→O10→Cr0	1	1.74	69.0
3	Cr0→O4→Cr0	2	1.94	88.0
4	Cr0→O1→Cr0	1	1.96	41.4
5	Cr0→N2→Cr0	1	2.03	37.1
6	Cr0→C11→Cr0	1	2.68	18.2
7	Cr0→C6→Cr0	1	2.82	18.2
8	Cr0→C11→O10→Cr0	2	2.90	23.5
9	Cr0→O4→O5→Cr0	4	2.92	23.4
10	Cr0→C8→Cr0	1	2.94	10.7
11	Cr0→Cr12→Cr0	1	2.95	14.7
12	Cr0→O1→O5→Cr0	2	2.95	10.1
13	Cr0→N2→O5→Cr0	2	3.02	10.1
14	Cr0→C6→O1→Cr0	2	3.04	19.0
15	Cr0→O1→O10→Cr0	2	3.06	7.25
16	Cr0→O10→C11→O10→Cr0	1	3.10	6.83
17	Cr0→O5→Cr0→O5→Cr0	1	3.12	7.65
18	Cr0→O3→O4→Cr0	2	3.26	6.14
19	Cr0→O3→O10→Cr0	2	3.21	4.43
20	Cr0→C8→N2→Cr0	2	2.23	8.69
21	Cr0→O1→C6→O1→Cr0	1	3.25	5.17
22	Cr0→O5→O10→Cr0	2	3.28	25.8
23	Cr0→N2→O10→Cr0	2	3.29	4.62
24	Cr0→N2→O1→Cr0	2	2.29	5.05
25	Cr0→O5→Cr0→O10→Cr0	2	2.29	31.3
26	Cr0→O4→O10→Cr0	2	3.34	5.88
27	Cr0→O15→Cr0	1	3.40	12.1
28	Cr0→Cr12→O4→Cr0	4	3.41	13.2
29	Cr0→O1→O3→Cr0	2	3.45	3.91
30	Cr0→O10→Cr0→O10→Cr0	1	3.47	5.44
31	Cr0→N2→O4→Cr0	2	3.47	4.46
32	Cr0→O3→Cr0→O5→Cr0	4	3.50	3.13
33	Cr0→N2→C8→N2→Cr0	1	3.52	2.47
34	Cr0→C11→O1→Cr0	2	3.58	6.35
35	Cr0→O16→Cr0	1	3.58	11.0
36	Cr0→C8→O1→Cr0	2	3.65	6.05
37	Cr0→C8→C6→Cr0	2	3.65	7.38
38	Cr0→C6→N2→Cr0	2	3.65	7.67
39	Cr0→O4→Cr0→O10→Cr0	2	3.67	2.49
40	Cr0→O15→O3→Cr0	4	3.85	9.90
41	Cr0→C8→C6→O1→Cr0	2	3.86	1.28
42	Cr0→O4→Cr0→O4→Cr0	2	3.88	4.83

43	Cr0→O3→Cr12→O3→Cr0	2	3.88	3.60
44	Cr0→O4→O1→Cr0	2	3.88	17.7
45	Cr0→O4→Cr0→O1→Cr0	2	3.90	12.8
46	Cr0→O5→O3→O5→Cr0	2	3.91	5.28
47	Cr0→O1→Cr0→O1→Cr0	1	3.91	2.58
48	Cr0→O5→O1→O5→Cr0	1	3.94	2.74
49	Cr0→O15→Cr12→Cr0	2	3.95	7.08
50	Cr0→O3→N2→Cr0	2	3.96	17.6
51	Cr0→O3→Cr0→N2→Cr0	2	3.97	11.9
52	Cr0→O5→N2→O5→Cr0	1	4.00	2.74
53	Cr0→O7→Cr0	1	4.01	7.72
54	Cr0→O7→C6→Cr0	2	4.03	25.5
55	Cr0→C11→O10→C11→Cr0	1	4.04	4.07
56	Cr0→C6→O7→C6→Cr0	1	4.05	19.2
57	Cr0→N2→Cr0→N2→Cr0	1	4.07	2.12
58	Cr0→O7→O1→Cr0	2	4.10	13.0
59	Cr0→C6→O1→C6→Cr0	1	4.12	6.32
60	Cr0→C6→O7→O1→Cr0	2	4.12	19.8
61	Cr0→ C11→O5→Cr0	2	4.13	7.67
62	Cr0→O16→Cr12→Cr0	2	4.13	6.70
63	Cr0→O16→O4→Cr0	2	4.13	5.26
64	Cr0→O1→O7→O1→Cr0	1	4.19	6.20
65	Cr0→C11→Cr0→O5→Cr0	2	4.24	3.10
66	Cr0→O7→C6→O1→Cr0	2	4.25	14.6
67	Cr0→O4→O5→O4→Cr0	2	4.29	7.39
68	Cr0→O4→O15→O4→Cr0	2	4.29	2.73
69	Cr0→C11→N2→Cr0	2	4.29	2.20
70	Cr0→C17→Cr0	1	4.30	7.01
71	Cr0→O4→O5→O1→Cr0	2	4.31	3.63
72	Cr0→O5→C11→O10→Cr0	2	4.33	5.28
73	Cr0→O1→O5→O1→Cr0	1	4.34	3.36
74	Cr0→O3→O5→N2→Cr0	2	4.38	3.87
75	Cr0→O4→O3→O4→Cr0	2	4.39	5.43
76	Cr0→ C11→O4→Cr0	2	4.39	3.90
77	Cr0→C11→Cr0→O10→Cr0	2	4.42	2.22
78	Cr0→C8→N2→C8→Cr0	1	4.42	1.65
79	Cr0→C11→O10→O5→Cr0	2	4.44	3.45
80	Cr0→N2→O5→N2→Cr0	1	4.47	3.45
81	Cr0→C6→O3→Cr0	2	4.48	4.08
82	Cr0→O10→O3→O10→Cr0	1	4.48	2.71
83	Cr0→C11→O10→O4→Cr0	2	4.50	3.06
84	Cr0→C6→O1→O3→Cr0	2	4.54	3.29
85	Cr0→C8→O4→Cr0	2	4.57	2.90
86	Cr0→O10→C11→O4→Cr0	2	4.60	2.05
87	Cr0→C17→O16→Cr0	2	4.62	4.79
88	Cr0→O13→Cr0	1	4.64	3.93
89	Cr0→N14→Cr0	1	4.65	4.49

90	Cr0→C8→N2→O4→Cr0	2	4.66	2.18
91	Cr0→C17→O4→Cr0	2	4.67	4.13
92	Cr0→C11→O1→O10→Cr0	2	4.68	2.83
93	Cr0→O4→C6→Cr0	2	4.68	8.91
94	Cr0→O3→O10→O3→Cr0	1	4.69	1.99
95	Cr0→C6→O7→C8→Cr0	2	4.69	2.71
96	Cr0→C6→O1→C8→Cr0	2	4.73	4.16
97	Cr0→O10→O4→O10→Cr0	1	4.75	1.97
98	Cr0→C6→Cr0→O4→Cr0	2	4.76	3.96
99	Cr0→Cr12→O1→Cr0	2	4.77	2.91
100	Cr0→O13→Cr12→Cr0	2	4.77	4.07
101	Cr0→N14→O4→Cr0	2	4.78	6.45
102	Cr0→O3→C8→Cr0	2	4.79	5.24
103	Cr0→O13→O3→Cr0	2	4.80	5.25
104	Cr0→Cr12→N2→Cr0	2	4.81	2.71
105	Cr0→N14→Cr12→Cr0	2	4.81	4.24
106	Cr0→O5→O10→O5→Cr0	1	4.83	2.65
107	Cr0→N2→O10→N2→Cr0	1	4.84	1.74
108	Cr0→C8→N2→C6→Cr0	2	4.85	3.07
109	Cr0→O7→C6→C8→Cr0	2	4.85	2.95
110	Cr0→O16→O5→Cr0	2	4.86	2.25
111	Cr0→O15→O10→Cr0	2	4.86	2.46
112	Cr0→C8→Cr0→O3→Cr0	2	4.88	2.06
113	Cr0→Cr12→Cr0→O3→Cr0	4	4.89	1.76
114	Cr0→O4→C6→O1→Cr0	2	4.90	5.27
115	Cr0→C6→N2→O1→Cr0	2	4.91	2.20
116	Cr0→O4→N14→O4→Cr0	1	4.91	2.78
117	Cr0→Cr12→O13→O3→Cr0	2	4.93	2.96
118	Cr0→Cr12→N14→O4→Cr0	2	4.95	3.34
119	Cr0→O3→O13→O3→Cr0	1	4.95	2.17
120	Cr0→C6→O1→O4→Cr0	2	4.97	4.27
121	Cr0→C8→O1→N2→Cr0	2	4.98	1.79
122	Cr0→O10→O5→O10→Cr0	1	5.00	2.99
123	Cr0→C6→O5→O4→Cr0	2	5.01	2.99
124	Cr0→C6→O5→O1→Cr0	2	5.04	3.02
125	Cr0→O3→C8→N2→Cr0	2	5.08	2.72
126	Cr0→C8→O5→O3→Cr0	2	5.09	1.87
127	Cr0→C11→O3→O10→Cr0	2	5.13	2.56
128	Cr0→O15→O1→Cr0	2	5.15	3.46
129	Cr0→C8→N2→O3→Cr0	2	5.15	1.92
130	Cr0→O7→O1→C6→Cr0	2	5.18	5.16
131	Cr0→C8→O5→N2→Cr0	2	5.18	2.31
132	Cr0→O15→N2→Cr0	2	5.19	3.19
133	Cr0→O7→C6→O7→Cr0	1	5.24	4.19
134	Cr0→O13→Cr12→O3→Cr0	2	5.24	1.63
135	Cr0→C6→O10→O1→Cr0	2	5.27	2.87
136	Cr0→N14→Cr12→O3→Cr0	2	5.28	1.38

137	Cr0→O16→N2→Cr0	2	5.35	2.87
138	Cr0→O16→O1→Cr0	2	5.39	3.44
139	Cr0→O15→O5→O4→Cr0	4	5.40	2.32

[a] The atom numbering scheme is shown in Figure 5.16. [b] *R* is the total distance travelled by the photoelectron divided by two. [c] The importance factor is the percent contribution of a path relative to the strongest MS path and includes Debye-Waller contributions.

Table A3.4 Debye-Waller factors for Model **III** of

$Na_2[Cr^{V}{}_2O_4(S\text{-ala})_2(OCH_3)_2].0{\cdot}5CH_3OH.0{\cdot}5(S\text{-alaH})$[a]

atom	σ^2 (Å^2)	atom	σ^2 (Å^2)
O1	0.0010(1)	N2	0.0021(4)
O3	0.0010(1)	O4	0.0010(1)
O5	0.0032(2)	C6	0.0048(9)
O7	0.006(1)	C8	0.029(1)
C9	0.030(1)	O10	0.0010(1)
C11	0.019(1)	Cr12	0.0051(2)
O13	0.030(1)	N14	0.030(6)
O15	0.0013(2)	O16	0.0010(1)
C17	0.0020(1)		

[a] The Monte-Carlo errors in the last significant figure are given in parentheses.

Table A3.5 Restraints used in the refinement of Model **VIII** of *cis*-$[Cr^{III}(phen)_2(OH_2)_2](NO_3)_3.2{\cdot}5H_2O$[a]

Restraints	
$S_0^2 \approx 0.9$ {0.2}	$\sigma^2_1 > 0.001$ {0.0005}
$\sigma^2_2 > 0.001$ {0.0005}	$\sigma^2_3 > 0.001$ {0.0005}
$\sigma^2_4 > 0.001$ {0.0005}	$\sigma^2_5 > 0.001$ {0.0005}
$\sigma^2_6 > 0.001$ {0.0005}	$\sigma^2_7 > 0.001$ {0.0005}
$\sigma^2_8 > 0.001$ {0.0005}	$\sigma^2_9 > 0.001$ {0.0005}
$\sigma^2_{10} > 0.001$ {0.0005}	$\sigma^2_{11} > 0.001$ {0.0005}
$\sigma^2_{12} > 0.001$ {0.0005}	$\sigma^2_{13} > 0.001$ {0.0005}
$\sigma^2_{14} > 0.001$ {0.0005}	$\sigma^2_{15} > 0.001$ {0.0005}
$\sigma^2_{16} > 0.001$ {0.0005}	$\sigma^2_{17} > 0.001$ {0.0005}
$\sigma^2_{18} > 0.001$ {0.0005}	$\sigma^2_{19} > 0.001$ {0.0005}
$\sigma^2_{20} > 0.001$ {0.0005}	$\sigma^2_{21} > 0.001$ {0.0005}
$\sigma^2_{22} > 0.001$ {0.0005}	$\sigma^2_{23} > 0.001$ {0.0005}
$\sigma^2_{24} > 0.001$ {0.0005}	$\sigma^2_{25} > 0.001$ {0.0005}
$\sigma^2_{26} > 0.001$ {0.0005}	$\sigma^2_{27} > 0.001$ {0.0005}
$\sigma^2_{28} > 0.001$ {0.0005}	$\sigma^2_{29} > 0.001$ {0.0005}
$\sigma^2_{30} > 0.001$ {0.0005}	$\sigma^2_{31} > 0.001$ {0.0005}
$\sigma^2_{32} > 0.001$ {0.0005}	$\sigma^2_{33} > 0.001$ {0.0005}
$\sigma^2_{34} > 0.001$ {0.0005}	$\sigma^2_1 < 0.02$ {0.01}
$\sigma^2_2 < 0.02$ {0.01}	$\sigma^2_3 < 0.02$ {0.01}
$\sigma^2_4 < 0.02$ {0.01}	$\sigma^2_5 < 0.02$ {0.01}
$\sigma^2_6 < 0.03$ {0.01}	$\sigma^2_7 < 0.03$ {0.01}
$\sigma^2_8 < 0.03$ {0.01}	$\sigma^2_9 < 0.03$ {0.01}
$\sigma^2_{10} < 0.03$ {0.01}	$\sigma^2_{11} < 0.03$ {0.01}
$\sigma^2_{12} < 0.03$ {0.01}	$\sigma^2_{13} < 0.03$ {0.01}
$\sigma^2_{14} < 0.03$ {0.01}	$\sigma^2_{15} < 0.03$ {0.01}
$\sigma^2_{16} < 0.03$ {0.01}	$\sigma^2_{17} < 0.03$ {0.01}
$\sigma^2_{18} < 0.03$ {0.01}	$\sigma^2_{19} < 0.03$ {0.01}
$\sigma^2_{20} < 0.03$ {0.01}	$\sigma^2_{21} < 0.03$ {0.01}
$\sigma^2_{22} < 0.03$ {0.01}	$\sigma^2_{23} < 0.03$ {0.01}
$\sigma^2_{24} < 0.03$ {0.01}	$\sigma^2_{25} < 0.03$ {0.01}
$\sigma^2_{26} < 0.03$ {0.01}	$\sigma^2_{27} < 0.03$ {0.01}
$\sigma^2_{28} < 0.03$ {0.01}	$\sigma^2_{29} < 0.03$ {0.01}
$\sigma^2_{30} < 0.03$ {0.01}	$\sigma^2_{31} < 0.03$ {0.01}
$\sigma^2_{32} < 0.03$ {0.01}	$\sigma^2_{33} < 0.03$ {0.01}
$\sigma^2_{34} < 0.03$ {0.01}	$\sigma^2_7 > (\sigma^2_3 + 0.001)$ {0.0005}
$\sigma^2_8 > (\sigma^2_3 + 0.001)$ {0.0005}	$\sigma^2_9 > (\sigma^2_3 + 0.001)$ {0.0005}
$\sigma^2_{13} > (\sigma^2_3 + 0.001)$ {0.0005}	$\sigma^2_{18} > (\sigma^2_{13} + 0.001)$ {0.0005}
$\sigma^2_{17} > (\sigma^2_{18} + 0.001)$ {0.0005}	$\sigma^2_{31} > (\sigma^2_1 + 0.001)$ {0.0005}
$\sigma^2_{32} > (\sigma^2_1 + 0.001)$ {0.0005}	$\sigma^2_{33} > (\sigma^2_2 + 0.001)$ {0.0005}
$\sigma^2_{34} > (\sigma^2_2 + 0.001)$ {0.0005}	Cr0–O1 ≈ 1.95 Å {0.05}
Cr0–N3 ≈ 2.06 Å {0.05}	N3–C7 ≈ 1.33 Å {0.02}
N3–C13 ≈ 1.37 Å {0.02}	C7–C8 ≈ 1.40 Å {0.02}
C8–C9 ≈ 1.36 Å {0.02}	C9–C18 ≈ 1.40 Å {0.02}

C13–C18 ≈ 1.41 Å {0.02}	C13–C14 ≈ 1.42 Å {0.02}
C16–C17 ≈ 1.34 Å {0.02}	C17–C18 ≈ 1.43 Å {0.02}
Cr0–O31 ≈ 3.95 Å {0.05}	Cr0–O32 ≈ 3.93 Å {0.05}
Cr0–O33 ≈ 4.03 Å {0.05}	Cr0–O34 ≈ 3.88 Å {0.05}
O1–O31 ≈ 2.56 Å {0.05}	O1–O32 ≈ 2.66 Å {0.05}
O2–O33 ≈ 2.63 Å {0.05}	O2–O34 ≈ 2.63 Å {0.05}
Cr0–O2 ≈ Cr0–O1 {0.02}	Cr0–N4 ≈ Cr0–N3 {0.02}
Cr0–N5 ≈ Cr0–N3 {0.02}	Cr0–N6 ≈ Cr0–N3 {0.02}
N4–C10 ≈ N3–C7 {0.02}	N5–C25 ≈ N3–C7 {0.02}
N6–C28 ≈ N3–C7 {0.02}	C10–C11 ≈ C7–C8 {0.02}
C25–C26 ≈ C7–C8 {0.02}	C28–C29 ≈ C7–C8 {0.02}
N4–C14 ≈ N3–C13 {0.02}	N5–C19 ≈ N3–C13 {0.02}
N6–C20 ≈ N3–C13 {0.02}	C19–C20 ≈ C13–C14 {0.02}
C22–C23 ≈ C16–C17 {0.02}	C11–C12 ≈ C8–C9 {0.02}
C26–C27 ≈ C8–C9 {0.02}	C29–C30 ≈ C8–C9 {0.02}
C12–C15 ≈ C9–C18 {0.02}	C24–C27 ≈ C9–C19 {0.02}
C21–C30 ≈ C9–C18 {0.02}	C14–C15 ≈ C13–C18 {0.02}
C19–C24 ≈ C13–C18 {0.02}	C20–C21 ≈ C13–C18 {0.02}
C15–C16 ≈ C17–C18 {0.02}	C21–C22 ≈ C17–C18 {0.02}
C23–C24 ≈ C17–C18 {0.02}	O1–Cr0–O2 ≈ 89° {5}
O1–Cr0–N3 ≈ 92° {5}	O1–Cr0–N4 ≈ 172° {5}
O1–Cr0–N5 ≈ 92° {5}	O1–Cr0–N6 ≈ 91° {5}
O2–Cr0–N3 ≈ 95° {5}	O2–Cr0–N4 ≈ 89° {5}
O2–Cr0–N5 ≈ 172° {5}	O2–Cr0–N6 ≈ 92° {5}
N3–Cr0–N4 ≈ 80° {5}	N3–Cr0–N5 ≈ 93° {5}
N3–Cr0–N6 ≈ 173° {5}	N4–Cr0–N5 ≈ 91° {5}
N4–Cr0–N6 ≈ 97° {5}	Cr0–N3–C7 ≈ 128° {2}
Cr0–N3–C13 ≈ 113° {2}	C7–N3–C13 ≈ 118° {2}
N3–C7–C8 ≈ 122° {2}	C7–C8–C9 ≈ 120° {2}
C8–C9–C18 ≈ 120° {2}	N3–C13–C18 ≈ 123° {2}
N3–C13–C14 ≈ 117° {2}	C14–C13–C18 ≈ 120° {2}
C9–C18–C13 ≈ 117° {2}	C9–C18–C17 ≈ 125° {2}
C13–C18–C17 ≈ 118° {2}	C16–C17–C18 ≈ 122° {2}
Cr0–O1–O31 ≈ 121° {5}	Cr0–O1–O32 ≈ 116° {5}
Cr0–O2–O33 ≈ 122° {5}	Cr0–O2–O34 ≈ 114° {5}
N5–Cr0–N6 ≈ N3–Cr0–N4 {2}	Cr0–N4–C10 ≈ Cr0–N3–C7 {2}
Cr0–N5–C25 ≈ Cr0–N3–C7 {2}	Cr0–N6–C28 ≈ Cr0–N3–C7 {2}
Cr0–N4–C14 ≈ Cr0–N3–C13 {2}	Cr0–N5–C19 ≈ Cr0–N3–C13 {2}
Cr0–N6–C20 ≈ Cr0–N3–C13 {2}	C10–N4–C14 ≈ C7–N3–C13 {2}
C25–N5–C19 ≈ C7–N3–C13 {2}	C28–N6–C20 ≈ C7–N3–C13 {2}
N4–C10–C11 ≈ N3–C7–C8 {2}	N5–C25–C26 ≈ N3–C7–C8 {2}
N6–C28–C29 ≈ N3–C7–C8 {2}	C10–C11–C12 ≈ C7–C8–C9 {2}
C25–C26–C27 ≈ C7–C8–C9 {2}	C28–C29–C30 ≈ C7–C8–C9 {2}
C11–C12–C15 ≈ C8–C9–C18 {2}	C26–C27–C24 ≈ C8–C9–C18 {2}
C29–C30–C21 ≈ C8–C9–C18 {2}	N4–C14–C15 ≈ N3–C13–C18 {2}
N5–C19–C24 ≈ N3–C13–C18 {2}	N6–C20–C21 ≈ N3–C13–C18 {2}
N4–C14–C13 ≈ N3–C13–C14 {2}	N5–C19–C20 ≈ N3–C13–C14 {2}

N6–C20–C19 ≈ N3–C13–C14 {2}	C13–C14–C15 ≈ C14–C13–C18 {2}
C20–C19–C24 ≈ C14–C13–C18 {2}	C19–C20–C21 ≈ C14–C13–C18 {2}
C12–C15–C14 ≈ C9–C18–C13 {2}	C27–C24–C19 ≈ C9–C18–C13 {2}
C30–C21–C20 ≈ C9–C18–C13 {2}	C12–C15–C16 ≈ C9–C18–C17 {2}
C27–C24–C23 ≈ C9–C18–C17 {2}	C30–C21–C22 ≈ C9–C18–C17 {2}
C14–C15–C16 ≈ C13–C18–C17 {2}	C19–C24–C23 ≈ C13–C18–C17 {2}
C20–C21–C22 ≈ C13–C18–C17 {2}	C17–C16–C15 ≈ C16–C17–C18 {2}
C22–C23–C24 ≈ C16–C17–C18 {2}	C23–C22–C21 ≈ C16–C17–C18 {2}

Atoms restrained to be approximately coplanar:

((N3–N4)×(C13–N4))^.(C14–N4) ≈ 0 {0.01}
((N3–N4)×(C13–N4))^.(C7–N4) ≈ 0 {0.01}
((N3–N4)×(C13–N4))^.(C8–N4) ≈ 0 {0.01}
((N3–N4)×(C13–N4))^.(C9–N4) ≈ 0 {0.01}
((N3–N4)×(C13–N4))^.(C10–N4) ≈ 0 {0.01}
((N3–N4)×(C13–N4))^.(C11–N4) ≈ 0 {0.01}
((N3–N4)×(C13–N4))^.(C12–N4) ≈ 0 {0.01}
((N3–N4)×(C13–N4))^.(C15–N4) ≈ 0 {0.01}
((N3–N4)×(C13–N4))^.(C16–N4) ≈ 0 {0.01}
((N3–N4)×(C13–N4))^.(C17–N4) ≈ 0 {0.01}
((N3–N4)×(C13–N4))^.(C18–N4) ≈ 0 {0.01}
((N3–N4)×(C13–N4))^.(Cr0–N4) ≈ 0 {0.01}

((N5–C19)×(N6–C19))^.(C20–C19) ≈ 0 {0.01}
((N5–C19)×(N6–C19))^.(C21–C19) ≈ 0 {0.01}
((N5–C19)×(N6–C19))^.(C22–C19) ≈ 0 {0.01}
((N5–C19)×(N6–C19))^.(C23–C19) ≈ 0 {0.01}
((N5–C19)×(N6–C19))^.(C24–C19) ≈ 0 {0.01}
((N5–C19)×(N6–C19))^.(C25–C19) ≈ 0 {0.01}
((N5–C19)×(N6–C19))^.(C26–C19) ≈ 0 {0.01}
((N5–C19)×(N6–C19))^.(C27–C19) ≈ 0 {0.01}
((N5–C19)×(N6–C19))^.(C28–C19) ≈ 0 {0.01}
((N5–C19)×(N6–C19))^.(C29–C19) ≈ 0 {0.01}
((N5–C19)×(N6–C19))^.(C30–C19) ≈ 0 {0.01}
((N5–C19)×(N6–C19))^.(Cr0–C19) ≈ 0 {0.01}

[a] The ranges of the restraints are given in parentheses.

Table A3.6 Constraints used in the refinement of Model **VIII** of *cis*-$[Cr^{III}(phen)_2(OH_2)_2](NO_3)_3.2{\cdot}5H_2O$

Constraints	
$\sigma^2_1 = \sigma^2_2$	$\sigma^2_4 = \sigma^2_3$
$\sigma^2_5 = \sigma^2_3$	$\sigma^2_6 = \sigma^2_3$
$\sigma^2_{10} = \sigma^2_7$	$\sigma^2_{25} = \sigma^2_7$
$\sigma^2_{28} = \sigma^2_7$	$\sigma^2_{11} = \sigma^2_8$
$\sigma^2_{26} = \sigma^2_8$	$\sigma^2_{29} = \sigma^2_8$
$\sigma^2_{12} = \sigma^2_9$	$\sigma^2_{27} = \sigma^2_9$
$\sigma^2_{30} = \sigma^2_9$	$\sigma^2_{14} = \sigma^2_{13}$
$\sigma^2_{19} = \sigma^2_{13}$	$\sigma^2_{20} = \sigma^2_{13}$
$\sigma^2_{18} = \sigma^2_{15}$	$\sigma^2_{21} = \sigma^2_{15}$
$\sigma^2_{24} = \sigma^2_{15}$	$\sigma^2_{17} = \sigma^2_{16}$
$\sigma^2_{22} = \sigma^2_{16}$	$\sigma^2_{23} = \sigma^2_{16}$
$x1 = x2$	$y1 = -y2$
$z1 = -z2$	$x3 = x6$
$y3 = -y6$	$z3 = -z6$
$z3 = -z4$	$z3 = z5$
$x4 = x5$	$x3 = x4$
$z13 = -z14$	$y4 = -y5$
$z13 = -z20$	$z13 = z19$
$y14 = -y19$	$x14 = x19$
$y13 = -y20$	$x13 = x20$
$z15 = -z18$	$z15 = z21$
$x15 = x24$	$z15 = -z24$
$x18 = x21$	$y15 = -y24$
$z16 = -z17$	$y18 = -y21$
$z16 = -z23$	$z16 = z22$
$y16 = -y23$	$x16 = x23$
$y17 = -y22$	$x17 = x22$
$y7 = -y28$	$x7 = x28$
$x8 = x29$	$z7 = -z28$
$z8 = -z29$	$y8 = -y29$
$y9 = -y30$	$x9 = x30$
$x10 = x25$	$z9 = -z30$
$z10 = -z25$	$y10 = -y25$
$y11 = -y26$	$x11 = x26$
$x12 = x27$	$z11 = -z26$
$z12 = -z27$	$y12 = -y27$

Table A3.7 Details of the SS and MS paths for Model **VIII** of *cis*-$[Cr^{III}(phen)_2(OH_2)_2](NO_3)_3.2{\cdot}5H_2O$

Path No.	Atoms in MS pathway[a]	Degeneracy	R[b] (Å)	Importance factor[c]
1	Cr0→O1→Cr0	2	1.93	100
2	Cr0→N4→Cr0	4	2.05	100
3	Cr0→C20→Cr0	4	2.89	41.2
4	Cr0→C25→Cr0	2	3.06	22.5
5	Cr0→C28→Cr0	2	3.06	22.5
6	Cr0→C20→N6→Cr0	8	3.15	28.6
7	Cr0→C25→N5→Cr0	4	3.22	27.2
8	Cr0→C7→N3→Cr0	4	3.22	27.3
9	Cr0→N4→N3→Cr0	4	3.37	6.91
10	Cr0→N5→C25→N5→Cr0	4	3.38	22.2
11	Cr0→N5→O1→Cr0	4	3.41	5.90
12	Cr0→N6→C20→N6→Cr0	2	3.42	3.02
13	Cr0→N4→C14→N4→Cr0	2	3.42	3.03
14	Cr0→N6→O2→Cr0	4	3.43	5.69
15	Cr0→N3→O2→Cr0	4	3.44	5.54
16	Cr0→N4→N6→Cr0	4	3.57	4.72
17	Cr0→C19→C20→Cr0	4	3.60	9.02
18	Cr0→C20→N5→Cr0	4	3.66	7.19
19	Cr0→C19→N6→Cr0	4	3.66	7.19
20	Cr0→O1→Cr0→O1→Cr0	2	3.87	4.14
21	Cr0→O34→Cr0	1	3.87	5.63
22	Cr0→O32→Cr0	1	3.93	5.98
23	Cr0→O31→Cr0	1	3.94	5.51
24	Cr0→O2→N5→Cr0	4	3.98	19.8
25	Cr0→O2→Cr0→N5→Cr0	4	3.99	25.0
26	Cr0→O33→Cr0	1	4.02	5.24
27	Cr0→N6→N3→Cr0	2	4.10	9.08
28	Cr0→N6→Cr0→N3→Cr0	2	4.11	12.8
29	Cr0→N5→Cr0→N5→Cr0	4	4.11	8.33
30	Cr0→C7→C13→Cr0	4	4.13	3.11
31	Cr0→C25→C19→Cr0	4	4.13	3.11
32	Cr0→O31→O1→Cr0	2	4.22	4.30
33	Cr0→O34→O2→Cr0	2	4.22	3.54
34	Cr0→C15→Cr0	4	4.26	18.4
35	Cr0→C13→N3→C13→Cr0	2	4.26	3.62
36	Cr0→C19→N5→C19→Cr0	2	4.26	3.61
37	Cr0→O32→O1→Cr0	2	4.26	3.78
38	Cr0→C21→C20→Cr0	4	4.27	19.6
39	Cr0→C24→C19→Cr0	4	4.27	19.6
40	Cr0→N4→C10→C14→Cr0	4	4.29	4.31
41	Cr0→N6→C28→C20→Cr0	4	4.29	4.31
42	Cr0→C13→C18→C13→Cr0	2	4.29	14.9

43	Cr0→C14→C15→C14→Cr0	2	4.29	14.9
44	Cr0→O33→O2→Cr0	2	4.29	4.03
45	Cr0→C28→N6→C20→Cr0	4	4.32	5.23
46	Cr0→C25→N5→C19→Cr0	4	4.32	5.23
47	Cr0→C26→Cr0	2	4.36	6.20
48	Cr0→C29→Cr0	2	4.36	6.19
49	Cr0→C15→N4→Cr0	4	4.38	11.2
50	Cr0→C21→N6→Cr0	4	4.38	11.2
51	Cr0→C25→N5→C25→Cr0	2	4.39	4.68
52	Cr0→C28→N6→C28→Cr0	2	4.39	4.68
53	Cr0→C13→C18→N3→Cr0	4	4.39	15.4
54	Cr0→C19→C24→N5→Cr0	4	4.39	15.4
55	Cr0→C26→N5→Cr0	4	4.40	9.80
56	Cr0→C29→N6→Cr0	4	4.40	9.80
57	Cr0→N6→C20→C28→Cr0	4	4.40	3.14
58	Cr0→N5→C19→C25→Cr0	4	4.40	3.14
59	Cr0→C11→C10→Cr0	4	4.41	10.2
60	Cr0→C29→C28→Cr0	4	4.41	10.2
61	Cr0→N3→C8→N3→Cr0	4	4.44	10.9
62	Cr0→C25→C26→N5→Cr0	4	4.45	11.3
63	Cr0→C7→C8→N3→Cr0	4	4.45	11.3
64	Cr0→C10→C11→C10→Cr0	2	4.46	6.81
65	Cr0→C28→C29→C28→Cr0	2	4.46	6.80
66	Cr0→N4→C10→N4→C14→Cr0	4	4.48	6.99
67	Cr0→N6→C28→N6→C20→Cr0	4	4.48	6.99
68	Cr0→C13→O1→Cr0	4	4.49	4.16
69	Cr0→N6→C21→N6→Cr0	4	4.49	9.65
70	Cr0→C13→N3→C13→N3→Cr0	4	4.52	4.46
71	Cr0→C14→N4→C14→N4→Cr0	4	4.52	4.45
72	Cr0→C13→N3→O1→Cr0	4	4.53	3.49
73	Cr0→C15→C14→N4→Cr0	4	4.54	9.17
74	Cr0→C21→C20→N6→Cr0	4	4.54	9.18
75	Cr0→C25→N5→C25→N5→Cr0	4	4.55	8.43
76	Cr0→C7→N3→C7→N3→Cr0	4	4.55	8.33
77	Cr0→N4→C10→C14→N4→Cr0	4	4.56	4.81
78	Cr0→N3→C7→C13→N3→Cr0	4	4.56	4.81
79	Cr0→C20→C21→C20→N6→Cr0	4	4.56	12.5
80	Cr0→C14→C15→C14→N4→Cr0	4	4.56	12.5
81	Cr0→C11→C10→N4→Cr0	4	4.57	7.35
82	Cr0→C8→C7→N3→Cr0	4	4.57	7.34
83	Cr0→N6→C20→N6→C28→Cr0	4	4.59	4.63
84	Cr0→N4→C14→N4→C10→Cr0	4	4.59	4.63
85	Cr0→N4→C11→C10→N4→Cr0	8	4.61	17.9
86	Cr0→C10→C11→C10→N4→Cr0	4	4.62	8.95
87	Cr0→C7→C8→C7→N3→Cr0	4	4.62	8.95
88	Cr0→C14→N6→Cr0	4	4.63	4.70
89	Cr0→N6→C21→C20→N6→Cr0	4	4.66	8.47

90	Cr0→N5→C24→C19→N5→Cr0	4	4.66	8.46
91	Cr0→C19→N5→N3→Cr0	4	4.67	4.68
92	Cr0→N4→N3→N4→Cr0	4	4.70	4.10
93	Cr0→N4→C10→N3→Cr0	8	4.70	5.93
94	Cr0→N4→C10→N4→N3→Cr0	8	4.70	10.3
95	Cr0→C14→O1→Cr0	4	4.72	7.75
96	Cr0→C19→N5→C20→Cr0	4	4.76	4.41
97	Cr0→C20→N6→C19→Cr0	4	4.76	4.41
98	Cr0→C19→C24→C20→Cr0	4	4.82	2.94
99	Cr0→C13→C18→C14→Cr0	4	4.82	2.94
100	Cr0→C19→Cr0→O2→Cr0	4	4.82	5.93
101	Cr0→C27→Cr0	2	4.83	6.96
102	Cr0→C30→Cr0	2	4.83	6.96
103	Cr0→C27→N6→Cr0	4	4.83	15.6
104	Cr0→C9→N3→Cr0	4	4.83	15.6
105	Cr0→N5→C27→N5→Cr0	2	4.84	8.89
106	Cr0→N6→C30→N6→Cr0	2	4.84	8.88
107	Cr0→N3→C20→Cr0	4	4.85	7.31
108	Cr0→N5→C25→C20→Cr0	8	4.93	5.72
109	Cr0→C13→Cr0→N6→Cr0	4	4.94	6.76
110	Cr0→C13→N4→N3→Cr0	4	4.98	2.79
111	Cr0→C19→N6→N5→Cr0	4	4.98	2.78
112	Cr0→O1→C10→Cr0	4	4.98	9.06
113	Cr0→N4→C10→N4→C13→Cr0	4	4.98	5.01
114	Cr0→N6→C28→N6→C19→Cr0	4	4.98	5.01
115	Cr0→O2→C19→N5→Cr0	4	4.99	3.62
116	Cr0→O2→Cr0→C25→Cr0	4	4.99	11.5
117	Cr0→C27→C19→Cr0	4	5.05	5.79
118	Cr0→C9→C13→Cr0	4	5.05	5.79
119	Cr0→C14→C12→N4→Cr0	4	5.06	7.05
120	Cr0→C13→C9→N3→Cr0	4	5.06	7.04
121	Cr0→N6→N4→N6→Cr0	4	5.08	4.85
122	Cr0→C14→C15→C13→N3→Cr0	4	5.08	3.31
123	Cr0→C20→C21→C19→N5→Cr0	4	5.08	3.31
124	Cr0→C14→N4→Cr0→O1→Cr0	4	5.09	3.31
125	Cr0→O1→Cr0→C14→N4→Cr0	4	5.09	2.56
126	Cr0→N6→C7→Cr0	4	5.09	9.56
127	Cr0→N6→Cr0→C7→Cr0	4	5.12	10.6
128	Cr0→N3→C20→N6→Cr0	4	5.12	3.25
129	Cr0→C27→C25→Cr0	4	5.14	4.09
130	Cr0→O2→C25→N5→Cr0	4	5.14	5.65
131	Cr0→C30→C28→Cr0	4	5.14	4.08
132	Cr0→N4→C12→C10→Cr0	4	5.15	5.28
133	Cr0→N3→C9→C7→Cr0	4	5.15	5.27
134	Cr0→O2→N5→C25→Cr0	4	5.15	5.32
135	Cr0→O1→Cr0→N4→C10→Cr0	4	5.15	7.80
136	Cr0→O2→Cr0→C25→N5→Cr0	4	5.15	7.45

137	Cr0→N3→C7→C18→Cr0	8	5.20	7.05
138	Cr0→C20→N6→N3→Cr0	4	5.20	2.49
139	Cr0→C20→N6→Cr0→N3→Cr0	4	5.21	3.90
140	Cr0→N6→Cr0→C13→N3→Cr0	4	5.21	2.90
141	Cr0→C9→C18→Cr0	4	5.24	2.64
142	Cr0→C27→C24→Cr0	4	5.24	2.64
143	Cr0→N6→C7→N3→Cr0	4	5.25	6.19
144	Cr0→C30→C21→C20→Cr0	4	5.26	3.66
145	Cr0→C27→C24→C19→Cr0	4	5.26	3.66
146	Cr0→C14→C15→C12→N4→Cr0	4	5.27	4.13
147	Cr0→C20→C21→C30→N6→Cr0	4	5.27	4.13
148	Cr0→C22→Cr0	2	5.27	5.16
149	Cr0→C16→Cr0	2	5.27	5.15
150	Cr0→N3→N6→C28→Cr0	4	5.27	5.81
151	Cr0→C7→N3→Cr0→N6→Cr0	4	5.28	8.01
152	Cr0→N3→C7→Cr0→N6→Cr0	4	5.28	7.56
153	Cr0→C22→C20→Cr0	4	5.30	9.87
154	Cr0→C16→C14→Cr0	4	5.30	9.87
155	Cr0→N4→C10→N4→O1→Cr0	4	5.31	4.60
156	Cr0→C19→C23→C19→Cr0	2	5.32	3.58
157	Cr0→C13→C17→C13→Cr0	2	5.32	3.58
158	Cr0→N5→C24→C25→N5→Cr0	8	5.32	5.77
159	Cr0→C27→C26→C25→Cr0	4	5.33	2.43
160	Cr0→C30→C29→C28→Cr0	4	5.33	2.42
161	Cr0→N4→C12→C11→C10→Cr0	4	5.33	3.36
162	Cr0→N6→C30→C29→C28→Cr0	4	5.33	3.36
163	Cr0→N3→C7→N3→N6→Cr0	4	5.43	5.32
164	Cr0→C21→N6→C20→Cr0	4	5.48	3.85
165	Cr0→C22→C19→Cr0	4	5.48	5.13
166	Cr0→C24→N5→C19→Cr0	4	5.48	3.85
167	Cr0→C16→C13→Cr0	4	5.48	5.12
168	Cr0→C17→C18→Cr0	4	5.48	5.21
169	Cr0→C16→C15→Cr0	4	5.48	5.21
170	Cr0→C13→C18→N3→C13→Cr0	4	5.49	5.09
171	Cr0→C19→C24→N5→C19→Cr0	4	5.50	5.09
172	Cr0→C17→C18→C13→Cr0	4	5.50	4.57
173	Cr0→C23→C24→C19→Cr0	4	5.50	4.57
174	Cr0→C14→C16→C13→Cr0	4	5.50	3.70
175	Cr0→C13→C17→C14→Cr0	4	5.50	3.70

[a] The atom numbering scheme is shown in Figure 5.20. [b] *R* is the total distance travelled by the photoelectron divided by two. [c] The importance factor is the percent contribution of a path relative to the strongest MS path and includes Debye-Waller contributions.

Table A3.8 Debye-Waller factors for Model **VIII** of

cis-$[Cr^{III}(phen)_2(OH_2)_2](NO_3)_3.2{\cdot}5H_2O$[a]

atom	σ^2 (Å^2)	atom	σ^2 (Å^2)
O1	0.0020(1)	N3	0.0010(1)
C7	0.0062(5)	C8	0.0300(1)
C9	0.0029(2)	C13	0.0084(3)
C17	0.0104(3)	C18	0.0094(3)

[a] The Monte-Carlo errors in the last significant figure are given in parentheses.

Table A3.9 Restraints used in the refinement of Model **XA** of *trans*-$[Cr^{III}(bpb)(OH_2)_2]ClO_4.H_2O$[a]

Restraints	
$S_0^2 \approx 0.9$ {0.2}	$\sigma^2_1 > 0.001$ {0.0005}
$\sigma^2_2 > 0.001$ {0.0005}	$\sigma^2_3 > 0.001$ {0.0005}
$\sigma^2_4 > 0.001$ {0.0005}	$\sigma^2_5 > 0.001$ {0.0005}
$\sigma^2_6 > 0.001$ {0.0005}	$\sigma^2_7 > 0.001$ {0.0005}
$\sigma^2_8 > 0.001$ {0.0005}	$\sigma^2_9 > 0.001$ {0.0005}
$\sigma^2_{10} > 0.001$ {0.0005}	$\sigma^2_{11} > 0.001$ {0.0005}
$\sigma^2_{12} > 0.001$ {0.0005}	$\sigma^2_{13} > 0.001$ {0.0005}
$\sigma^2_{14} > 0.001$ {0.0005}	$\sigma^2_{15} > 0.001$ {0.0005}
$\sigma^2_{16} > 0.001$ {0.0005}	$\sigma^2_{17} > 0.001$ {0.0005}
$\sigma^2_{18} > 0.001$ {0.0005}	$\sigma^2_{19} > 0.001$ {0.0005}
$\sigma^2_{20} > 0.001$ {0.0005}	$\sigma^2_{21} > 0.001$ {0.0005}
$\sigma^2_{22} > 0.001$ {0.0005}	$\sigma^2_{23} > 0.001$ {0.0005}
$\sigma^2_{24} > 0.001$ {0.0005}	$\sigma^2_{25} > 0.001$ {0.0005}
$\sigma^2_{26} > 0.001$ {0.0005}	$\sigma^2_1 < 0.02$ {0.01}
$\sigma^2_2 < 0.02$ {0.01}	$\sigma^2_3 < 0.02$ {0.01}
$\sigma^2_4 < 0.02$ {0.01}	$\sigma^2_5 < 0.02$ {0.01}
$\sigma^2_6 < 0.02$ {0.01}	$\sigma^2_7 < 0.02$ {0.01}
$\sigma^2_8 < 0.02$ {0.01}	$\sigma^2_9 < 0.02$ {0.01}
$\sigma^2_{10} < 0.02$ {0.01}	$\sigma^2_{11} < 0.02$ {0.01}
$\sigma^2_{12} < 0.02$ {0.01}	$\sigma^2_{13} < 0.03$ {0.01}
$\sigma^2_{14} < 0.03$ {0.01}	$\sigma^2_{15} < 0.03$ {0.01}
$\sigma^2_{16} < 0.03$ {0.01}	$\sigma^2_{17} < 0.02$ {0.01}
$\sigma^2_{18} < 0.03$ {0.01}	$\sigma^2_{19} < 0.03$ {0.01}
$\sigma^2_{20} < 0.03$ {0.01}	$\sigma^2_{21} < 0.02$ {0.01}
$\sigma^2_{22} < 0.02$ {0.01}	$\sigma^2_{23} < 0.03$ {0.01}
$\sigma^2_{24} < 0.03$ {0.01}	$\sigma^2_{25} < 0.03$ {0.01}
$\sigma^2_{26} < 0.02$ {0.01}	$\sigma^2_7 > (\sigma^2_2 + 0.001)$ {0.0005}
$\sigma^2_{13} > (\sigma^2_7 + 0.001)$ {0.0005}	$\sigma^2_{14} > (\sigma^2_{13} + 0.001)$ {0.0005}
$\sigma^2_{17} > (\sigma^2_1 + 0.001)$ {0.0005}	$\sigma^2_{18} > (\sigma^2_1 + 0.001)$ {0.0005}
$\sigma^2_{20} > (\sigma^2_1 + 0.001)$ {0.0005}	$\sigma^2_{21} > (\sigma^2_1 + 0.001)$ {0.0005}
$\sigma^2_{19} > (\sigma^2_{18} + 0.001)$ {0.0005}	$\sigma^2_{11} > (\sigma^2_9 + 0.001)$ {0.0005}
N1–C17 ≈ 1.35 Å {0.05}	N1–C21 ≈ 1.34 Å {0.05}
C17–C18 ≈ 1.38 Å {0.05}	C18–C19 ≈ 1.38 Å {0.05}
C19–C20 ≈ 1.36 Å {0.05}	C20–C21 ≈ 1.37 Å {0.05}
N2–C7 ≈ 1.41 Å {0.05}	N2–C9 ≈ 1.34 Å {0.05}
C9–O11 ≈ 1.23 Å {0.05}	C9–C17 ≈ 1.50 Å {0.05}
C7–C8 ≈ 1.42 Å {0.05}	C7–C13 ≈ 1.39 Å {0.05}
C13–C14 ≈ 1.38 Å {0.05}	C14–C15 ≈ 1.38 Å {0.05}
Cr0–O5 < 3.0 {0.1}	Cr0–O6 < 3.0 {0.1}
N1–Cr0–N2 ≈ 81° {10}	N1–Cr0–N4 ≈ 108° {10}
N2–Cr0–N3 ≈ 82° {10}	Cr0–N1–C17 ≈ 112° {5}
Cr0–N1–C21 ≈ 129° {5}	C17–N1–C21 ≈ 118° {5}
Cr0–N2–C7 ≈ 114° {5}	Cr0–N2–C9 ≈ 119° {5}

C7–N2–C9 ≈ 126° {5}	N2–C9–O11 ≈ 129° {5}
N2–C9–C17 ≈ 110° {5}	O11–C9–C17 ≈ 120° {5}
N2–C7–C8 ≈ 115° {5}	N2–C7–C13 ≈ 126° {5}
C8–C7–C13 ≈ 120° {5}	N1–C17–C9 ≈ 117° {5}
N1–C17–C18 ≈ 121° {5}	C9–C17–C18 ≈ 121° {5}
N1–C21–C20 ≈ 122° {5}	C17–C18–C19 ≈ 119° {5}
C18–C19–C20 ≈ 119° {5}	C19–C20–C21 ≈ 119° {5}
C7–C13–C14 ≈ 120° {5}	C13–C14–C13 ≈ 120° {5}
O5–Cr0–N1 > 80 {1}	O5–Cr0–N2 > 80 {1}
O5–Cr0–N3 > 80 {1}	O5–Cr0–N4 > 80 {1}
O6–Cr0–N1 > 80 {1}	O6–Cr0–N2 > 80 {1}
O6–Cr0–N3 > 80 {1}	O6–Cr0–N4 > 80 {1}
Atoms restrained to be approximately coplanar:	
((C7–C13)×(C8–C13))^.(C14–C13) ≈ 0 {0.01}	
((C7–C13)×(C8–C13))^.(C15–C13) ≈ 0 {0.01}	
((C7–C13)×(C8–C13))^.(C16–C13) ≈ 0 {0.01}	
((C7–C13)×(C8–C13))^.(N2–C13) ≈ 0 {0.01}	
((C7–C13)×(C8–C13))^.(N3–C13) ≈ 0 {0.01}	
((C7–C13)×(C8–C13))^.(C9–C13) ≈ 0 {0.01}	
((C7–C13)×(C8–C13))^.(C10–C13) ≈ 0 {0.01}	
((C7–C13)×(C8–C13))^.(O11–C13) ≈ 0 {0.01}	
((C7–C13)×(C8–C13))^.(O12–C13) ≈ 0 {0.01}	
((N1–C17)×(C18–C17))^.(C19–C17) ≈ 0 {0.01}	
((N1–C17)×(C18–C17))^.(C20–C17) ≈ 0 {0.01}	
((N1–C17)×(C18–C17))^.(C21–C17) ≈ 0 {0.01}	

[a] The ranges of the restraints are given in parentheses.

Table A3.10 Constraints used in the refinement of Model **XA** of *trans*-$[Cr^{III}(bpb)(OH_2)_2]ClO_4.H_2O$

Constraints	
$\sigma^2_1 = \sigma^2_4$	$\sigma^2_2 = \sigma^2_3$
$\sigma^2_7 = \sigma^2_8$	$\sigma^2_9 = \sigma^2_{10}$
$\sigma^2_{11} = \sigma^2_{12}$	$\sigma^2_{13} = \sigma^2_{16}$
$\sigma^2_{14} = \sigma^2_{15}$	$\sigma^2_{17} = \sigma^2_{22}$
$\sigma^2_{18} = \sigma^2_{23}$	$\sigma^2_{19} = \sigma^2_{24}$
$\sigma^2_{20} = \sigma^2_{25}$	$\sigma^2_{21} = \sigma^2_{26}$
$x1 = x4$	$y1 = -y4$
$z1 = z4$	$x2 = x3$
$y2 = -y3$	$z2 = z3$
$x7 = x8$	$y7 = -y8$
$z7 = z8$	$x9 = x10$
$y9 = -y10$	$z9 = z10$
$x11 = x12$	$y11 = -y12$
$z11 = z12$	$x13 = x16$
$y13 = -y16$	$z13 = z16$
$x14 = x15$	$y14 = -y15$
$z14 = z15$	$x17 = x22$
$y17 = -y22$	$z17 = z22$
$x18 = x23$	$y18 = -y23$
$z18 = z23$	$x19 = x24$
$y19 = -y24$	$z19 = z24$
$x20 = x25$	$y20 = -y25$
$z20 = z25$	$x21 = x26$
$y21 = -y26$	$z21 = z26$

Table A3.11 Details of the SS and MS paths for Model **XA** of *trans*-$[Cr^{III}(bpb)(OH_2)_2]ClO_4.H_2O$

Path No.	Atoms in MS pathway[a]	Degeneracy	R[b] (Å)	Importance factor[c]
1	Cr0→N2→Cr0	2	1.94	100
2	Cr0→O5→Cr0	1	1.95	49.9
3	Cr0→O6→Cr0	1	2.03	51.4
4	Cr0→N1→Cr0	2	2.07	96.2
5	Cr0→C7→Cr0	2	2.82	26.0
6	Cr0→C10→Cr0	2	2.87	44.6
7	Cr0→C22→Cr0	2	2.87	42.3
8	Cr0→C7→N2→Cr0	4	3.08	16.2
9	Cr0→C9→N2→Cr0	4	3.08	31.8
10	Cr0→C26→Cr0	2	3.10	32.8
11	Cr0→C17→N1→Cr0	4	3.15	23.0
12	Cr0→O5→N3→Cr0	2	3.19	5.11
13	Cr0→N2→N3→Cr0	2	3.23	4.77
14	Cr0→O6→N3→Cr0	2	3.26	10.5
15	Cr0→C26→N4→Cr0	4	3.26	38.5
16	Cr0→N4→N3→Cr0	4	3.28	10.1
17	Cr0→N2→C9→N2→Cr0	2	3.29	7.81
18	Cr0→O5→N2→Cr0	2	3.30	4.34
19	Cr0→N2→C7→N2→Cr0	2	3.35	2.73
20	Cr0→N4→O6→Cr0	4	3.37	10.0
21	Cr0→N4→C26→N4→Cr0	2	3.42	13.8
22	Cr0→N1→C17→N1→Cr0	2	3.42	3.63
23	Cr0→C7→C8→Cr0	2	3.52	3.97
24	Cr0→C7→N3→Cr0	4	3.57	6.76
25	Cr0→C22→N3→Cr0	4	3.57	9.32
26	Cr0→N4→O5→Cr0	2	3.61	3.63
27	Cr0→C17→C9→Cr0	4	3.62	11.5
28	Cr0→C10→N4→Cr0	4	3.68	8.25
29	Cr0→N1→O5→Cr0	2	3.71	6.03
30	Cr0→N4→N1→Cr0	2	3.78	4.90
31	Cr0→N3→Cr0→N3→Cr0	2	3.88	7.38
32	Cr0→O5→Cr0→O5→Cr0	1	3.89	3.47
33	Cr0→O5→O6→Cr0	2	3.94	13.4
34	Cr0→N2→N4→Cr0	4	3.96	27.0
35	Cr0→O6→Cr0→N2→Cr0	4	3.97	4.28
36	Cr0→O5→Cr0→O6→Cr0	2	3.98	16.9
37	Cr0→C8→O6→Cr0	4	4.00	3.72
38	Cr0→N3→Cr0→N1→Cr0	4	4.01	32.1
39	Cr0→N4→Cr0→N3→Cr0	4	4.01	4.49
40	Cr0→O6→Cr0→O6→Cr0	1	4.06	3.35
41	Cr0→C9→C7→Cr0	4	4.07	3.75
42	Cr0→O11→Cr0	2	4.07	20.2

43	Cr0→O12→C10→Cr0	4	4.09	43.1
44	Cr0→N1→Cr0→O6→Cr0	4	4.10	3.48
45	Cr0→C10→O12→C10→Cr0	2	4.10	25.9
46	Cr0→C10→O6→Cr0	4	4.12	4.38
47	Cr0→C21→C17→Cr0	4	4.14	4.84
48	Cr0→N4→Cr0→N4→Cr0	2	4.14	5.58
49	Cr0→C16→Cr0	2	4.17	10.7
50	Cr0→O11→N2→Cr0	4	4.17	26.6
51	Cr0→C9→O5→Cr0	4	4.18	3.20
52	Cr0→C13→C7→Cr0	4	4.18	21.0
53	Cr0→C9→011→N2→Cr0	4	4.19	27.4
54	Cr0→C7→C13→C7→Cr0	2	4.20	12.7
55	Cr0→C18→Cr0	2	4.20	17.4
56	Cr0→C7→N2→C7→Cr0	2	4.22	1.88
57	Cr0→C9→N2→C7→Cr0	4	4.22	5.95
58	Cr0→C9→N2→C9→Cr0	2	4.22	8.00
59	Cr0→C17→N1→C17→Cr0	2	4.22	6.36
60	Cr0→C32→C22→Cr0	4	4.23	33.8
61	Cr0→C17→C18→C17→Cr0	2	4.25	19.1
62	Cr0→N3→O12→N3→Cr0	2	4.27	10.1
63	Cr0→N2→C9→C7→Cr0	4	4.28	4.24
64	Cr0→C13→N2→Cr0	4	4.30	13.0
65	Cr0→O11→C9→N2→Cr0	4	4.30	15.7
66	Cr0→N4→C26→C22→Cr0	4	4.30	5.18
67	Cr0→C7→C13→N2→Cr0	4	4.31	13.5
68	Cr0→C18→N1→Cr0	4	4.33	20.6
69	Cr0→N3→C8→C10→Cr0	4	4.33	3.12
70	Cr0→C17→O5→Cr0	4	4.34	3.30
71	Cr0→C26→N4→C22→Cr0	4	4.34	6.90
72	Cr0→C17→N1→N2→Cr0	4	4.35	3.15
73	Cr0→C17→C18→N1→Cr0	4	4.35	19.7
74	Cr0→C9→N3→Cr0	4	4.36	4.76
75	Cr0→C8→N3→N2→Cr0	4	4.37	2.19
76	Cr0→C10→N3→N2→Cr0	4	4.37	5.69
77	Cr0→C25→Cr0	2	4.37	7.43
78	Cr0→C7→N1→Cr0	4	4.40	2.71
79	Cr0→C25→N4→Cr0	4	4.41	14.1
80	Cr0→C8→N3→N4→Cr0	4	4.42	3.03
81	Cr0→C25→C26→Cr0	4	4.42	14.3
82	Cr0→C9→N2→N1→Cr0	4	4.42	2.81
83	Cr0→N1→C17→C21→Cr0	4	4.42	4.29
84	Cr0→N3→C16→N3→Cr0	2	4.43	4.67
85	Cr0→N3→O5→N3→Cr0	2	4.44	3.43
86	Cr0→C13→C7→N2→Cr0	4	4.45	6.84
87	Cr0→C26→N3→Cr0	4	4.45	2.60
88	Cr0→C26→N4→C26→Cr0	2	4.45	6.84
89	Cr0→N1→C20→N1→Cr0	2	4.45	5.89

90	Cr0→N4→C23→N4→Cr0	2	4.45	7.19
91	Cr0→C26→C25→N4→Cr0	4	4.46	10.8
92	Cr0→C26→N4→N3→Cr0	4	4.47	3.02
93	Cr0→C26→C25→C26→Cr0	2	4.47	6.08
94	Cr0→N3→O6→N3→Cr0	2	4.49	3.11
95	Cr0→N3→N4→N3→Cr0	2	4.49	3.02
96	Cr0→C18→C17→N1→Cr0	4	4.50	10.0
97	Cr0→N3→N2→N3→Cr0	2	4.53	3.43
98	Cr0→O6→N2→O6→Cr0	2	4.58	3.13
99	Cr0→C20→C21→N1→Cr0	4	4.58	6.57
100	Cr0→N1→N2→N1→Cr0	2	4.62	3.08
101	Cr0→C22→N2→Cr0	4	4.64	10.5
102	Cr0→O11→C17→Cr0	4	4.66	2.73
103	Cr0→O6→N1→O6→Cr0	2	4.67	2.86
104	Cr0→C10→O12→C22→Cr0	4	2.67	3.90
105	Cr0→C8→N1→Cr0	4	4.69	6.28
106	Cr0→C16→C7→Cr0	4	4.70	2.07
107	Cr0→C10→N3→C7→Cr0	4	4.70	1.96
108	Cr0→N4→O6→N4→Cr0	2	4.70	2.84
109	Cr0→C7→N2→C8→Cr0	4	4.71	3.08
110	Cr0→C22→N3→C8→Cr0	4	4.71	1.72
111	Cr0→C9→N2→C17→Cr0	4	4.71	6.10
112	Cr0→C7→C13→C8→Cr0	4	4.72	2.50
113	Cr0→C8→Cr0→N2→Cr0	4	4.76	2.73
114	Cr0→C22→N4→C10→Cr0	4	4.76	5.27
115	Cr0→C17→N4→Cr0	4	4.77	10.2
116	Cr0→C21→O5→Cr0	4	4.77	6.11
117	Cr0→C18→C9→Cr0	4	4.78	2.86
118	Cr0→C9→Cr0→N2→Cr0	4	4.81	2.77
119	Cr0→C24→Cr0	2	4.81	12.2
120	Cr0→C17→Cr0→N3→Cr0	4	4.81	7.01
121	Cr0→C17→C18→C9→Cr0	4	4.81	3.61
122	Cr0→C22→Cr0→N3→Cr0	4	4.81	3.56
123	Cr0→C19→N1→Cr0	4	4.82	20.8
124	Cr0→N1→C19→N1→Cr0	2	4.83	10.2
125	Cr0→O12→C10→C22→Cr0	4	4.84	5.34
126	Cr0→C8→N2→N3→Cr0	4	4.86	3.27
127	Cr0→C22→N3→N2→Cr0	4	4.86	3.81
128	Cr0→C9→O11→N1→Cr0	4	4.86	4.28
129	Cr0→C17→N1→N4→Cr0	4	4.86	6.91
130	Cr0→C18→N2→Cr0	4	4.87	3.08
131	Cr0→C26→N4→C10→Cr0	4	4.87	2.58
132	Cr0→N2→C9→C8	4	4.88	2.60
133	Cr0→C7→Cr0→N4→Cr0	4	4.89	3.92
134	Cr0→C13→C7→C8→Cr0	4	4.89	2.38
135	Cr0→C9→N1→N2→Cr0	4	4.89	4.18
136	Cr0→C17→C18→N2→Cr0	4	4.89	4.05

137	Cr0→C7→C13→N3→Cr0	4	4.90	2.78
138	Cr0→C8→N2→N1→Cr0	4	4.90	2.38
139	Cr0→O11→C9→N1→Cr0	4	4.90	4.69
140	Cr0→N4→C9→Cr0	4	4.91	15.1
141	Cr0→C21→N1→O5→Cr0	4	4.91	4.19
142	Cr0→C22→N3→N4→Cr0	4	4.91	4.43
143	Cr0→N3→C17→N1→Cr0	4	4.92	3.70
144	Cr0→N4→Cr0→C9→Cr0	4	4.94	16.8
145	Cr0→C9→Cr0→N1→Cr0	4	4.94	3.13
146	Cr0→C22→Cr0→N1→Cr0	4	3.94	6.87
147	Cr0→N2→C7→C17→Cr0	4	4.95	2.02
148	Cr0→N4→C7→N2→Cr0	4	4.95	2.60
149	Cr0→N4→C26→C10→Cr0	4	4.97	3.46
150	Cr0→C20→C17→Cr0	4	4.98	1.26
151	Cr0→N2→C26→Cr0	4	4.99	12.6
152	Cr0→N1→C20→C17→Cr0	4	5.02	1.41
153	Cr0→C24→C22→Cr0	4	5.03	8.84
154	Cr0→N3→Cr0→C21→Cr0	4	5.04	12.5
155	Cr0→C17→N1→N3→Cr0	4	5.04	2.48
156	Cr0→C17→C19→N1→Cr0	4	5.04	7.36
157	Cr0→N4→C22→N1→Cr0	4	5.05	3.18
158	Cr0→C26→Cr0→O5→Cr0	4	5.05	1.81
159	Cr0→C10→N3→N1→Cr0	4	5.10	7.55
160	Cr0→N2→C9→N4→Cr0	4	5.12	6.86
161	Cr0→C24→C26→Cr0	4	5.13	5.84
162	Cr0→N1→C19→C21→Cr0	4	5.14	5.36
163	Cr0→N4→C26→N2→Cr0	4	5.15	7.99
164	Cr0→C14→Cr0	2	5.16	4.82
165	Cr0→C21→N1→N3→Cr0	4	5.16	7.63
166	Cr0→N1→C21→C18→Cr0	4	5.16	4.18
167	Cr0→C22→C7→Cr0	4	5.17	1.91
168	Cr0→C26→Cr0→N4→Cr0	4	5.17	2.23
169	Cr0→C14→C7→Cr0	4	5.18	8.25
170	Cr0→C7→N3→C7→Cr0	2	5.19	0.64
171	Cr0→N3→C8→O12→Cr0	4	5.19	2.14
172	Cr0→C17→N2→C8→Cr0	4	5.19	1.60
173	Cr0→C8→C15→C8→Cr0	2	5.20	3.12
174	Cr0→C24→C23→Cr0	4	5.20	4.01
175	Cr0→C22→N3→C22→Cr0	2	5.20	2.09
176	Cr0→C18→C19→N1→Cr0	4	5.20	3.53
177	Cr0→C19→C18→C17→Cr0	4	5.22	5.05
178	Cr0→N2→C9→C13→Cr0	4	5.23	2.77
179	Cr0→C7→O6→N2→Cr0	4	5.23	2.24
180	Cr0→C25→C22→N4→Cr0	4	5.26	1.83
181	Cr0→C19→C20→Cr0	4	5.27	2.78
182	Cr0→C25→C24→N4→Cr0	4	5.28	2.35
183	Cr0→O11→C9→O11→Cr0	2	5.31	5.78

184	Cr0→O11→N2→C9→Cr0	4	5.31	6.62
185	Cr0→C24→C25→C26→Cr0	4	5.32	2.88
186	Cr0→C9→O6→N2→Cr0	4	5.35	3.16
187	Cr0→C15→C16→Cr0	4	5.35	4.30
188	Cr0→O5→N1→O5→Cr0	2	5.36	2.57
189	Cr0→C15→C16→C8→Cr0	4	5.37	4.17
190	Cr0→C14→C8→Cr0	4	5.37	3.74
191	Cr0→C13→C14→C7→Cr0	4	5.37	4.04
192	Cr0→C8→C14→C7→Cr0	4	5.39	3.13
193	Cr0→C18→N1→C17→Cr0	4	5.40	5.33
194	Cr0→C15→N3→Cr0	4	5.41	3.59
195	Cr0→N2→O6→C26→Cr0	4	5.43	2.43
196	Cr0→C7→C14→N2→Cr0	4	5.43	3.55
197	Cr0→C13→N2→C7→Cr0	4	5.44	2.66
198	Cr0→C15→C8→N3→Cr0	4	5.45	3.35
199	Cr0→C17→O6→N1→Cr0	4	5.45	2.98
200	Cr0→C15→C16→N3→Cr0	4	5.48	3.63
201	Cr0→C10→C9→Cr0	2	5.48	2.59
202	Cr0→C10→N2→C9→Cr0	4	5.50	5.27
203	Cr0→C9→O5→N2→Cr0	4	5.53	3.40

[a] The atom numbering scheme is shown in Figure 5.23. [b] *R* is the total distance travelled by the photoelectron divided by two. [c] The importance factor is the percent contribution of a path relative to the strongest MS path and includes Debye-Waller contributions.

Table A3.12 Debye-Waller factors for model **XA** of

trans-$[Cr^{III}(bpb)(OH_2)_2]ClO_4.H_2O$[a]

atom	σ^2 (Å^2)	atom	σ^2 (Å^2)
N1	0.0010(1)	N2	0.0011(1)
O5	0.0026(4)	O6	0.0010(1)
C7	0.021(1)	C9	0.0010(1)
O11	0.0024(2)	C13	0.022(1)
C14	0.030(1)	C17	0.0026(3)
C18	0.0020(1)	C19	0.0030(6)
C20	0.031(1)	C21	0.0037(4)

[a] The Monte-Carlo errors in the last significant figure are given in parentheses.

Table A3.13 Restraints used in the refinement of Model **XII** of *trans*-[Cr^{III}(bpb)Cl(OH_2)].DMF[a]

Restraints	
$S_0^2 \approx 0.9$ {0.2}	$\sigma^2_1 > 0.001$ {0.0005}
$\sigma^2_2 > 0.001$ {0.0005}	$\sigma^2_3 > 0.001$ {0.0005}
$\sigma^2_4 > 0.001$ {0.0005}	$\sigma^2_5 > 0.001$ {0.0005}
$\sigma^2_6 > 0.001$ {0.0005}	$\sigma^2_7 > 0.001$ {0.0005}
$\sigma^2_8 > 0.001$ {0.0005}	$\sigma^2_9 > 0.001$ {0.0005}
$\sigma^2_{10} > 0.001$ {0.0005}	$\sigma^2_{11} > 0.001$ {0.0005}
$\sigma^2_{12} > 0.001$ {0.0005}	$\sigma^2_{13} > 0.001$ {0.0005}
$\sigma^2_{14} > 0.001$ {0.0005}	$\sigma^2_{15} > 0.001$ {0.0005}
$\sigma^2_{16} > 0.001$ {0.0005}	$\sigma^2_{17} > 0.001$ {0.0005}
$\sigma^2_{18} > 0.001$ {0.0005}	$\sigma^2_{19} > 0.001$ {0.0005}
$\sigma^2_{20} > 0.001$ {0.0005}	$\sigma^2_{21} > 0.001$ {0.0005}
$\sigma^2_{22} > 0.001$ {0.0005}	$\sigma^2_{23} > 0.001$ {0.0005}
$\sigma^2_{24} > 0.001$ {0.0005}	$\sigma^2_{25} > 0.001$ {0.0005}
$\sigma^2_{26} > 0.001$ {0.0005}	$\sigma^2_1 < 0.02$ {0.01}
$\sigma^2_2 < 0.02$ {0.01}	$\sigma^2_3 < 0.02$ {0.01}
$\sigma^2_4 < 0.02$ {0.01}	$\sigma^2_5 < 0.02$ {0.01}
$\sigma^2_6 < 0.02$ {0.01}	$\sigma^2_7 < 0.02$ {0.01}
$\sigma^2_8 < 0.02$ {0.01}	$\sigma^2_9 < 0.02$ {0.01}
$\sigma^2_{10} < 0.02$ {0.01}	$\sigma^2_{11} < 0.02$ {0.01}
$\sigma^2_{12} < 0.02$ {0.01}	$\sigma^2_{13} < 0.03$ {0.01}
$\sigma^2_{14} < 0.03$ {0.01}	$\sigma^2_{15} < 0.03$ {0.01}
$\sigma^2_{16} < 0.03$ {0.01}	$\sigma^2_{17} < 0.02$ {0.01}
$\sigma^2_{18} < 0.03$ {0.01}	$\sigma^2_{19} < 0.03$ {0.01}
$\sigma^2_{20} < 0.03$ {0.01}	$\sigma^2_{21} < 0.02$ {0.01}
$\sigma^2_{22} < 0.02$ {0.01}	$\sigma^2_{23} < 0.03$ {0.01}
$\sigma^2_{24} < 0.03$ {0.01}	$\sigma^2_{25} < 0.03$ {0.01}
$\sigma^2_{26} < 0.02$ {0.01}	$\sigma^2_7 > (\sigma^2_2 + 0.001)$ {0.0005}
$\sigma^2_{13} > (\sigma^2_7 + 0.001)$ {0.0005}	$\sigma^2_{14} > (\sigma^2_{13} + 0.001)$ {0.0005}
$\sigma^2_{17} > (\sigma^2_1 + 0.001)$ {0.0005}	$\sigma^2_{18} > (\sigma^2_1 + 0.001)$ {0.0005}
$\sigma^2_{20} > (\sigma^2_1 + 0.001)$ {0.0005}	$\sigma^2_{21} > (\sigma^2_1 + 0.001)$ {0.0005}
$\sigma^2_{19} > (\sigma^2_{18} + 0.001)$ {0.0005}	$\sigma^2_{11} > (\sigma^2_9 + 0.001)$ {0.0005}
N1–C17 ≈ 1.35 Å {0.05}	N1–C21 ≈ 1.34 Å {0.05}
C17–C18 ≈ 1.38 Å {0.05}	C18–C19 ≈ 1.38 Å {0.05}
C19–C20 ≈ 1.36 Å {0.05}	C20–C21 ≈ 1.37 Å {0.05}
N2–C7 ≈ 1.41 Å {0.05}	N2–C9 ≈ 1.34 Å {0.05}
C9–O11 ≈ 1.23 Å {0.05}	C9–C17 ≈ 1.50 Å {0.05}
C7–C8 ≈ 1.42 Å {0.05}	C7–C13 ≈ 1.39 Å {0.05}
C13–C14 ≈ 1.38 Å {0.05}	C14–C15 ≈ 1.38 Å {0.05}
Cr0–O5 < 3.0 {0.1}	Cr0–Cl6 < 3.5 {0.1}
N1–Cr0–N2 ≈ 81° {10}	N1–Cr0–N4 ≈ 108° {10}
N2–Cr0–N3 ≈ 82° {10}	Cr0–N1–C17 ≈ 112° {5}
Cr0–N1–C21 ≈ 129° {5}	C17–N1–C21 ≈ 118° {5}
Cr0–N2–C7 ≈ 114° {5}	Cr0–N2–C9 ≈ 119° {5}

C7–N2–C9 ≈ 126° {5}	N2–C9–O11 ≈ 129° {5}
N2–C9–C17 ≈ 110° {5}	O11–C9–C17 ≈ 120° {5}
N2–C7–C8 ≈ 115° {5}	N2–C7–C13 ≈ 126° {5}
C8–C7–C13 ≈ 120° {5}	N1–C17–C9 ≈ 117° {5}
N1–C17–C18 ≈ 121° {5}	C9–C17–C18 ≈ 121° {5}
N1–C21–C20 ≈ 122° {5}	C17–C18–C19 ≈ 119° {5}
C18–C19–C20 ≈ 119° {5}	C19–C20–C21 ≈ 119° {5}
C7–C13–C14 ≈ 120° {5}	C13–C14–C13 ≈ 120° {5}
O5–Cr0–N1 > 80 {1}	O5–Cr0–N2 > 80 {1}
O5–Cr0–N3 > 80 {1}	O5–Cr0–N4 > 80 {1}
Cl6–Cr0–N1 > 80 {1}	Cl6–Cr0–N2 > 80 {1}
Cl6–Cr0–N3 > 80 {1}	Cl6–Cr0–N4 > 80 {1}
Atoms restrained to be approximately coplanar:	
((C7–C13)×(C8–C13))^.(C14–C13) ≈ 0 {0.01}	
((C7–C13)×(C8–C13))^.(C15–C13) ≈ 0 {0.01}	
((C7–C13)×(C8–C13))^.(C16–C13) ≈ 0 {0.01}	
((C7–C13)×(C8–C13))^.(N2–C13) ≈ 0 {0.01}	
((C7–C13)×(C8–C13))^.(N3–C13) ≈ 0 {0.01}	
((C7–C13)×(C8–C13))^.(C9–C13) ≈ 0 {0.01}	
((C7–C13)×(C8–C13))^.(C10–C13) ≈ 0 {0.01}	
((C7–C13)×(C8–C13))^.(O11–C13) ≈ 0 {0.01}	
((C7–C13)×(C8–C13))^.(O12–C13) ≈ 0 {0.01}	
((N1–C17)×(C18–C17))^.(C19–C17) ≈ 0 {0.01}	
((N1–C17)×(C18–C17))^.(C20–C17) ≈ 0 {0.01}	
((N1–C17)×(C18–C17))^.(C21–C17) ≈ 0 {0.01}	

[a] The ranges of the restraints are given in parentheses.

Table A3.14 Constraints used in the refinement of Model **XII** of *trans*-[Cr^{III}(bpb)Cl(OH_2)].DMF

Constraints	
$\sigma^2_1 = \sigma^2_4$	$\sigma^2_2 = \sigma^2_3$
$\sigma^2_7 = \sigma^2_8$	$\sigma^2_9 = \sigma^2_{10}$
$\sigma^2_{11} = \sigma^2_{12}$	$\sigma^2_{13} = \sigma^2_{16}$
$\sigma^2_{14} = \sigma^2_{15}$	$\sigma^2_{17} = \sigma^2_{22}$
$\sigma^2_{18} = \sigma^2_{23}$	$\sigma^2_{19} = \sigma^2_{24}$
$\sigma^2_{20} = \sigma^2_{25}$	$\sigma^2_{21} = \sigma^2_{26}$
$x1 = x4$	$y1 = -y4$
$z1 = z4$	$x2 = x3$
$y2 = -y3$	$z2 = z3$
$x7 = x8$	$y7 = -y8$
$z7 = z8$	$x9 = x10$
$y9 = -y10$	$z9 = z10$
$x11 = x12$	$y11 = -y12$
$z11 = z12$	$x13 = x16$
$y13 = -y16$	$z13 = z16$
$x14 = x15$	$y14 = -y15$
$z14 = z15$	$x17 = x22$
$y17 = -y22$	$z17 = z22$
$x18 = x23$	$y18 = -y23$
$z18 = z23$	$x19 = x24$
$y19 = -y24$	$z19 = z24$
$x20 = x25$	$y20 = -y25$
$z20 = z25$	$x21 = x26$
$y21 = -y26$	$z21 = z26$

Table A3.15 Details of the SS and MS paths for Model **XII** of *trans*-[Cr^{III}(bpb)Cl(OH_2)].DMF

Path No.	Atoms in MS pathway[a]	Degeneracy	R[b] (Å)	Importance factor[c]
1	Cr0→O5→Cr0	1	1.91	100
2	Cr0→N3→Cr0	2	1.98	100
3	Cr0→N4→Cr0	2	2.07	98.0
4	Cr0→Cl6→Cr0	1	2.32	38.6
5	Cr0→C22→Cr0	2	2.86	28.6
6	Cr0→C7→Cr0	2	2.88	46.1
7	Cr0→C9→Cr0	2	2.88	46.9
8	Cr0→C26→Cr0	2	3.09	26.8
9	Cr0→C10→N3→Cr0	4	3.10	33.1
10	Cr0→C8→N3→Cr0	4	3.14	27.5
11	Cr0→C22→N4→Cr0	4	3.14	17.9
12	Cr0→N2→O5→Cr0	4	3.24	10.9
13	Cr0→C26→N4→Cr0	4	3.25	34.5
14	Cr0→N2→N3→Cr0	2	3.28	5.44
15	Cr0→N1→N2→Cr0	4	3.32	11.4
16	Cr0→N2→C9→N2→Cr0	2	3.32	8.10
17	Cr0→N3→C8→N3→Cr0	2	3.40	5.53
18	Cr0→N4→C26→N4→Cr0	2	3.41	13.1
19	Cr0→N4→C22→N4→Cr0	2	3.42	3.1
20	Cr0→Cl6→N3→Cr0	4	3.54	6.77
21	Cr0→N1→O5→Cr0	2	3.58	4.02
22	Cr0→C17→N2→Cr0	4	3.59	8.32
23	Cr0→C8→C7→Cr0	2	3.59	7.62
24	Cr0→Cl6→N4→Cr0	4	3.61	6.55
25	Cr0→C7→N3→Cr0	4	3.62	10.8
26	Cr0→C10→C22→Cr0	4	3.63	10.9
27	Cr0→N4→O5→Cr0	2	3.66	6.42
28	Cr0→C9→N1→Cr0	4	3.70	9.85
29	Cr0→N4→N1→Cr0	2	3.79	5.88
30	Cr0→O5→Cr0→O5→Cr0	1	3.83	4.16
31	Cr0→N3→Cr0→O5→Cr0	4	3.90	1.23
32	Cr0→N3→Cr0→N3→Cr0	2	3.97	7.70
33	Cr0→N3→N1→Cr0	4	4.00	28.8
34	Cr0→C7→O5→Cr0	4	4.01	5.67
35	Cr0→C9→O5→Cr0	4	4.04	5.45
36	Cr0→N3→Cr0→N1→Cr0	4	4.05	33.5
37	Cr0→N4→Cr0→N3→Cr0	4	4.05	4.95
38	Cr0→O11→Cr0	2	4.09	20.9
39	Cr0→O11→C9→Cr0	4	4.10	44.9
40	Cr0→C9→C7→Cr0	4	4.11	5.68
41	Cr0→C9→O11→C9→Cr0	2	4.11	30.2
42	Cr0→C26→C22→Cr0	4	4.14	3.39

43	Cr0→N1→Cr0→N1→Cr0	2	4.14	6.52
44	Cr0→C18→Cr0	2	4.19	19.3
45	Cr0→O5→Cl6→Cr0	2	4.20	8.67
46	Cr0→O12→N3→Cr0	4	4.20	26.6
47	Cr0→C9→O11→N2→Cr0	4	4.21	30.3
48	Cr0→C23→C22→Cr0	4	4.22	36.9
49	Cr0→C22→N4→C22→Cr0	2	4.22	2.35
50	Cr0→C9→N2→C9→Cr0	2	4.22	9.30
51	Cr0→C16→Cr0	2	4.23	18.4
52	Cr0→O5→Cr0→Cl6→Cr0	2	4.23	11.2
53	Cr0→C17→C18→C17→Cr0	2	4.24	22.3
54	Cr0→C13→C7→Cr0	4	4.25	36.7
55	Cr0→C9→N2→C7→Cr0	4	4.26	9.85
56	Cr0→C7→C13→C7→Cr0	2	4.26	23.2
57	Cr0→C7→N2→C7→Cr0	2	4.29	7.79
58	Cr0→N1→C21→C17→Cr0	4	4.30	3.83
59	Cr0→N2→O11→N2→Cr0	2	4.31	10.3
60	Cr0→C18→N1→Cr0	4	4.32	22.1
61	Cr0→O11→C9→N2→Cr0	4	4.32	18.1
62	Cr0→C26→N4→C22→Cr0	4	4.32	4.85
63	Cr0→N2→C9→C7→Cr0	4	4.33	6.28
64	Cr0→C17→C18→N1→Cr0	4	4.34	23.7
65	Cr0→C25→Cr0	2	4.35	9.19
66	Cr0→C13→N2→Cr0	4	4.35	22.1
67	Cr0→C7→C13→N2→Cr0	4	4.37	23.3
68	Cr0→N2→C7→C9→Cr0	4	4.37	5.17
69	Cr0→C10→N2→Cr0	4	4.39	4.56
70	Cr0→C17→N1→N2→Cr0	4	4.39	3.02
71	Cr0→C25→N4→Cr0	4	4.39	16.6
72	Cr0→C9→N2→N3→Cr0	4	4.40	5.95
73	Cr0→C25→C26→Cr0	4	4.40	16.3
74	Cr0→N1→C17→C21→Cr0	4	4.41	2.95
75	Cr0→C21→N1→C21→Cr0	2	4.43	3.33
76	Cr0→C8→N3→N2→Cr0	4	4.43	3.58
77	Cr0→C9→N2→N1→Cr0	4	4.44	3.48
78	Cr0→N4→C25→N4→Cr0	2	4.44	6.96
79	Cr0→N1→C18→N1→Cr0	2	4.44	8.23
80	Cr0→C26→C25→N4→Cr0	4	4.45	13.2
81	Cr0→C8→N4→Cr0	4	4.45	4.27
82	Cr0→C26→C25→C26→Cr0	2	4.46	7.30
83	Cr0→C7→N2→N1→Cr0	4	4.47	4.30
84	Cr0→N2→C13→N2→Cr0	2	4.48	8.07
85	Cr0→C21→N2→Cr0	4	4.48	2.14
86	Cr0→C21→N4→Cr0	4	4.48	1.94
87	Cr0→O5→N2→O5→Cr0	2	4.49	3.59
88	Cr0→C23→C22→N4→Cr0	4	4.49	11.8
89	Cr0→C26→N4→N3→Cr0	4	4.50	2.75

90	Cr0→C13→C7→N2→Cr0	4	4.51	12.9
91	Cr0→C20→C21→N1→Cr0	4	4.56	7.73
92	Cr0→N2→O5→N2→Cr0	2	4.57	3.85
93	Cr0→N3→N4→N3→Cr0	2	4.57	3.37
94	Cr0→N3→N2→N3→Cr0	2	4.58	3.69
95	Cr0→C21→O5→Cr0	4	4.63	3.76
96	Cr0→Cl6→Cr0→Cl6→Cr0	1	4.64	1.40
97	Cr0→N1→N2→N1→Cr0	2	4.65	3.40
98	Cr0→C22→N2→Cr0	4	4.66	7.73
99	Cr0→O12→C22→Cr0	4	4.66	2.95
100	Cr0→C9→O11→C17→Cr0	4	4.68	4.14
101	Cr0→C9→N2→C17→Cr0	4	4.71	5.51
102	Cr0→C8→N1→Cr0	4	4.74	9.98
103	Cr0→C22→N3→C8→Cr0	4	4.74	2.31
104	Cr0→C10→N3→C7→Cr0	4	4.74	3.49
105	Cr0→C16→C7→Cr0	4	4.76	4.03
106	Cr0→C21→N1→O5→Cr0	2	4.76	1.58
107	Cr0→C17→N1→C9→Cr0	4	4.77	4.73
108	Cr0→C17→N4→Cr0	4	4.77	7.90
109	Cr0→C8→N3→C7→Cr0	4	4.78	6.67
110	Cr0→C8→C16→C7→Cr0	4	4.78	4.97
111	Cr0→C23→C10→Cr0	4	4.79	3.54
112	Cr0→C19→Cr0	2	4.79	13.5
113	Cr0→N1→C21→O5→Cr0	4	4.79	2.31
114	Cr0→C24→N4→Cr0	4	4.80	23.1
115	Cr0→C22→C23→C10→Cr0	4	4.81	4.06
116	Cr0→N1→C19→N1→Cr0	2	4.81	12.4
117	Cr0→N4→Cl6→N2→Cr0	4	4.83	3.35
118	Cr0→C25→N4→O5→Cr0	2	4.84	1.78
119	Cr0→O12→C10→C22→Cr0	4	4.84	4.91
120	Cr0→C22→Cr0→N2→Cr0	4	4.85	4.62
121	Cr0→C22→Cr0→N3→Cr0	4	4.85	2.89
122	Cr0→C7→Cr0→N3→Cr0	4	4.86	4.13
123	Cr0→C10→Cr0→N3→Cr0	4	4.87	2.96
124	Cr0→C17→N1→N4→Cr0	4	4.87	6.01
125	Cr0→C10→O12→N4→Cr0	4	4.87	5.32
126	Cr0→C21→N1→C9→Cr0	4	4.88	2.45
127	Cr0→C17→N2→N3→Cr0	4	4.88	3.13
128	Cr0→C22→C23→N3→Cr0	4	4.90	4.91
129	Cr0→C7→N3→N3→Cr0	4	4.92	5.05
130	Cr0→O12→C10→N4→Cr0	4	4.92	5.70
131	Cr0→C17→N2→N1→Cr0	4	4.92	3.73
132	Cr0→N4→C9→Cr0	4	4.92	17.3
133	Cr0→N2→C9→C8→Cr0	4	4.93	3.98
134	Cr0→C22→Cr0→N1→Cr0	4	4.93	5.92
135	Cr0→N2→C22→N4→Cr0	4	4.94	3.26
136	Cr0→C10→N4→N3→Cr0	4	4.95	4.81

137	Cr0→C7→Cr0→N4→Cr0	4	4.95	5.87
138	Cr0→N1→Cr0→C10→Cr0	4	4.95	19.8
139	Cr0→C9→Cr0→N1→Cr0	4	4.95	3.74
140	Cr0→C13→C7→C8→Cr0	4	4.95	5.51
141	Cr0→C7→C13→N3→Cr0	4	4.96	4.83
142	Cr0→C8→N2→N1→Cr0	4	4.96	3.70
143	Cr0→C20→C17→Cr0	4	4.97	1.45
144	Cr0→N2→C7→C17→Cr0	4	4.98	2.53
145	Cr0→C18→C17→C9→Cr0	4	4.98	4.71
146	Cr0→N1→C21→C9→Cr0	4	4.98	3.12
147	Cr0→N1→C8→N3→Cr0	4	5.00	3.97
148	Cr0→C21→Cr0→O5→Cr0	4	5.00	1.60
149	Cr0→C24→C22→Cr0	4	5.01	8.95
150	Cr0→N1→C20→C17→Cr0	4	5.01	1.76
151	Cr0→N2→C26→Cr0	4	5.02	11.1
152	Cr0→C17→C19→N1→Cr0	4	5.02	8.52
153	Cr0→N1→C17→N4→Cr0	4	5.05	2.90
154	Cr0→N3→Cr0→C21→Cr0	4	5.07	11.3
155	Cr0→C22→N4→N2→Cr0	4	5.08	1.94
156	Cr0→C19→C21→Cr0	4	5.11	6.25
157	Cr0→C9→N2→N4→Cr0	4	5.12	8.50
158	Cr0→N4→C24→C26→Cr0	4	5.12	6.03
159	Cr0→N2→C9→N4→Cr0	4	5.14	7.48
160	Cr0→N1→C21→C18→Cr0	4	5.15	4.40
161	Cr0→C21→Cr0→N1→Cr0	4	5.16	1.96
162	Cr0→C19→C18→Cr0	4	5.18	4.46
163	Cr0→N4→C26→N2→Cr0	4	5.18	7.33
164	Cr0→C21→N1→N3→Cr0	4	5.18	7.19
165	Cr0→C22→N3→C22→Cr0	2	5.19	0.86
166	Cr0→C23→C24→N4→Cr0	4	5.19	4.51
167	Cr0→C8→C17→Cr0	4	5.20	2.07
168	Cr0→C24→C23→C22→Cr0	4	5.20	5.68
169	Cr0→N2→C7→O11→Cr0	4	5.22	3.53
170	Cr0→C15→Cr0	2	5.23	9.74
171	Cr0→C17→C19→C17→Cr0	2	5.24	1.96
172	Cr0→O5→N4→O5→Cr0	2	5.25	3.08
173	Cr0→C20→C17→N1→Cr0	4	5.25	2.01
174	Cr0→C19→C20→Cr0	4	5.25	3.20
175	Cr0→C15→C8→Cr0	4	5.25	17.0
176	Cr0→C8→N2→C8→Cr0	2	5.26	2.47
177	Cr0→C20→C19→N1→Cr0	4	5.26	3.12
178	Cr0→C7→C14→C7→Cr0	2	5.27	6.50
179	Cr0→N2→C9→C13→Cr0	4	5.29	4.51
180	Cr0→C24→C25→C26→Cr0	4	5.30	3.19
181	Cr0→O12→N3→C10→Cr0	4	5.32	7.62
182	Cr0→O12→C10→O12→Cr0	2	5.32	6.31
183	Cr0→C23→N4→C22→Cr0	4	5.39	4.92

184	Cr0→C14→C13→Cr0	4	5.42	8.84
185	Cr0→N4→N1→C9→Cr0	4	5.42	2.97
186	Cr0→C15→C16→Cr0	4	5.44	8.74
187	Cr0→C15→C7→Cr0	4	5.44	7.80
188	Cr0→C16→C15→C8→Cr0	4	5.44	8.49
189	Cr0→C8→O5→N3→Cr0	4	5.45	3.66
190	Cr0→C8→C14→C7→Cr0	4	5.46	6.44
191	Cr0→C15→N3→Cr0	4	5.47	7.14
192	Cr0→C9→C10→Cr0	2	5.49	2.77
193	Cr0→C7→C14→N2→Cr0	4	5.50	7.29

[a] The atom numbering scheme is shown in Figure 5.26. [b] *R* is the total distance travelled by the photoelectron divided by two. [c] The importance factor is the percent contribution of a path relative to the strongest MS path and includes Debye-Waller contributions.

Table A3.16 Debye-Waller factors for model **XII** of *trans*-[Cr^{III}(bpb)Cl(OH_2)].DMF[a]

atom	σ^2 (Å^2)	atom	σ^2 (Å^2)
N1	0.0010(1)	N2	0.0010(1)
O5	0.0020(7)	Cl6	0.0038(3)
C7	0.0020(1)	C9	0.0010(1)
O11	0.003(1)	C13	0.0030(1)
C14	0.0040(1)	C17	0.020(1)
C18	0.0020(1)	C19	0.0030(6)
C20	0.030(1)	C21	0.018(1)

[a] The Monte-Carlo errors in the last significant figure are given in parentheses.